UNIVERSITY OF CAMBRIDGE

Ubiquitination of proteins involved in metabolism and immunomodulatory drug sensitivity in lymphocytes

Rebecca Ann Harris

Darwin College

Department of Pathology

December 2021

This thesis is submitted for the degree of Doctor of Philosophy

CANCER RESEARCH UK | CAMBRIDGE CENTRE

Declaration

This thesis is the result of my own work and includes nothing which is the outcome of work done in collaboration except as declared in the preface and specified in the text.

It is not substantially the same as any work that has already been submitted before for any degree or other qualification except as declared in the preface and specified in the text.

This thesis does not exceed the prescribed 60,000 word limit for the School of Biological Sciences Degree Committee.

_____

Rebecca Ann Harris

Acknowledgements

Firstly, I must thank supervisor, Professor Heike Laman, for her continuous guidance and encouragement over the past four years, and for helping me to navigate a PhD through the uncertainty of a global pandemic. I am grateful for the time that you have dedicated to me, and the ideas and knowledge that you have shared. You have struck the perfect balance of supporting me, whilst giving me space to learn and grow as an independent researcher, and I leave your lab with a confidence instilled by you.

To past and present members of the Laman lab, my journey would not have been complete without you. I have watched the lab grow since I joined, and it became a brighter place with every one of you. Thank you for your help, encouragement, laughter, and long lunch breaks. Special thanks must go to Beth, for passing on all your knowledge and for your patience in the early days of my PhD when you were the only person around to answer my questions. I am also especially grateful to Sara who has been the best desk neighbour and source of support that I could ask for, and who I will sorely miss.

Many thanks go to my mentor, Professor Klaus Okkenhaug, for his advice throughout my PhD, and to his lab for willingly sharing their T cell expertise. I would also like to thank Professor Christian Frezza, Dr Ming Yang, and Dr Christina Schmidt for their knowledge, time and resources dedicated to my metabolomics experiments.

I would like to thank Global Biotech Revolution and my amazing GapSummit organising team. At times, we all thought we had bitten off more than we could chew in organising such a large event (twice, thanks to COVID!). Perhaps without realising, you rallied me through the challenges of a PhD and served as a reminder that science is exciting, even when my own experiments hit hurdles.

I would not have made it here without my family. Thanks go to my grandparents who always encourage me to strive for the best, my brothers for their healthy sibling rivalry and votes of confidence, and to my incredible parents. Mum and Dad, you gave me the foundations to achieve this PhD and I always have your unconditional support, thank you.

Finally, I must thank Alex, who has stood with me through every step in this journey. We have celebrated the highs, and your belief in me has helped me through the lows. You never fail to make me smile at the end of a long day. You have always known when to let me work late, and when to take me off to the Peak District for a break. Those weekends away with you and Annie have kept me going, and now I can just enjoy our next adventure.

Abstract

Proteins undergo post-translational modifications, such as ubiquitination and phosphorylation, which can alter their activity, localisation and stability, making a cell responsive to its internal and external environment. Ubiquitin ligases and kinases comprise large enzyme families which catalyse such reactions. The SCF-type E3 ubiquitin ligase sub-family utilise F-box proteins as the substrate targeting component. However, alongside promoting ubiquitination, the F-box protein Fbxo7 can also function as a scaffold and stabilise a subset of proteins, including Cdk6. Cdk6 is activated through binding the D-type cyclins, and historically, a key role has been as a cell cycle regulatory kinase that inactivates G1 checkpoint proteins. More recently, wider roles for Cdk6 have been identified, including as an inhibitor of glycolysis. Notably, Cdk6 has pro-survival activity in T acute lymphoblastic leukaemia (T-ALL) cells due to the phosphorylation and inhibition of glycolytic enzymes, including the rate-limiting gatekeeper, phosphofructokinase (PFKP). Our screens for Fbxo7-interacting partners identified a set of candidates that overlapped as cyclin D/Cdk6 substrates and included PFKP. Further study revealed that Fbxo7 promotes two post-translational modifications on PFKP, ubiquitination and phosphorylation, and specifically promotes Cdk6 activity. Analysis in T-ALL cells suggest that Fbxo7 inhibits the assembly of active PFKP complexes to ultimately inhibit glycolysis. This is confirmed in a murine model of reduced Fbxo7 expression, whose $CD4^+$ T cells show higher levels of glycolytic flux, alongside various other metabolic defects including altered nucleotide biosynthesis and arginine metabolism. This places Fbxo7 as a negative regulator of glycolysis and unveils other diverse roles in metabolism, which may contribute to viability and activation defects observed in these Fbxo7-deficient murine T cells. Given that Fbxo7 negatively regulates glycolysis via PFKP, I also investigated how glucose regulates Fbxo7, as feedback loops in glucose signalling are commonplace in metabolic networks. I discovered Fbxo7 is a dose-dependent, glucose responsive protein in numerous cell types, which is both transcriptionally downregulated and targeted for autophagy in response to glucose starvation. Moreover, data suggest that Fbxo7 is responsive to other stresses, including oxidative stress, placing Fbxo7 as a nexus to link various cellular stress responses to metabolic reprogramming. In addition to PFKP, Fbxo7 has also been shown to recognise a protein called cereblon (CRBN), which is another E3 ubiquitin ligase. CRBN is of clinical relevance because its expression is required for the efficacy of immunomodulatory drugs (IMiDs) in multiple myeloma (MM), which primarily enable the recognition of neo-substrates by CRBN to elicit their anti-cancer effects. We sought to investigate a role for Fbxo7 in MM cells. We show that Fbxo7 promotes CRBN ubiquitination and propose that this targets CRBN for proteasomal degradation, which may have relevance for IMiD sensitivity. Together, these data identify two novel substrates for Fbxo7 ubiquitination and reveal a role for Fbxo7 in lymphocytes. We demonstrate that Fbxo7 expression is responsive to cellular stress and propose that Fbxo7 levels may fine-tune metabolism under different physiological and pathological conditions.

Table of Contents

List of Figures

CHAPTER 1: Introduction

CHAPTER 3: Fbxo7 as a regulator of glycolysis and wider T cell metabolism

CHAPTER 4: Fbxo7 regulation under cellular stress

CHAPTER 5: A role for Fbxo7 in regulating the immunomodulatory drug target, CRBN

List of Tables

CHAPTER 2: Materials and Methods

Abbreviations

1C	1 carbon metabolism	DMSO	Dimethyl sulfoxide
2-DG	2-deoxy-D-glucose	DN	Double negative
AD	Alzheimer's disease	DP	Double positive
ADCC	Antibody-dependent cellular cytotoxicity	EMT	Epithelial-to-mesenchymal transition
ALCL	Anaplastic large cell lymphoma	FAO	Fatty acid oxidation
AML	Acute myeloid leukaemia	FAS	Fatty acid synthesis
APC	Antigen presenting cell	FBP	F-box protein
BafA	Bafilomycin A1	FBS	Fetal bovine serum
BMSC	Bone marrow stromal cells	FP	Fbxo7-PI31
CAF	Cancer-associated fibroblast	H_2DCFDA	2′,7′-Dichlorofluorescin diacetate
CAR	Chimeric antigen receptor	H_2O_2	Hydrogen peroxide
Cdk	Cyclin-dependent kinase	HBD	Helical bundle domain
CELMoDs	Cereblon E3 ligase-modulating drugs	HECT	Homologous to E6-associated protein C-terminus
CHX	Cycloheximide	HRMS	Hybrid quadrupole-orbitrap mass spectrometer
Co-NTA	Cobalt NTA agarose affinity resin	HSPCs	Haematopoietic stem and progenitor cells
CRL	Cullin RING ligase	ID	Intellectual disability
CTL	Cytotoxic T lymphocyte	IMiD	Immunomodulatory drug
CULT	Cereblon domain of unknown activity, binding cellular ligands and thalidomide	IP	Immunoprecipitation
DC	Dendritic cell	LC-MS	Liquid chromatography-mass spectrometry
DCAF	DDB1-CUL4 associated factors	LLD	LON-like domain
DLBCL	Diffuse large B cell lymphoma	mAb	Monoclonal antibody

MHC	Major histocompatability complex	qRT-PCR	Quantitative reverse transcription polymerase chain reaction
MM	Multiple myeloma	RBR	RING-in-between-RING
MS	Mass spectrometry	RING	Really interesting new gene
MW	Molecular weight	ROS	Reactive oxygen species
NEM	N-Ethylmaleimide	Rot/AA	Rotenone / Antimycin A
NK	Natural killer	RT	Room temperature
NTD	N-terminal domain	SCF	Skp1-Cullin 1-Fbox
OXPHOS	Oxidative phosphorylation	shRNA	Short hairpin ribonucleic acid
P/S	Penicillin and streptomycin	siRNA	Short interfering ribonucleic acid
PAABD	Phospho-amino acid binding domain	SP	Single positive
pAb	Polyclonal antibody	T-ALL	T acute lymphoblastic leukaemia
PBS	Phosphate buffered saline	TCR	T cell receptor
PCA	Principle component analysis	Th1, Th2, Th17	Helper T cell subsets
PCR	Polymerase chain reaction	Tm	Memory T cell
PEI	Polyethylenimine	TME	Tumour microenvironment
PFA	Paraformaldehyde	Tn	Naïve T cell
PI	Propidium iodide	Treg	Regulatory T cell
PMSF	Phenylmethylsulfonyl fluoride	Ub	Ubiquitin
PPP	Pentose phosphate pathway	Ubl	Ubiquitin-like
PROTAC	Proteolysis-targeting chimera	UPS	Ubiquitin proteasome system
PRR	Proline rich region	WT	Wild type
PTM	Post-translational modification	Y2H	Yeast two-hybrid

CHAPTER 1

Introduction

Ubiquitin Proteasome System

Protein turnover is critical for many cellular processes including the cell cycle, DNA repair and differentiation, and it is essential that proteins can be specifically targeted for degradation in a spatial and temporal manner. The ubiquitin proteasome system (UPS) is this bridge between cellular signalling pathways and highly regulated protein degradation.

Ubiquitin is a 76 amino acid protein which is highly conserved in eukaryotes and can be conjugated to the lysine residues of target proteins as a post-translational modification. Proteins are ubiquitinated in a three-step enzymatic cascade which involves an E1 ubiquitin-activating enzyme, E2 ubiquitin-conjugating enzyme, and E3 ubiquitin-protein ligase[1–3] (Fig.1.1). The process begins with an ATP-dependent reaction in which a thioester bond is formed between the C-terminal carboxyl group of ubiquitin and a catalytic cysteine residue in the E1. Charging the E1 with ubiquitin induces a conformational change that reveals a negatively charged groove, and this enables its recognition by two conserved lysine residues in an E2 enzyme. In the second step, a catalytic cysteine residue in the E2 active site attacks the E1-ubiquitin complex to form another thioester bond and transfer the ubiquitin molecule to the E2 enzyme. Finally, it is the role of the E3 ligase to bring the E2 and substrate in close proximity and catalyse the formation of an isopeptide bond between the lysine ε-amino group of the substrate and the C-terminal carboxyl of ubiquitin, thereby ubiquitinating the substrate.

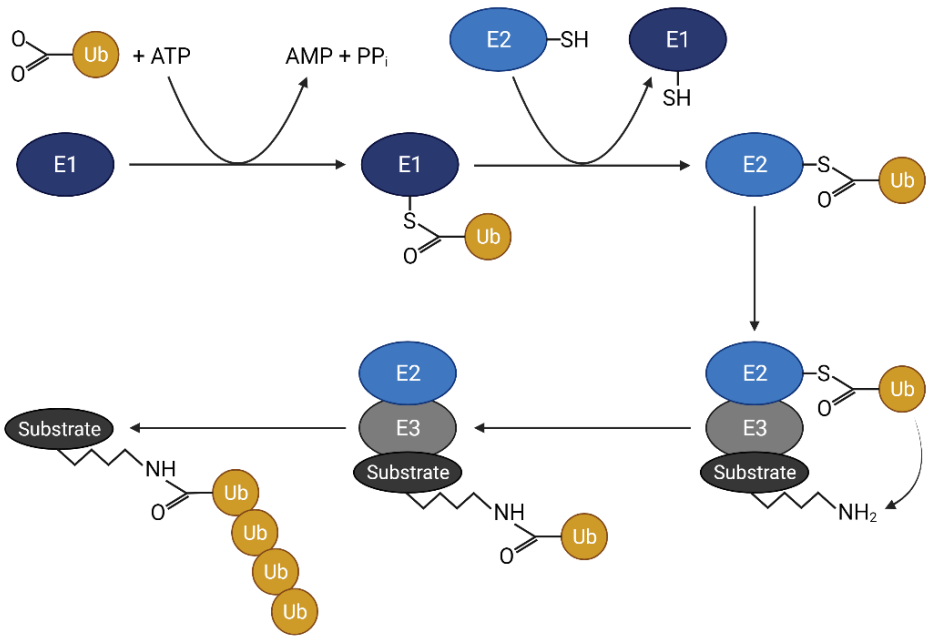

Figure 1.1: The ubiquitination enzymatic cascade.

Small ubiquitin molecules are added sequentially to protein lysine residues through the action of an E1 ubiquitin-activating enzyme, E2 ubiquitin-conjugating enzyme, and E3 ubiquitin-protein ligase.

The widespread roles for ubiquitination in cellular signalling place requirements for multiplicity, complexity, and responsiveness in the system. Firstly, a vast array of substrates must be targeted, and this diversity is obtained by permutations of E1, E2 and E3 enzymes, with one E2 able to interact with many different E3s and vice versa. In humans there are two E1 ubiquitin-activating enzymes (UBE1 & UBA6)[1], ~40 E2 ubiquitin-conjugating enzymes[34], and over 600 E3 ubiquitin-protein ligases[5,6], which results in enormous variation. It is also necessary for the system to be dynamic in order to rapidly respond to signalling cascades within the cell. This occurs in part by maintaining a pool of cellular ubiquitin that may be free, or bound to an E1/E2/E3 enzyme or a substrate, at any given time[7]. Like any protein, the size of the ubiquitin pool can be altered by protein transcription and degradation but, importantly for this dynamic system, the reaction can also be reversed by deubiquitinating enzymes (DUBs) to release substrate-bound ubiquitin back into the free ubiquitin pool[8]. A further level of complexity is added by the post-translational modification of ubiquitin by both phosphorylation and acetylation[9,10]. Under normal growth conditions the concentration of phosphorylated ubiquitin is low, but this can be increased by signalling cascades[11,12] and ultimately impact its interactions with other proteins such as DUBs[12] to change the outcome or duration of the ubiquitin signal.

Ubiquitin can be conjugated to proteins in different ways, and this affects the fate of the target protein. The addition of a single ubiquitin molecule to a target protein is termed monoubiquitination, whilst multi-monoubiquitination refers to the addition of multiple single ubiquitin molecules across the length of the target protein. However, ubiquitin itself also contains seven internal lysine residues (K6, K11, K27, K29, K33, K48 and K63) and an N-terminal methionine residue (M1), which can themselves be ubiquitinated to form polyubiquitin chains[9,13,14]. The chain linkage topology and length are determined by the E2 enzymes, and multiple E2s may work synchronously to add subsequent ubiquitin molecules to a polyubiquitin chain[4]. For example, K48-linked polyubiquitin chains are the most abundant topology and typically target the substrate for proteasomal degradation, although studies have also shown non-proteolytic functions[15]. Meanwhile, K63-linked chains have been shown to induce lysosomal targeting, DNA repair, NFκB activation and innate immune responses[16]. The remaining linkage types are less well characterised, but data does indicate a role for K6 chains in the removal of damaged mitochondria[11], K33 chains in Golgi trafficking[17], and K27 chains in DNA repair and autoimmunity[18,19]. Ubiquitin can also form heterotypic chains where different linkage types are present in the same polyubiquitin chain, and these may be linear or branched. Although these chains are less well studied, functions are increasingly being discovered, such as the anaphase-promoting complex (APC/C) which assembles branched chains that are efficient proteasome degradation signals and enhance the turnover of cell-cycle regulators[20]. Whilst it was once believed that each chain linkage conferred a distinct outcome, these rules are increasingly being broken, and the field is moving

towards a model whereby each ubiquitination event falls onto a complex spectrum of signalling or degradation outcomes[21].

Whilst the E1-E2-E3 cascade is sufficient for most ubiquitin events, the efficient ubiquitination of some targets requires the additional action of an E4 ubiquitin ligase. To date, only a small handful of E4 enzymes have been identified[22–26], and their role is primarily to complement the action of E3s by either stimulating E3 function or extending existing polyubiquitin chains. In this regard, they may be considered as ubiquitin chain elongation factors. Many E4 enzyme are structurally related to E3s and may even possess E3 ligase activity[27]. The first E4 to be described, yeast UFD2, is one such enzyme[27–29] and its two human homologues, UBE4A and UBE4B, also show E3/E4 activity[30–33]. Notably, UBE4B promotes the polyubiquitination of p53 by E3 ligase Hdm2 to ultimately yield p53 degradation, and is involved in p53 regulation in both brain tumours[32] and breast cancer[33], illustrating the regulatory significance of this novel subset of enzymes.

1..1 E3 ubiquitin ligases

There are three classes of E3 ligase: the HECT (Homologous to E6-associated protein C-terminus) domain, RBR (RING-in-between-RING) domain and RING (Really Interesting New Gene)-finger type E3s[6,34]. The HECT-domain and RBR-domain families require a two-step reaction whereby ubiquitin is first transferred to a catalytic cysteine on the E3 before being added to the substrate. Conversely, the most abundant RING-finger type E3s facilitate the transfer of ubiquitin from the E2 directly to the substrate in a single step (as illustrated in Fig. 1.1). These RING-finger type ligases can function as monomers, or form homo- and hetero-dimers and multi-subunit complexes that may augment their enzymatic efficiency[35].

The Cullin-RING ligases (CRL) are an example of multi-subunit RING E3s[36,37] (Fig. 1.2). This family of E3s have the common feature of being built upon one of seven cullin scaffold proteins that bind a RING-box protein (Rbx1 or Rbx2) at their C-terminal globular domain, and this RING-box protein in turn recruits the E2 ligase. The N-terminal stalk of the cullin scaffold binds an adaptor protein that tethers the substrate-recruiting component via an adaptor-binding motif. Whilst the cullin structures are largely similar, there is a variable sequence in this N-terminal stalk that determines which adaptor protein, and therefore substrate-recognition component, may join the complex.

One example is CRL1, or SCF (Skp1-Cullin 1-Fbox), E3 ligases[36,37] (Fig. 1.2). These are built upon a cullin1 backbone and comprise an Rbx1 protein for E2 recruitment, and a Skp1 adaptor protein which in turn binds a variable F-box protein (FBP). Upon substrate binding to the FBP, the ubiquitin charged E2 and

substrate are brought in close proximity to enable the transfer of the ubiquitin to the target protein. A second example is the CRL4 complex (Fig. 1.2) which is built upon a cullin4A backbone and employs a Damaged DNA Binding protein 1 (DDB1) adaptor protein instead of Skp1[38,39]. This DDB1 adaptor binds a DDB1-CUL4 associated factors (DCAF) which serves as the substrate-recruiting component.

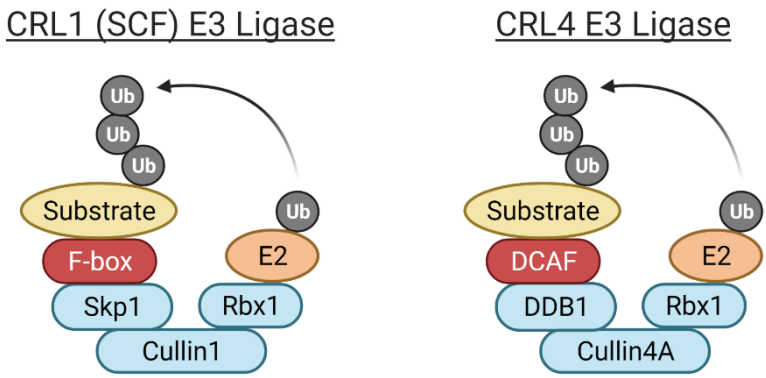

Figure 1.2: Schematic of example Cullin-RING ligases (CRL).

Cullin-RING ligases are a subfamily of RING-type E3 ligases and are commonly built upon a cullin scaffold, which binds an Rbx1 protein at its C-terminus. The N-terminal stalk of different cullin proteins bind alternative adaptor proteins. Shown here is CRL1 (left) which uses a Skp1 adaptor to bind an F-box protein, and CRL4 (right) which uses a DDB1 adaptor to bind a DCAF protein. Both F-box and DCAF proteins recruit substrates to the CRL complex to enable the transfer of ubiquitin molecules from an E2 enzyme to the lysine residues of target proteins.

Substrate recruitment to CRL complexes is a tightly regulated response to cellular stimuli and typically occurs via recognition of a short peptide motif known as a degron[5,37]. Whilst some CRLs will recognise unmodified sequences[40–43], many integrate cellular signalling pathways and rely upon post-translational modifications (PTMs) for substrate recognition. Often, degrons contain one or more phosphorylated residues and these phospho-degrons can enable the rapid translation of a protein kinase signalling cascade into a ubiquitination response. Other PTMs reported to enable substrate binding include the recognition of glycosylated substrates by SCF^{Fbxo2} and SCF^{Fbxo6} [44,45], and acetyl-degrons by SCF^{Fbxl17} [46]. Sometimes these peptide degrons cannot be recognised by CRL subunits directly and co-factors are required. This is exemplified by $CRL4^{Cdt2}$ which recognises substrates with PIP-motif degrons, such as Ctd1 and p21, that are docked onto an essential PCNA co-factor[47–49]. Furthermore SCF^{Skp2} (Fbxl1) requires a Cks1 accessory protein to recognise and recruit phosphorylated p27 and p130 to the SCF^{Skp2} complex[50–52]. Interestingly, recent studies indicate that substrate binding can also be regulated by metabolic co-factors, such as the positive regulation of SCF^{Fbxl5} ubiquitination

of IRP2 by iron[53]. Although recognition is frequently via a linear peptide motif, evidence suggests that non-canonical degrons may also take the form of protein domains[54]. This domain-based recognition gives the potential for protein modifications or functions that influence its 3D structure to directly impact ubiquitination. To increase stringency of the UPS, these various modes of recognition may be combined to enable precise recognition of specific substrates by CRL complexes.

CRL assembly and substrate engagement forms a regulatory circuit where the availability of substrate and cognate CRL maintain a dynamic system. It is widely believed that the availability and localisation of substrate-receptors (SRs, e.g., F-box protein or DCAF) may determine the CRL complexes formed, with turnover of SRs often regulated by autoubiquitination in the absence of their substrates[36,55–57]. Neddylation is another critical PTM in the regulation of the CRL system and it has long been understood that the attachment of NEDD8 onto cullin backbones stimulates CRL activity[58,59]. Subsequently, several studies culminated to define a cycle whereby NEDD8 conjugation drives SR exchange, and hence directs ubiquitination[43,60–64]. Briefly, upon substrate ubiquitination and release, the COP9 signalosome (CSN) mediates deneddylation of the substrate-free CRL. This enables the binding of the Cand1 exchange factor which removes the empty SR and resets the cycle for another SR. To this end, substrate binding protects the cognate SR from displacement by Cand1, hence the substrate availability itself is a driver for CRL assembly. Importantly, these mechanisms ultimately regulate the levels of CRL in the cell and maintain dynamic ubiquitination activity that enables a cell to rapidly adapt to intrinsic and extrinsic signals.

1..2 F-box proteins (FBPs)

FBPs are the substrate-recruiting components of CRL1 / SCF E3 ubiquitin ligases. To date there have been 69 identified in humans[65], and they are characterised by the presence of a 40 amino acid F-box domain which binds to the Skp1 adaptor. F-box proteins are further sub-divided into three categories based on the motifs present in their substrate binding domain; namely a series of leucine rich repeats (Fbxl family), WD40 repeats (Fbxw family) or other or non-recognisable motifs (Fbxo family)[55,66]. Although FBPs are essential for the formation of SCF complexes, a study found that over half of all human FBPs showed <10% assembly into SCF complexes[62]. It is conceivable that this pool of free FBPs is involved in the growing number of SCF-independent functions that have been identified through the ongoing characterisation of these proteins. In fact, over 12% of human FBPs are recognised to have non-canonical functions that may involve alternative protein binding partners or intrinsic enzymatic activity[55].

1..2.1 Fbxo7

Fbxo7 is a predominantly cytoplasmic protein[67] which, alongside its characteristic F-box domain, contains an N-terminal ubiquitin-like (Ubl) domain and largely unstructured C-terminal proline-rich region (PRR), both of which are involved in mediating protein-protein interactions. The central portion of the protein also contains domains involved in specific protein interactions, namely PI31 via a globular Fbxo7-PI31 (FP) domain, and a Cdk6 binding domain that forms a bi-partite recognition site in conjunction with the PRR[55,68] (Fig. 1.3). *FBXO7* comprises 9 exons which can form three protein coding transcripts, termed isoforms 1-3. Isoform 1 is the most abundantly expressed and, at 522 amino acids, is the longest and contains all the aforementioned domains. However, isoforms 2 and 3 have alternative 5' exons and both lack the Ubl domain[55].

Fbxo7 is the fifth most abundant SCF in cultured cells[69] so it is unsurprising that the number of validated SCF^{Fbxo7} substrates is growing. The first to be identified was HURP, a mitotic spindle protein that is expressed during G2/M and regulates chromosome congression and alignment. Following HURP phosphorylation by cyclin B/Cdk1, SCF^{Fbxo7} ubiquitinates HURP via K48-linked chains to mark its proteasomal degradation[70]. As HURP is reported to be overexpressed in colon, breast and hepatocellular carcinomas, and is a negative regulator for p53[70,71], Fbxo7 may therefore function as a tumour suppressor in this context.

Several SCF^{Fbxo7} substrates are implicated in NFκB signalling and, in this context, Fbxo7 may have both tumour suppressive and oncogenic roles. cIAP and TRAF2 can both function as E3 ubiquitin ligases and, in response to TNF signalling, they interact to ubiquitinate RIP1 and promote the activation of the IKK signalosome to ultimately promote NFκB signalling and cell survival[72,73]. K63-linked ubiquitination by SCF^{Fbxo7} inhibits both cIAP and TRAF2 activity, thereby reducing NFκB signalling[74,75] and conferring a tumour suppressive role for Fbxo7. Similarly, SCF^{Fbxo7} ubiquitination of the NFκB transcriptional enhanceosome cofactor, UXT-V2, targets it for proteasomal degradation and also negatively regulates NFκB signalling[76]. In contrast, K63-linked ubiquitination of NRAGE by SCF^{Fbxo7} increases the formation of active NRAGE-TAK1-TAB1 complexes to instead promote NFκB signalling[77]. NRAGE has context-dependent roles in cancer and can promote progression of hepatocellular carcinoma[78] but suppresses proliferation, migration and invasion in human breast cancer cells[79]. Lastly, p105, a precursor to NFκB, is an apparent pseudo-substrate for SCF^{Fbxo7}. Whilst ubiquitination by SCF^{Fbxo7} stabilises p105 and enhances proliferation, an enzymatically inactive Fbxo7 mutant also stabilises p105, suggesting that the ubiquitination is spurious and the simple binding of Fbxo7 is sufficient to protect p105 from the proteolytic ubiquitination by other ligases[80]. Together, these studies characterise numerous cancer-relevant substrates for SCF^{Fbxo7}.

Other SCF^{Fbxo7} substrates have disease relevance beyond cancer. A high-throughput proteomic screen identified 338 potential substrates of SCF^{Fbxo7} and two additional substrates were validated from this list: Tomm20 and GSK3β[81]. Tomm20 is a mitochondrial translocase that induces mitophagy and is associated with Parkinson's disease[82–84]. SCF^{Fbxo7} promotes the mono- and di-ubiquitination of Tomm20 but, similarly to p105, Fbxo7 can also stabilise this substrate independently of SCF complex formation[81]. On the other hand, GSK3β is negatively regulated by SCF^{Fbxo7} K63-linked ubiquitination which, given the involvement of GSK3β in the Wnt signalling pathway and widespread roles in the cell cycle, proliferation, differentiation and apoptosis, could implicate Fbxo7 in diseases such as cancer, diabetes and Parkinson's disease[81,85]. Another substrate with disease relevance is the ribosomal protein RPL23 which acts as a sensor of cellular stress. SCF^{Fbxo7} ubiquitination of RPL23 results in its degradation and disrupts the RPL23-MDM2-p53 axis to prevent neuronal cell death, providing a link to neurodegenerative conditions[86]. Proteasome mis-regulation has been linked to human disease[87], and Fbxo7 has two known substrates that regulate proteasome activity. PSMA2 engages essential interactions between proteasomal subunits, and its ubiquitination by SCF^{Fbxo7} has been proposed to account for reduced proteasome assembly and activity in Fbxo7 KD cells[88]. Similarly, Fbxo7 interacts with the BAG6 complex which regulates proteasome activity, and ubiquitinates one of the subunits, GET3. This K27/29-linked polyubiquitination promotes the cytoplasmic localisation of BAG6 subunits and efficient assembly of the complex, to ultimately promote proteasome activity[89]. Indeed, reduced UPS activity and an accumulation of polyubiquitinated proteins were observed in the fibroblasts of a Parkinsonism-pyramidal syndrome patient with an $Fbxo7^{S123X}$ mutation[90], further highlighting the importance of Fbxo7 in this pathway and disease. In summary, the canonical substrates of SCF^{Fbxo7} are clearly involved in a plethora of biological pathways and diseases, yet the important functions of Fbxo7 also go beyond its ligase activity.

As F-box proteins are increasingly characterised a growing number of SCF-independent functions have been identified, and Fbxo7 is a prime example. The FP domain of Fbxo7 mediates both Fbxo7 homodimerisation and heterodimerisation with the proteasome regulator PI31, further implicating Fbxo7 in proteasome regulation. PI31 was first discovered as a proteasome inhibitor *in vitro*[91,92] but conflicting evidence published since suggests varied and context-specific roles in cells[68,93]. Fbxo7 shares homology with an orthologue in drosophila called nutcracker, and dimerization of nutcracker with DmPI31 was shown to stabilise DmPI31 and promote proteasome activity[94,95], suggesting a role for Fbxo7 in proteasome activation. Consistent with this, evidence suggests that Fbxo7 may also stabilise PI31 in mammalian cells but this was not associated with a change in proteasome activity[93]. PI31 is however reported to inhibit the production and maturation of the immunoproteasome, a variant of the constitutive proteasome, in mammals[96]. Interestingly, it has been shown that Fbxo7

can dimerise with PI31 in the presence of Skp1[97], suggesting that PI31 may have a role in modulating the activity of SCF^{Fbxo7}. Whilst the presence of this heterodimerization is clear and the crystal structure has been solved[97], the molecular outcome and impacts on the proteasome are still interesting areas for investigation.

Mutations in Fbxo7 have been associated with both sporadic Parkinson's disease and autosomal recessive early-onset Parkinsonism[68]. The precise mechanisms for this pathogenicity are unknown and likely multifaceted but partly reply upon a second non-canonical role for Fbxo7, in the removal of damaged mitochondria by mitophagy. In this context, the reduced membrane potential of damaged mitochondria is sensed by the mitochondrial kinase PINK1, stimulating its auto-phosphorylation and activation. In collaboration with PINK1, Fbxo7 facilitates the recruitment of the E3 ligase Parkin to form a complex at the mitochondrial membrane. Phosphorylation by PINK1 then activates Parkin E3 ligase activity and triggers the ubiquitination of mitochondrial proteins to initiate mitophagy (Fig. 1.3)[68,98]. There is strong evidence that this recruiting function of Fbxo7 is required for mitophagy and that some Parkinson's disease associated *FBXO7* mutations impair this pathway[98]. In addition, PINK1 has recently been identified as a substrate for ubiquitination by SCF^{Fbxo7}, which targets it for proteasomal degradation[99]. This is particularly interesting as it implies a role for Fbxo7, not just downstream of PINK1, but in regulating PINK1 itself, and hence may serve as a feedback mechanism to terminate the mitophagy response.

As highlighted by some of its ubiquitination substrates, Fbxo7 is also implicated in cancer, and displays oncogenic potential in a variety of cell types. Fbxo7 overexpression is observed in human tumour biopsies from colorectal adenocarcinoma and lung cancer[67], as well as human T cell lymphoma and anaplastic large cell lymphoma (ALCL) (unpublished). Moreover, its overexpression in fibroblasts triggered invasiveness and tumour formation in nude mice in a Cdk6-dependent manner[67]. This oncogenic capacity for Fbxo7 is restricted by p53, as an increase in Fbxo7 expression reduced proliferation of WT haematopoietic stem and progenitor cells (HSPCs) but increased proliferation in p53 null equivalents. In addition, when adoptively transferred into irradiated mice, these Fbxo7-expressing p53-null HSPCs significantly induced the formation of T cell lymphoma when compared to their WT-p53 counterparts[100].

This oncogenic potential may be attributed in part to the role of Fbxo7 as a cell cycle regulator. Fbxo7 directly interacts with and stabilises Cdk6, acting as a scaffold for the assembly of cyclin D3-Cdk6 complexes and thereby promoting S phase entry[67,101]. Interestingly, Fbxo7 can also bind and stabilise p27, a protein with opposing roles in cell cycle regulation[67]. Like Fbxo7, p27 can serve as an assembly factor for cyclin D-Cdk4/6 complexes and the two proteins can work in concert or independently in

this setting[67]. In contrast, p27 also acts to inhibit Cdk2 activity, thereby inhibiting cell cycle progression[67,102]. Thus, Fbxo7 can promote cell cycle progression, primarily through promoting Cdk6 activity, or inhibit it by stabilising p27.

Fbxo7 is particularly important in haematopoietic cells of both the myeloid and lymphoid lineage, and this may partly be attributed to the juxtaposing roles in cell cycle regulation. Both B cells and erythrocytes lacking Fbxo7 cycle faster *in vitro* due to reduced levels of p27[102,103]. They also show increased proliferation and impaired cellular differentiation in a hypomorphic Fbxo7-deficient mouse, in which the Fbxo7 locus is disrupted by a LacZ insertion ($Fbxo7^{LacZ/LacZ}$), and there are elevated pro-B and pro-erythroblast populations in this model[102]. This defective erythropoiesis causes anaemia, extramedullary haematopoiesis, and splenomegaly[103,104]. Interestingly, study of the transcription factors that regulate the human *FBXO7* promotor found enrichment of multiple transcription factor binding sites, many of which had roles in haematopoietic development[105]. In the context of T cells, there are opposing roles for Fbxo7 cell cycle regulation at different stages of T cell development[106]. The $Fbxo7^{LacZ/LacZ}$ mouse displayed thymic hypoplasia caused by reduced proliferation and increased apoptosis at the double negative (DN) stages of T cell development, and this was attributed to an observed lack of Cdk6 activity. The defective thymocytes resulted in fewer $CD4^+$ and $CD8^+$ T cells in the periphery but, paradoxically, these mutant T cells expanded more rapidly upon activation due to reduced levels of p27. There was a proportional increase in $CD4^+$ and $CD8^+$ effector T cells in both the blood and spleen, with an increase in IL-2, IFNγ (Th1 cytokines) and IL-10 (Th2/Treg cytokine), and $CD44^{High}$ $CD62L^{Low}$ markers, suggesting a skewed differentiation profile towards regulatory T cells and effector memory T cells respectively[104,106]. Interestingly, these mice are also more sensitive to morbidity following systemic infection with *Salmonella typhimurium*[104]. Surprisingly, the generation of a mouse with T-cell specific ablation of Fbxo7, reversed several of these phenotypes, including thymic atrophy, changes to T cell phenotypes, and sensitivity to *Salmonella* infection[104], suggesting that some phenotypes may be driven by T cell extrinsic factors. Despite this, there is substantial evidence for a pivotal role for Fbxo7 in cells of haematopoietic lineage, in particular through differentially regulating the cell cycle across different cell types and developmental stages.

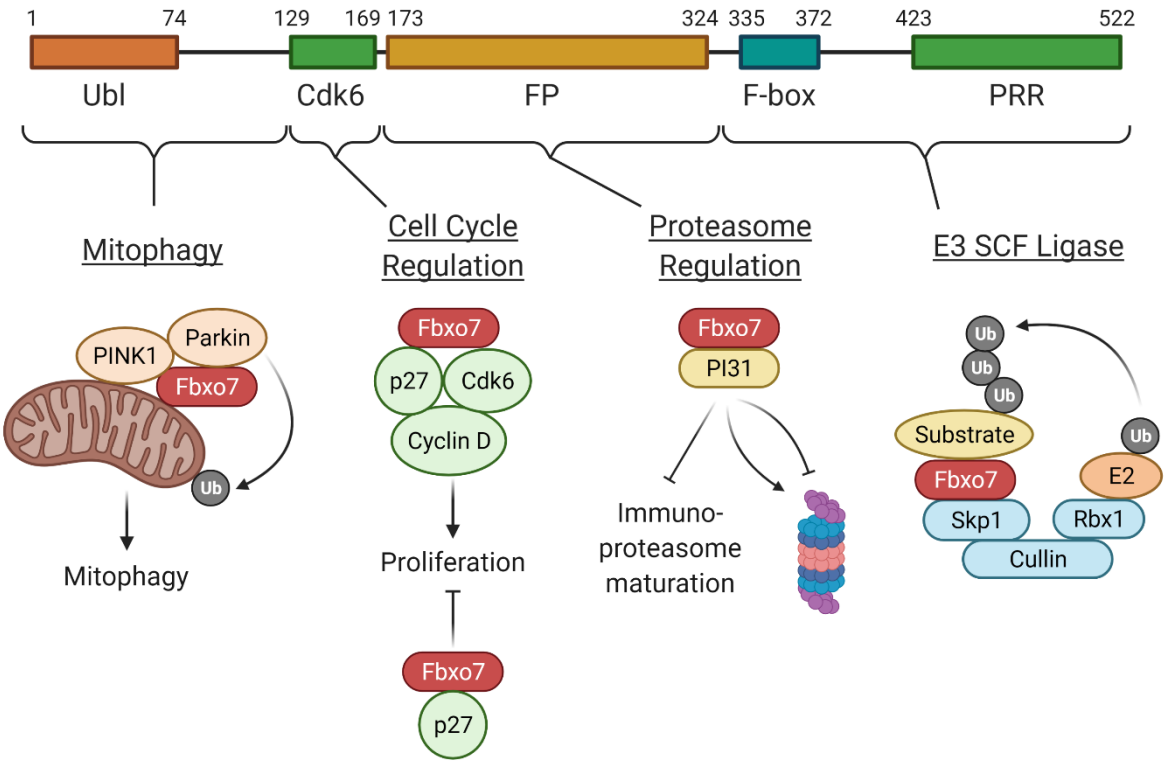

Figure 1.3: Domains and functions of Fbxo7.

Fbxo7 has a canonical function as an SCF E3 ligase, ubiquitinating numerous target proteins to alter their stability and activity, and this largely relies on the F-box domain for SCF complex formation, and the PRR for substrate binding. Other domains mediate SCF-independent functions for Fbxo7. Fbxo7 can promote mitophagy by acting in concert with PINK1 to recruit Parkin to damaged mitochondria, via the Fbxo7 Ubl domain. Activated Parkin ubiquitinates mitochondrial proteins to initiate mitophagy. Fbxo7 can stabilise Cdk6 via a bipartite binding site that involves the Cdk6-binding domain and PRR. Fbxo7 may paradoxically activate the cell cycle by promoting the assembly of cyclin D3-Cdk6 complexes or inhibit it by stabilising p27. The central FP domain mediates Fbxo7 homodimerisation, and heterodimerisation with PI31, conferring mixed roles for Fbxo7 in proteasome and immunoproteasome regulation.

Ubl: ubiquitin-like domain. Cdk6: Cdk6-binding domain. FP: Fbxo7-PI31 dimerisation domain. PRR: proline rich region.

1..2.2 Cdk6

Progression through the cell cycle is driven by the heterodimerisation of regulatory cyclins and catalytic cyclin dependent kinases (Cdks). For example, Cdk4 and Cdk6 form complexes with D-type cyclins (cyclin D1, D2, and D3) in G1 to enable progression into S phase. This is largely governed by the availability of cyclin D which increases in response to external mitogenic stimuli, enabling the integration of signals and coupling of tissue homeostasis to proliferation[107,108]. However, complex formation can also be restricted by the Cip/Kip family of pan-Cdk inhibitors (e.g. p27) and INK4 (e.g. $p16^{INK4A}$) proteins which are specific Cdk4/6 inhibitors that compete with cyclin D binding[109,110]. Nonetheless, once cyclin D-Cdk4/6 complexes are formed, they translocate into the nucleus where they are activated by phosphorylation by the Cdk-activating kinase complex (CAK). The Rb family of tumour suppressor proteins (Rb, p107 and p130) ordinarily sequester the E2F transcription factor but their phosphorylation by active cyclin D-Cdk4/6 complexes trigger the release of E2F and the subsequent expression of late G1/S phase genes such as cyclin E. This signals progression past the G1-S restriction point, allowing cyclin E-Cdk2 to hyper-phosphorylate Rb, further relieving E2F inhibition and promoting S phase entry[110]. In this manner, Cdk4/6 can play an important role in tumorigenesis and promote aberrant cell cycling through the inhibition of Rb tumour suppressor proteins.

Some Cdks have alternative functions beyond the cell cycle, such as Cdk6 which operates distinctly from its close homologue Cdk4, as a transcriptional regulator largely independently of kinase activity (reviewed in [110]). Through this action, cyclin D-Cdk6 can interact with STAT3 to promote the transcription of the $p16^{INK4A}$ inhibitor in an autoregulatory feedback mechanism[111,112]. However, many of these transcriptional activities confer an oncogenic role for Cdk6, particularly in haematopoietic lineages. Cdk6 can bind, alongside c-Jun, to induce VEGF-A expression and promote angiogenesis[111,112], and act as a transcriptional inhibitor of EGR1 to enable HSPCs to exit quiescence and promote proliferation of leukemic stem cells[113,114]. Cdk6 can also promote tumour formation in haematopoietic cells by promoting the expression of p53 antagonists PRMT5, PPMID and MDM4 to induce a transcriptional programme that counteracts the p53 response to oncogenic stimuli[115]. Cells lacking Cdk6 activity therefore have a selective pressure to mutate p53 during transformation, leading to an emergence of p53 mutations in cancers with low Cdk6[115]. Lastly, Cdk6 is also a positive regulator of inflammatory cytokines via NFκB signalling[116,117] and has been shown to act downstream of Notch signalling to facilitate thymocyte development and tumorigenesis in T cells[118–120]. In short, there is growing appreciation for Cdk6 as a transcriptional regulator that can function in either a tumour promoting or suppressive manner depending on the cellular context.

There have been numerous studies using Cdk6 mouse models and these have unveiled interesting requirements for Cdk6 in different settings, particularly in the haematopoietic system. Cdk6 is

expressed throughout mammalian tissues but most abundantly so in lymphoid organs[121]. Two different strains of Cdk6$^{-/-}$ mice displayed normal proliferation in most cell types but showed thymic hypoplasia and reduced cellularity in the spleen[119,122], characteristics reminiscent of the Fbxo7 hypomorphic mouse. This was attributed to a block in T cell development[119,122] as Cdk6 kinase activity is required downstream of Notch signalling as mentioned above[118,119]. Alongside the lymphoid phenotypes, these mice also exhibited erythroid defects including anaemia, though evidence of deficiencies in common haematopoietic precursors is contradictory between the two models[118,119,122]. Interestingly, it was only when Cdk4 was also deleted that severe anaemia resulted in embryonic lethality but, even then, organogenesis and proliferation was still normal in most cell types[119]. Together these studies show that, whilst Cdk6 is required for differentiation and proliferation in haematopoietic cells, there may be a compensatory mechanism for Cdk4/6 in the cell cycle in most other tissues.

Dysregulation or overexpression of Cdk6 is frequently observed in cancer and it is therefore an attractive therapeutic target. The first generation of Cdk inhibitors showed pan-Cdk activity and were abandoned due to poor efficacy and high toxicity, but specific Cdk4/6 inhibitors (palbociclib, ribociclib, and abemaciclib) have showed greater promise[123]. Palbociclib is approved by the FDA for the treatment of advanced hormone receptor-positive breast cancer and shows promise in clinical trials for other indications including haematopoietic cancers, lung cancer and colorectal cancer[124]. The small molecule kinase inhibitor primarily works by preventing the phosphorylation of Rb, resulting in G1 arrest and reduced proliferation. However, additional activities have been observed after prolonged exposure, including increased tumour neoantigen presentation and induction of autophagy[107]. Interestingly, Cdk4/6 inhibitors also demonstrate direct effects on specific lymphocyte populations that may be present in the tumour microenvironment. Specifically, Cdk4/6 inhibition enhances CD4^{+} T cell activity *in vitro*[125] and preferentially suppresses proliferation of Treg cells[126], possibly potentiating an anti-tumour immune response. The roles for Cdk6 in both cell cycle and transcriptional regulation justify its title as a central node in oncogenesis and tumour maintenance and make it an attractive and viable target for therapeutic intervention.

1..3 DDB1-CUL4 associated factors (DCAFs)

Like FBPs in CRL1 complexes, DCAFs (also termed DDB1-binding/WD40 domain (DWD) or CUL4–DDB1-associated WDR (CDW) proteins) are the substrate-recruiting subunits for CRL4 E3 ubiquitin ligases (Fig. 1.2). Whilst less extensively studied than their FBP counterparts, there are estimated to be 60-90 DCAFs encoded in the human genome[38,39,127], implying a large and significant protein family. Both DCAFs and their DDB1 adaptor are WD40-containing proteins, with DDB1 comprising three β-propellers each of seven WD40 repeats. DCAFs contain one to three copies of a common WDxR motif within their WD40 repeats that is believed to mediate binding to DDB1[38,128], however, some DCAF proteins lack this conserved motif so other modes of binding must exist[127].

1..3.1 CRBN

Study of one DCAF, cereblon (CRBN), has exploded since first reported in 2004[129] due to its crucial role in the efficacy of immunomodulatory drugs (IMiDs). CRBN is an evolutionary conserved protein of 442 amino acids in humans and is comprised of three domains (Fig. 1.4): an N-terminal seven-stranded β-sheet (NTD), a central α-helical bundle domain (HBD), and a C-terminal domain of eight β-sheets (also known as Cereblon domain of Unknown activity, binding cellular Ligands and Thalidomide (CULT)). Part of the NTD and HBD together resemble the structure of ATP-dependent Lon proteases (LON-like domain, LLD), with a helical insertion. Surprisingly, CRBN binding to DDB1 is not via a WDxR motif, but instead this helical insertion at residues 188 - 248, representing a novel mode of DDB1 binding[130,131].

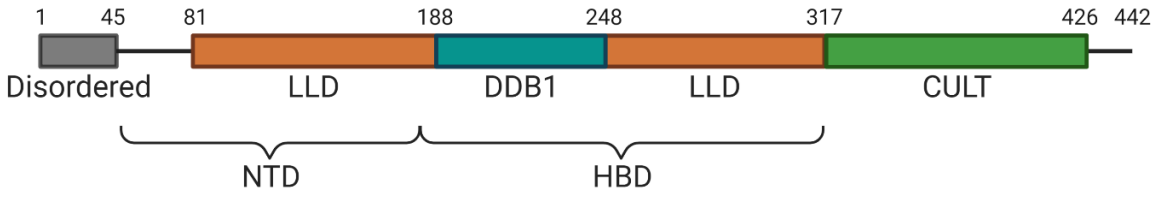

Figure 1.4: Domains of CRBN.

The CRBN protein can be divided into distinct domains. The NTD and HBD domains of CRBN together form a LLD that contains an insertion of α-helices through which the DDB1 adaptor protein binds. The C-terminal CULT domain mediates binding to several CRBN ligands and immunomodulatory drugs.

NTD: N-terminal domain. HBD: helical bundle domain. CULT: Cereblon domain of Unknown activity, binding cellular Ligands and Thalidomide. LLD: Lon-like domain. DDB1: DDB1-binding domain.

Several substrates for $CRL4^{CRBN}$ have been identified that are involved in neuronal and brain function, particularly intellectual disability (ID). Founding work in CRBN function discovered the interaction of the large conductance Ca^{2+}- and voltage-activated K^+ (BK) channels and voltage-gated Cl^- (CLC-2) channels with CRBN[132,133]. Both have since been validated as $CRL4^{CRBN}$ substrates, with CLC-1 and CLC-2 undergoing typical polyubiquitination and degradation[134,135]. Meanwhile, polyubiquitination of the BK channel retains it in the endoplasmic reticulum, a step found to be important in preventing epileptogenesis[136]. Interestingly, a subsequent study revealed that ID-associated CRBN mutations disrupt the CRBN-BK interaction and instead both CRBN and BK are directed to SCF^{Fbxo7} for polyubiquitination and proteasomal degradation[137]. Another $CRL4^{CRBN}$ substrate associated with ID is MEIS2[130], a transcription factor required for many aspects of human development[138,139], including proper limb formation. MEIS2 interacts with CRBN via the CULT domain, and ubiquitination promotes degradation[130].

Regulation of these substrates is proposed to contribute to the role of CRBN in brain function. CRBN is widely expressed in the brain[133,140] where it has an evolutionary conserved role in insects, mammals, and zebrafish[141,142]. Although germline and forebrain-specific CRBN deficient mice show no gross abnormality, they do display lower fear conditioning[143], implicating CRBN in learning. This was corroborated by a mouse model with a neuron-specific deletion of CRBN which exhibits cognitive defects including impaired learning and memory[137]. Interestingly, this was specifically linked to misregulation of the BK channel, as the phenotype was partially rescued by BK activation[137,141]. In humans, two CRBN mutations (an R419X truncation[129] and C391R missense mutation[144]) have been identified in families presenting with autosomal-recessive non-syndromic intellectual disability, further implicating CRBN in brain function and human neurological disorders.

Beyond brain function, CRBN is also implicated in metabolism. Glutamine synthetase functions in glutamine synthesis, and glutamate and ammonia detoxification, and is subject to negative regulation by $CRL4^{CRBN}$. Specifically, glutamine induces the acetylation of glutamine synthetase and this signals the ubiquitination and degradation by $CRL4^{CRBN}$, providing an example of acetyl-degron recognition by the CULT domain of CRBN[145]. In addition, CRBN modulates AMP-activated protein kinase (AMPK), a master regulator of energy metabolism that is critically involved in energy sensing. The mode of CRBN-dependent regulation is still debated, with reports that CRBN competitively binds the AMPKα subunit to inhibit complex formation[146], or that $CRL4^{CRBN}$ promotes AMPKα and AMPKγ polyubiquitination and degradation[147,148]. Nonetheless, CRBN-deficient mice have elevated active AMPK in the liver and show reduced weight gain compared to wildtype mice when fed a high-fat diet[149], so the physiological impact of this metabolic regulation is evident.

Like many CRL substrate receptors, CRBN also has ubiquitin-independent functions. CRBN is reported to act as a chaperone to mediate proper folding and maturation of two transmembrane proteins, CD147 and MCT1[150]. CD147 is a glycoprotein involved in a plethora of biological processes including proliferation and survival, and it acts as an essential chaperone for the lactate transporter MCT1. This chaperone-like function for CRBN promotes protein localisation to the membrane and the assembly of active CD147-MCT1 complexes, essential for cell homeostasis and metabolic regulation. In addition, CRBN can negatively regulate TLR4 signalling independently of the CRL^{CRBN} complex. TLR signalling activates TRAF6 to function as an E3 ubiquitin ligase which ubiquitinates both itself and downstream regulatory subunits to ultimately promote NFκB activation. CRBN interacts with TRAF6 to inhibit the ubiquitination cascade, prevent NFκB activation and ultimately reduce the pro-inflammatory response[151]. Indeed $CRBN^{-/-}$ mice show elevated pro-inflammatory cytokines and decreased survival in response to LPS challenge[151], implicating CRBN in innate immune modulation via TLR signalling.

1..3.2 Immunomodulatory drugs (IMiDs) in multiple myeloma

IMiDs are a class of drugs that are analogues of thalidomide, a synthetic glutamic acid derivative. Thalidomide was developed in the 1950s when it was prescribed as an antiemetic during pregnancy, with the devastating outcome of causing severe birth defects due to its teratogenic side effects. Despite its clinical withdrawal, IMiD research continued, and thalidomide was later discovered to be an effective treatment for multiple myeloma (MM)[152]. MM is a B cell malignancy typified by the aberrant expansion of plasma cells in the bone marrow. It is the second most common haematological cancer, accounting for 10%[153], with an estimated 176,000 cases worldwide in 2020[154]. Historically, there were limited treatment options for MM and the repurposing of thalidomide, amongst other advances, have improved the estimated 5-year survival in the UK to 52.3%[155]. IMiDs are now the mainstay for standard MM treatment regimens, with thalidomide analogue lenalidomide widely prescribed, and pomalidomide used for relapsed/refractory disease[156]. The next generation of this drug class (now renamed as Cereblon E3 ligase-modulating drugs (CELMoDs)) show efficacy in lenalidomide and pomalidomide-resistant patients, and in other haematological malignancies such as acute myeloid leukaemia (AML) and diffuse large B cell lymphoma (DLBCL)[157]. Crucially, IMiDs have revolutionised treatment options for MM patients and continue to be the basis for successive generations of therapeutics.

Soon after the approval of IMiDs for MM, CRBN was identified as their primary target, responsible for both the teratogenicity of thalidomide[158] and the anti-MM properties[159] (Fig. 1.5). Two groups independently discovered that $CRL4^{CRBN}$ ubiquitinates two Ikaros family transcription factors for

degradation in the presence of IMiDs[160,161]. Ikaros (IKZF1) and Aiolos (IKZF3) play a vital role in B cell maturation and MM cell survival through the modulation of downstream targets *IRF4* and *MYC*[162,163]. Since this discovery of IKZF1 and IKZF3 in 2014, a host of other IMiD-dependent CRBN neo-substrates have been identified. CK1α is known to promote MM pathogenesis through the sustained activation of p53 and signalling pathways such as PI3K/AKT and NFκB[164,165], and is a lenalidomide-specific neo-substrate for $CRL4^{CRBN}$ [165]. Importantly, this also promotes lenalidomide efficacy in a subset of myelodysplastic syndrome[166] and exemplifies how the subtle differences in IMiD structure can produce significant biological effects. Another such example is the pomalidomide-specific ubiquitination of ARID2 by $CRL4^{CRBN}$ [167]. ARID2 is a subunit of the chromatin remodelling complex PBAF and is involved in the transcriptional regulation of *MYC*[167]. This may be a contributing factor to the increased potency of pomalidomide over lenalidomide. Meanwhile, other $CRL4^{CRBN}$ neo-substrates are responsible for the undesirable side-effects of IMiDs. SALL4 is a transcription factor critical in limb development and is ubiquitinated for degradation by $CRL4^{CRBN}$ in the presence of thalidomide[168], hence likely contributing to the teratogenic effects. Moreover, IMiD binding can disrupt the recognition of physiological CRBN substrates such as MEIS2[130,145,150], another key protein in human development.

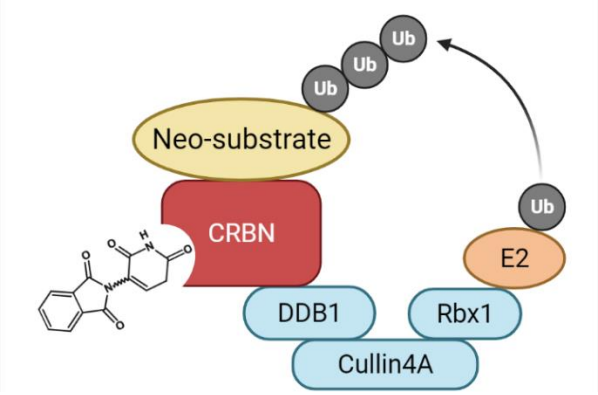

Figure 1.5: Immunomodulatory drugs promote neo-substrate recognition by $CRL4^{CRBN}$. The binding of IMiDs such as thalidomide (shown) to the CULT domain of CRBN modifies substrate recognition to promote the ubiquitination of neo-substrates such as IKZF1 and IKZF3 by $CRL4^{CRBN}$.

As the name suggests, IMiDs also carry immunomodulatory effects and augment both the innate and adaptive anti-tumour immune responses to MM cells. MM induces immune paresis through the secretion of immunosuppressive TGF-β, IL-10, IL-6, and VEGF. Together these inhibit the function of T cells and natural killer (NK) cells and impair antigen presentation by dendritic cells (DCs)[169,170]. Ultimately, this compromised immune signalling enables MM cell survival and immune evasion. As IMiDs are frequently used in combination therapies, including with the anti-inflammatory drug dexamethasone, it has been difficult to dissect their immunomodulatory effects in patients.

Nonetheless, IMiDs have been shown to promote T cell activation by both enhancing antigen presentation by DCs[171], and independently triggering the CD28 co-stimulatory marker on T cells to abrogate the requirement for a co-stimulatory signal entirely[172]. In addition, IMiDs enhance the activity of the transcription factor AP-1[173], a key driver for IL-2 production in T cells. IL-2 induces T cell proliferation and activation, and both IL-2 and T cell proliferation are elevated upon IMiD treatment[170,174]. Interestingly, T cells demonstrate a skewed ratio of T effector subsets Th1 and Th2 in response to IMiD treatment[175], with increased secretion of Th1 cytokines IL-2 and IFN-γ and a decrease in Th2/Treg cytokines IL-4 and IL-10[169]. The elevated IL-2 also promotes the activation of NK cells of the innate immune system, which have a cytotoxic function[176,177]. Lenalidomide increases NK cell proliferation, cytotoxicity and antibody-dependent cellular cytotoxicity (ADCC) *in vitro*[174,176,177]. Alongside immune evasion, MM cells also require an interaction with bone marrow stromal cells (BMSCs) to promote their survival and IMiDs disrupt this by downregulating the expression of cell surface adhesion molecules, partially through inhibiting TNFα production[170]. The secretion of VEGF and β-FGF from MM cells and BMSCs is also downregulated in response to IMiD treatment, to exert anti-angiogenic effects[169]. Overall, the impact of IMiDs on tumour immune surveillance and the microenvironment are multifaceted and ongoing research is vital to understand drug combinations to give optimal anti-tumour effects.

Whilst IMiDs have vastly improved MM patient survival, IMiD resistance prevails in a subset of patients. Early in IMiD research, it was discovered that CRBN expression is required for IMiD efficacy, and CRBN depletion led to MM cell resistance to both lenalidomide and pomalidomide[159]. Importantly, high CRBN expression is associated with improved clinical outcomes to IMiDs[159], whilst mutations in *CRBN* can contribute to IMiD resistance[178]. Recently, the RUNX transcription factors were discovered to bind IKZF1 and IKZF3 and protect them from CRBN-mediated degradation, thus IMiD resistance may be overcome by combination with RUNX inhibitors *in vitro*[179]. Finally, it has been proposed that antioxidative capacity may be used as a biomarker for IMiD sensitivity as lower antioxidative capacity correlates with IMiD sensitivity in MM patients[180]. Plasma cells generate intracellular reactive oxygen species (ROS) through disulphide bond formation in immunoglobulin production and are sensitive to drugs that elevate this ROS or target antioxidative pathways. A study found that IMiDs inhibit thioredoxin reductase, an enzyme involved in hydrogen peroxide decomposition, in a CRBN-dependent manner, and this increases intracellular ROS[181]. MM cells with a lower oxidative capacity are more vulnerable to the oxidative stress-induced cytotoxic effect of IMiDs, whilst those with increased capacity may emerge as IMiD resistant[180,181]. The IMiD resistance pathways are not yet completely understood, though it is clear that CRBN status is a critical factor in IMiD sensitivity.

Metabolism

1..4 Cellular metabolic pathways

Metabolic pathways are complex and interlinked, and the flow of metabolites between pathways can have a profound impact on cellular functions, affecting processes such as proliferation, differentiation, and survival. Metabolism can be subdivided into catabolic reactions that breakdown molecules for energy production and anabolic reactions that generate molecules for biosynthesis, and the balance between these two states is precisely orchestrated to provide energy homeostasis for the cell (Fig. 1.6).

Glucose is one of the most favourably catabolised molecules in most cells[182] and proper regulation of central carbon metabolism is vital to meet both the bioenergetic and biosynthetic demands of a cell. Glucose import can occur via two sodium glucose transporters (SGLTs) and 14 GLUT proteins, which vary in their affinity to glucose and expression in different cell types or developmental stages[183]. Following glucose uptake, it is rapidly phosphorylated to glucose-6-phosphate (G6P), ensuring retention within the cell[184]. There are several fates for G6P, one of which being conversion to glycogen to provide a storage reserve for times of energy deficit, such as starvation and exercise, and this primarily occurs within the liver and skeletal muscle[185]. G6P can also be catabolised to pyruvate via glycolysis. Pyruvate has two potential fates and is typically converted into lactate under anaerobic conditions or, in the presence of oxygen, is transported into the mitochondria where it forms acetyl CoA and feeds the tricarboxylic acid (TCA) cycle. The TCA cycle is essential for the production of NADH and $FADH_2$, which act as reducing agents for oxidative phosphorylation (OXPHOS) within the mitochondria. During OXPHOS, the electron transport chain utilises NADH and $FADH_2$ oxidation to generate an electrochemical proton gradient across the inner mitochondrial membrane, and ATP synthase uses this to ultimately generate ATP from ADP and phosphate. This process also generates ROS due to inefficient electron transfer. This central carbon metabolism is the major source of cellular energy via ATP.[182,186–189]

However, glucose does not always yield pyruvate, and glycolytic intermediates can feed into several anabolic pathways. Another fate for G6P is redirection into the pentose phosphate pathway (PPP) [186–188,190], where it is decarboxylated through a series of redox reactions to produce ribose-5-phosphate (R5P) and generate NADPH. This branch is termed the oxidative PPP and is a major source of NADPH, thus pivotal in maintaining cellular redox state. In the non-oxidative PPP, enzymes TKT and TALDO transfer carbon units from pentoses (5-carbon sugars) to generate fructose-6-phosphate (F6P) and glyceraldehyde-3-phosphate (G3P) that can feed back into glycolysis. Similarly, the reverse reactions can redirect F6P and G3P into the non-oxidative PPP to recruit additional glycolytic intermediates. The PPP enzymes are subject to allosteric regulation to enable cells to adapt to changing metabolic

demands. For example, the first enzyme in the oxidative PPP, G6P dehydrogenase (G6PD), is negatively regulated by NADPH to adjust oxidative PPP flux according to cellular redox state[191]. Alongside ensuring redox homeostasis, the PPP is pivotal for nucleotide biosynthesis, as R5P is converted to phosphoribosyl pyrophosphate (PRPP) which forms the backbone for both purine and pyrimidine rings[187,190,192]. Nucleotide biosynthesis, amongst other physiological processes including amino acid homeostasis and glutathione generation, also requires 1-carbon (1C) units derived from the folate and methionine cycles which are collectively termed 1C metabolism. These cycles redistribute carbon groups from glycine, methionine or serine (imported or synthesised *de novo* from 3-phosphoglutarate (3PG) in the serine synthesis pathway) to various acceptor molecules for biosynthesis[192,193]. Through pathways such as the PPP and serine synthesis, glycolytic intermediates can be redirected to generate essential biosynthetic molecules such as nucleotides and amino acids and play a role in maintaining the redox state of a cell.

In addition to glucose, cells rely on other fuel sources to feed metabolic pathways. Glutamine is widely catabolised by glutaminolysis and provides α-ketoglutarate (αKG) to enter the TCA cycle[182,187]. Glutamine uptake has been demonstrated as essential for lipid synthesis, as citrate from the TCA cycle is converted back to acetyl-CoA in the cytosol where it utilised for fatty acid synthesis (FAS)[194]. Conversely, fatty acids may be catabolised via fatty acid oxidation (FAO) as an alternative source of acetyl-CoA. Another amino acid central to cellular metabolism is arginine[195]. Arginine is a non-essential amino acid which can be imported or synthesised from citrulline and aspartate in the urea cycle. It is one of the most versatile amino acids and can be catabolised to serve as a precursor to several metabolites including polyamines and nitric oxide[195]. There are therefore several other crucial metabolic pathways that can be used to complement central glucose metabolism.

The metabolic pathways employed by a cell are driven by its energetic and biosynthetic requirements. ATP is produced by both glycolysis and OXPHOS, but at a ratio of 2 molecules in glycolysis and up to 36 molecules in OXPHOS[182]. This makes OXPHOS far more efficient in terms of ATP production. Nonetheless, aerobic glycolysis may be favoured in actively proliferating cells, as its intermediates supply pathways for macromolecular synthesis, including nucleotides and amino acids as described above.

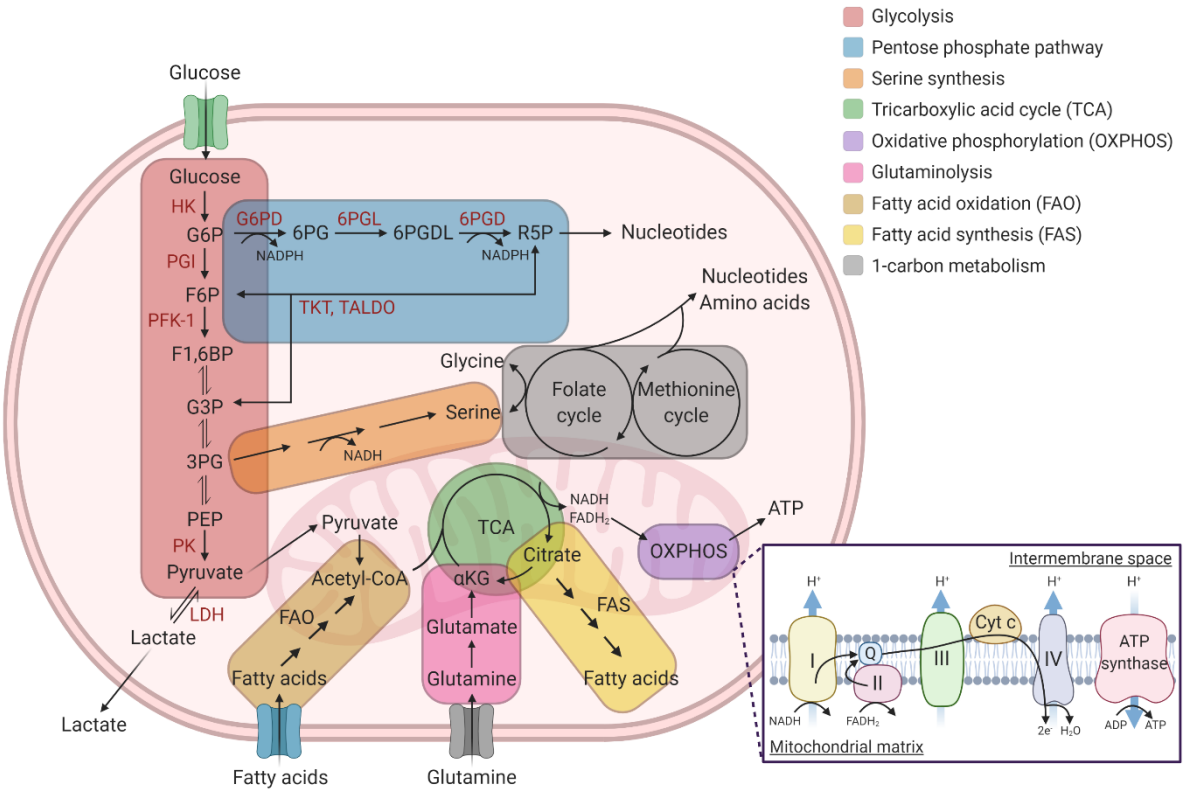

Figure 1.6: An overview of central cellular metabolic pathways.

The metabolic pathways employed by a cell are driven by its energetic and biosynthetic requirements. Glucose is a primary energy source and its catabolism via glycolysis (red), the tricarboxylic acid cycle (green) and oxidative phosphorylation (purple) generates essential ATP for the cell. However, the intermediates generated in glycolysis can also feed into biosynthetic pathways such as the pentose phosphate pathway (blue) and serine synthesis pathway (orange) which, alongside 1-carbon metabolism (grey), ultimately yield nucleotides, amino acids and reducing agents. Similarly, the TCA cycle intermediate citrate can be used for fatty acid synthesis (yellow). Other important fuel sources can feed into the TCA cycle, including fatty acids via fatty acid oxidation (brown), and glutamine via glutaminolysis (pink). Metabolites are in black, metabolic enzymes are in red.

G6P: Glucose 6-phosphate. F6P: Fructose 6-phosphate. F1,6BP: Fructose 1,6-bisphosphate. G3P: Glyceraldehyde 3-phosphate. 3PG: 3-phosphoglycerate. PEP: Phosphoenolpyruvate. 6PG: 6-phosphogluconic acid. 6PGDL: 6-phoshogluconolactone. R5P: Ribose 5-phosphate. αKG: α-Ketoglutarate. HK: Hexokinase. PGI: Phosphoglucose isomerase. PFK-1: Phosphofructokinase-1. PK: Pyruvate kinase. LDH: Lactate dehydrogenase. G6PD: Glucose-6-phosphate dehydrogenase. 6-PGL: Phosphogluconolactonase. 6PGD: 6-phosphogluconate dehydrogenase. TKT: Transketolase. TALDO: Transaldolase. TCA cycle: Tricarboxylic acid cycle. OXPHOS: Oxidative phosphorylation. FAO: Fatty acid oxidation. FAS: Fatty acid synthesis.

1..5 T cell metabolism

The immune system functions to neutralise disease-causing pathogens or aberrant cells such as cancer, whilst maintaining the integrity of healthy host cells. It can be broadly divided into two arms: the innate and adaptive immune systems. The innate response is the rapid first line of defence and is characterised by broad specificity towards common pathogen features. In contrast, the adaptive immune system comprises a cellular response to specific antigens and retains immunological memory to mount a rapid response to secondary infections. The major cell types of the adaptive immune system are T cells and B cells, which are effector cells in cell-mediated and humoral immunity respectively.

The life cycle of a T cell progresses from thymic progenitors to mature, activated T cells that differentiate to several distinct effector T cell subsets, or quiescent memory T cells that elicit an efficient recall response. The energy requirements of the cell changes dramatically during these stages and thus a dynamic metabolic reprogramming occurs (Fig. 1.7). In fact, immunometabolism is tightly linked to T cell function, and disrupting certain pathways can block T cell development or skew differentiation profiles.

1..5.1 Metabolism in T cell development

T cell development is a process whereby common lymphoid progenitors from the bone marrow undergo sequential maturation and selection steps in distinct regions of the thymus[196] to produce mature naïve T cells. The early thymic progenitors that colonise the thymus lack a T cell receptor (TCR) and mature T cell markers such as CD4 or CD8, thus are called double negative (DN) thymocytes. These DN thymocytes may be further subdivided into four stages based on expression of the adhesion molecule CD44, and the IL-2 receptor α-chain CD25: DN1 ($CD44^+CD25^-$), DN2 ($CD44^+CD25^+$), DN3 ($CD44^-CD25^+$) and DN4 ($CD44^-CD25^-$)[197]. Rearrangement of the TCR β-chain locus occurs as cells transition through DN2 to DN3, and the functionality of this TCRβ chain is tested via the β-selection checkpoint in DN3[198,199]. This β-chain pairs with the surrogate pre-Tα chain to produce a pre-TCR[200] which, alongside Notch signalling, enables progression into DN4 where the cells undergo rapid proliferation[201,202]. Notch signalling drives progression through the DN stages and is important for β-selection. Importantly, Notch promotes GLUT1 upregulation and glycolysis in pre-T cells via activation of the PI3K/AKT pathway, and this metabolic regulation is essential for the survival of pre-T cells through the β-selection checkpoint[203]. AKT knock-out causes a DN3 block in thymocyte development, with pre-T cells showing reduced glucose uptake and increased apoptosis, due in part to the impaired

glycolytic metabolism[204]. This illustrates the importance of the PI3K/AKT pathway for the metabolic reprogramming required for T cell development.

Following β-selection, cells upregulate CD4 and CD8 expression to become double positive (DP) cells which rearrange their TCR α-chain and maintain dependence on glycolysis. PTEN is a major negative regulator of PI3K, and it impairs glycolysis to cause developmental defects in thymocytes, as mice with elevated PTEN expression present with fewer DP cells that have reduced proliferative capacity[205], further demonstrating the reliance on PI3K/AKT signalling. These DP cells next undergo vital rounds of positive and negative selection of the mature αβTCR to ensure correct affinity for antigen/MHC complexes and remove strongly self-reactive T cells[206]. Many cells will undergo apoptosis at this stage, but those that survive downregulate either co-receptor to yield naïve CD4 or CD8 single positive T cells.

Whilst most T cells express an αβTCR, up to 5% of T cells have a distinct γδ chain[207]. γ- and δ-chain rearrangement occurs alongside β-chain rearrangement in DN2 and the differentiation between T cells expressing an αβ or γδ TCR occurs in DN3, driven partly by metabolism. mTOR signalling drives many metabolic pathways and is transmitted via mTORC1 and mTORC2 complexes[208]. Loss of mTORC1 signalling in thymocytes impairs glycolysis and instead promotes OXPHOS, resulting in elevated ROS in DN3 cells. This profile drives a preference for γδ T cell generation, thus coupling cellular metabolic status to the αβ / γδ ratio and determination of cell fate[209].

1..5.2 Metabolic reprogramming upon T cell activation

Naïve $CD4^+$ or $CD8^+$ T cells circulate in the periphery, screening for their cognate antigen displayed on a major histocompatibility complex (MHC) by an antigen presenting cell (APC). During this process, T cell survival and homeostasis is maintained by transient interactions between TCR and MHC, and cytokines such as IL-7[210,211]. Metabolites play a vital role in this homeostasis, with adenosine import shown to maintain IL-7R expression to promote the naïve T cell state[212]. Throughout immune surveillance, T cells maintain a low basal metabolism whereby they uptake minimal glucose to fuel a reliance on the TCA cycle and OXPHOS[213,214]. Metabolism is restrained to this level in newly circulating naïve T cells through reduced mTORC1 activity and c-Myc expression, two positive regulators of glycolysis[215–217].

T cell activation occurs when a TCR engages with its cognate peptide antigen presented on MHC. Sufficient TCR signalling results in a clustering of TCRs at the T cell/APC interface, and generation of an immunological synapse[218]. A second co-stimulatory signal is required to elicit a full T cell response

as opposed to anergy, and this is provided by B7 on the APC surface binding to CD28 on the T cell[219]. Whilst these two signals are sufficient to mount a T cell response, a third cytokine priming signal may polarise T cell differentiation and promote specific effector functions[219]. Together these signals initiate a proliferative burst called clonal expansion that amplifies the T cell response and requires extensive metabolic reprogramming.

T cell activation is characterised by a predominantly glycolytic programme that is upregulated within 6 hours of T cell activation, independently of CD28 co-stimulation[214]. This early TCR signalling activates pyruvate dehydrogenase kinase (PDK1) which subsequently inhibits pyruvate dehydrogenase (PDH) to prevent pyruvate conversion to acetyl-CoA and instead drive lactate production[214,220]. Maintenance of this aerobic glycolytic state through late-stage T cell activation requires transcriptional and translational remodelling. The upregulation of glycolysis is largely directed through the PI3K/AKT signalling pathway which is activated upon TCR engagement and co-stimulation[221–223]. mTOR is activated downstream of this pathway and PDK1, and promotes glycolysis via activation of the transcription factors c-Myc and HIF1α[216,224,225]. The importance of mTOR in T cell activation has been demonstrated by its inhibition by rapamycin, which is strongly immunosuppressive to T cells[226]. Importantly, both c-Myc and HIF1α induce the upregulation of the glucose transporter GLUT1, glycolytic enzymes such as HK2, and lactate dehydrogenase (LDH), to increase glucose uptake and glycolysis that supports proliferation of activated T cells[216,223,224,227–229]. Several biosynthetic pathways stemming from glycolysis are also upregulated upon T cell activation, such as the PPP and serine synthesis[216,230], and extracellular serine is also critically required for the generation of 1C units, nucleotide synthesis and proliferation of activated T cells[230]. The metabolism of other amino acids also increases with T cell activation, with leucine[231], arginine[232] and cysteine[233] all required for T cell metabolic fitness. Moreover, glutamine is of particular importance as it is required to replenish TCA cycle intermediates in a process called anaplerosis[234,235] and provide nitrogen for amino acid and nucleotide biosynthesis, and glutamine depletion impairs T cell proliferation *in vitro*[236,237]. Both c-Myc and ERK play a vital role in stimulating glutaminolysis through the upregulation of enzymes such as glutaminase[237,238]. Together, PI3K/AKT and ERK/MAPK are two major signalling cascades induced by T cell activation and these are integrated to confer a distinct metabolic programme in activated T cells.

Despite the shift to glycolysis, there remains an important role for mitochondrial metabolism in activated T cells, as OXPHOS is elevated following TCR engagement to sustain activation and proliferation[239–241]. Critically, the generation of mitochondrial ROS provides an additional activation signal to T cells by activating NFAT and promoting IL-2 production[239], and treatment with antioxidants to dampen this blocks T cell proliferation in response to infection[242]. Nonetheless, a deleterious threshold of ROS still exists in T cells, and glutathione is required to buffer the elevated ROS from

OXPHOS. Quantitative proteomics revealed that T cell activation induced proteome remodelling and mitochondrial biogenesis to produce specialised mitochondria with elevated 1C metabolism that were essential for glutathione synthesis[243]. Inhibition by SHMT2 depletion caused increased DNA damage and reduced T cell survival[243], highlighting the importance of mitochondrial 1C metabolism and antioxidant capacity in T cell activation and survival.

1..5.3 Metabolic control of T cell differentiation

Nutrient availability and the predominant metabolic pathways govern T cell differentiation and function, and T cell subsets display distinct metabolic profiles (Fig. 1.7). Mature, activated and differentiated T cells may fall into several categories including cytotoxic T cells, T helper cells, regulatory T cells, and memory T cells.

The largest subsets of $CD4^+$ T helper cells are pro-inflammatory Th1, Th2 and Th17 cells, and these are amongst the best studied in terms of metabolic influence. T helper cells all show a predominance of glycolysis that is largely driven by mTOR signalling[225,244–246]. Th1 cells function to activate cell-mediated immunity and are induced by the presence of IL-22 and IFNy, which promote expression of the T-bet transcription factor to drive Th1 differentiation[225,247]. Activated mTORC1 in Th1 cells phosphorylates T-bet to enhance IFNy production and is required for Th1 differentiation[248]. Importantly, the production of IFNy also relies on specific metabolic regulation as its expression can be controlled by two metabolic enzymes. GAPDH and LDH can both bind the 3' UTR of IFNy mRNA to sequester it from translation, and thus mediate cytokine production[214,241]. It is only upon upregulation of aerobic glycolysis that these enzymes release the mRNA to enable efficient IFNy production[214,241]. Moreover, LDH exerts epigenetic control over IFNy and is required for histone acetylation of the IFNy locus to promote its production in T cells[249]. In addition to glycolysis, Th1 cells rely on glutaminolysis to produce αKG, a metabolite shown to enhance T-bet expression[250] and in the absence of glutamine, cells will instead differentiate to regulatory subtypes[250,251]. Th2 cells drive humoral immunity through the stimulation of B cells and are the most glycolytic T helper subset[252]. Driven by IL-4 and IL-2 cytokines, the STAT6 and GATA3 transcription factors directs Th2 differentiation[253,254], whilst mTORC2 is specifically required for the associated metabolic reprogramming[255]. In addition to elevated glycolysis, airway Th2 cells also show increased lipid metabolism in an allergy model, and this is required for Th2 differentiation and effector functions[256]. Finally, the metabolic drivers of Th17 differentiation are of particular interest, as Th17 cells are involved in mucosal immunity and inflammation and are pertinent in autoimmune diseases such as multiple sclerosis and rheumatoid arthritis[257]. IL-6, IL-21 and TGF-β trigger activation of the RORγt transcription factor responsible for Th17 differentiation[257,258]. Th17

cells have elevated HIF1α compared to other T helper subsets and this is proposed to maintain glycolysis[245], whilst they also rely heavily on FAS[259]. In fact, HIF1α knockout and FAS inhibition both impair Th17 differentiation and instead promote regulatory T cell subsets[245,259], thus posing interesting therapeutic targets for treating diseases with Th17 immune pathology. Th17 cells may also present with heterogenous metabolic states due to elevated plasticity[260]. Th17 cells have been described with both stemness-associated features and lower anabolic metabolism, or higher metabolic activity to drive Th1-like responses, and this is centrally regulated by mTORC1 signalling[260]. Ultimately, our current understanding of the metabolic component to T helper differentiation illustrates how environmental cues may skew T cell profiles and highlights avenues to target this in disease therapeutics.

Regulatory T cells (Treg) play an essential role in maintaining peripheral tolerance and are characterised by a catabolic profile and secretion of IL-10, TGF-β and IL-35 immunosuppressive cytokines. Natural Treg (nTreg) may arise from $CD4^+$ cells directly in the thymus, whereas induced Tregs (iTreg) can develop in the periphery following $CD4^+$ T cell activation and TGF-β signalling[261,262]. Both are reliant on expression of the transcription factor Foxp3 that counteracts the PI3K/AKT-induced glycolytic programme and suppresses Myc expression to diminish anabolic metabolism, whilst also upregulating OXPHOS[246,263]. In addition, Treg cells utilise FAO which is directly activated in response to TGF-β and AMPK signalling[252,264]. The metabolic features of Treg cells enhance their suppressive capacity and give a survival advantage in nutrient depleted conditions[246,263], such as the tumour microenvironment, and hence they may prevail and stifle the host immune response in such environments.

$CD8^+$ cytotoxic T lymphocytes (CTLs) play a vital role in the elimination of intracellular infections and the immune response to malignant cells. They are characterised by the release of perforin and granzyme B at the immunological synapse to directly kill target cells. Analogous to $CD4^+$ T helper cells, CTLs import high levels of glucose for catabolism by aerobic glycolysis, and this abolishes the GAPDH and LDH RNA-binding functions that mediate cytokine mRNA stability and expression[214,241,249]. Notably, LDH may exert this moonlighting function on three critical CTL cytokines: IFNγ, TNFα and IL-2[214]. CTLs also rely on FAS, and deletion of a critical FAS enzyme, acetyl-CoA carboxylase, impairs $CD8^+$ T cell proliferation, persistence and survival which can be rescued by supplementation with exogenous fatty acids[265].

Most effector T cells undergo apoptosis after antigen clearance but some return to a more quiescent state and become memory T cells (Tm), enabling a rapid response following antigen rechallenge. The metabolic distinction between these two fates may begin as early as the first cell division following

TCR engagement, when asymmetric cell division can occur to distribute a greater portion of amino acid transporters, mTORC1 and c-Myc into the cell proximal to the APC[266,267]. This results in elevated glycolysis in this cell, supporting terminal T effector differentiation, whereas the distal cell has a less glycolytic composition that favours Tm differentiation[266,267]. Mitochondrial dynamics may similarly control cell fate, as evidence suggests that effector T cells induce mitochondrial fission to encourage glycolysis, whereas Tm cells maintain fused networks[268]. $CD8^+$ Tm cells are the best characterised Tm cells and require the inhibition of glycolysis[269] and upregulation of FAO and OXPHOS[270,271], to ultimately yield a more quiescent metabolic profile that preserves long-lived memory cells. The activation of FAO is in a TRAF6 and AMPK-dependent manner, and mice with a T cell-specific deletion of TRAF6 fail to sustain an efficient Tm population[270]. Despite this dependence on FAO, Tm cells do not import high levels of fatty acids, and glucose is primarily used to support both FAO and OXPHOS in these cells[272]. Similarly, IL-7 drives the import of glycerol in Tm cells and subsequent triglyceride synthesis can fuel FAO and promote Tm survival[273]. Interestingly, $CD8^+$ Tm cells also have elevated mitochondrial mass and spare respiratory capacity compared to $CD8^+$ effector T cells[271], further illustrating their reliance on mitochondrial metabolism.

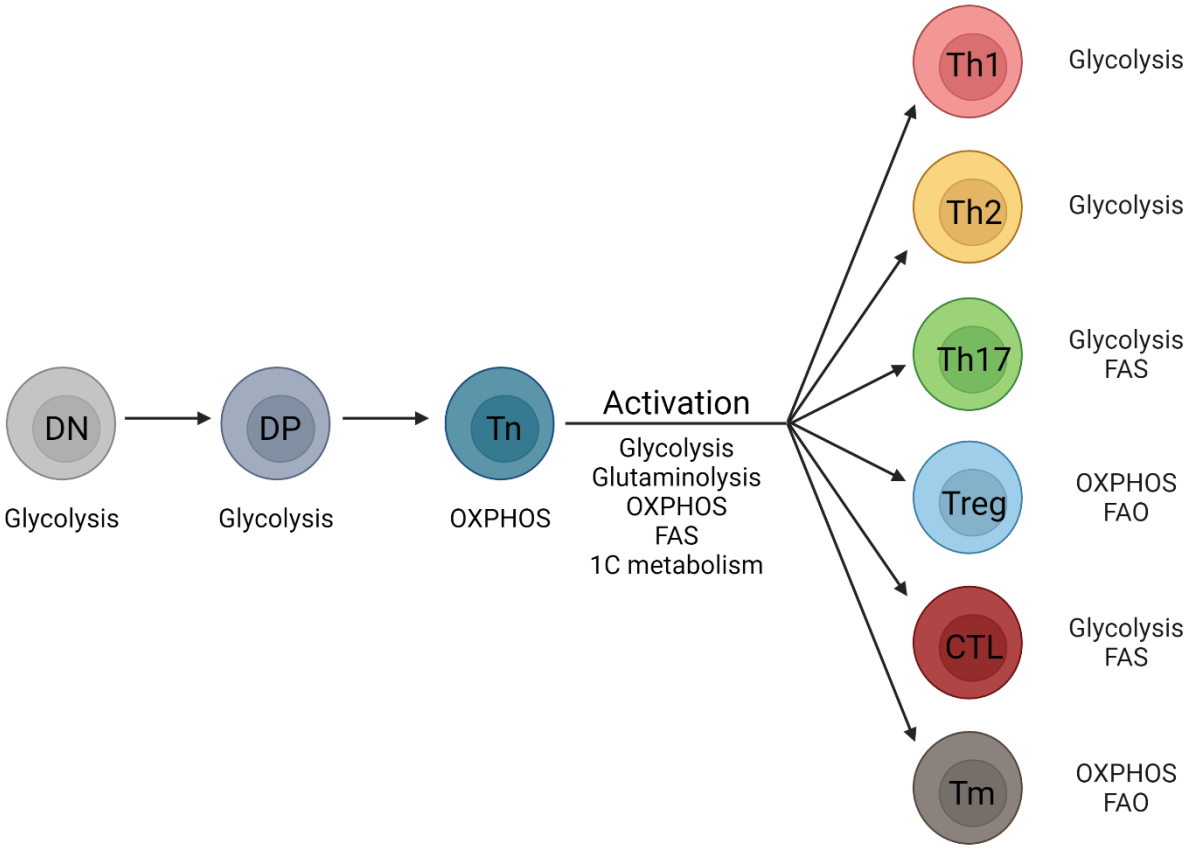

Figure 1.7: Metabolic reprogramming through the lifecycle of a T cell.

Through development, double negative thymocytes upregulate glycolysis to progress through the β-selection checkpoint and promote proliferation in DN4. This glycolytic profile is maintained in double positive thymocytes. Mature naïve T cells switch to a quiescent metabolic state in which minimal glucose is utilised to sustain OXPHOS. Upon activation, T cells undergo significant metabolic reprogramming to upregulate glycolysis and glutaminolysis, whilst maintaining a critical level of OXPHOS. There is also an upregulation of anabolic pathways including FAS and 1C metabolism to support proliferation. Nutrient availability and the metabolic profile of a T cell can skew differentiation to distinct T cell subsets. Pro-inflammatory Th1, Th2 and Th17 cells, and $CD8^+$ CTLs maintain high levels of aerobic glycolysis, whereas promoting catabolic metabolism with a dominance of OXPHOX and FAO polarises to regulatory and memory T cell differentiation. All T cell developmental stages and mature subsets employ a variety of metabolic pathways and those listed here are purely the dominant pathways.

DN: Double negative thymocytes. DP: Double positive thymocytes. Tn: Naïve T cell. Th1, Th2, Th17: T helper subsets. Treg: Regulatory T cell. CTL: Cytotoxic T lymphocyte. Tm: Memory T cell. OXPHOS: Oxidative phosphorylation. FAS: Fatty acid synthesis. FAO: Fatty acid oxidation.

1..6 Cancer metabolism

Cancer is a complex and diverse disease that is defined as the uncontrolled proliferation of abnormal cells. This cellular transformation occurs through the multi-step acquisition of mutations that give rise to malignant characteristics. Six hallmarks of cancer were outlined by Hanahan and Weinberg in 2000 to describe the biological capabilities required for neoplastic disease, namely sustained proliferative signalling, insensitivity to growth suppressors, resistance to cell death, replicative immortality, sustained angiogenesis, and tissue invasion and metastasis[274]. These features have since been expanded to include the reprogramming of energy metabolism and evasion of immune destruction[275]. Moreover, Hanahan and Weinberg also highlighted genomic instability and tumour-promoting inflammation as two enabling characteristics that underpin tumorigenesis[275].

Cancer metabolism has its roots in the observation made by Otto Warburg that cancer cells utilise excessive glucose to generate lactate through the process of aerobic glycolysis, a phenomenon coined the Warburg effect[276]. Early study of cancer metabolism sought to understand the purpose of this aerobic glycolysis which is an inefficient source of ATP, and the recognition that it supports biosynthesis to sustain proliferation was a turning point[182]. Research has extensively characterised the metabolic pathways in cancer and common features have emerged across cancer types[277–280]. More recently, appreciation has grown for metabolic influence beyond energy and biomass generation, as a driver of redox homeostasis, metastasis, and tumorigenesis itself. Moreover, there is growing interest in the tumour microenvironment and its role in influencing the heterogeneity of cancer metabolism. Ultimately, the metabolism of cancer cells and the tumour microenvironment both pose an exciting avenue for therapeutic targeting.

1..6.1 Features of cancer metabolism

Whilst the metabolic features of cancer may be influenced by a plethora of factors such as genotype and tissue origin, several common themes have emerged and are highlighted by recent pan-cancer transcriptomic analyses[277–280]. These cancer metabolic profiles share parallels with the reprogramming upon T cell activation, as common pathways prevail in rapidly proliferating cells from both physiological and pathological settings (Fig. 1.8). Elevated glucose uptake and aerobic glycolysis are characteristic of cancer[277–280] and may be upregulated by mutations in signalling molecules such as Myc, ATK, mTOR and HIF. In fact, meta-analysis of GLUT1 overexpression in solid tumours found that studies report up to 85% of tumours have elevated GLUT1[281], and this augmented glucose uptake is routinely employed for cancer diagnosis using ^{18}F-fluorodeoxyglucose PET imaging[282]. Whilst lactate production is elevated in cancer cells, many glycolytic intermediates are also redirected into various

anabolic pathways, particularly for nucleotide biosynthesis[277]. Cancer cells may increase flux into the PPP through overexpression of the non-oxidative PPP enzymes, TKT and TALDO[283,284], and the loss of p53-mediated repression of G6PD by mutations that abolish binding[285]. Similarly, cancer cells may utilise glucose-derived carbon for glycine and serine synthesis to fuel 1C metabolism, as has been shown in melanoma by the amplification of serine biosynthesis enzyme phosphoglycerate dehydrogenase (PHDGH)[286]. Notably, meta-analysis of mRNA profiles from almost 2000 tumours identified 1C metabolism as the highest scoring pathway and the 1C enzyme mitochondrial folate-coupled dehydrogenase (MTHFD2) was the most consistently overexpressed[287], further implicating 1C upregulation as a common feature in cancer. As aerobic glycolysis does not yield pyruvate, cancer cells replenish TCA cycle metabolites through anaplerosis, and over 50% of this comes from amino acids[288]. Glutamine is particularly important and the upregulation of glutamine transporters through mechanisms such as c-Myc activation is reported in many cancers, promoting glutaminolysis to fuel the TCA cycle[238,289–291].

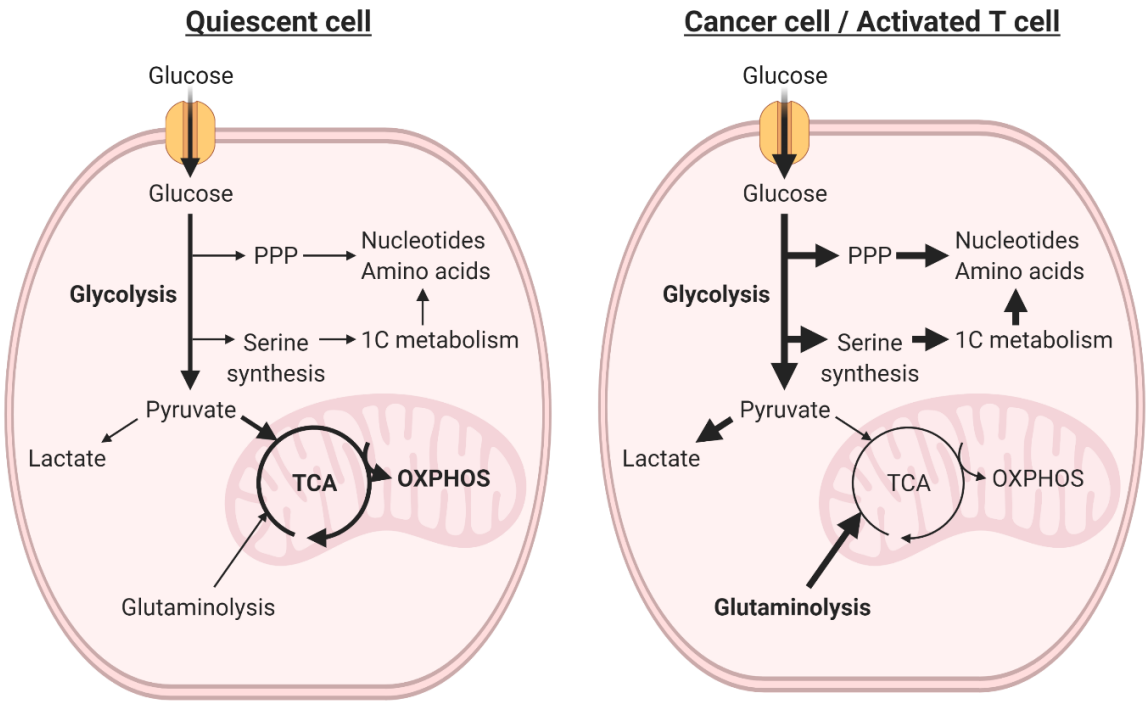

Figure 1.8: Common features of metabolic reprogramming in cancer and T cell activation.

Similar metabolic reprogramming occurs during tumorigenesis and upon T cell activation, as both cell types upregulate biomass production to sustain rapid proliferation. Cancer cells and activated T cells display high levels of aerobic glycolysis to produce lactate, and an increase in flux into the emanating PPP and serine synthesis biosynthetic pathways, which subsequently fuels 1C metabolism and generation of nucleotides and amino acids. These cells also upregulate the catabolism of amino acids such as glutamine to replenish intermediates of the TCA cycle.

PPP: Pentose phosphate pathway. TCA: Tricarboxylic acid cycle. OXPHOS: Oxidative phosphorylation.

Unlike the pathways described above, others display greater inter-tumour heterogeneity. For example, expression of TCA cycle and OXPHOS genes vary between cancer types[277–280], suggesting divergent roles. The importance of mitochondrial function in cancer has been heavily debated and, whilst the Warburg effect was once considered a response to mitochondrial dysfunction[276,292], growing evidence demonstrates that OXPHOS does occur in cancer and may be upregulated in certain populations including cancer stem cells and therapy resistant clones[293–295]. The electron transport chain is one source of ROS in cancer cells, taking the form of superoxide O_2^- that is reduced to H_2O_2 [296]. ROS may have juxtaposing roles in cancer, as moderate localised ROS can support tumorigenesis and maintain proliferation whereas detrimentally high ROS can induce cell death. For example, H_2O_2 can oxidise cysteine residues in proteins such as PTEN to promote proliferation, survival and invasion[297,298], and reducing ROS levels by specifically enhancing mitochondrial antioxidative capacity can impair cancer progression[299,300]. In contrast, cancer cells may upregulate proteins involved in antioxidant defences, such as TP53 Induced Glycolysis Regulatory Phosphatase (TIGAR) which promotes the oxidative PPP[301–303], and reducing the antioxidative capacity of these cells may render them more susceptible to ROS-induced apoptosis[304]. These differential signalling outcomes may predominate at different stages of cancer progression, illustrating the dynamic nature of cancer metabolism.

One feature of cancer progression that is increasingly understood to arise from metabolic signalling is metastasis. The epithelial-mesenchymal transition (EMT) is the process through which epithelial cells lose their cell-cell interactions and demonstrate migratory and invasive properties. This occurs physiologically such as in development and tissue repair[305], but is also a common feature of metastatic disease. Several metabolites may promote EMT, including lactate, ROS and acetyl-CoA which are all commonly elevated in cancer cells[306–309]. Subsequent metabolic reprogramming is also required during cell migration and adoption into a new metastatic niche. Detachment from the extracellular matrix may induce significant oxidative stress, thus cancer cells upregulate antioxidative pathways such as NADPH generation via the folate pathway[310]. Moreover, a switch to catabolic metabolism occurs to promote cell survival in circulation[311]. Upon colonisation, metastatic cells must adapt to their new tumour microenvironment as tissues may have disparate nutrient availabilities, such as limited serine and glycine in the brain[312]. Thus, different metabolic signatures are required for different tissue metastases. Given the implication of metastases on patient survival, identifying metastasis-promoting metabolic pathways is of great interest and may present novel therapeutic strategies.

Intra-tumour genomic heterogeneity is widely recognised[313], and cancer metabolism is now considered to be similarly heterogeneous. The metabolic profile changes throughout cancer progression and within different tumour subpopulations and is ultimately the result of cooperation between intrinsic and extrinsic factors.

1..6.2 Cell-intrinsic drivers for cancer metabolism

Cancer metabolic reprogramming is largely driven by mutations in the signalling pathways that drive metabolism. One example mentioned above is the mutation of p53 which can produce a protein incapable of binding and inhibiting G6PD, thus upregulating PPP in cancer cells[285]. Other examples include mutations in the PI3K/AKT pathway which promote GLUT1 expression and increase glycolytic enzyme activity[314,315]; and mutations that activate c-Myc or deactivate Rb to increase the expression of glutamine transporters[238,291]. Splice variations are also shown to drive metabolic reprogramming in cancer, such as via the re-expression of the pyruvate kinase M2 isoform which critically drives aerobic glycolysis compared to the M1 counterpart[316]. Further study showed that c-Myc overexpression controls this deregulated splicing, by upregulating hnRNP RNA-binding proteins that favour PKM2[317]. Ultimately, these tumorigenic mutations and protein dysregulation abolish a cells reliance on growth factors and external signals to promote nutrient uptake and metabolism. In this manner the change in metabolic programme may support tumorigenesis.

In some cases, metabolic imbalance may precede genetic alterations in oncogenes or tumour suppressors, and metabolites themselves may initiate transformation by disrupting metabolism, epigenetics, and genetic integrity. Such metabolites are known as oncometabolites[318]. Oncometabolites can aberrantly accumulate from disrupted metabolic pathways caused by mutations in metabolic enzymes and are traditionally TCA cycle metabolites[318]. The first oncometabolite identified was D-2-hydroxyglutarate (D2HG) which arises from mutations in the TCA cycle enzyme isocitrate dehydrogenase 1 / 2 (IDH1/2) that give neomorphic enzyme activity[319,320]. These mutations commonly occur in >80% of grade 2/3 gliomas[318], suggesting they are a driver mutation in glioma transformation. D2HG is also suggested to promote leukemic transformation since it can induce DNA hypermethylation, impair haematopoietic differentiation and increase expression of stem/progenitor cell markers[321]. D2HG and other TCA cycle oncometabolites such as succinate and fumarate typically promote tumorigenesis through the inhibition of αKG-dependent dioxygenases such as the epigenetic TET enzymes[320,321] and DNA repair ALKBH enzymes[322], ultimately promoting genetic instability and genome-wide epigenetic alterations[318,320–323]. More recently it has been proposed that lactate may be an oncometabolite, as an increase in both endogenous and exogenous lactate in breast cancer cells affects the transcription of oncogenes such as *MYC* and *RAS*, the *BRCA1/2* tumour suppressors, transcription factors such as *HIF1α*, and genes involved in cell cycle progression and proliferation[324]. Oncometabolites are particularly valuable for use as cancer biomarkers and, as they are a vulnerability specific to cancer cells, may also be targeted with anti-cancer therapies[325,326].

1..6.3 The tumour microenvironment in metabolic reprogramming

Cancer metabolism is also subject to environmental cues that drive dynamic metabolic adaptation, leading to metabolic heterogeneity in different tumour niches. The tumour microenvironment (TME) comprises stromal and endothelial cells that support cancer progression and infiltrating immune cells. As highlighted for metastases, the tissue context of a cancer cell may require different metabolic adaptations. For example, cancers such as leukaemia, lymphoma, breast, and lung commonly upregulate OXPHOS genes, whereas they are reduced in brain and colon neoplasms[277]. Moreover, the dysregulation of signalling molecules such as Myc may induce different metabolic effects in different tissues[327,328], further suggesting crosstalk with environmental factors.

Several environmental gradients occur within a tumour, including those of nutrients, oxygen, and stromal interactions. Hypoxia, particularly at the core of a solid tumour, stabilises HIF1α which can upregulate glucose transporters, glycolytic enzymes, LDH and PDK1, as previously explained in the context of T cells[224,228]. There is also evidence that HIF1α can upregulate both glutamine import[329] and catabolism[330] in response to hypoxia. Given the augmented uptake of nutrients to sustain cancer cell proliferation, and the competing requirements of other tumour-infiltrating cells, nutrient deprivation occurs in the TME. To overcome this, cancer cells may use opportunistic modes of nutrient acquisition and upregulate nutrient scavenging pathways to satisfy their metabolic demands[331]. For instance, AMPK activation by low cellular energy induces lysosomal gene expression, thus promoting functional lysosomes and autophagy in response to metabolic stress[332]. The significance of this pathway is highlighted by autophagy inhibitors which cause tumour regression in mouse models of non-small cell lung cancer and pancreatic ductal adenocarcinoma[332–334]. Similarly, the use of micropinocytosis to obtain an extracellular source of amino acids, nucleotides, fats, and sugars can promote cancer survival, and confer resistance to standard chemotherapies that target biosynthetic pathways[335,336]. Cancer cells may also overcome nutrient deprivation via a symbiotic relationship with stromal cells such as cancer associated fibroblasts (CAFs). Lactate and glutamine released by CAFs may be consumed and metabolised by cancer cells to fuel the TCA cycle[337,338], and they may also provide cysteine to leukaemic cells to promote glutathione synthesis and resistance to oxidative stress[339].

The metabolism of cancer cells and infiltrating immune cells is similarly intertwined and can have profound effects on the anti-tumour immune response. The balance between cells with anti-tumour activity such as NK cells, inflammatory macrophages and Th1, CTL and Tm cells, and those with immunosuppressive functions such as anti-inflammatory macrophages and Treg cells, is influenced by nutrient availability and signals in the TME. Glucose depletion in the TME correlates with reduced $CD8^+$ T cell infiltration and can lead to impaired cytokine production, T cell hypo-responsiveness and exhaustion[340–343]. The high extracellular lactate is also immunosuppressive and inhibits NFAT-driven T

cell activation and IFNγ production[344], elevates NADH and reductive stress which inhibits glycolysis, serine synthesis and T cell proliferation[345], and blocks CTL cytokine release and lytic granule exocytosis[346]. Moreover, lactate acidosis impairs the innate immune response through mechanisms such as polarisation to immunosuppressive M2 macrophages[347]. Some cancers overexpress the IDO1/TDO2 enzymes that metabolise tryptophan to kynurenine[348] and the impact of this on T cell function is two-fold. Tryptophan depletion from the TME can induce cell cycle arrest and anergy in T cells, whilst the accumulated kynurenine suppresses effector T cell function, stimulates apoptosis and polarises to Treg[349]. Finally, cancer frequently sustains chronic antigen stimulation and engagement of T cell inhibitory receptors such as PD-1, and this can drive T cells into a dysfunctional metabolic and exhausted state[350]. These signals maintain FAO, downregulate GLUT1 and HK2 and impair glycolysis[351,352], and T cell function may be partially restored by GLUT1 overexpression in a B cell leukaemia model[352]. There is a plethora of mechanisms through which cancer cells can induce an immunosuppressive TME, and understanding the metabolic interdependence between cancer and infiltrating immune cells can help to direct immunotherapies.

1..6.4 Metabolism as a therapeutic target

Knowledge of the underlying metabolic composition of both cancer and immune cells can reveal novel therapeutic targets. Modulating metabolism for cancer treatment may be broadly divided into two avenues: (1) targeting cancer metabolism to inhibit tumour progression and adjust the TME; and (2) targeting immunometabolism to improve the anti-cancer immune activity. These approaches show great promise when used synchronously, such as to create a less hostile TME that improves the survival of metabolically fit T cells from adoptive transfer[189,353,354].

T cell transfer therapy has been an exciting addition to our anti-cancer arsenal in recent decades and may be further enhanced by considering the metabolic programmes of cells. T cell transfer therapy involves the isolation of tumour-specific patient T cells (adoptive transfer therapy), or the *ex vivo* modification of T cells to express a synthetic chimeric antigen receptor (CAR-T cell therapy), and their subsequent expansion *in vitro* before being reinfused back to the patient with the aim of improving the anti-tumour immune response. To ensure the success of these therapies the reintroduced T cells must be stable and robust antigen-specific cells with Tm-like longevity, and manipulating their metabolism to reduce glycolysis and promote mitochondrial integrity, OXPHOS and FAS may promote these features[269,355–357]. For example, pharmacologically inhibiting glycolysis and glutaminolysis during *ex vivo* conditioning can both improve T cell survival, cytokine production and cytotoxicity upon reinfusion[269,355,356]. Moreover, altering the cell culture nutrient composition may alter T cell longevity,

such as elevating L-arginine to promote OXPHOS over glycolysis and induce a Tm phenotype with improved persistence and anti-tumour efficacy[232]. The metabolism of CAR-T cells may also be manipulated via genetic editing. The inclusion of different domains in the CAR construct can elicit different metabolic responses[358–360], for example dual stimulation of the 4-1BB and OX40 domains of TNF-receptors enhances both glycolysis and OXPHOS in melanoma[360]. Interestingly, CAR-T cells may also be adapted to the TME via genetic editing and have been engineered with features such as overexpressed catalase to metabolise H_2O_2 and thus reduce oxidative stress and improve cytotoxic function[361].

The combination of T cell transfer therapies with other therapies can improve their efficiency. As mentioned, targeting cancer metabolism to reduce the tumour burden and create an environment that supports the survival and function of transferred T cells. For example, proton pump inhibitors reduce acidification of the TME and can improve the efficacy of immunotherapy[362], whilst pre-treatment with drugs that downregulate IDO1 in lymphoma cells improves CAR-T cell activity *in vivo*[363]. Finally, the combination with checkpoint inhibitors such as anti-PD-1 can reprogramme T cell metabolism to revitalise glycolysis and T cell function in anergic cells[189,351,354].

1..7 PFKP

Phosphofructokinase (PFK-1) is termed the "gatekeeper" of glycolysis as it catalyses the first committed and rate limiting step: the phosphorylation of fructose-6-phosphate (F6P) to fructose-1,2-bisphosphate (F1,6BP). The regulation of PFK-1 activity therefore mediates the flux of carbon into glycolysis or the redirection of glycolytic intermediates into the PPP to promote NADPH and nucleotide synthesis. PFK-1 exists in three isoforms that share 67-70% sequence homology[364] and are found primarily in platelets (PFKP), muscle (PFKM), or liver (PFKL), though all three also localise in other tissues[365,366]. PFKP is of interest as the major isoform implicated in human cancer[367–369]. PFKP has 8 transcript variants with isoform 1 being the longest at 784 amino acids (Fig. 1.9A). It is comprised of an N-terminal catalytic domain which contains 3 substrate binding regions, and C-terminal regulatory domain. PFKP monomers are unstable and readily denature but, upon oligomerisation, dimers may be partially active and tetramers are fully active[370–374]. The crystal structure of the mammalian PFKP tetramer in complex with ATP-Mg^{2+} and ADP have both been solved to 3 Å, and this illustrates how the PFKP tetramer is an antiparallel assembly of two dimers, with an active site positioned between the two subunits of each dimer (Fig. 1.9B)[371]. The activity of PFKP requires an ATP-Mg^{2+} cofactor which is bound to each subunit, in the active site, and ATP hydrolysis results in conformational changes that may facilitate the release of products[371].

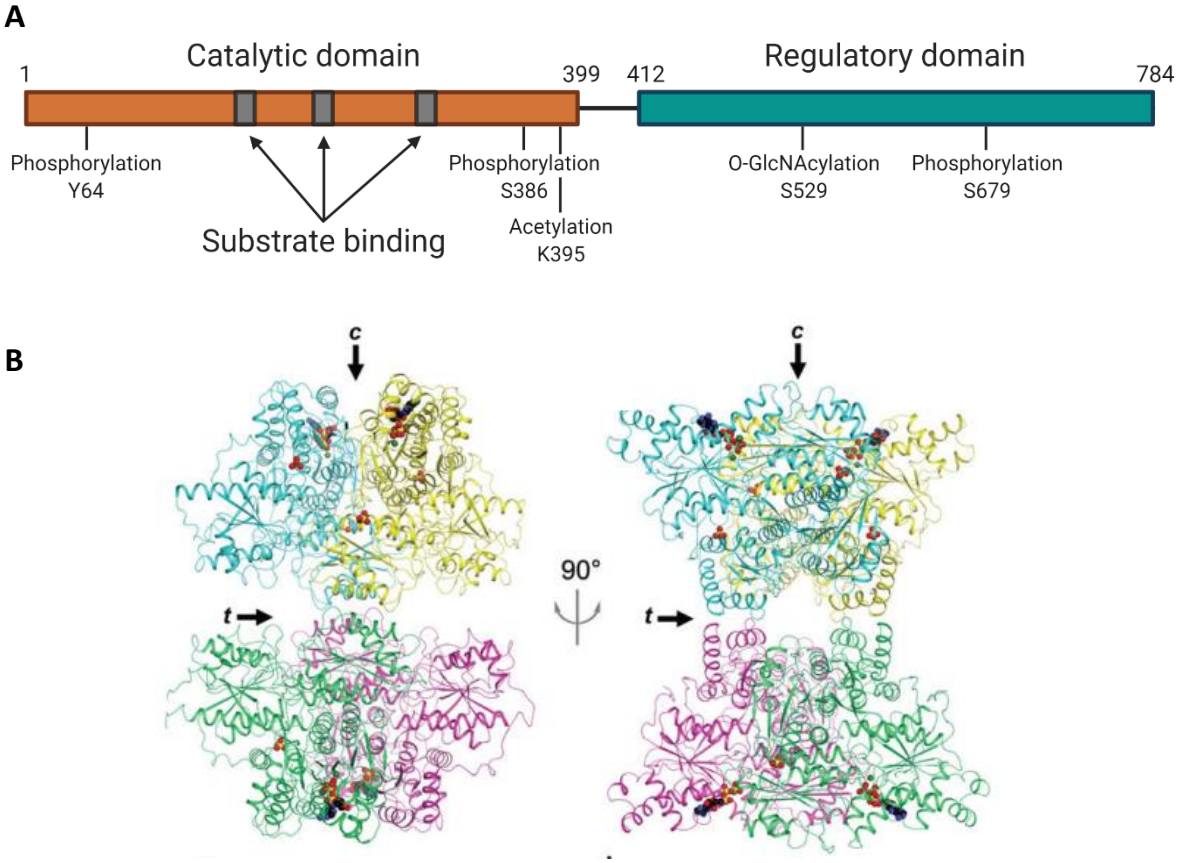

Figure 1.9: Domain and oligomeric structure of PFKP.

(A) PFKP is divided into two domains: an N-terminal catalytic domain that contains three substrate binding regions, and a C-terminal regulatory domain. Both domains contain amino acids that are subject to post-translational modification to regulate PFKP activity, some of which are annotated.

(B) Ribbon diagrams of PFKP tetramers which show the relative positions of the two anti-parallel dimers. Each PFKP monomer is individually coloured. “c” and “t” indicate the catalytic and tetrameric interfaces respectively. Image taken from Webb et al. 2015.

PFK-1 is subject to allosteric regulation by several metabolites, and these largely alter the distribution between dimer and tetramer states. Fructose-2,6-bisphosphate (F2,6BP) is the most potent PFK-1 activator[373–375] and is converted to/from F6P by the bifunctional enzyme PFKFB (6-phosphofructo-2-kinase / fructose-2,6-bisphosphatase) to enable reciprocal regulation of glycolysis and gluconeogenesis[376]. Binding of F2,6BP to the PFK-1 regulatory domain promotes tetramers, and hence enzymatic activity, in the presence of abundant F6P substrate[373–375]. A high concentration of ADP, AMP and cAMP similarly stabilise PFK-1 tetramers to drive activity[364,372]. Conversely, lactate and citrate provide negative feedback from anaerobic glycolysis and the TCA cycle respectively, and promote the dissociation of PFK-1 to dimers[364,372]. The regulation of PFK-1 by ATP is interesting as it displays a dual effect due to the presence of both a catalytic and allosteric ATP binding site[372–374]. PFK-1 is activated by low concentrations of ATP (1 mM), but inhibited by ATP binding at higher concentrations[372–374], although this inhibitory effect can be overcome by F2,6BP[373,374]. PFK-1 is also regulated by binding to microtubules, f-actin and calmodulin (CaM), though this is largely demonstrated experimentally using purified PFKM[370,377–380]. The association of PFKM with microtubules stabilises the dimeric form and hence inhibits enzymatic activity[364]. In contrast, hormones such as serotonin, insulin, and epinephrine can all promote phosphorylation of tetrameric PFKM which increases its affinity for f-actin and stabilises the active state[364,377–379]. Interestingly, PFKM binding to CaM promotes dissociation to dimers but these dimers maintain full enzymatic activity[370,380]. In this manner, high Ca^{2+} concentrations may promote fully active CaM-bound PFKM dimers which have independence from other allosteric regulators[380]. Ultimately, PFK-1 can integrate multiple signals to dynamically alter its activity and hence the cellular metabolic state.

Mutations in PFK-1 are associated with glycogen storage disease type VII (Tarui disease)[381], and PFK-1 expression is suggested to play a critical role in metabolic reprogramming in cancer[364]. As previously noted, PFKP is the most prominent PFK-1 isoform in cancer, and its aberrant expression has been observed in breast cancer, B and T cell leukaemia, glioblastoma, and clear cell renal carcinoma, amongst others[368,369,390,382–389]. These alterations in PFKP activity may arise from genetic amplification, disrupted transcriptional or post-translational control, or somatic mutations, of which 44 have been identified in cancer and many are predicted to affect ligand interactions and enzymatic activity[371]. Ultimately PFKP upregulation in cancer typically promotes glycolysis, increases proliferation, and stimulates invasion and metastasis due to elevated lactate production. In particular, elevated PFKP is associated with poor prognosis in lung[382,383] and breast cancer[368,384,385] and diminishing PFKP activity can decrease migration and invasion[385]. As such, PFKP is a proposed prognostic biomarker for several cancer types including lung[382], triple negative breast cancer[386] and medulloblastoma[387]. Nonetheless, it has recently been shown that PFKP overexpression is associated with improved prognosis in clear

cell renal carcinoma and correlates with an augmented anti-tumour response including elevated $CD4^+$ and $CD8^+$ infiltrating T cells[391], thus illustrating some complexity of PFKP's role in cancer metabolism.

Disrupted transcriptional control of PFKP is common in cancer, and several transcriptional regulators have been identified that drive metabolic reprogramming via PFKP. Most recently, the transcription factor YY1, which is overexpressed in prostate cancer, was identified to bind alongside BRD4 to upregulate PFKP and promote glycolysis and cancer progression[392]. Conversely, BRCA1 and its binding partner ZBRK1 can form a transcriptional repression complex at the PFKP promotor to inhibit PFKP expression, thus BRCA1 deficiency in breast cancer drives metabolic reprogramming, glycolysis, and cancer progression[393]. Transcriptional control of PFKP has also been implicated in metastatic disease. In triple negative breast cancer, hypoxia in the TME activates HIF1α which upregulates PFKP[384]. This elevated PFKP, in concert with the stabilisation of citrate synthase, results in the accumulation of citrate which promotes metastasis in response to hypoxic conditions[384]. Similarly, PFKP upregulation by the transcription factor KLF4 is also shown to promote glycolysis and metastasis in breast cancer[368]. In contrast, the EMT transcriptional repressor SNAI1 has been shown to transcriptionally inhibit PFKP to suppress glycolysis and promote metabolite diversion into the PPP to facilitate breast cancer cell survival under metabolic and oxidative stress[367]. This exemplifies how both glycolysis and the PPP can be advantageous to cancer cells, and the regulation of PFKP to drive either pathway may be context dependent.

PFKP is also regulated post-translationally to enable a rapid physiological response to cellular signalling, and this may too be disrupted in cancer. O-GlcNAcylation is a form of glycosylation in which N-acetylglucosamine modifications such as UDP-GlcNAc are added to proteins. UDP-GlcNAc is synthesised from key metabolites including glucose and acetyl-CoA, and thus serves as a nutrient sensor to reflect the metabolic status of a cell[394]. PFK-1 may be modified by O-GlcNAcylation at S529 in response to hypoxia and glucose starvation, which blocks F2,6BP binding and hence favours low oligomeric states of PFK-1[395]. In cancer cells, this inhibition of PFK-1 activity and redirection to the PPP provides a proliferative advantage[395]. Similarly, the phosphorylation of PFKP by cyclin D/Cdk6 at S679 dissociates PFKP tetramers and drives the PPP to promote survival of T-ALL cells experiencing oxidative stress[304]. Moreover, this phosphorylated dimeric PFKP can be translocated to the nucleus where, in concert with c-Myc, it induces expression of the CXCR4 receptor involved in chemotaxis and stimulates invasion in mice and *in vitro* primary human samples[396,397]. This outlines a mechanism whereby PFKP phosphorylation by Cdk6 can promote cancer cell survival via upregulation of the PPP, and invasion via transcriptional activity of nuclear PFKP. In other instances, PFKP phosphorylation may activate the enzyme and potentiate signalling cascades. The activation of EGFR promotes PFKP acetylation at K395, and subsequent phosphorylation at Y64, and this phosphorylated PFKP may in turn enhance PI3K/AKT

activation[398]. Activated AKT can phosphorylate PFKP at S386 to inhibit ubiquitination and degradation by TRIM21, providing a positive feedback mechanism for PFKP regulation[388]. This axis promotes glycolysis and tumour proliferation in response to PI3K/AKT signalling in glioblastoma[388]. Phosphorylation at S386 can also reduce PFKP ubiquitination by HDR1, an E3 ubiquitin ligase that targets PFKP for degradation and inhibits glycolysis in breast cancer cells in a tumour-suppressive manner[399]. The assortment of PTMs on PFKP (Fig. 1.8) enable the rapid reprogramming of glycolysis in response to environmental cues and signalling cascades, and this is frequently commandeered by cancer cells to promote cancer progression.

As a central player in cancer cell metabolic reprogramming, PFK-1 is an attractive therapeutic target and two possible strategies for PFK-1 targeting have been proposed. Firstly, the small molecule acetylsalicylic acid (aspirin) has been found to disrupt the PFK-1 quaternary structure and inhibit glycolysis in breast cancer cells, suggesting that this may contribute to its anti-tumour properties[400]. Secondly, drugs may be employed to disrupt PFK-1 interaction with the cytoskeleton, such as the antifungal derivative clotrimazole that promotes dissociation of PFK-1 from the cytoskeleton and correlates with reduced viability in lung carcinoma and colon adenocarcinoma cells[401]. PFK-1 activity may also be disrupted indirectly using PFKFB3 inhibitors to reduce production of the F2,6BP allosteric activator. PFK-158 is a novel PFKFB3 inhibitor that has shown promise in reducing glycolysis and endometrial cancer cell survival *in vitro* when used in combination with standard chemotherapy drugs[402]. Nonetheless, there are challenges associated with targeting PFK-1, particularly since glucose is a major energy source throughout the body so toxicities need to be carefully assessed.

1..8 F-box proteins in metabolism

Given the scale of the ubiquinome and broad influence of FBPs, it is unsurprising that numerous FBPs play pivotal roles in both homeostatic metabolic regulation and its reprogramming in disease. This may be through their ligase activity or via one of their growing SCF-independent functions.

Skp2 (Fbxl1) is one of the best characterised FBPs and is a known oncogene reported to be overexpressed in a variety of cancers[403–405]. Skp2 has over 40 identified substrates[406], many of which are tumour suppressor proteins such as the Cdk inhibitor p27. Alongside its crucial role in cell cycle progression, Skp2 has also been implicated in the metabolic reprogramming of cancer cells to aerobic glycolysis, in part through its role as a transcriptional co-activator for Myc[407]. Upon EGF signalling or in times of metabolic stress (such as in the TME), AMPK phosphorylates Skp2 to stabilise its ligase activity[408]. This increases the ubiquitination of the Skp2 substrate Akt, which translocates to the cell membrane where it is activated[409]. Activated Akt promotes glucose uptake by increasing the expression and translocation of GLUT receptors, and glycolytic flux via the upregulation of HK2 and activation of PFKFB3[409–411]. In breast cancer, this metabolic reprogramming has been linked to progression in tumour models and Skp2 overexpression correlates with increased Akt activation and poor prognosis in patients[409]. Similarly, Akt has been shown to promote aerobic glycolysis in human glioblastoma lines and leukemic cells from transformed mice, rendering them susceptible to glucose removal[412]. Together, this metabolic function and cell cycle role make Skp2 an attractive therapeutic target and its inhibition has been shown to sensitise cells to Herceptin and anti-EGFR therapy[408,409].

In contrast, Fbxw7 is a recognised tumour suppressor protein and is arguably the FBP with the most diverse metabolic influence. Approximately 6% of primary human cancers have a mutation in *FBXW7*[413]. Fbxw7 degradative targets include SREBP transcription factors[414] that regulate enzymes for lipid synthesis; PGC-1α[415], a transcriptional co-activator that promotes mitochondrial biogenesis and OXPHOS; and mTOR[416] which is associated with various metabolic pathways. However, the best characterised metabolic role for Fbxw7 is as a negative regulator of glycolysis and its expression inversely correlates with glucose metabolic activity in a mouse xenograft model and pancreatic cancer patients[417]. Fbxw7 ubiquitinates the glycolytic enzyme Eno1 and signals its degradation, thereby directly reducing glycolytic flux[418]. Fbxw7 can also indirectly limit glycolysis by ubiquitinating transcription factors HIF1α and c-Myc[417,419,420], implicating Fbxw7 as a negative regulator of glycolysis[417,419,420]. It is worth noting that c-Myc is a tightly regulated protein which can also be targeted for degradation by Fbxl3 in co-operation with the CRY2 co-factor. Interestingly, miR-181d targets Fbxl3 and CRY2 to promote aerobic glycolysis in colorectal cancer, and this has been implicated in cancer progression[421].

The cell cycle and metabolism work in concert to ensure proliferation only occurs when it is metabolically viable, and FBPs function as regulators of this crosstalk. APC/C-Cdh1 ubiquitinates a number of proteins involved in the progression to S-phase and thus maintains cells in G1[422], but has also been shown to ubiquitinate PFKFB3[423], glutaminase-1 (GLS1)[424] and isocitrate dehydrogenase 3β (IDH3β)[425], signalling their degradation and inhibiting glycolysis, glutaminolysis and the TCA respectively. Consequently, the high APC/C activity through G1 keeps levels of these enzymes low, but they accumulate when APC/C falls in late G1 and an increase in metabolic flux is observed[426,427]. As the cell moves into S-phase another FBP, β-TRCP, increases. In an example of collaboration between FBPs, β-TRCP also ubiquitinates PFKFB3 to ensure a short peak of glycolysis in late G1, whereas GLS1 and glutaminolysis remain active through S-phase[424,428]. Unsurprisingly, this system is often dysregulated in cancer and the tumour suppressive APC/C-Cdh1 is mutated or downregulated in many cancers including colon, prostate, breast, ovary, brain and liver[429,430]. Mechanistically it has been shown that the accumulation of the TCA enzyme IDH3β promotes the G1/S transition in esophageal squamous cell carcinoma cells and IDH3β overexpression correlates with poor survival in these patients[425]. It would therefore be interesting to ascertain whether this bidirectional relationship between the cell cycle and metabolism contributes to the progression of other APC/C-Cdh1 mutated cancers.

The degree of ROS production and antioxidative capacity is a by-product of metabolism and the previously mentioned Fbxw7 and β-TRCP are two FBPs involved in sensing oxidative stress. The transcription factor Nrf2 is a master regulator of redox homeostasis and initiates transcription of anti-apoptotic genes and detoxifying enzymes. β-TRCP ubiquitinates both Nrf1 and Nrf2[431,432], whilst Fbxw7 ubiquitinates Nrf1[433], to result in their degradation and thereby regulate the cellular stress response. Fbxl17 can also play a role, as it ubiquitinates an Nrf2 regulator called BACH1 to activate Nrf2 transcription profiles, hence lowering the threshold required for an oxidative stress response[434].

Whilst the metabolic roles discussed thus far utilise the canonical ligase function of FBPs, Fbxl10 affects an array of metabolic pathways through its action as a histone demethylase. In fact, transcriptome analysis of Fbxl10 overexpressing fibroblasts revealed that approximately 50% of all Fbxl10-regulated genes are involved in metabolism[435]. Such genes include antioxidant enzymes such as NAD(P)H quinone oxidoreductase-1 (Nqo1) and peroxiredoxin-4 (Prdx4) which are induced by Fbxl10 to protect from oxidative stress in mouse embryonic fibroblasts[436]. Data on the role of Fbxl10 in glycolysis and its oncogenic or tumour suppressor properties are conflicted. Metabolomic analysis of HeLa cells identified Fbxl10 as a positive regulator of glycolysis and pyrimidine synthesis[437]. In contrast, Fbxl10 silencing by miR-448 was shown to increase glycolysis in gastric cancer, as Fbxl10 was discovered as a transcriptional repressor of Myc expression, portraying a tumour suppressive function[438]. Paradoxically, Fbxl10 has also been shown to induce a Myc transcriptional profile, this

time in a KRAS-mutated pancreatic cancer allograft model. In this case, Fbxl10 promoted the expression of genes involved in protein synthesis and OXPHOS and cooperated with KRAS to drive tumour progression[439]. The induction of OXPHOS by Fbxl10 is also reported to drive the development of leukaemia in transgenic mice[440]. Taken together, these data implicate Fbxl10 in an array of metabolic processes and suggest that its role in metabolism is tissue and context dependent.

Whilst much of the literature investigates the role of FBPs in regulating the Warburg effect, FBPs have also been implicated in mitochondrial function and this can have widespread consequences in disease. Cardiolipin synthase 1 (CLS1) catalyses the synthesis of cardiolipin, a lipid found on the inner mitochondrial membrane. Fbxo15 ubiquitinates CLS1 in response to phosphorylation by PINK1, resulting in impaired cardiolipin synthesis and disrupted mitochondrial function, and this can result in acute lung injury with *Staphylococcus aureus* infection[441]. Fbxl7 overexpression can also damage mitochondria resulting in depolarisation, reduced ATP output, and ultimately apoptosis. This toxic effect is via increased proteasomal degradation of the Fbxl7 target survivin, which is important for mitochondrial bioenergetics[442]. Interestingly, survivin expression is associated with poor prognosis in many cancers[443], suggesting Fbxl7 and reduced mitochondrial output may restrict cancer progression.

The regulation of metabolism by FBPs is a phenomenon that is evolutionarily conserved, and examples can also be found in yeast. One example is Grr1 in *Saccharomyces cerevisiae* which is broadly involved in regulating the switch from glycolysis to gluconeogenesis. When high levels of glucose are sensed, Grr1 ubiquitinates its substrates to ultimately induce expression of glucose transporter genes and genes involved in carbon assimilation[444]. Conversely, after glucose depletion, Grr1 ubiquitination of Tye7 (a transcription factor for glycolytic genes) and PFK27 (a glycolysis second messenger equivalent to mammalian PFK2) dampen glycolysis[445]. Mdm30 is another FBP which works in opposition to Grr1 to fine-tune the transcription of genes involved in galactose assimilation, and in conjunction with FBP Mfb1 to regulate mitochondrial function[444].

The significance of FBPs in several metabolic pathways is evident, and they provide a mechanism to rapidly adjust metabolic output to intrinsic and extrinsic signals, such as to support cell cycle progression or respond to cellular stress. The use of small molecules to inhibit FBPs in cancer therapy is already established[446] and recent examples show promise in targeting FBPs to modulate metabolism, such as a novel Skp2 inhibitor which restricts tumour growth in a mouse colorectal cancer xenograph model, partly by the downstream inhibition of HK2 and reduced glycolysis[447]. Whilst the cells metabolic network is extensive and its effects may be complex and difficult to dissect, research into mechanisms of metabolic regulation continues to build our understanding and reveal novel therapeutic avenues to target metabolism in disease.

Thesis aims

1..9 Characterising a role for Fbxo7 in metabolism

Fbxo7 is involved in multiple cellular processes via SCF-dependent and independent functions. Of particular significance is the ability of Fbxo7 to bind Cdk6 and promote the assembly of Cdk6-cyclin D complexes. Prior to this PhD, Wang, et al.[304] described a pro-survival role for Cdk6 in T-ALL cells via the phosphorylation and inhibition of the glycolytic enzyme PFKP, to ultimately reduce glycolysis and buffer oxidative stress. We therefore hypothesised that Fbxo7, as a Cdk6 scaffolding protein, may also function in glycolytic regulation. This was further supported by data from a yeast two-hybrid screen which identified the C-terminus of PFKP as an Fbxo7 binding partner.

To investigate a role for Fbxo7 in metabolism I planned to validate PFKP as a substrate for Fbxo7 and to explore the reliance of their interaction on Cdk6. I subsequently sought to explore the downstream effects of Fbxo7 on the metabolism and function of T-ALL cells and primary $CD4^+$ T cells from an Fbxo7-deficient mouse.

Since feedback loops in glucose signalling are commonplace in metabolic networks, I also hypothesised that Fbxo7 may be subject to regulation by glucose availability. Consequently, I set out to determine whether Fbxo7 is regulated by metabolic or oxidative stress; to outline the mechanisms by which this may occur; and to explore whether the loss of Fbxo7 would increase the sensitivity of cells to such stresses.

1..10 Investigating CRBN as a substrate for Fbxo7

CRBN is the primary target for IMiDs and its expression correlates with improved clinical outcomes, with *CRBN* mutations or depletion contributing to IMiD resistance. In the context of intellectual disability, Song, et al.[137] reported that mutant CRBN may be redirected to SCF^{Fbxo7} for polyubiquitination and proteasomal degradation. We therefore hypothesised that Fbxo7 may modulate CRBN to affect IMiD sensitivity. To test this theory, I wanted to establish whether WT CRBN is a substrate for ubiquitination by Fbxo7 and its effect on CRBN stability. I sought to investigate the effect of the IMiD, lenalidomide, on Fbxo7 and CRBN proteins, and to ascertain whether the loss of Fbxo7 altered MM cell sensitivity to lenalidomide.

CHAPTER 2

Materials and Methods

Cell culture and analysis

2..1 Standard cell culture

Cells were maintained in culture medium as detailed in Table 2.1, supplemented with heat-inactivated fetal bovine serum (FBS) (Gibco) and 100 U/mL penicillin and streptomycin (P/S) (Gibco), and were incubated at 37°C in a humidified 5% CO_2 atmosphere. Cells were sub-cultured every 2-3 days to ensure adherent cells were <90% confluent, and suspension cells were at a density of $0.4x10^6$ to $1x10^6$ cells/mL. Where viral vector selection was required, normal culture medium was supplemented with 2 µg/mL puromycin (Sigma). To vary glucose concentration, cells were cultured in RPMI or DMEM without glucose, supplemented with 10% FBS, 100 U/mL penicillin and streptomycin, and glucose solution (Thermo Scientific) as required.

Table 2.1: Cell lines and standard culture media used.

Cell line	Species	Cell type	Properties	Medium
CCRF-CEM	Human	Acute lymphoblastic leukaemia	Suspension	RPMI-1640 + 10% serum
MOLT-4	Human	Acute lymphoblastic leukaemia	Suspension	RPMI-1640 + 10% serum
Jurkat E6	Human	Acute T cell leukaemia	Suspension	RPMI-1640 + 10% serum
HEK293T	Human	Embryonic kidney	Adherent	DMEM + 10% serum
Phoenix-ECO	Human	HEK293T based retrovirus producer line	Adherent	DMEM + 10% serum
OPM2	Human	Multiple myeloma	Suspension	RPMI-1640 + 10% serum
MM1S	Human	Multiple myeloma	Mixed	RPMI-1640 + 10% serum
U266	Human	Multiple myeloma	Suspension	RPMI-1640 + 10% serum
Nalm6	Human	B cell precursor leukaemia	Suspension	RPMI-1640 + 10% serum

2..2 Drug treatment

Where indicated, cells were treated with 10 µM or 25 µM MG132 (Sigma), 200 nM bafilomycin A1 (BafA) (Santa Cruz Biotechnology), 100 µg/mL cycloheximide (CHX) (Sigma), 1 µM palbociclib (Sigma), 1-10 µM lenalidomide (Insight Biotechnology), or 0.1 µM Cdk6 PROTAC for the indicated durations. Control samples were treated with the appropriate vehicle control. Cdk6 PROTAC 1 was kindly provided by Sarbjit Singh and Amarnath Natarajan (Eppley Institute for Cancer Research, University of

Nebraska)[448], Cdk6 PROTAC 2 was kindly provided by Yu Rao and Zimo Yan (School of Pharmaceutical Sciences, Tsinghua University)[449].

2..3 Transient transfection of adherent cells

8-24 hours prior to transfection, cells were seeded so that they reached 50-80% confluency at the time of transfection. DNA was diluted in Opti-MEM reduced serum media (Gibco), and polyethylenimine (PEI) (Polysciences) or FuGENE (Promega) transfection reagent was added at a ratio of 3 µL/µg DNA. The mix was vortexed, incubated for 15 min at room temperature (RT) and added dropwise to cells. A maximum of 10 µg DNA was added to 90 mm dishes, 4 µg to 60 mm dishes, and 1.5 µg to 6 well plates. Within each experiment, the DNA added to each dish was normalised by the addition of an equivalent empty vector construct. Cells were harvested 48 hours after transfection.

2..4 siRNA transfection with Lipofectamine RNAiMAX

8-24 hours prior to transfection, HEK293T cells were seeded in a 60 mm dish in 2 mL DMEM containing 5% FBS and without P/S antibiotics so they were 50-80% confluent at the time of transfection. Suspension cells were sub-cultured in RPMI containing 5% FBS and without P/S antibiotics so that they would be at approximately $0.7x10^6$/mL at the time of transfection. 10 µL Lipofectamine RNAiMAX (Thermo Scientific) transfection reagent and 1.5 µL siRNA (at 100 µM) were each added to 250 µL Opti-MEM in separate tubes, and incubated for 5 min at RT. The contents of the two tubes were gently mixed and incubated for a further 15 min at RT before being added dropwise to cells. The final concentration of siRNA was 60 nM. A minimum of 12 hours later, media was replaced to contain 10% FBS. When further DNA transfection was required, cells were transfected as in section 2.3, 24 hours after siRNA delivery. Cells were harvested for analysis 48 hours after siRNA transfection.

Fbxo7 siRNA sequence: UACCCGAUUUACAAUUACAUU.

2..5 Electroporation of suspension cells

Suspension cells were electroporated using the Neon Transfection System 100 µL Kit (Thermo Scientific), mostly as per manufacturer's instructions. Briefly, suspension cells were washed in PBS and resuspended in Resuspension Buffer R or alternative sucrose-based buffer[450] (250 mM sucrose and 1 mM $MgCl_2$ in DPBS). DNA constructs or siRNA were added at the appropriate concentration, and cells were electroporated using 100 µL Neon Tips. Cell densities, DNA/siRNA concentrations and electroporation parameters are summarised in Table 2.2. Following electroporation, $1x10^6$ cells were immediately placed into 1 mL pre-warmed media without antibiotics, in a 24 well plate. Cells were harvested for analysis 48 hours after electroporation.

Table 2.2: Settings for electroporation of suspension cells using the Neon Transfection System.

Cell type	Transfection	Cell number / 100 µL tip	Electroporation parameters
CCRF-CEM	DNA, 5 µg	$2x10^6$	Pulse voltage: 1230 V Pulse width: 40 ms Pulse number: 1
MOLT-4	DNA, 5 µg	$2x10^6$	Pulse voltage: 1230 V Pulse width: 40 ms Pulse number: 1
U266	siRNA, 50 nM	$0.5x10^6$	Pulse voltage: 1650 V Pulse width: 20 ms Pulse number: 1
	siRNA, 100 nM	$0.5x10^6$	Pulse voltage: 1650 V Pulse width: 20 ms Pulse number: 1
	siRNA, 50 nM	$1x10^6$	Pulse voltage: 1050 V Pulse width: 30 ms Pulse number: 1
	siRNA, 100 nM	$1x10^6$	Pulse voltage: 1050 V Pulse width: 30 ms Pulse number: 1

2..6 Retroviral transduction of suspension cells for shRNA knockdown of Fbxo7

90 mm dishes of viral packaging cell line Phoenix-ECO were transfected with 3 µg retroviral plasmid of interest and 2 µg viral envelope VSVG using FuGENE reagent as described in section 2.3. 24 hours after transfection, the media was changed to that of the recipient cells, and recipient cells were sub-cultured so they would reach approximately $1x10^6$/mL following culture overnight. The following day the virus-containing conditioned media was removed from Phoenix-ECO cells, filtered through a 0.45 µm filter and 4 µg /mL polybrene was added. To transduce cells, $1x10^6$ recipient cells (approximately 1 mL volume) and 2 mL viral media were added to a 6 well plate and centrifuged at 2000 rpm for 30 minutes before being returned to the incubator. To repeat this process the following day, cells were harvested, pelleted by centrifugation, and resuspended in 1 mL fresh media. A further 2 mL conditioned viral media was added, and the centrifugation repeated. After the final infection, 1 mL fresh media was added to the cells, and they were incubated for 2-3 days prior to selection in puromycin. Fbxo7 shRNA sequence: CGCTGAGTCAATTCAAGATAAT.

2..7 Plasmids

Table 2.3: Plasmids used in this thesis.

Plasmid backbone	Insert	Tag	Selection	Use
MSCV	Empty	-	GFP and puromycin	Retroviral transduction
MSCV	Fbxo7 miR30 short hairpin	-	GFP and puromycin	Retroviral transduction
pcDNA3.1	Empty	-	-	Transfection
pcDNA3.1	Fbxo7 (1-522)	-	-	Transfection
pcDNA3.1	Fbxo7 (1-522)	FLAG (N-terminal)	-	Transfection
pcDNA3.1	Fbxo7 (ΔFbox)	FLAG (N-terminal)	-	Transfection
pcDNA3.1	Fbxo7 (R498X)	FLAG (N-terminal)	-	Transfection
pcDNA3.1	Fbxo7 (1-398)	FLAG (N-terminal)	-	Transfection
pcDNA3.1	Fbxo7 (89-522)	FLAG (N-terminal)	-	Transfection
pcDNA3.1	PFKP	-	-	Transfection
pcDNA3.1	PFKP	HA (N-terminal)	-	Transfection
pcDNA3.1	CRBN	FLAG (N-terminal)	-	Transfection
pcDNA3.1	Skp1	-	-	Transfection
pcDNA3.1	Rbx1	Myc (N-terminal)	-	Transfection
pcDNA3.1	Cullin1	-	-	Transfection
pCMV	Ubiquitin	6xHis-Myc (N-terminal)	-	Transfection

2..8 Cell cycle analysis

CCRF-CEM and MOLT-4 cells were incubated with 1 μM palbociclib or DMSO for 24 hours. Cells were harvested, washed in PBS, and slowly resuspended in ice-cold 70% ethanol by vortexing. Cells were fixed for at least 24 hours by incubating at 4^{o}C, washed in PBS, and stained with propidium iodide (PI) for 30 min. Samples were analysed on a Cytek DxP8 flow cytometer.

2..9 Use of experimental mice

All experiments in mice were performed in accordance with the UK Animals (Scientific Procedures) Act 1986 and ARRIVE guidelines. Animal licences were approved by the Home Office and the University of Cambridge's Animal Welfare & Ethical Review Body Standing Committee. Experiments were performed under Home Office licence PPL 70/9001. Fbxo7^{LacZ} mice (Fbxo7 tm1a(EUCOMM)Hmgu on a C57BL/6J background) were bred as heterozygous crosses. WT, heterozygous and homozygous littermates were harvested between 6-9 weeks. Where littermates were not available, mice of a similar age were compared. Both male and female mice were used for experiments.

2..10 Preparation of mouse tissue

The thymus, pancreas, liver and lung were harvested from WT Fbxo7^{LacZ} mice. The thymus was passed through a 40 µm cell strainer to obtain a single cell suspension. The pancreas, liver and lung were minced with a scalpel and incubated with 1 mL trypsin at 37^{o}C for 15-30 min, then passed through a 40 µm cell strainer. Cells from each tissue were divided into five cultures in RPMI media supplemented with 10% FBS and 100 U/mL P/S, and glucose or 100 µM hydrogen peroxide (H_2O_2) (Fisher Scientific) were added as indicated. Cells were incubated for 3 hours at 37^{o}C in a humidified 5% CO_2 atmosphere, before being harvested.

2..11 Murine CD4^{+} T cell isolation and activation

Spleens were harvested from WT, heterozygous or homozygous Fbxo7^{LacZ} mice and passed through a 40 µm cell strainer to obtain a single cell suspension. Cells were diluted to 1x10^{7}/mL in PBS and viable lymphocytes were separated with an equal volume of mouse Lympholyte® Cell Separation Media by centrifugation at 1250g for 20 minutes. CD4^{+} T cells were then isolated by negative selection using the MojoSort Mouse CD4 T Cell Isolation Kit (Biolegend). Briefly, splenocytes were resuspended to 1x10^{8}/mL in MojoSort Buffer, transferred to ice, and incubated for 15 min with 50 µL biotin-antibody cocktail/mL sample, followed by 50 µL streptavidin nanobeads/mL sample for a further 15 min. Tubes were incubated on a magnet for 5 min at RT to remove labelled cells and the supernatant was removed. Streptavidin-nanobeads were washed in MojoSort Buffer and incubated on the magnet for 5 min for a second separation. The two unlabelled fractions were pooled. Isolated CD4^{+} T cells were seeded at 1x10^{6} /mL in RPMI supplemented with 10% FBS, 100 U/mL P/S and 5 µM β-mercaptoethanol (β-ME) (Merck). To activate, cells were added to plates coated with 2 µg/mL α-CD3 (clone 145-2C11) and containing 2 µg/mL soluble α-CD28 (clone 37.51) and incubated for the indicated duration. Where indicated, 40 ng/mL IL-2 was added 48 hours after T cell activation to maintain cells in culture.

2..12 Flow cytometry analysis of murine T cells

Cell viability and activation were measured by flow cytometry. $1x10^6$ cells were Fc blocked with α-CD16/32 (eBioscience) in FACS buffer (1% BSA in PBS) for 10 min on ice, then stained with 0.5 µL each of α-CD4 PE (clone GK1.5, eBioscience), α-CD25 PE-Cy7 (clone H1.2F3, Biolegend) and α-CD69 FITC (clone H1.2F3, eBioscience), and Fixable Viability Dye eFluor 780 (eBioscience) at 1:5000, for 30 min on ice in the dark. Cells were washed twice in cold FACS buffer and either analysed immediately or fixed in 2% paraformaldehyde (PFA) in PBS for 15 min at RT, then washed once in FACS buffer before being stored at 4°C. Samples were analysed on a CytoFLEX S flow cytometer.

2..13 Intracellular ROS detection

At time intervals following *in vitro* activation of murine $CD4^+$ T cells, cells were harvested, washed with PBS, and incubated at $1x10^6$ cells/mL in PBS containing 5 µM 2',7'-Dichlorofluorescin diacetate (H_2DCFDA) (Sigma) for 45 min in the dark at 37°C. Cells were washed twice in PBS, stained with propidium iodide (PI) and the fluorescence signal was analysed on a CytoFLEX S flow cytometer.

2..14 Seahorse extracellular flux analysis

Human T cell lines and purified $CD4^+$ T cells from mice were analysed using the Seahorse XF Glycolytic Rate Assay Kit (Agilent). 24 hours prior to the assay, a Seahorse XF96 Cell Culture Microplate (Agilent) was coated with 25 µL of 22.4 µg/mL Cell-Tak solution (Corning) and incubated for 20 min at RT. The wells were washed twice using 200 µL sterile water and left to dry at RT prior to storing the plate at 4°C overnight. The XFe96 Sensor Cartridge (Agilent) was hydrated with sterile water and incubated, alongside an aliquot of Seahorse XF Calibrant (Agilent), at 37°C overnight in a non-CO_2 incubator. On the day of the assay, the sterile water in the XFe96 Sensor Cartridge was replaced with warm Seahorse XF Calibrant and allowed to equilibrate for at least 1 hour at 37°C in a non-CO_2 incubator. Cells were harvested and resuspended in warm Seahorse XF RPMI medium (Agilent), supplemented with 2 mM glutamine (Thermo Scientific), 10 mM glucose (Thermo Scientific) and 1 mM pyruvate (Thermo Scientific), at pH 7.4. Cells were plated into the Cell-Tak-coated Seahorse XF96 Cell Culture Microplate (Agilent) at $3x10^5$ cells/well, briefly centrifuged to adhere, and incubated at 37°C for 45-60 min in a non-CO_2 incubator. Cells were analysed using the Seahorse XF Glycolytic Rate Assay Kit (Agilent) with of 0.5 µM rotenone/antimycin A (Rot/AA) and 50 mM 2-deoxy-D-glucose (2-DG). The assay was run at 37°C on a Seahorse XF96 analyser (Agilent) and data was analysed using Wave software (Agilent)

2..15 Metabolite extraction

For metabolite profiling, murine $CD4^+$ T cells were isolated and activated in a 12 well plate for 48 hours. For ^{13}C stable isotope tracing, murine $CD4^+$ T cells were isolated and activated in a 12 well plate with culture media containing 2 g/L D-Glucose-1,2- $^{13}C_2$ (Sigma) for 24 hours. To extract metabolites, cells

were harvested, washed twice in PBS and resuspended in 200 µL ice cold metabolite extraction solution (50% LC–MS grade methanol, 30% LCMS grade acetonitrile, 20% ultrapure water, 5 µM valine-d8 as internal standard) per $1x10^6$ cells. Cells were incubated in a dry ice-methanol bath for 20 min, then at 4°C with shaking for 15 min. Samples were centrifuged at 13000 rpm for 20 min and the supernatant was collected into autosampler vials for LC-MS analysis.

2..16 Metabolite measurement by LC-MC

Kindly performed by Dr Ming Yang.

LC-MS chromatographic separation of metabolites was achieved using a Millipore Sequant ZICpHILIC analytical column (5 µm, 2.1 × 150 mm) equipped with a 2.1 × 20 mm guard column (both 5 mm particle size) with a binary solvent system. Solvent A was 20 mM ammonium carbonate, 0.05% ammonium hydroxide; Solvent B was acetonitrile. The column oven and autosampler tray were held at 40°C and 4°C, respectively. The chromatographic gradient was run at a flow rate of 0.200 mL/min as follows: 0–2 min: 80% B; 2-17 min: linear gradient from 80% B to 20% B; 17-17.1 min: linear gradient from 20% B to 80% B; 17.1-22.5 min: hold at 80% B. Samples were randomized and analysed with LC–MS in a blinded manner with an injection volume of 5 µl. Pooled samples were generated from an equal mixture of all individual samples and analysed interspersed at regular intervals within sample sequence as a quality control. Metabolites were measured with a Thermo Scientific Q Exactive Hybrid Quadrupole-Orbitrap Mass spectrometer (HRMS) coupled to a Dionex Ultimate 3000 UHPLC. The mass spectrometer was operated in full-scan, polarity-switching mode, with the spray voltage set to +4.5 kV/-3.5 kV, the heated capillary held at 320°C, and the auxiliary gas heater held at 280°C. The sheath gas flow was set to 25 units, the auxiliary gas flow was set to 15 units, and the sweep gas flow was set to 0 units. HRMS data acquisition was performed in a range of m/z = 70–900, with the resolution set at 70,000, the AGC target at $1x10^6$, and the maximum injection time at 120 ms. Metabolite identities were confirmed using two parameters: (1) precursor ion m/z was matched within 5 ppm of theoretical mass predicted by the chemical formula; (2) the retention time of metabolites was within 5% of the retention time of a purified standard run with the same chromatographic method.

2..17 Metabolomics data analysis

Kindly performed by Dr Ming Yang and Dr Christina Schmidt.

Chromatogram review and peak area integration were performed using the Thermo Fisher software Tracefinder (v.5.0). Correction for natural abundance was performed using the Accucor Package (v.0.2.3)[451] and the fractional enrichment was visualised using stacked bar graphs. For the total pools, the peak area for each detected metabolite was subjected to the “Filtering 80% Rule”, half minimum missing value imputation, and normalized against the total ion count (TIC) of the sample to correct

any variations introduced from sample handling through instrument analysis. Sample were excluded after performing testing for outliers based on geometric distances of each point in the PCA score analysis as part of the muma package (v.1.4)[452]. Afterwards, PCA analysis was performed using the R base package stats (v.4.0.5) (https://www.r-project.org/) with the function prcomp and visualised using the autoplot function of ggplot2 (v.3.3.3)[453] after loading the ggfortify package (v.0.4.11)[454,455]. Differential metabolomics analysis was performed using the R package "gtools"(v.3.8.2) (https://cran.r-project.org/web/packages/gtools/index.html) to calculate the Log2FC using the functions "foldchange" and "foldchange2logratio" (parameter base=2) . The corresponding p-value was calculated using the R base package stats (v.4.0.5) with the function "t.test" (SIMPLIFY = F). Volcano plots were generated using the EnhancedVolcano package (v. 1.8.0)[456].

Biochemistry

2..18 Cell lysis

Cells were harvested, washed in PBS, resuspended in an appropriate volume of lysis buffer and kept on ice. Cells were lysed in the required buffer supplemented with 1 mM sodium fluoride (Sigma), 0.1 mM sodium orthovanadate (Sigma), 1X protease inhibitor cocktail (Sigma), 1 mM phenylmethylsulfonyl fluoride (PMSF) (AppliChem), and, where appropriate, 5 mM N-Ethylmaleimide (NEM) (Sigma) to inhibit deubiquitinating enzymes. For lysis in RIPA or KCl buffers, cells were incubated on ice for 30 min with periodic vortexing. For lysis in tween lysis buffer, cells were disrupted with mild sonication (2 x 5 sec at power level 6) using a Branson sonifier microtip. All lysates were clarified by centrifugation at 13000 rpm for 20 min at 4°C and the supernatant was transferred to a clean tube. Protein concentration was measured by BCA assay (Pierce) according to the manufacturer's instructions, and samples were normalised accordingly.

2..19 Immunoblotting

Samples were mixed with an equal volume of 2X Laemmli loading dye and incubated for 5 min at 95°C to denature the proteins. Denatured samples were run alongside Precision Plus Protein™ Dual Color Standards (Bio-Rad) on an SDS-PAGE gel in Tris-Glycine running buffer (Geneflow), and then transferred to PVDF membranes (Millipore) using a Bio-Rad semi-dry transfer cell. Membranes were blocked with 5% milk in 0.05% PBS-T for 1 hour at RT and probed with primary antibody in 5% milk/PBS-T overnight at 4°C. Membranes were washed 3 x 5 min in PBS-T, incubated with secondary antibody in 5% milk/PBS-T for 1 hour at RT, and then washed a further 3 x 5 min in PBS-T. Bands were detected using ECL Western Blotting Detection Reagents (GE Healthcare), Pierce™ SuperSignal™ West Pico PLUS Chemiluminescent Substrate (Thermo Scientific) or Immobilon Western Chemiluminescent HRP Substrate (Merck Millipore) and exposed on a film (FujiFilm or Konica) or captured using a Syngene G:BOX Chemi-XRQ instrument. Signals were analysed using ImageJ software and normalised by the loading control.

2..20 Immunoprecipitation

Cells were transfected and lysed as described in sections 2.3 and 2.18. Cells were lysed in KCl lysis buffer for α-FLAG immunoprecipitation (IP), RIPA lysis buffer for α-HA IP, and tween lysis buffer for α-Fbxo7 and α-Cdk6 IP. A 40 µL aliquot of total lysate was removed from each sample and stored at -20°C. For anti-FLAG and anti-HA immunoprecipitation (IP), the remaining lysate was incubated with either pre-washed 12.5 µL 80% anti-FLAG® M2 Affinity Gel (Sigma) or 30 µL anti-HA agarose (Sigma) for 4 hours at 4°C with rotation. For IPs with other antibodies, lysates were cleared with 10 µL pre-washed Protein A/G PLUS-Agarose (Santa Cruz) for 30 min at 4°C with rotation. The cleared lysates

were transferred to a fresh tube and incubated with antibody for 1 hour at 4°C with rotation, then 20 µL Protein A/G PLUS-Agarose was added and samples were incubated for a further 2 hours. Beads were washed 4 times in lysis buffer and resuspended directly in 20-40 µL 2X Laemmli loading buffer.

2..21 Antibodies

Table 2.4: Immunoblot and immunoprecipitation antibodies used in this thesis.

Antibody	Species	Supplier	Use	Dilution
Fbxo7	Rabbit polyclonal	In-house[67]	Immunoblot	1:1000
Fbxo7	Mouse monoclonal	Santa Cruz (sc-271763)	Immunoblot	1:500
Fbxo7	Rabbit polyclonal	Aviva (ARP43128_P050)	Immunoprecipitation	1 µg
PFKP	Rabbit monoclonal	Cell Signalling (8164)	Immunoblot	1:1000
PFKP	Rabbit polyclonal	Abcam (ab233109)	Immunoblot	1:1000
Cdk6	Rabbit polyclonal	Santa Cruz (sc-177)	Immunoblot Immunoprecipitation	1:1000 0.4 µg
Cdk6	Rabbit monoclonal	Cell Signalling (13331)	Immunoblot	1:1000
HA	Rabbit monoclonal	Cell Signalling (3724)	Immunoblot	1:1000
Myc	Rabbit polyclonal	Cell Signalling (2272)	Immunoblot	1:1000
FLAG	Mouse monoclonal	Sigma (F3165)	Immunoblot	1:5000
Skp1	Mouse monoclonal	BD (610530)	Immunoblot	1:1000
Cul1	Rabbit polyclonal	Santa Cruz (sc-11384)	Immunoblot	1:1000
p-Rb (Ser780)	Rabbit monoclonal	Cell Signalling (8180)	Immunoblot	1:1000
GAPDH	Rabbit polyclonal	Sigma (G9545)	Immunoblot	1:5000
Actin	Rabbit polyclonal	Sigma (A2066)	Immunoblot	1:5000
Tubulin	Mouse monoclonal	Sigma (T6557)	Immunoblot	1:2000
-	Rabbit IgG	Merck (12-370)	Immunoprecipitation	
Anti-Mouse	Donkey	Jackson Lab (715-035-151)	Immunoblot (secondary antibody)	1:5000
Anti-Rabbit	Donkey	Jackson Lab (711-035-152)	Immunoblot (secondary antibody)	1:10000

2..22 Purification and quantification of SCF complexes

HEK293T cells were transfected with plasmids encoding Skp1, Cullin1 and Myc-Rbx1, alongside the appropriate FLAG-Fbxo7 construct. 48 hours after transfection, cells were harvested and lysed in KCl lysis buffer and SCF complexes were purified by anti-FLAG IP, as described in section 2.20. After the incubation, beads were washed 3 times in lysis buffer and twice in elution buffer, and protein was eluted with 20 µL 100 µg/mL FLAG peptide (Sigma) for 1-2 hours at 4°C with rotation. Beads were pelleted, and the eluate was removed and stored at -20°C in 15% glycerol. The purified SCF complexes were resolved by SDS-PAGE alongside known BSA standards, stained with Coomassie Blue (Generon), and quantified based on the Fbxo7 and cullin1 band density using ImageJ software. Purified complexes were also run on a second SDS-PAGE to western blot for each component.

2..23 In vitro ubiquitination assays

To purify substrate for *in vitro* ubiquitination, HEK293T cells were transfected with 5 µg HA-PFKP which was immunoprecipitated with anti-HA agarose 48 hours after transfection, as described in section 2.20. After the incubation, beads were washed 3 times in lysis buffer and twice in elution buffer, and protein was eluted with 30 µL 300 µg/mL HA peptide (Sigma) for 1-2 hours at 4°C with rotation. Beads were pelleted, and the eluate was removed and stored at -20°C in 15% glycerol. For the *in vitro* ubiquitination assay, a ubiquitin mix was prepared with 100 nM E1 (UBE1, Bio-Techne), 500 nM E2 (UbcH5a, Bio-Techne), 20 µM human recombinant ubiquitin (Santa Cruz) and 2 mM ATP (Bio-Techne) in 1X ubiquitin conjugation reaction buffer (Bio-Techne). This was incubated for 5 min at RT then added to 100 nM SCF and 1 µL HA-PFKP substrate and incubated for 1 hour at 30°C. The entire 10 µL reaction was mixed with an equal volume of 2X Laemmli loading buffer, resolved by SDS-PAGE and analysed by immunoblotting.

2..24 In cellulo ubiquitination assays

HEK293T cells were transfected with His-tagged ubiquitin, PFKP, and FLAG-Fbxo7 constructs, and cells were treated with 25 µM MG132 for 4 hours prior to lysis. Cells were harvested and a 10% portion was lysed in RIPA buffer as the total lysate sample. The remaining cells were resuspended in Co-NTA lysis buffer, disrupted with mild sonication (2 x 10 sec at power level 6) using a Branson sonifier microtip, and clarified by centrifugation at 13000 rpm for 20 min at 4°C. This supernatant was added to 50 µL of pre-washed Super Cobalt NTA Agarose Affinity Resin (Generon) and incubated for 4 hours at 4°C with rotation. The beads were washed once in Co-NTA lysis buffer, once in Co-NTA wash buffer, and twice in Co-NTA wash buffer containing 0.1% Triton-X 100 (VWR), with an incubation of 5 min at RT between each wash. Proteins were eluted in 50 µL Co-NTA elution buffer for 20 min at RT with shaking. Both lysate and eluate were resolved by SDS-PAGE and analysed by immunoblotting.

2..25 Cdk6 biosensor assay

CCRF-CEM cells were collected and lysed in lysis buffer (PBS, 0.2% NP-40, 1 mM EDTA, protease inhibitor cocktail (Sigma) and 2 mM PMSF. Note: No phosphatase inhibitors). Cells treated with 1 µM palbociclib (Sigma) for 24 hours were used as a control. 60 µg protein was plated into a 96 well Fluotrac™ 200 plate (Greiner) in triplicate. The assay was performed in 200 µL PBS supplemented with 5 mM $MgCl_2$ and 0.5 mM ATP, and 200 nM Cdk6 peptide biosensor kindly provided by May Morris (Institut des Biomolécules Max Mousseron, University of Montpellier)[457]. Changes in fluorescence emission of the TAMRA-labelled peptide biosensor were recorded at 30°C on a FLUOstar Omega (BMG) (excitation 560 nm / emission 590 nm). Biosensor fluorescence was subtracted from the samples containing protein lysate, and relative fluorescence was calculated.

2..26 200 kDa cut-off ultrafiltration

$5x10^7$ CCRF-CEM cells were collected per sample and lysed in lysis buffer (25 mM Tris-HCl pH 7.5, 150 mM NaCl, 1 mM EDTA, 5% glycerol, 1% NP-40, 10 mM β-glycerophosphate) with a protease inhibitor cocktail (Sigma) and other inhibitors (1 mM PMSF, 10 mM NaF, 1 mM Na_3VO_4). 1 mM AMP (Acros Organics) or 10 mM citrate (Sigma) were also added to the lysis buffer as controls where indicated. Equal amounts of protein were filtered using the Disposable Ultrafiltration Units with molecular weight 200 kDa cut-off (USY-20, Advantec MFS). 30 µg of total lysate or filtrate (<200 kDa) were resolved by SDS-PAGE and immunoblotted with the indicated antibodies.

Molecular biology

2..27 Genotyping PCR

Ear biopsy samples were collected and digested in Chelex solution (10% Chelex 100 resin (Bio-Rad), 0.1% Tween-20, 20 µg proteinase K (Sigma)) for 45 min at 50°C. Proteinase K was inactivated by a subsequent incubation for 30 min at 95°C. 1 µL genomic DNA was added to a PCR master mix of 1X OneTaq® Quick-Load® Master Mix (NEB), 0.4 µM forward primer, 0.2 µM WT reverse primer and 0.2 µM transgenic reverse primer (sequences in Table 2.7) and amplified by PCR as detailed in Table 2.5. The reaction amplifying the WT allele produces a 197 bp product, whereas the reaction amplifying the transgene produces a 362 bp product. PCR products were separated by electrophoresis in a TAE agarose DNA gel with 1X SYBR Safe DNA Gel Stain (Invitrogen), and bands imaged on a Syngene G:BOX Chemi-XRQ instrument.

Table 2.5: Genotyping PCR cycling conditions.

Temperature	Time	Cycles
92°C	5 min	1
92°C	30 sec	35
62°C	30 sec	
72°C	30 sec	
72°C	5 min	1
4°C	∞	

2..28 RNA extraction and cDNA synthesis

RNA was extracted from $7x10^6$ cells using the RNeasy Plus Mini Kit (Qiagen) according to the manufacturer's instructions. Cells were homogenised by passing 6 times through a 21-gauge needle and passed through a gDNA eliminator spin column prior to RNA extraction. RNA concentration was measured by A260nm on a Nanodrop ND-1000 spectrometer. 1 µg RNA was used to synthesise cDNA in a 20 µL reaction volume using the QuantiTect Reverse Transcription Kit (Qiagen) according to the manufacturer's instructions. Controls without reverse transcriptase were included to check for genomic DNA contamination.

2..29 qRT-PCR

qRT-PCR reactions were performed in triplicate by creating a mix of 1X SYBR® Green JumpStart™ Taq ReadyMix™ (Sigma), 0.4 µM primers (as listed in Table 2.7), and 2 µL cDNA (diluted 1:2). Reactions were run on an Eppendorf Mastercycler® ep realplex instrument as detailed in Table 2.6. Relative gene expression was calculated using the Pfaffl analysis method[458] with normalisation to housekeeping genes (actin, cyclophilin and HPRT).

Table 2.6: qRT-PCR cycling conditions.

Temperature	Time	Cycles
95°C	2 min	1
95°C	15 sec	45
58°C	20 sec	
72°C	15 sec	
76°C	8 sec	
Read		
Melt curve analysis from 65°C to 95°C to confirm product specific amplification		

2..30 Primers

Table 2.7: Primer sequences used in this thesis (5' to 3').

Description	Forward primer	Reverse primer
Mouse Fbxo7^{LacZ} Genotyping PCR	CAGGATCAGGGAACGCCTGT	WT: TGCAGGGTGAATAGCACTTCC Transgene: CACAACGGGTTCTTCTGTTAGTCC
Human Fbxo7 qRT-PCR	TTCCSGGACCTAACCCCATCTT	CGACCCCTGCTGGGTCTAA
Human Actin qRT-PCR	CACCATTGGCAATGAGCGGTTC	AGGTCTTTGCGGATGTCCACGT
Mouse Fbxo7 qRT-PCR	GCAGCCAAAGTGTACAAAG	AGGTTCAGTACTTGCCGTGTG
Mouse Actin qRT-PCR	KiCqStart® mouse M1_Actb	
Mouse Cyclophilin qRT-PCR	CCTTGGGCCGCGTCTCCTT	CACCCTGGCACATGAATCCTG
Mouse HPRT qRT-PCR	KiCqStart® mouse M1_Hprt	

Buffers and solutions

Table 2.8: Formulations of buffers and solutions used in this thesis.

Buffer	Use	Formulation
Sucrose based buffer	Neon electroporation	DPBS, 250 mM sucrose, 1 mM $MgCl_2$
FACS buffer	Flow cytometry	1X PBS, 1% BSA
Metabolite extraction solution	Metabolite extraction	50% LC–MS grade methanol, 30% LCMS grade acetonitrile, 20% ultrapure water, 5 µM valine-d8 as internal standard
RIPA lysis buffer	Cell lysis	50 mM Tris-HCl pH 7.5, 150 mM NaCl, 1% NP-40, 0.1% SDS, 0.5% sodium deoxycholate
KCl lysis buffer	Cell lysis	50 mM Tris-HCl pH 7.5, 225 mM KCl, 1% NP-40
Tween lysis buffer	Cell lysis	50 mM HEPES pH 7.5, 150 mM NaCl, 1 mM EDTA, 2.5 mM EGTA, 10% glycerol, 1 mM DTT, 0.1% Tween-20, 10 mM β-glycerophosphate
2X Laemmli loading dye	Gel electrophoresis	125 mM Tris pH 6.8, 4% SDS, 20% glycerol, 0.02% bromophenol blue, 10% β-ME
PBS-T	Immunoblot	PBS, 0.05% Tween-20
Elution buffer	FLAG and HA-tagged protein elution	10 mM HEPES, 225 mM KCl, 1.5 mM $MgCl_2$, 0.1% NP-40
Co-NTA lysis buffer	*In cellulo* ubiquitination assay	6 M guanidinium-HCl, 100 mM Na_2HPO_4/NaH_2PO_4, 10 mM Tris-HCl pH 8, 5 mM imidazole, 10 mM β-ME
Co-NTA wash buffer	*In cellulo* ubiquitination assay	8 M urea, 100 mM Na_2HPO_4/NaH_2PO_4, 10 mM Tris-HCl pH 6.8, 5 mM imidazole, 10 mM β-ME
Co-NTA elution buffer	*In cellulo* ubiquitination assay	200 mM imidazole, 150 mM Tris-HCl pH 6.8, 30% glycerol, 5% SDS, 720 mM β-ME
Specialised lysis buffer	Cdk6 biosensor assay	PBS, 0.2% NP-40, 1 mM EDTA
Specialised lysis buffer	200 kDa cut-off ultrafiltration	25 mM Tris-HCl pH 7.5, 150 mM NaCl, 1 mM EDTA, 5% glycerol, 1% NP-40, 10 mM β-glycerophosphate
Chelex solution	Genomic DNA extraction	10% chelex 100 resin, 0.1% Tween-20, 20 µg proteinase K

Data analysis and statistics

2..31 Cancer gene dependency scores

This thesis used DepMap 21Q3 dependency data for *FBXO7*, which had been generated from a CRISPR-Cas9 screen (available at https://depmap.org)[459]. Samples were grouped by their predefined lineage, and lineages with fewer than 5 cell lines were excluded from analyses. Final analyses included 1020 cell lines.

2..32 Quantification and statistical analysis

Immunoblot analyses were quantified using ImageJ processing software. All data are presented as mean ± standard deviation. Statistical differences were calculated using Student's two-tailed t tests with a significant cut-off of $p < 0.05$.

CHAPTER 3

Fbxo7 as a regulator of glycolysis and wider T cell metabolism

Introduction

Ubiquitination regulates an array of cellular processes including the cell cycle, DNA repair, differentiation, and metabolism. F-box proteins are the substrate-recruiting components of SCF E3 ubiquitin ligases and are therefore critical for the targeting of this post-translational modification (PTM). To date, Fbxo7 has been found to promote the ubiquitination of 12 substrates and only one-third of these ubiquitination events result in canonical proteasomal degradation[70,76,86,99], whilst the other substrates are stabilised, re-localised or have their activity altered by SCF^{Fbxo7} [74,77,80,81,89,460]. Fbxo7 also has SCF-independent functions, including binding to Cdk6 to scaffold the assembly of Cdk6-cyclin D complexes to promote cell cycle progression[67,101]. Cdk6 is of particular importance in hematopoietic cells and additional roles in regulating specific transcription factors and cellular functions have been reported in this lineage. This includes pro-survival activity in T acute lymphoblastic leukaemia (T-ALL) cells due to the phosphorylation and inhibition of glycolytic enzymes, including the rate-limiting gatekeeper, phosphofructokinase (PFKP)[304]. In this instance, phosphorylation of PFKP at S679 dissociates active PFKP tetramers to inhibit glycolysis and instead promote the pentose phosphate pathway (PPP) to buffer oxidative stress. Cdk6 inhibition with the small molecule kinase inhibitor palbociclib depletes NADPH and glutathione and sensitises T-ALL cells to oxidative stress-induced apoptosis, in a PFKP and PKM2 dependent manner (Fig. 3.0). This work, published just before the start of my PhD, piqued our interest due to the role of Fbxo7 in Cdk6 stabilisation, and suggested that Fbxo7 might play a part in metabolic regulation.

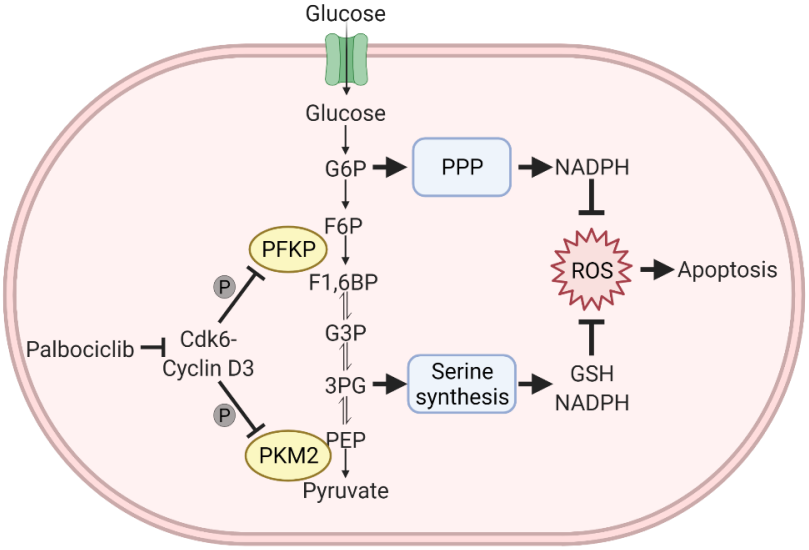

Figure 3.0: Regulation of glycolysis by Cdk6-cyclin D3.

Cdk6-cyclin D3 complexes can phosphorylate and inhibit two key glycolytic enzymes, PFKP and PKM2, to redirect metabolites into the pentose phosphate pathway (PPP) and serine synthesis pathways respectively. These biosynthetic pathways generate reducing molecules which neutralise detrimental reactive oxygen species (ROS). Inhibition of Cdk6 by palbociclib upregulates glycolysis and sensitises T-ALL cells to oxidative stress-induced apoptosis.

Amongst previous screens to identify Fbxo7-interacting proteins, a yeast two-hybrid (Y2H) assay was performed using aa 334-522 of Fbxo7, which spans the F-box domain and the substrate-binding proline rich region, as bait. A TaKaRa Mate & Plate™ human B and T cell cDNA library fused to a Gal4 activation domain was used as prey. 28 unique proteins were identified as candidate binding partners of Fbxo7, of which the C-terminus of PFKP was one (aa 385-784). This putative interaction between Fbxo7 and PFKP, alongside the regulation of PFKP by Cdk6, indicated that Fbxo7 may have a yet uncharacterised function in regulating glycolysis. In this chapter I aimed to validate the Y2H results and confirm whether PFKP is a ubiquitination substrate of Fbxo7 and explore the dependence of this mechanism on Cdk6. I then investigated the downstream effects of Fbxo7 on the metabolism and function of T-ALL cells and primary $CD4^+$ T cells from an Fbxo7-deficient mouse.

Results

3..1 PFKP is a substrate for ubiquitination by Fbxo7

To validate the interaction between Fbxo7 and PFKP in mammalian cells, I immunoprecipitated endogenous Fbxo7 from the T-ALL cell line, CCRF-CEM. Both isoforms 1 and 2 of Fbxo7 were isolated, at 70 kDa and 60 kDa respectively, and immunoblot analyses confirm the co-immunoprecipitation of PFKP, demonstrating a specific interaction between endogenous Fbxo7 and PFKP in these cells (Fig. 3.1).

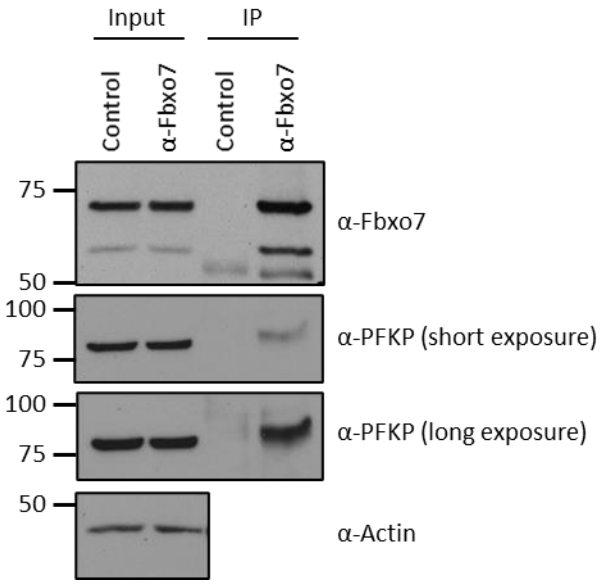

Figure 3.1: PFKP co-immunoprecipitates with endogenous Fbxo7 in CEM-CCRF cells. CEM cell lysates were immunoprecipitated with α-Fbxo7 or an isotype matched control antibody, followed by immunoblot analysis with the indicated antibodies. (n=2)

Since F-box proteins are the substrate-recruiting components of SCF-type E3 ligases, I next tested whether PFKP is a substrate for ubiquitination by SCF^{Fbxo7}. To generate SCF^{Fbxo7} ligases, HEK293T cells were transfected with N-terminally FLAG-tagged Fbxo7 constructs (WT, ΔFbox, and C-terminal truncation mutants R498X and 1-398) (Fig. 3.2A), alongside other SCF holoenzyme components Skp1, Cullin1 and Myc-tagged Rbx1. The resulting WT and mutant SCF E3 ubiquitin ligases were isolated by FLAG immunoprecipitation, quantified by Coomassie staining alongside BSA standards (Fig. 3.2B) and immunoblotted for the SCF subunits (Fig. 3.2C). Whilst WT Fbxo7, the pathogenic R498X mutation, and the 1-398 truncation all efficiently co-immunoprecipitated the other SCF subunits, Fbxo7-ΔFbox failed to form an SCF complex since the F-box domain is required to bind Skp1 and hence may be used as a negative control for subsequent assays.

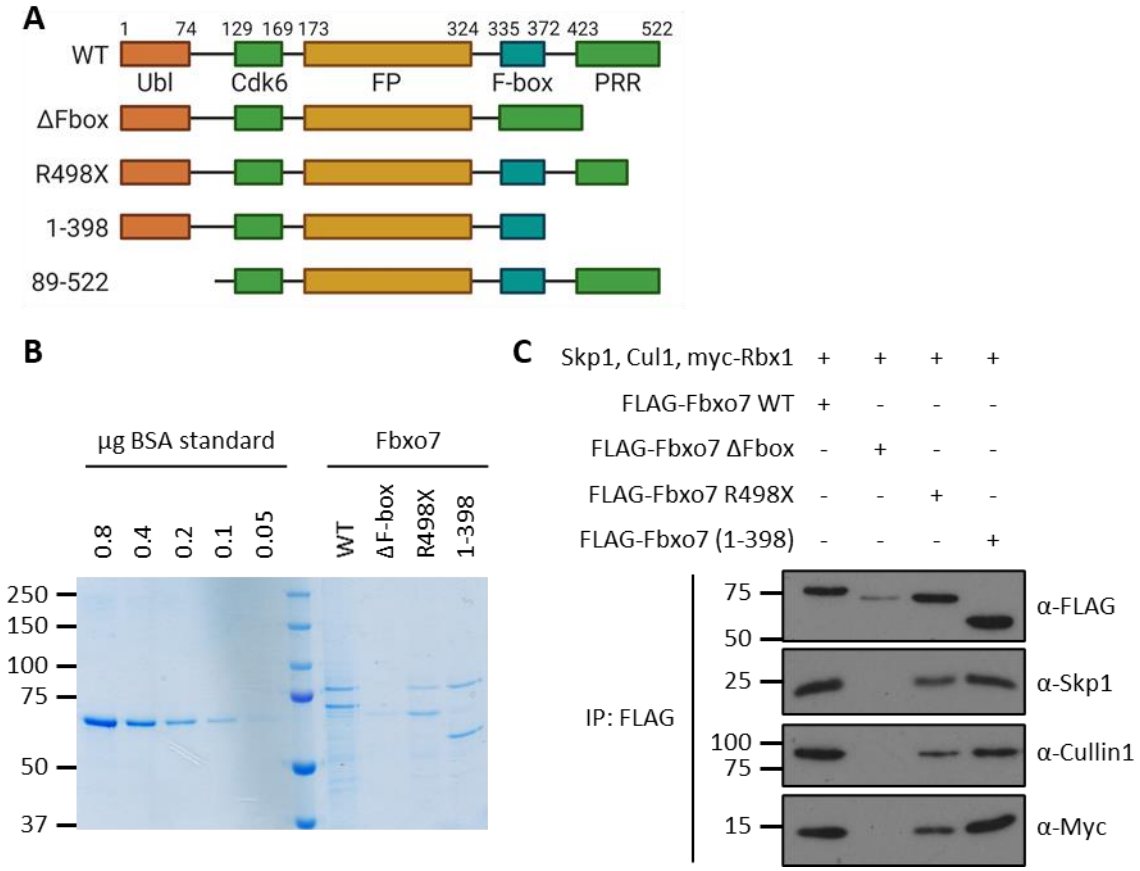

Figure 3.2: Purification of mutant SCF^{Fbxo7} complexes.

(A) Schematic of Fbxo7 constructs used to make SCF ligases and for *in cellulo* ubiquitination assays. All contain an N-terminal FLAG tag (not shown). Ubl: ubiquitin-like domain. Cdk6: Cdk6-binding domain. FP: Fbxo7-PI31 dimerization domain. PRR: proline rich region.

(B) & (C) FLAG-Fbxo7 constructs were transfected into HEK293T cells alongside Skp1, Cullin1 (Cul1) and myc-Rbx1, and SCF complexes were isolated by FLAG immunoprecipitation. Purified SCF ligases were (B) quantified by densitometry analysis of a Coomassie gel containing BSA standards, and (C) analysed by western blot to confirm the presence of SCF holoenzyme components.

In vitro ubiquitination assays were performed by mixing the SCF^{Fbxo7} complexes described in Fig.3.2, with HA-PFKP purified by immunoprecipitation from HEK293T cells, and a ubiquitin mix (Fig. 3.3A). Upon addition of SCF^{Fbxo7}, there is an increased smear of high molecular weight (MW) bands representing polyubiquitinated PFKP (Fig. 3.3, lane 8 vs. lane 6). As expected, this polyubiquitination was dependent on the F-box domain and SCF complex formation (Fig. 3.3, lane 9). Interestingly, neither of the C-terminally truncated Fbxo7 ligases promoted PFKP polyubiquitination (Fig. 3.3, lanes 10 & 11) despite the successful recruitment of SCF subunits (Fig. 3.2C), indicating the C-terminus of Fbxo7, as used in the Y2H, was required for PFKP ubiquitination.

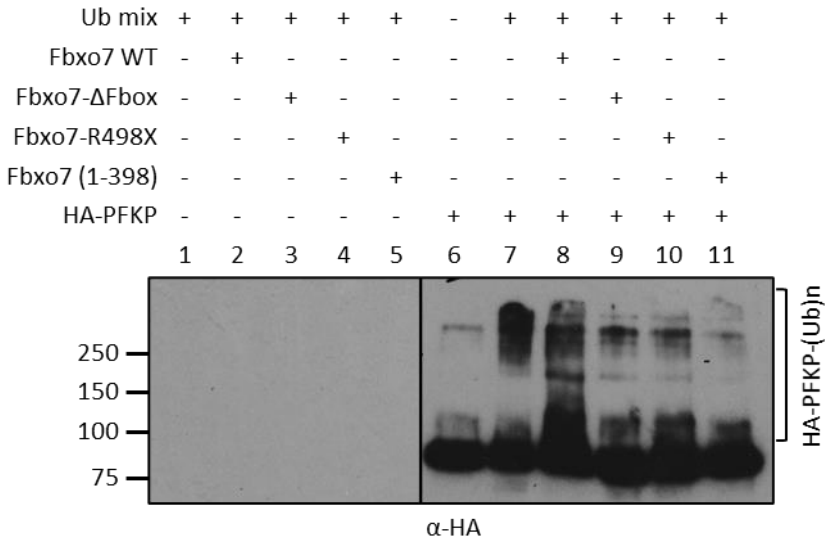

Figure 3.3: HA-PFKP is ubiquitinated by SCF^{Fbxo7} ***in vitro*.**

Equal concentrations of purified SCF^{Fbxo7} complexes were incubated with an activated ubiquitin (Ub) mix (ubiquitin buffer, UBE1, UbcH5a and ATP) in the presence of absence of purified HA-PFKP and analysed by immunoblotting. (n=2)

To corroborate this, I also performed *in cellulo* ubiquitination assays in HEK293T cells expressing a control or *FBXO7*-targetting shRNA, which would reduce background PFKP ubiquitination by Fbxo7. These cells were transfected with His-tagged ubiquitin, PFKP and FLAG-Fbxo7 constructs, and ubiquitinated proteins were isolated via the His-tag using cobalt-NTA affinity resin (Fig. 3.4). Immunoblot analyses showed a reduction in His-ubiquitinated PFKP in cells with an Fbxo7 shRNA knockdown compared to control (Fig. 3.4, lane 4 vs. lane 2). Re-expression of WT Fbxo7 markedly increased PFKP polyubiquitination (Fig. 3.4, lane 5), and this was lower when the ΔFbox mutant was expressed (Fig. 3.4, lane 6). Interestingly, the ΔFbox mutant still showed some increase above the empty vector control (Fig. 3.4, lane 4) despite its inability to recruit SCF subunits. Expression of C- and N-terminal truncated Fbxo7 also reduced polyubiquitination compared to WT (Fig. 3.4, lanes 7 & 8), indicating that both the C-terminal PRR and N-terminal Ubl domain are required for SCF^{Fbxo7} ubiquitination activity towards PFKP.

Together, these data show that an interaction occurs between Fbxo7 and PFKP resulting in PFKP ubiquitination by SCF^{Fbxo7}, and this modification is dependent on both the N- and C-termini of Fbxo7.

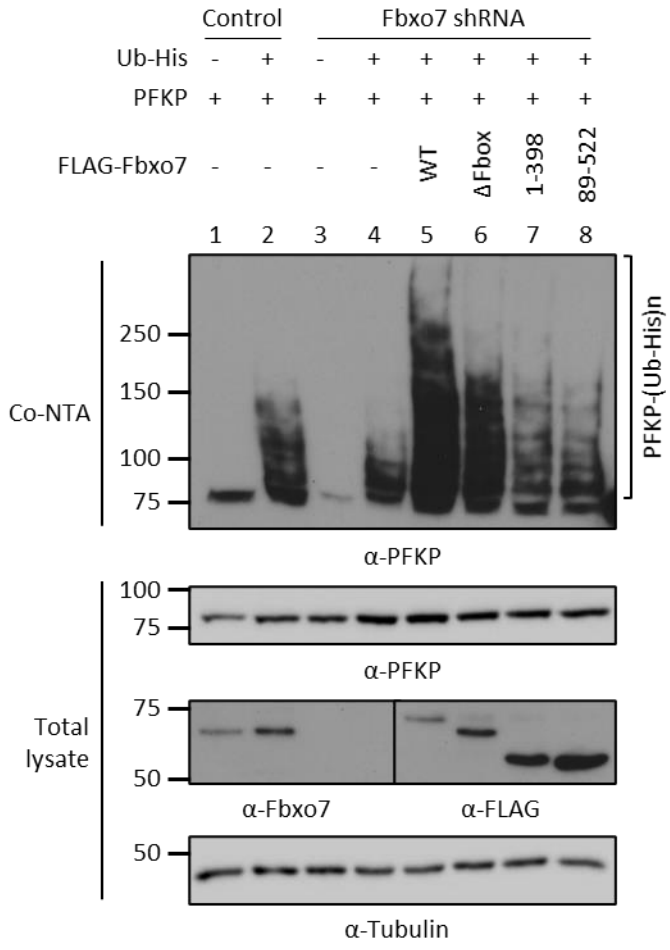

Figure 3.4: Fbxo7 ubiquitinates PFKP *in cellulo.*

HEK293T cells stably expressing a control or Fbxo7 shRNA were transfected with the plasmids indicated, treated with 25 μM MG132 for 4 hours and lysed in a denaturing buffer. Ubiquitinated proteins were isolated using a cobalt-NTA affinity resin (Co-NTA) to the His-tag on ubiquitin. Immunoblot for PFKP shows the degree of ubiquitination following expression of each Fbxo7 construct (n=3).

3..2 Fbxo7 ubiquitinates PFKP and promotes Cdk6-dependent phosphorylation

Given published data showing Fbxo7 directly binds and activates Cdk6[67,101], and Cdk6 phosphorylates PFKP[304], I reasoned that there may be interplay between these three proteins and sought to delineate their mechanistic relationship. Since phospho-degrons are a common recognition motif for SCF E3 ligases, I first investigated whether Cdk6 was required for Fbxo7 to interact with, or ubiquitinate PFKP. For this I used two tools: the Cdk4/6 kinase inhibitor palbociclib, and two Cdk6-specific PROTAC degraders[448,449]. Inhibition of Cdk4/6 in palbociclib-treated CCRF-CEM cells was verified by cell cycle analysis and G1 arrest was observed following 24 hours of treatment (Fig. 3.5A). Since HEK293T cells have disrupted cell cycle regulation, Cdk4/6 inhibition was instead confirmed by directly measuring a reduction in phophoSer780, a Cdk4/6-specific phospho-acceptor in the retinoblastoma protein (Rb) (Fig. 3.5B). The two Cdk6 PROTACs used are both based upon palbociclib as the substrate-binding ligand, and a pomalidomide warhead to recruit CRBN E3 ligase (Fig. 3.6A). CCRF-CEM cells were treated with a titration of each PROTAC for 4 or 24 hours prior to cell lysis and analysis by immunoblot (Fig. 3.6B). Both PROTACs induced a dose-dependent decrease in Cdk6 protein levels after just 4 hours, with the efficacy of PROTAC 2 slightly surpassing that of PROTAC 1, particularly at this earlier time point. Both PROTACs also displayed the hook effect, a competition-induced phenomenon arising from the formation of binary complexes at the detriment of tertiary target/PROTAC/E3 complexes at high PROTAC concentrations. Interestingly, immunoblot analysis of Fbxo7 protein levels identified a dose-dependent decrease in Fbxo7 following treatment with higher concentrations of PROTAC 1 (approximately 40% reduction with 5 µM PROTAC), though this was not observed with PROTAC 2. Considering these observations, subsequent experiments were performed by treating cells with 0.1 µM PROTAC for 24 hours – a dose with near-ablation of Cdk6 protein (97% loss of protein expression) but no reduction in Fbxo7 protein levels that may confound the data.

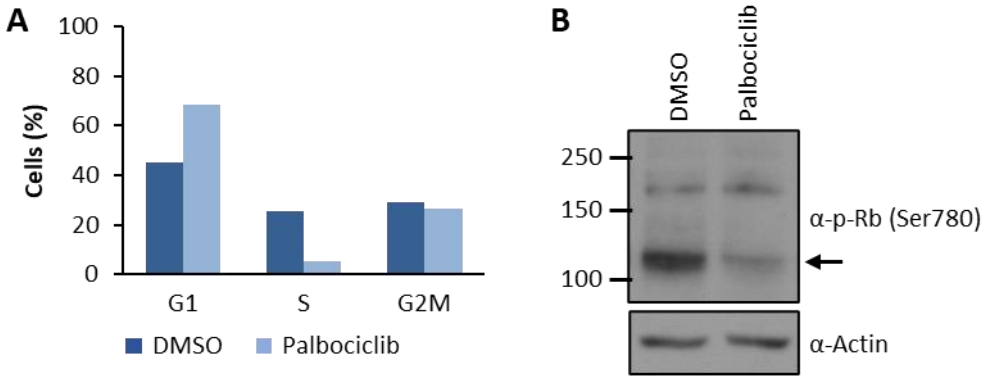

Figure 3.5: Inhibition of Cdk4/6 by palbociclib.

(A) Inhibition of Cdk4/6 by palbociclib in CCRF-CEM cells was verified by cell cycle analysis using propidium iodide staining (n=2). (B) Inhibition of Cdk4/6 by palbociclib in HEK293T cells was verified by immunoblotting cell lysates for phospho-Rb at Ser780 (n=1).

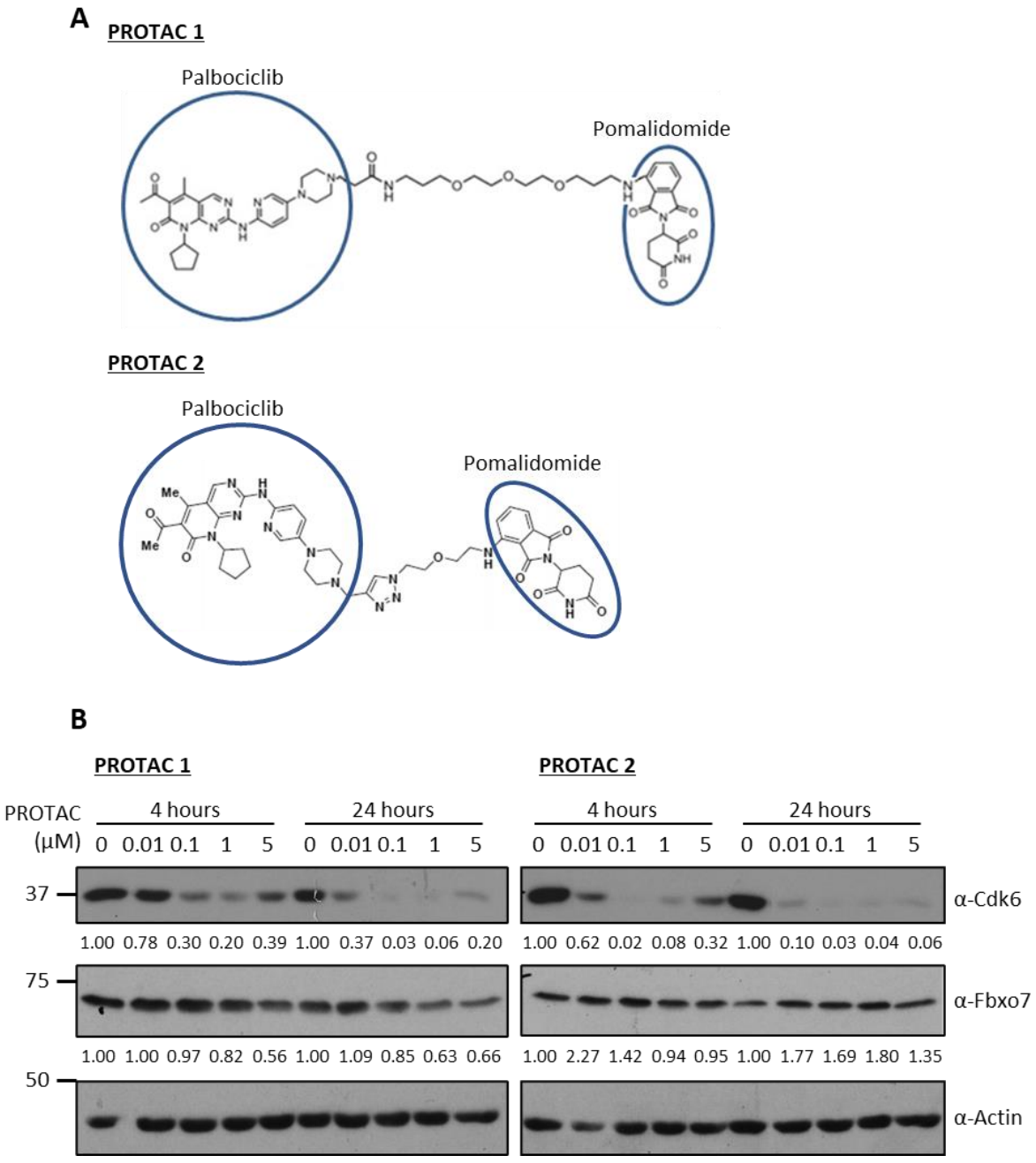

Figure 3.6: Cdk6 PROTACs induce degradation of Cdk6 in a dose-dependent manner.

(A) Chemical structures of the two Cdk6 PROTACs used, indicating the palbocicblib-based substrate binding ligand and pomalidomide warhead. PROTAC 1[448] and PROTAC 2[449] were kindly gifted by collaborators.

(B) CCRF-CEM cells were treated with a titration of each PROTAC for 4 hr or 24 hr prior to lysis and analysis by immunoblot. (n=1)

To investigate whether Cdk6 was required for the interaction between Fbxo7 and PFKP, CCRF-CEM cells were treated with vehicle control (DMSO), 1 µM palbociclib or 0.1 µM Cdk6 PROTAC for 24 hours, prior to Fbxo7 immunoprecipitation (Fig. 3.7). PFKP co-immunoprecipitated with Fbxo7 in cells treated with palbociclib (Fig. 3.7, lane 3) and in Cdk6-PROTAC-treated cells (Fig. 3.7, lanes 4 & 5), demonstrating that neither Cdk6 activity nor its presence was necessary for Fbxo7 binding to PFKP.

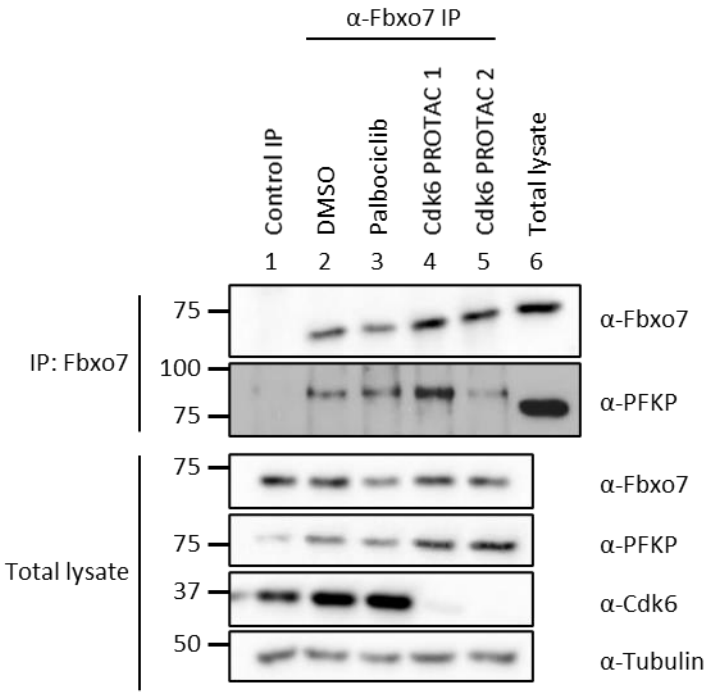

Figure 3.7: PFKP co-immunoprecipitates with Fbxo7 in the absence of Cdk6.
CCRF-CEM cells were treated with 1 µM palbociclib, 0.1 µM of Cdk6 PROTAC or vehicle control for 24 hours. Fbxo7 was immunoprecipitated from cell lysates, followed by immunoblot analysis with the indicated antibodies. (n=3).

I next tested whether Cdk6 activity was required for SCF^{Fbxo7}-mediated ubiquitination of PFKP. HEK293T cells expressing a control or Fbxo7-targeting shRNA were transfected with PFKP and treated with 1 µM palbociclib or vehicle control (DMSO) for 24 hours prior to cell lysis and analysis by immunoblot (Fig. 3.8). As previously observed, PFKP ubiquitination was reduced upon Fbxo7 knockdown (Fig. 3.8, lane 2 vs. lane 5) and enhanced with Fbxo7 overexpression (Fig. 3.8, lane 2 vs. lane 3). Interestingly, palbociclib treatment did not alter PFKP ubiquitination (Fig. 3.8, lane 2 vs. lane 4), indicating that Cdk6 activity is not required for SCF^{Fbxo7} ubiquitination of PFKP and further confirming an independence from Cdk6.

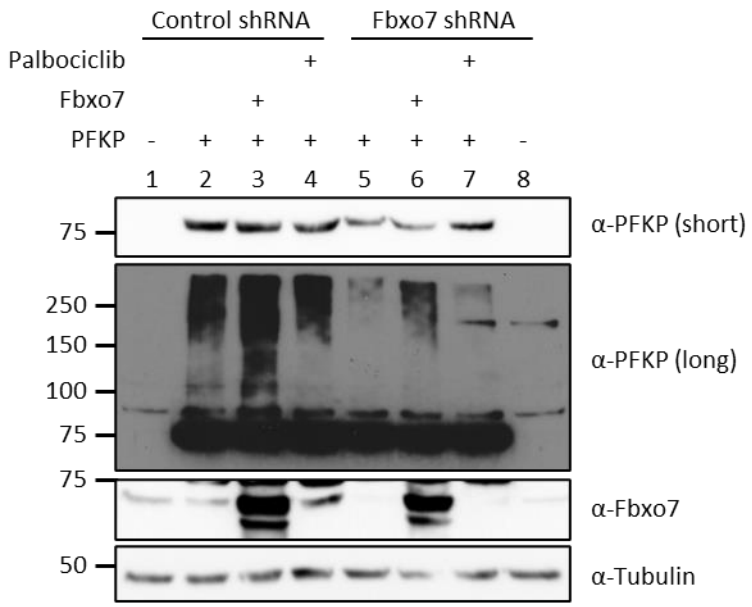

Figure 3.8: SCF^{Fbxo7} **ubiquitinates PFKP in the absence of Cdk6 kinase activity.** HEK293T cells expressing a control or Fbxo7 shRNA were transfected and treated with 1 µM palbociclib for 24 hours as indicated. Cells were treated with 10 µM MG132 prior to cell lysis and analysis by immunoblot. Immunoblot for PFKP shows the degree of ubiquitination. (n=2)

Since Cdk6 was dispensable for Fbxo7 to interact with and ubiquitinate PFKP, I tested whether Fbxo7 was required for the interaction between Cdk6 and PFKP in T-ALL cells. Cdk6 was immunoprecipitated from CCRF-CEM and MOLT-4 cells expressing a control or two different Fbxo7-targeting shRNAs (Fig. 3.9). In both cell lines, immunoblots show co-immunoprecipitation of PFKP with Cdk6 in the presence of Fbxo7 (Fig. 3.9, lane 4), but this interaction is lost upon Fbxo7 knockdown (Fig. 3.9, lanes 5 & 6). These data show Fbxo7 is required for a Cdk6-PFKP interaction in T-ALL cells and suggest that Fbxo7 would be required for the Cdk6 phosphorylation of PFKP reported by Wang, *et al*[304]. To test this, I used a fluorescent peptide biosensor to measure Cdk6 activity[457]. The bipartite biosensor comprises a C-terminal peptide sequence based upon PFKP and containing the PFKP S679 Cdk6-phosphorylation site reported by Wang, *et al*[304], conjugated to an N-terminal phospho-amino acid binding domain (PAABD) which specifically recognises phosphorylated substrate (Fig. 3.10A). Cdk6 kinase activity and biosensor phosphorylation is measured via a TAMRA dye incorporated into the peptide sequence, which undergoes a change in fluorescence upon PAABD binding to the substrate. Lysates from CCRF-CEM cells expressing a control or Fbxo7 shRNA were analysed with this biosensor, and those with an Fbxo7 knockdown showed reduced Cdk6 activity, comparable to the palbociclib-treated controls (Fig. 3.10B). These data show Fbxo7 is required for Cdk6 interaction with, and activity towards, PFKP.

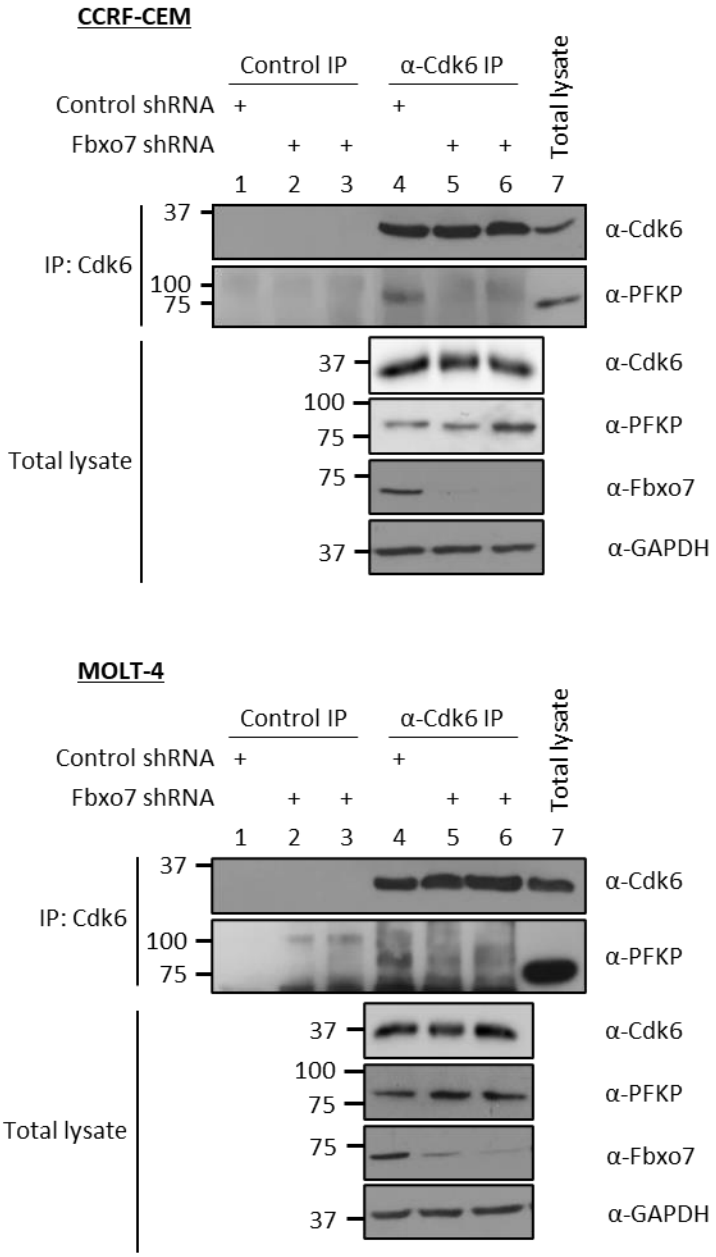

Figure 3.9: PFKP co-immunoprecipitation with Cdk6 is dependent on Fbxo7. CCRF-CEM and MOLT-4 cells expressing a control or two different Fbxo7 shRNAs were lysed. Cell lysates were immunoprecipitated with α-Cdk6 or an isotype matched control antibody, followed by immunoblot analysis with the indicated antibodies. (n=1)

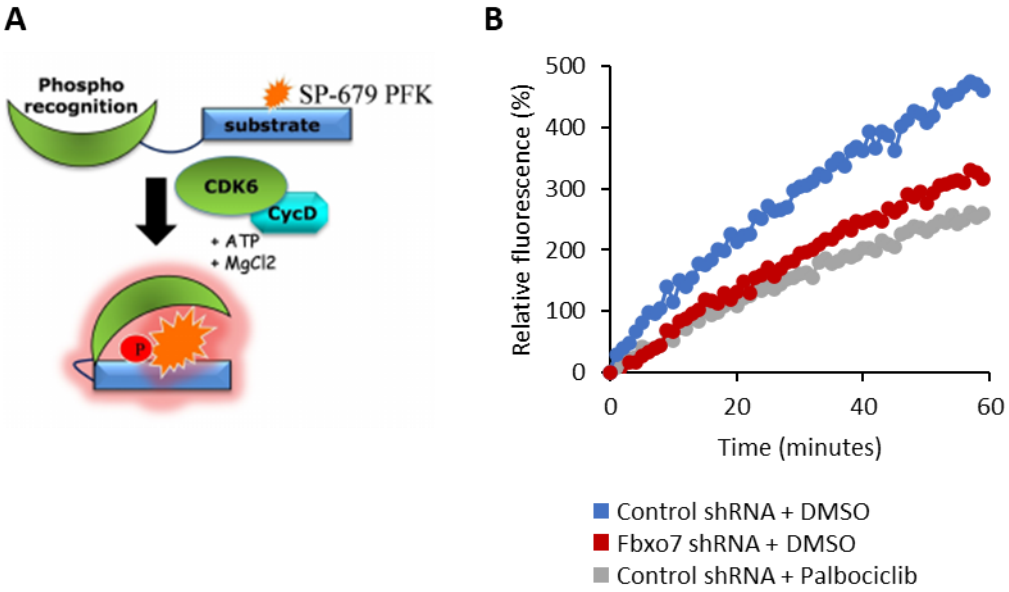

Figure 3.10: A Cdk6 biosensor shows that Fbxo7 promotes Cdk6 kinase activity.

(A) Schematic of the Cdk6 biosensor which comprises a C-terminal PFKP-based peptide sequence that contains a TAMRA dye (represented by orange spikes), and N-terminal phospho-recognition domain. Upon biosensor phosphorylation, the phospho-recognition domain binds to the substrate and this confirmational change induces a change in TAMRA dye fluorescence to report Cdk6 activity in a dose-dependent fashion.

(B) CCRF-CEM cells expressing a control or Fbxo7 shRNA were treated with 1 µM palbociclib or vehicle control for 24 hours as indicated. Kinase activity is measured in a dose-dependent manner by fluorescence of the Cdk6 biosensor and presented as a relative increase (%) from the fluorescence at time 0 min. (n=1)

Together, these data indicate a mechanism whereby Fbxo7 promotes two PTMs, namely the Cdk6-independent ubiquitination and Cdk6-dependent phosphorylation of PFKP (Fig. 3.11). Notably, the data suggest that Fbxo7 may act as a chaperone to recruit and activate Cdk6 to promote the phosphorylation of PFKP.

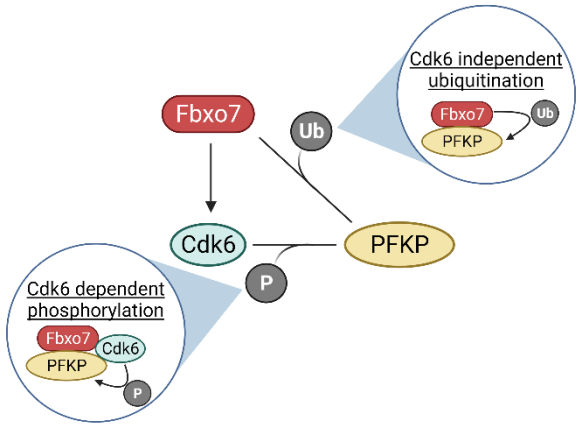

Figure 3.11: Schematic of Fbxo7-dependent post-translational modifications on PFKP.

Fbxo7 promotes two independent post-translational modifications on PFKP: Cdk6-independent ubiquitination, and Cdk6-dependent phosphorylation.

3..3 The post-translational modification of PFKP does not signal protein degradation

One common outcome of ubiquitination is proteasomal degradation, so I sought to determine whether ubiquitination by Fbxo7 results in PFKP degradation. I first examined whether Fbxo7 and PFKP protein levels correlated in HEK293T and CCRF-CEM cells expressing a control or Fbxo7-targeting shRNA by immunoblot analyses using a monoclonal antibody (mAb) to PFKP (Fig. 3.12). This showed a greater than 2-fold increase in PFKP protein upon Fbxo7 knockdown in both cell types, suggesting that PFKP was targeted for degradation in the presence of Fbxo7. To support this, I performed a cycloheximide chase experiment to examine PFKP stability but found no change in PFKP half-life in cells with reduced Fbxo7 (Fig. 3.13A). Moreover, there was no accumulation of PFKP with proteasome inhibition by MG132 treatment in CCRF-CEM or HEK293T cells (Fig. 3.13B), which would be expected if PFKP was targeted by the proteasome.

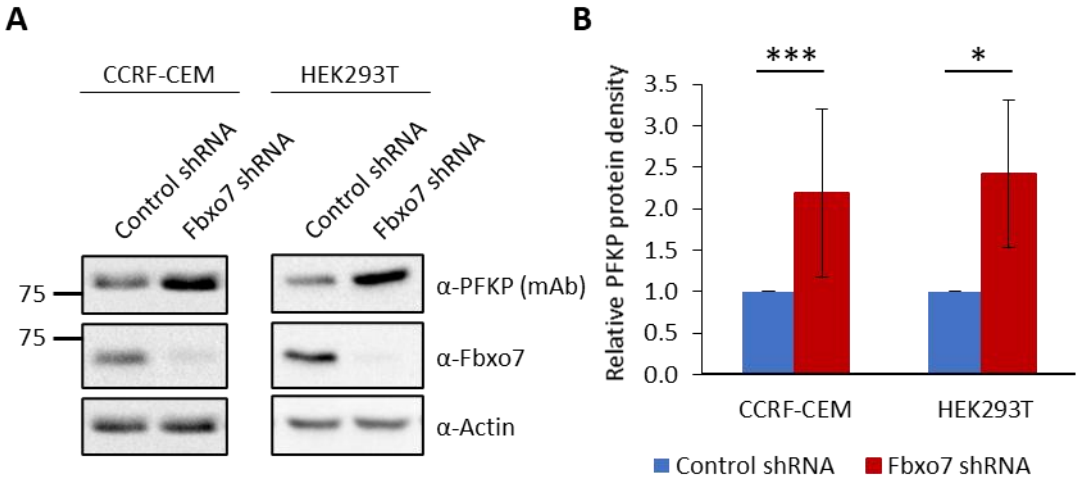

Figure 3.12: PFKP protein levels inversely correlate with Fbxo7 expression, when measured using a monoclonal α-PFKP antibody.

Lysates from CCRF-CEM and HEK293T cells expressing a control or Fbxo7 shRNA were analysed by immunoblot. (A) shows a representative image. (B) The relative intensity of protein expression was quantified using ImageJ and normalised to actin expression. (CCRF-CEM n=6, HEK293T n=10). * $p<0.05$, *** $p<0.001$

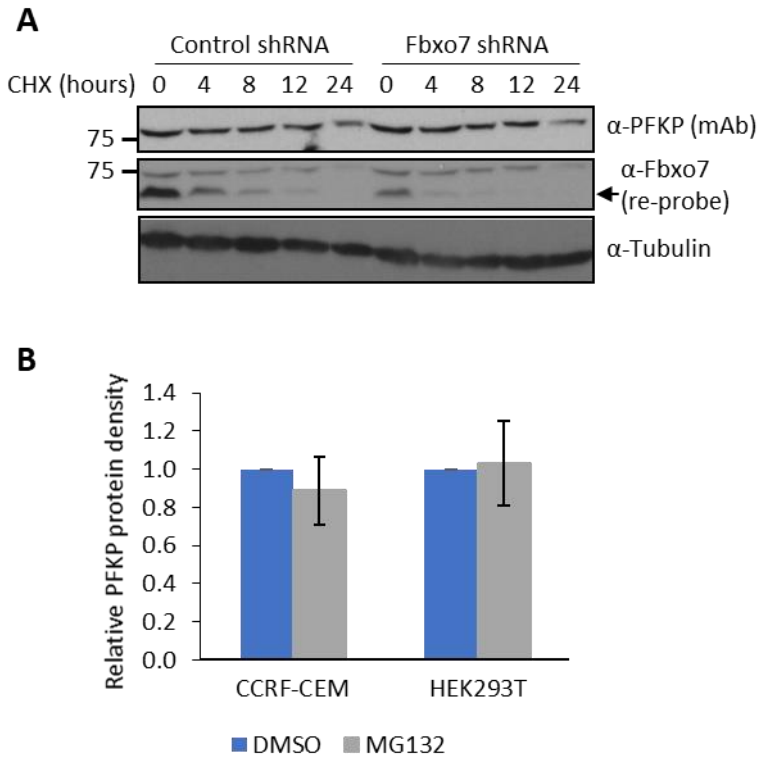

Figure 3.13: PFKP half-life is unchanged in the absence of Fbxo7, and PFKP does not accumulate with MG132 treatment (monoclonal α-PFKP).

(A) Representative immunoblot for PFKP half-life in CCRF-CEM cells expressing a control or Fbxo7 shRNA and treated with cycloheximide for up to 24 hours. (n=2)

(B) Cells were treated with DMSO or 10 μM MG132 for 4 hours and lysed. Proteins were resolved by SDS-PAGE to immunoblot for PFKP, and levels were quantified. (CCRF-CEM n=2, HEK293T n=3)

Given these conflicting data, and that a mAb detects a single epitope which may be affected by PTMs, I also measured PFKP protein levels with a polyclonal antibody (pAb). In contrast to the results with the mAb, there was no change in total PFKP protein levels in CCRF-CEM cells with an Fbxo7 knockdown (Fig. 3.14 A & B). However, immunoblotting with the pAb detected a cross-reacting higher MW band at 90 kDa which showed a 38% reduction in cells with Fbxo7 knockdown ((Fig. 3.14A & B). This was further supported by immunoblot analysis of HEK293T cells expressing a control or Fbxo7 shRNA, which also showed a proportional shift towards the lower MW band in the absence of Fbxo7 (Fig. 3.14C). However, it should be noted that, in contrast to CCRF-CEM cells, the higher 90 kDa form was predominant in HEK293T cell lysates. To lastly confirm this in primary cells, I isolated splenic $CD4^+$ T cells from heterozygous or homozygous Fbxo7-deficient mice, in which the *FBXO7* locus is disrupted by a *LacZ* insertion between exons 3 and 4. Lysates from these cells were analysed by immunoblot and also display a 37% reduction in the higher MW band in the absence of Fbxo7, despite no change to total PFKP (Fig. 3.14D). Together these data suggest that Fbxo7 promotes a distinct slower migrating form of PFKP across multiple cell types.

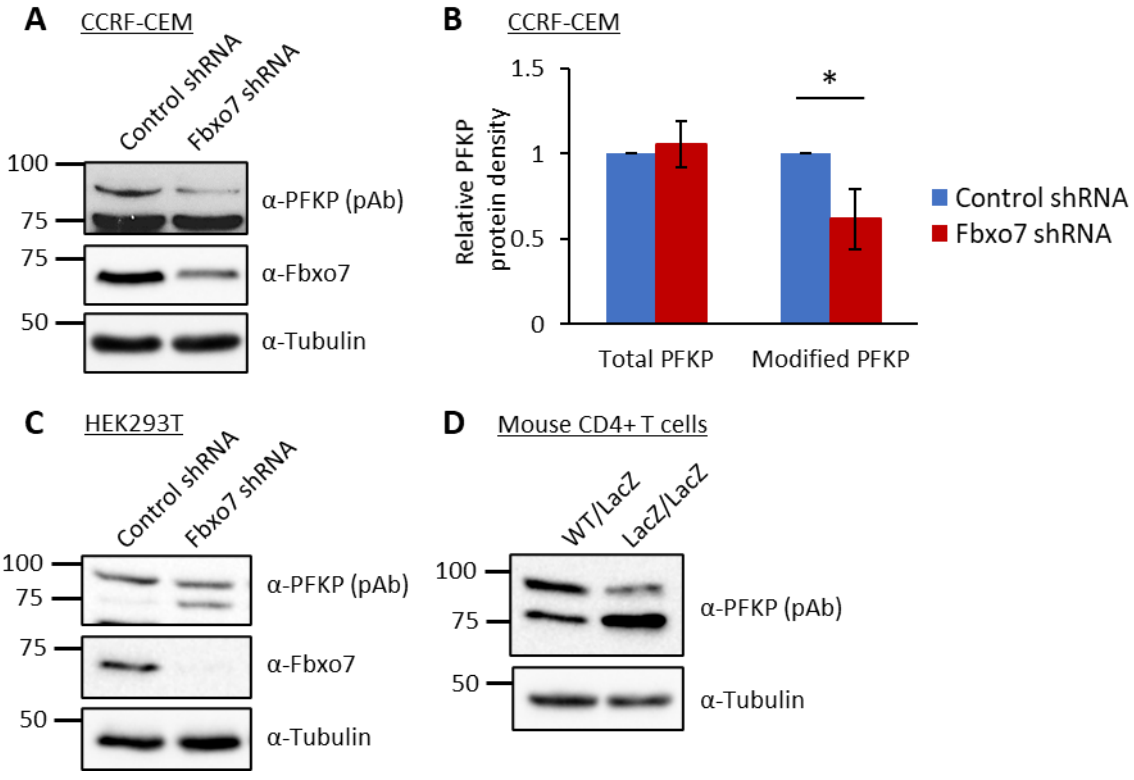

Figure 3.14: Fbxo7 knockdown reduces expression of a higher MW PFKP species (polyclonal α-PFKP). Lysates from (A-B) CCRF-CEM and (C) HEK293T cells expressing a control or Fbxo7 shRNA, and (D) $CD4^+$ T cells isolated from $Fbxo7^{WT/LacZ}$ or $Fbxo7^{LacZ/LacZ}$ mice, were analysed by immunoblot. (A, C and D) Representative images. (B) Quantification showing the relative levels of total PFKP and modified 90 kDa PFKP in CCRF-CEM cell lysates. (CCRF-CEM n=4, HEK293T n=4, Mouse $CD4^+$ T cells n=1). * $p<0.05$

To evaluate the detection of these two bands by the different antibodies, I immunoprecipitated PFKP from CCRF-CEM cells using the α-PFKP mAb and analysed the precipitated proteins using both the mAb and pAb α-PFKP antibodies (Fig. 3.15). Interestingly, two bands were detected in each case, but analysis with the mAb showed a predominance of the lower band, whilst the pAb gave a stronger upper band. These data corroborate that the two α-PFKP antibodies preferentially detect different sub-populations of PFKP in cell lysates. In addition, I immunoprecipitated Fbxo7 from these cell lysates to determine whether Fbxo7 preferentially interacts with one population of PFKP (Fig. 3.15). Interestingly, analysis with both antibodies showed the immunoprecipitation of PFKP at approximately 90 kDa and it was detected more strongly with the pAb, suggesting that Fbxo7 predominantly interacts with the higher MW species of PFKP.

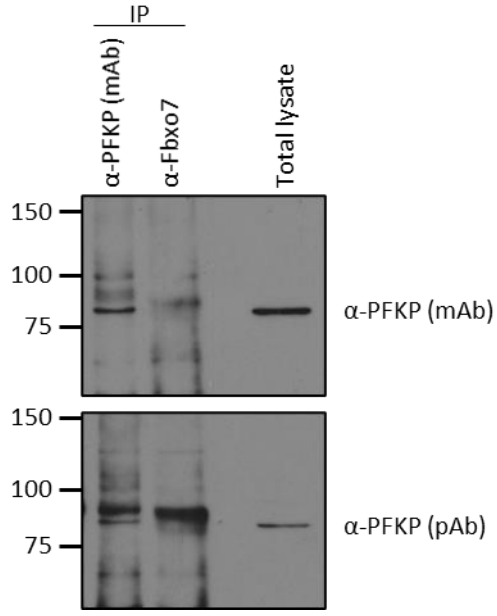

Figure 3.15: α-PFKP monoclonal and polyclonal antibodies detect different subpopulations of PFKP. Cell lysates from CCRF-CEM cells were immuno-precipitated using monoclonal α-PFKP or α-Fbxo7 as indicated, followed by immunoblot analysis with monoclonal α-PFKP (mAb) or polyclonal α-PFKP (pAb). (n=2)

This small increase in MW on a western blot may represent a PTM. As the predominance of this 10-15 kDa shift positively correlated with Fbxo7 expression, I reasoned that it may be a multi-mono- or di-ubiquitinated form of PFKP. To test this, I treated HEK293T cells with an Fbxo7-targeting siRNA and complemented back WT and ΔFbox Fbxo7, to determine whether the modification is dependent on SCF^{Fbxo7} ubiquitin ligase activity (Fig 3.16). As expected, immunoblot analysis with pAb α-PFKP showed an increase in the lower 80 kDa band with Fbxo7 knockdown (Fig. 3.16 lane 2 vs lane 1). However, this was reversed by the overexpression of both WT and ΔFbox Fbxo7 constructs (Fig. 3.16 lanes 3 and 4), which mimicked the scrambled siRNA control (Fig. 3.16 lane 1). This suggests that the upper modified population does not represent a ubiquitinated form of PFKP by Fbxo7, though these data do not rule out ubiquitination by another E3 ubiquitin ligase. Importantly, this increase in the abundance of the lower MW species of PFKP is rescued by the increased expression of Fbxo7 but is not dependent on its ligase activity.

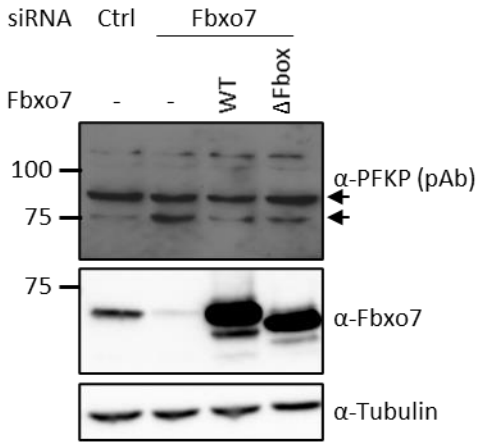

Figure 3.16: Restoration of Fbxo7 expression reduces levels of low molecular weight PFKP. HEK293T cells were treated with a control or Fbxo7-targeting siRNA and transfected with Fbxo7 WT or ΔFbox as indicated. Cells were lysed and lysates were analysed by immunoblot with the indicated antibodies. (n=3)

To further test the effect of Fbxo7 on the stability of these PFKP sub-populations, I treated CCRF-CEM cells with cycloheximide for up to 8 hours and this time analysed PFKP levels in cell lysates using the pAb α-PFKP antibody (Fig. 3.17A). Reminiscent of the mAb data (Fig. 3.13A), analysis with the pAb did not show any change in the half-life of either PFKP sub-population. Similarly, CCRF-CEM cells treated with proteasome inhibitor MG132 did not show any change in PFKP levels or population distributions compared to vehicle control (Fig. 3.17B). Together these data indicate that, whilst Fbxo7 promotes a change in the balance between higher and lower MW species, this is not ubiquitination by Fbxo7 and the loss of Fbxo7 does not promote the degradation of PFKP.

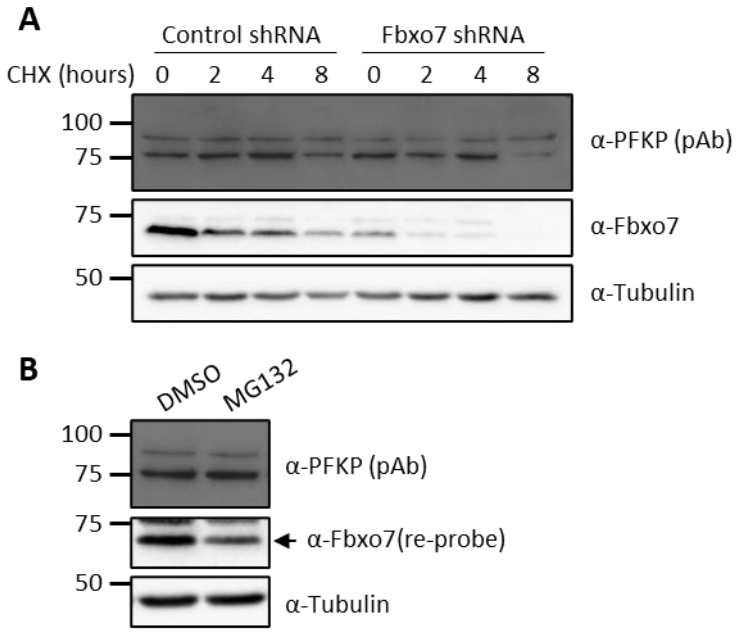

Figure 3.17: PFKP half-life is unchanged in the absence of Fbxo7, and the distribution between higher and lower MW populations is unaffected by MG132 treatment.

(A) Representative immunoblot for PFKP half-life in CCRF-CEM cells expressing a control or Fbxo7 shRNA and treated with cycloheximide for up to 8 hours. (n=2)

(B) Representative immunoblot for PFKP levels in CCRF-CEM cells treated with DMSO or 10 μM MG132 for 4 hours (n=2)

3..4 Fbxo7 knockdown reduces the proportion of inactive monomer/dimer forms of PFKP

A major mechanism for PFKP regulation is the formation and dissociation of tetrameric complexes, as PFKP is most enzymatically active as a tetramer. I therefore investigated whether Fbxo7 expression affects the distribution of PFKP complexes between tetramer and monomer/dimer forms. Total cell lysates from CCRF-CEM cells expressing a control or Fbxo7-targeting shRNA were passed over an ultrafiltration unit with molecular mass 200 kDa cutoff to separate monomers (86 kDa) and dimers (172 kDa) from active tetramers (344 kDa). As controls, allosteric regulators of PFKP were added to total cell lysates prior to filtration to promote (AMP) or dissociate (citrate) PFKP tetramers. The filtrates (<200 kDa fraction) containing the smaller monomer/dimer forms were then analysed, alongside the lysates prior to filtration (Fig. 3.18A). Immunoblots showed that Fbxo7 knockdown did not change total levels of PFKP, as before, but instead reduced the amount of inactive monomer/dimer forms by 75% (Fig. 3.18A and 3.18B), suggesting a change in distribution of PFKP into active tetramers.

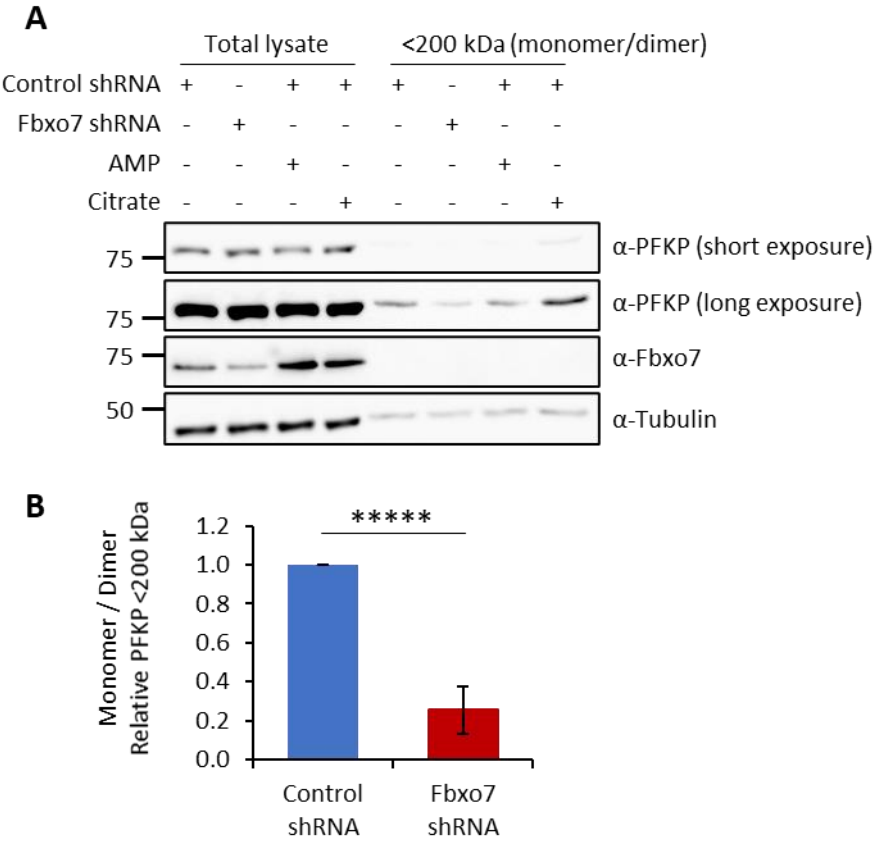

Figure 3.18: Fbxo7 knockdown decreases the proportion of PFKP in inactive monomer/dimer forms. Lysates from CCRF-CEM cells expressing a control or Fbxo7 shRNA were passed over a 200 kDa molecular weight cut-off filter to separate PFKP monomers (86 kDa) and dimers (172 kDa) from tetramers (344 kDa). 1 mM AMP and 10 mM citrate were added to lysates as controls to respectively promote or dissociate PFKP tetramers. Total lysates and <200 kDa fractions were resolved by SDS-PAGE and analysed by immunoblot. (A) Representative immunoblot. (B) Quantification of PFKP in <200 kDa fraction. (n=4) ***** $p<0.0005$

3..5 T cells lacking Fbxo7 show increased glycolysis and reduced viability and activation

As my data indicated that Fbxo7 regulates the active state of the rate-limiting glycolytic enzyme PFKP, I reasoned that glycolysis may be affected. To test this, I used the Agilent Seahorse Glycolytic Rate Assay which measures the extracellular acidification above a monolayer of cells to quantify glycolysis (Fig. 3.19). The assay first measures the basal glycolysis of cells, then injects a rotenone/antimycin A mix to inhibit mitochondrial complexes I and III, block mitochondrial activity and push the cell into compensatory glycolysis as an indicator of cellular glycolytic capacity. A second injection of glucose analogue 2-DG inhibits glycolysis and serves as an internal control. T-ALL cell lines CCRF-CEM and Jurkat E6 expressing a control or Fbxo7 shRNA were analysed. I found that Fbxo7 knockdown increased both basal and compensatory glycolysis in CCRF-CEM cells, by 48% and 26% respectively, whilst Jurkat E6 cells showed a 20% rise in compensatory glycolysis (Fig. 3.20A). These data indicate higher levels of glycolysis in malignant T cells with reduced Fbxo7. To demonstrate that this effect on glycolysis was not limited to cancer cell lines, I also tested primary T cells from our Fbxo7-deficient mouse. Splenic $CD4^+$ T cells were isolated and activated for 48 hours *in vitro* prior to analysis by Seahorse Glycolytic Rate Assay (Fig. 3.20B). Fbxo7-deficient T cells exhibited significantly higher basal glycolysis and a smaller increase in compensatory glycolysis, further indicating elevated glycolysis in cells with reduced Fbxo7 expression.

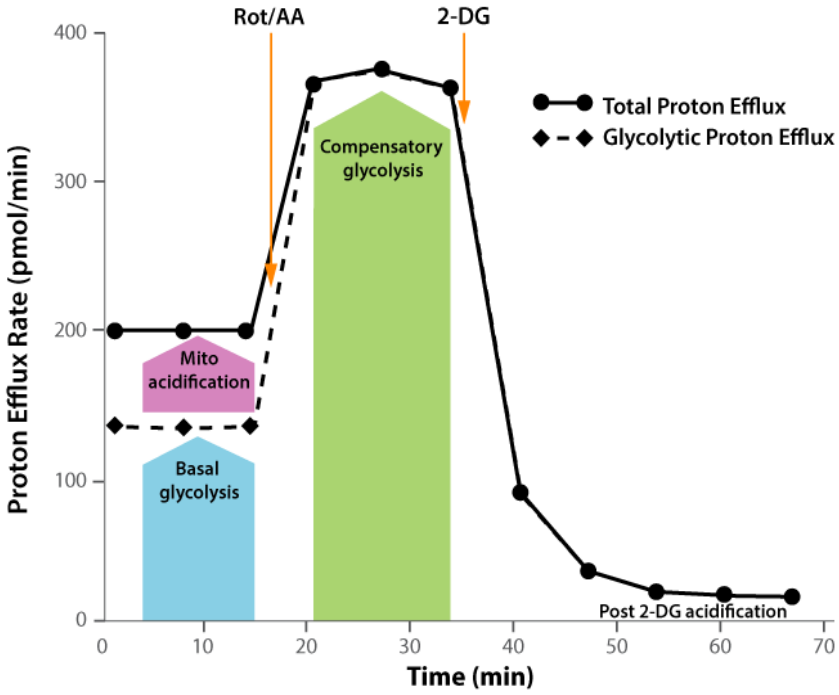

Figure 3.19: Agilent Seahorse XF Glycolytic rate assay profile.

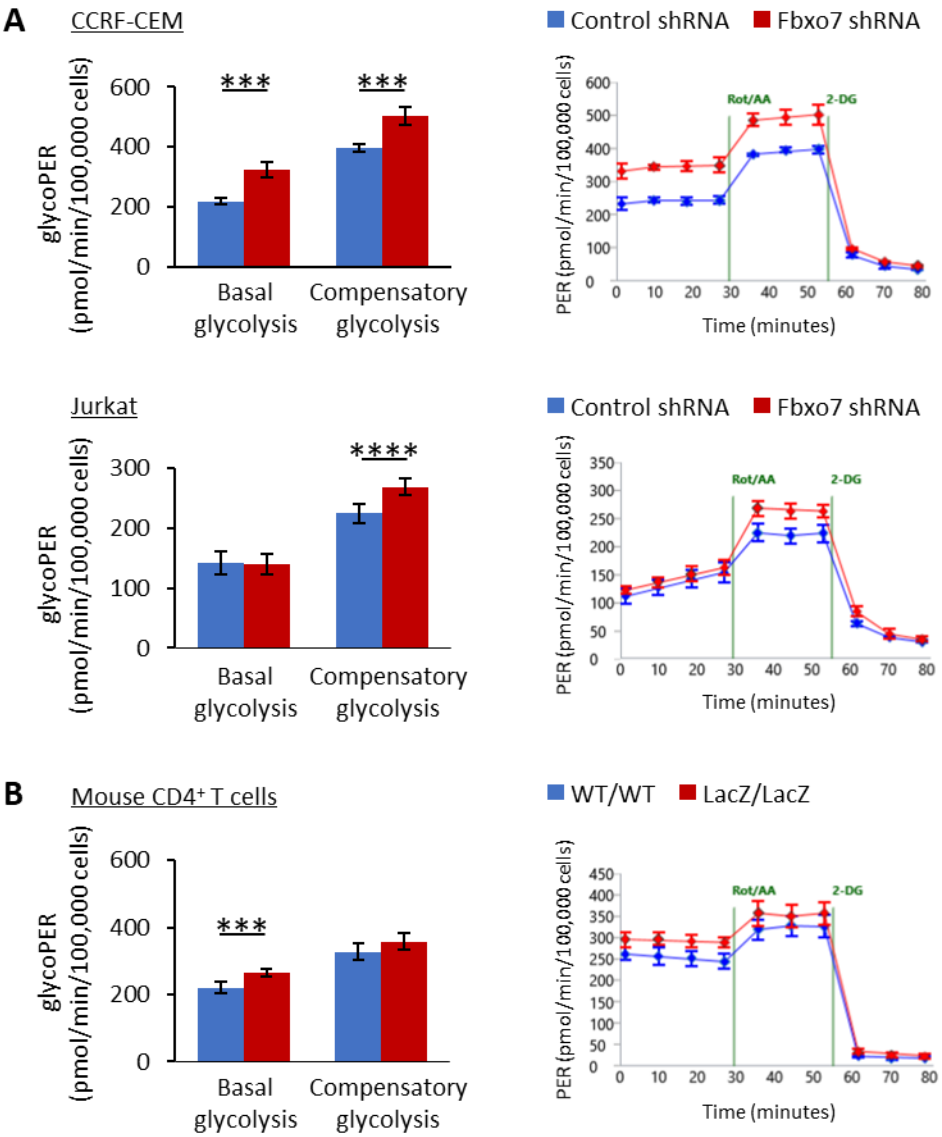

Figure 3.20: T-ALL cells and splenic CD4⁺ T cells with reduced Fbxo7 expression have higher levels of glycolysis.

(A) CCRF-CEM (top) and Jurkat E6 (bottom) cells expressing a control or Fbxo7 shRNA were analysed by the Agilent Seahorse Glycolytic Rate Assay. (n=4)

(B) CD4⁺ T cells were isolated from WT or Fbxo7$^{LacZ/LacZ}$ mice and activated for 48 hours *in vitro* prior to analysis with the Agilent Seahorse Glycolytic Rate Assay. (n=2)

*** p<0.005, **** p<0.001

I hypothesised that enhanced glycolysis in T cells lacking Fbxo7 might divert metabolites away from the PPP and impair their capacity to buffer ROS. To test this, I stained $CD4^+$ T cells with cell permeable H_2DCFDA to measure cellular ROS in naïve cells or at time intervals following activation, when both glycolysis and ROS generation are usually upregulated (Fig. 3.21). As expected, ROS were generated in response to T cell activation and both WT and Fbxo7-deficient cells showed a 2.2-fold increase in DCF fluorescence following 24 hours of activation (Fig. 3.21A). Interestingly, Fbxo7-deficient cells showed higher DCF fluorescence than WT and, in both naïve and activated conditions, $CD4^+$ T cells from mutant mice displayed a 27-34% increase in ROS compared to WT (Fig. 3.21B). A sample of activated cells were treated with the antioxidant N-acetylcysteine for 2 hours prior to staining with H_2DCFDA to confirm that the increase in 525 nm fluorescence is specific to elevated ROS (Fig. 3.21B and 3.21C). Together, these data demonstrate that $CD4^+$ T cells lacking Fbxo7 have elevated ROS in both naïve and activated states.

Given the altered metabolic state of these primary $CD4^+$ T cells, I examined other functional outputs including cell viability and activation. I noted that after *in vitro* activation for 24 hours, the viability of Fbxo7-deficient T cells was significantly reduced by 1.9-fold compared to WT cells (Fig. 3.22). Moreover, the activation of mutant cells was delayed and plateaued at 14.2% lower than WT (Fig. 3.23A), despite the increase in cell size upon T cell blasting being comparable between WT and mutant cells (Fig. 3.23B). Together these data suggest that Fbxo7 reduces ROS levels and promotes the viability and activation of $CD4^+$ T cells.

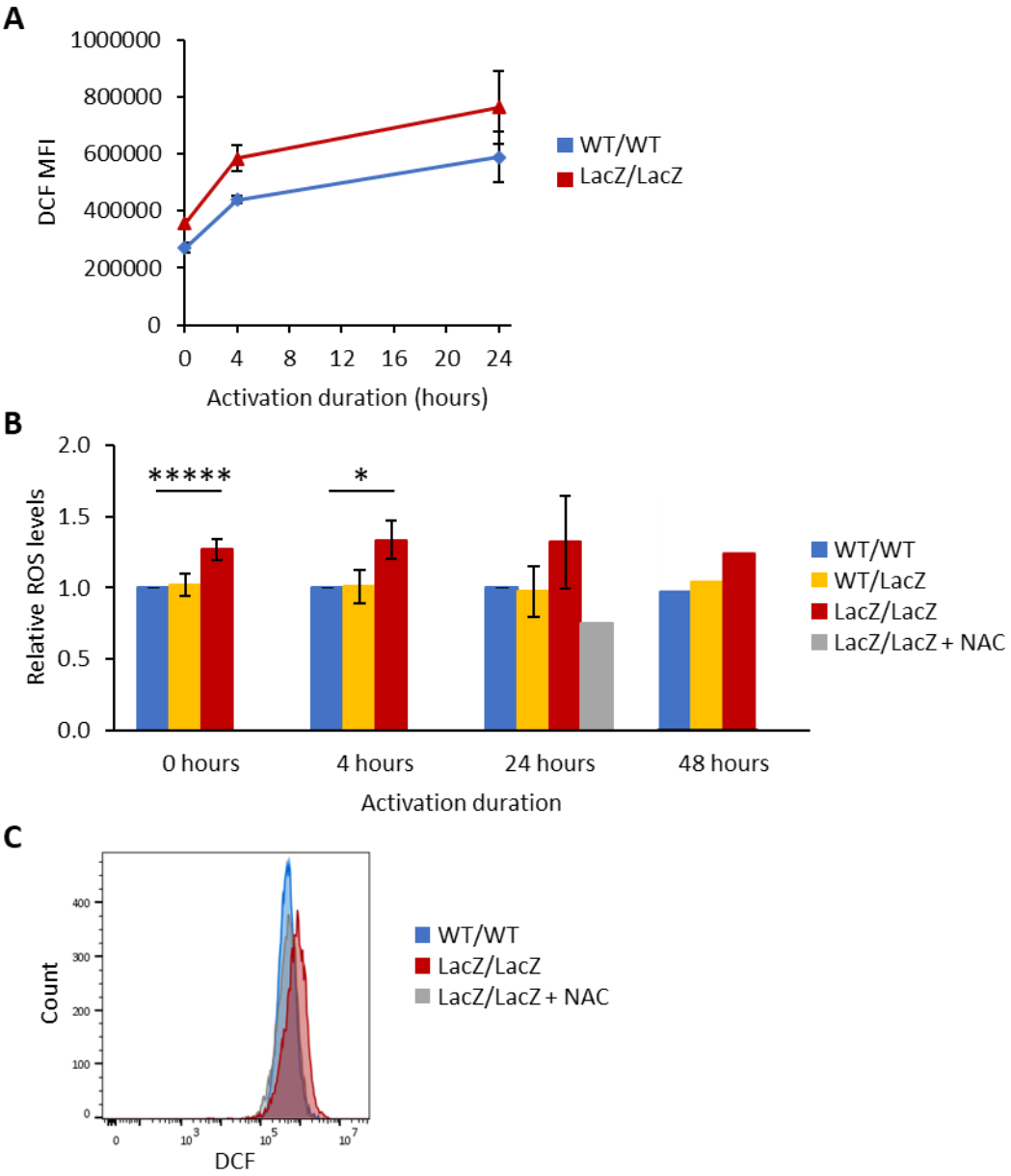

Figure 3.21: CD4⁺ T cells lacking Fbxo7 have elevated cellular ROS compared to WT.

CD4⁺ T cells were isolated and activated *in vitro* for the indicated duration prior to analysis using H_2DCFDA dye to measure cellular ROS. Where indicated, cells were pre-treated with 5 mM NAC for 2 hours prior to addition of the dye.

(A) Increase in cellular ROS over 24 hours of activation. (B) Relative ROS levels in WT, heterozygous and homozygous mutant cells at time intervals following T cell activation. (C) Example flow cytometry histogram.

(0, 4, 8 hours n≥3, 48 hours n=2) * $p<0.05$,***** $p<0.0005$

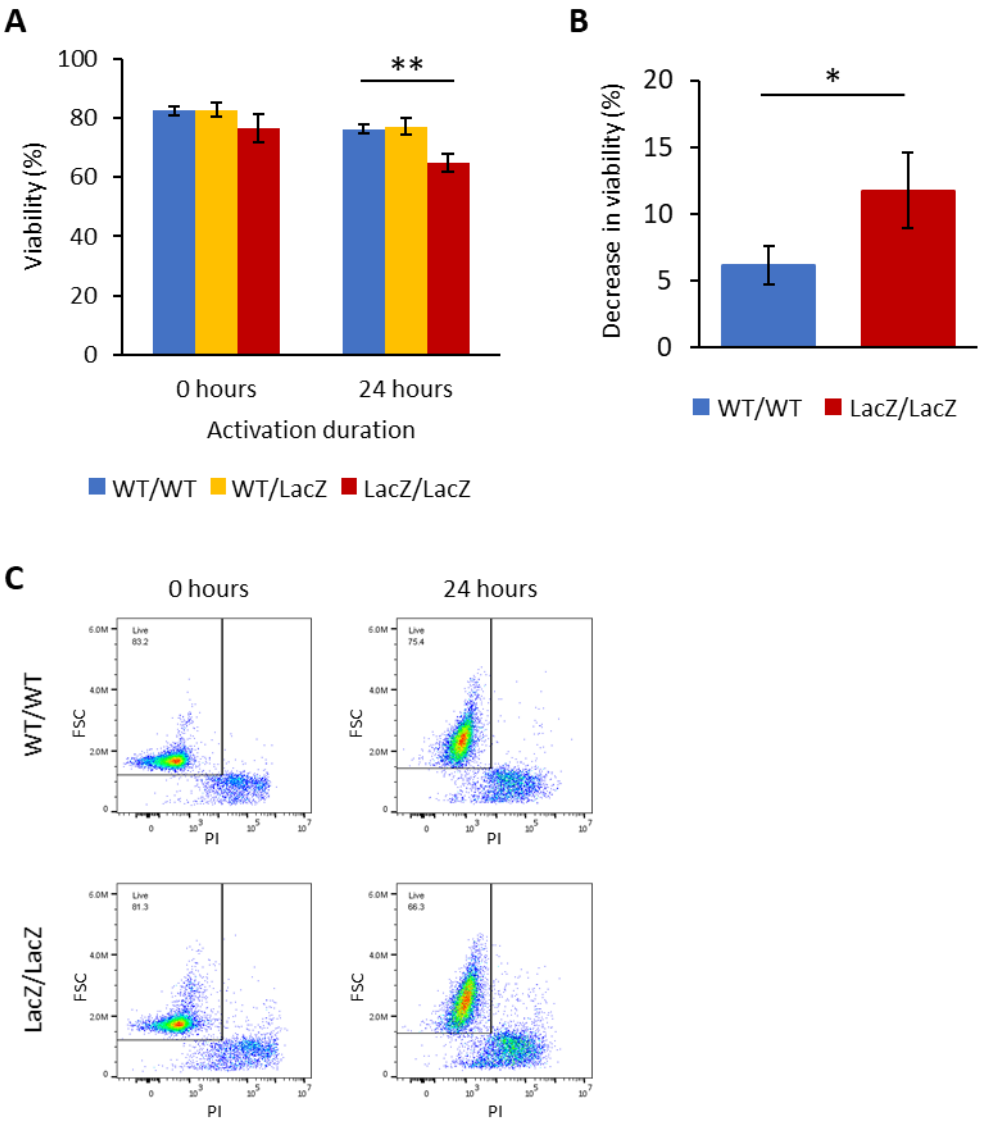

Figure 3.22: CD4⁺ T cells lacking Fbxo7 have reduced viability compared to WT.

The viability of isolated CD4⁺ T cells was analysed by PI staining upon isolation and following 24 hours of activation *in vitro*.

(A) Viability of cells. (B) Decrease in viability over 24 hours of activation. (C) Example flow cytometry plots. (n=3) * $p<0.05$, ** $p<0.01$

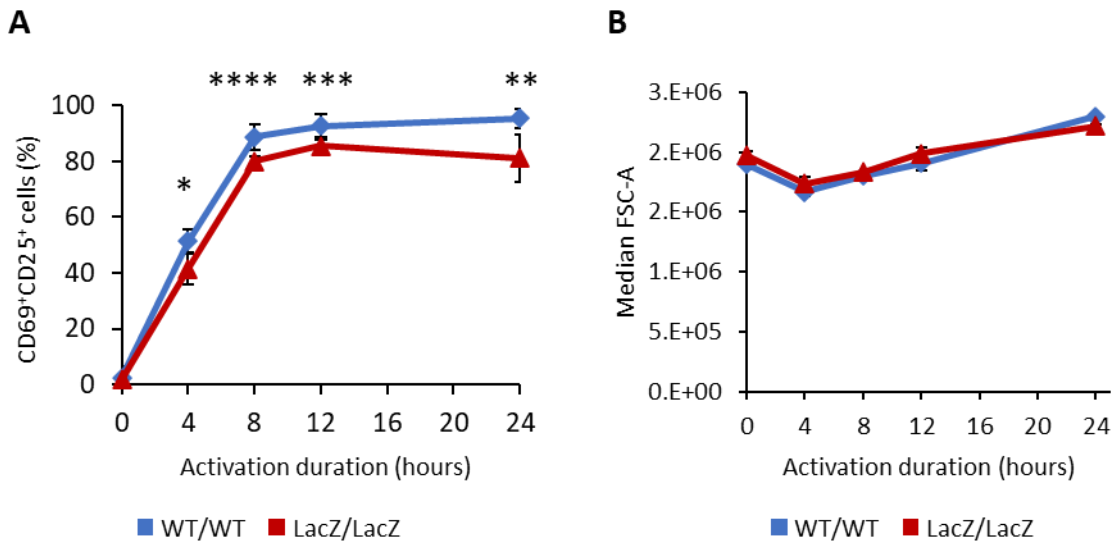

Figure 3.23: CD4⁺ T cells lacking Fbxo7 activate less efficiently *in vitro*.

$CD4^+$ T cells isolated from WT or $Fbxo7^{LacZ/LacZ}$ mice were activated *in vitro* for the indicated duration. (A) Activation was measured by both CD69 and CD25 expression over 24 hours, and (B) Median FSC was measured as an indicator of cell size. (n≥3) * p<0.05, ** p<0.01, *** p<0.005, **** p<0.001

To explore the wider impact of Fbxo7 on T cell metabolism, I performed untargeted metabolomics profiling on activated splenic $CD4^+$ T cells using liquid chromatography mass spectrometry (LC-MS). Principle component analysis shows discrete clusters of WT and $Fbxo7^{LacZ/LacZ}$ mutant samples, illustrating divergent metabolic profiles (Fig. 3.24A). These variations were multifaceted and will be discussed in further detail in subsequent sections. Importantly, among these differences was a pronounced accumulation of lactate, pyruvate, and late-stage glycolytic intermediates in mutant T cells, each showing a 1.7 to 2.1-fold increase compared to WT (Fig 3.24B and Fig. 3.25). Interestingly, consumption-release (CoRe) analysis of metabolites in the cell culture media show that, whilst glucose uptake was comparable, mutant T cells released less lactate and pyruvate (Fig. 3.25).

An accumulation of metabolites may occur due to increased flux through the pathway, or a downstream blockage. Therefore, to attribute this metabolite accumulation to glycolytic flux, I completed a stable isotope tracing study with $CD4^+$ T cells activated for 24 hours in the presence of Glucose-1,2-$^{13}C_2$ (Fig. 3.26). m+2 labelled lactate is derived directly from glycolysis, whilst m+1 labelled lactate is generated via the oxidative arm of the PPP. As hypothesised, there was a 59.5% increase in m+2 lactate in T cells from Fbxo7-deficient mice compared to WT, confirming an increase in lactate formation via glycolysis. Surprisingly, m+1 lactate was also elevated by 67.9%, indicating greater flux through the oxidative PPP.

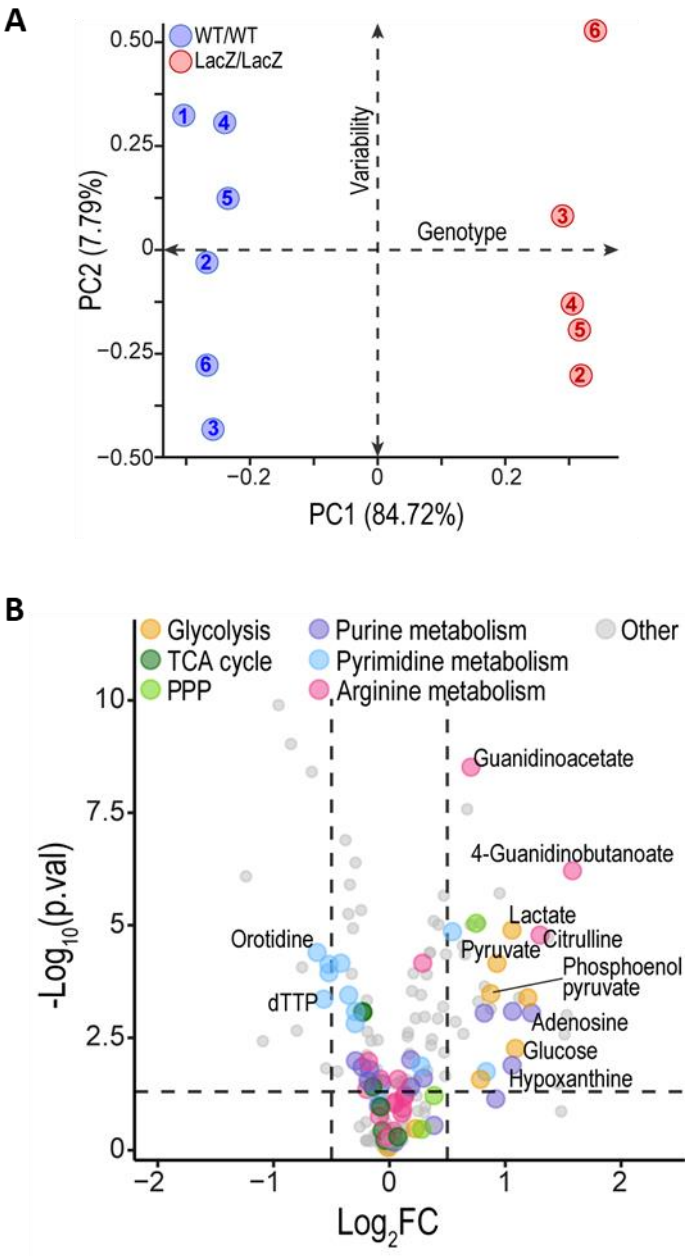

Figure 3.24: Metabolomic analysis of Fbxo7-deficient T cells highlights broad metabolic alterations.

Untargeted metabolomics profiling was performed on $CD4^+$ T cells from WT or $Fbxo7^{LacZ/LacZ}$ mice, activated for 48 hours. (n=6)

(A) Principal component analysis of intracellular metabolite ion intensities.

(B) Volcano plot of differentially expressed metabolites in $Fbxo7^{LacZLacZ}$ $CD4^+$ T cells compared to WT.

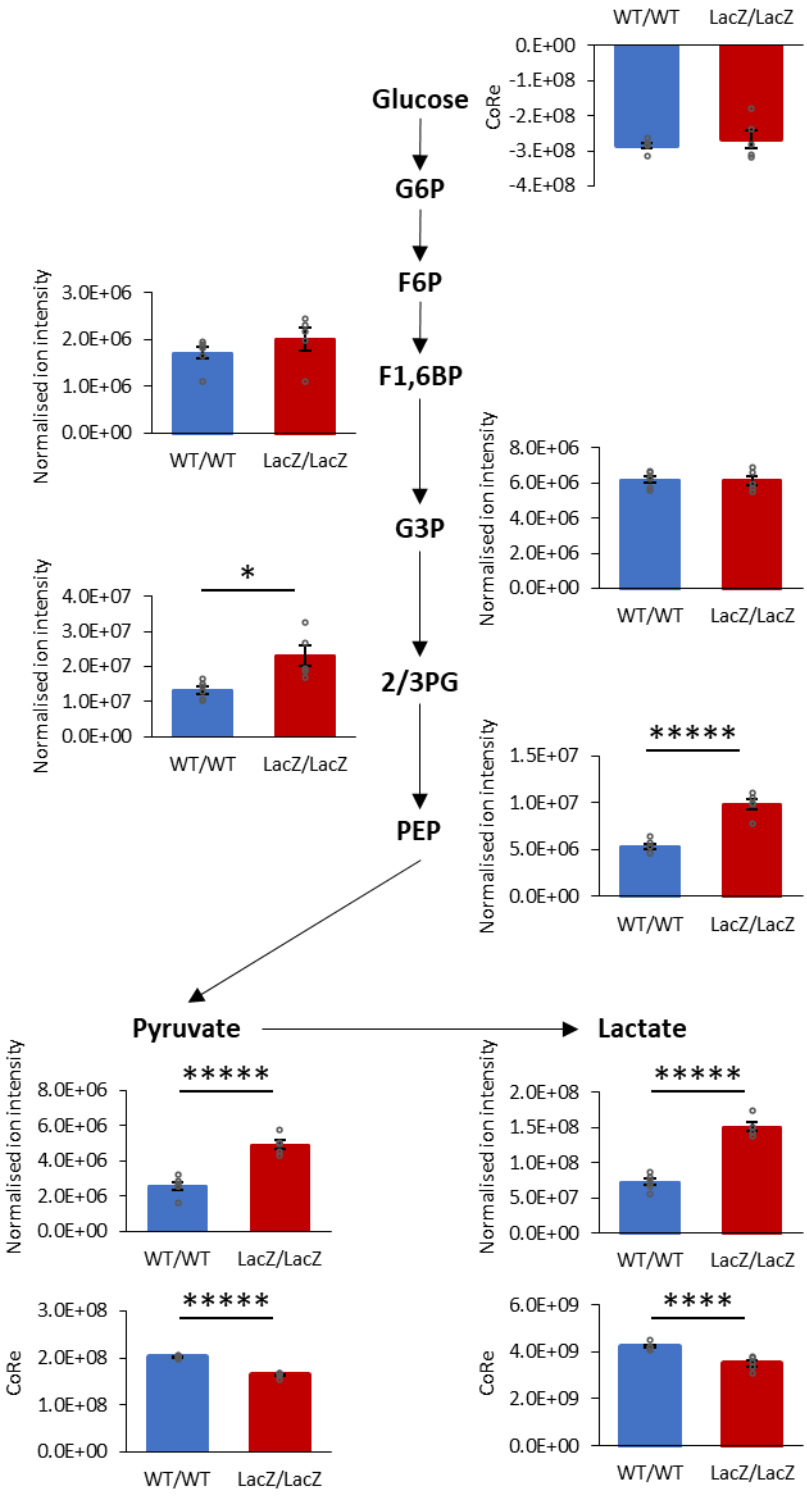

Figure 3.25: Metabolomic analysis of Fbxo7-deficient T cells shows changes to glycolytic metabolites.

Untargeted metabolomics profiling on $CD4^+$ T cells from WT or $Fbxo7^{LacZLacZ}$ mice shows changes to glycolytic intracellular ion intensities and consumption-release (CoRe) of metabolites from cell culture media.

(n=6) * p<0.05, ** p<0.01, *** p<0.005, **** p<0.001, ***** p<0.0005

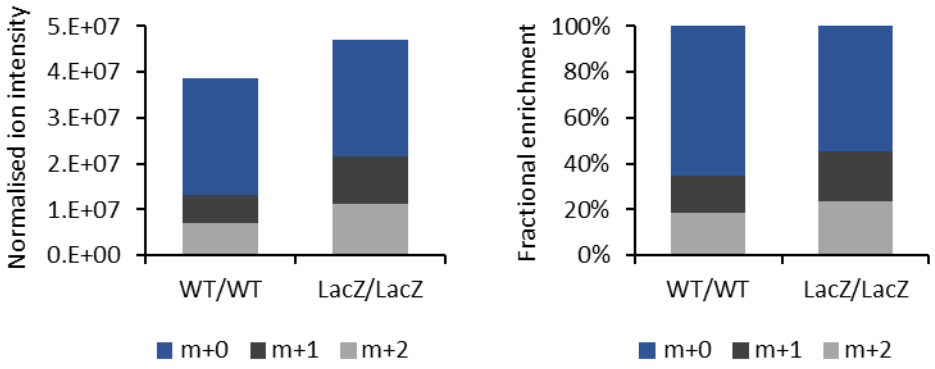

Figure 3.26: Carbon tracing analysis confirms an increase in glucose-derived lactate in Fbxo7-deficient T cells.

$CD4^+$ T cells from WT or $Fbxo7^{LacZ/LacZ}$ mice were activated for 24 hours in the presence of glucose-1,2-$^{13}C_2$ then subjected to metabolomics analysis. m+1 and m+2 intracellular lactate are derived from radio-labelled glucose. Normalised ion intensity (left) is a measure of ion abundance, fractional enrichment (right) shows the proportion of cellular lactate in each labelled pool. (n=6)

3..6 T cells lacking Fbxo7 show broad metabolic alterations

Beyond glucose metabolism, other differences were highlighted by my metabolic fingerprinting study in activated $CD4^+$ T cells from WT or $Fbxo7^{LacZ/LacZ}$ mice. Among these was a notable nucleotide imbalance. I observed elevated intracellular levels of pyrimidine precursors including carbamoyl aspartate, dihydroorotate and orotate in T cells lacking Fbxo7 (Fig. 3.27). This was accompanied by increased consumption of aspartate, a pyrimidine precursor, from the cell culture medium, and lower release of intermediates such as carbamoyl aspartate and dihydroorotate. Despite the seemingly augmented pyrimidine synthesis, intracellular pyrimidine levels were reduced in mutant T cells, suggesting a defect in pyrimidine synthesis or increased pyrimidine usage in these cells. Unlike pyrimidines, gross changes to intracellular purine levels were not observed, and only subtle variation was detected in AMP, IMP and GMP levels (Fig. 3.28). However, purine metabolism intermediates adenosine, hypoxanthine, xanthine and uric acid were all increased approximately 2-fold intracellularly in Fbxo7-deficient cells, and extracellular release of both xanthine and uric acid was increased. This is suggestive of increased purine metabolism in mutant T cells. Together these data imply a role for Fbxo7 in nucleotide synthesis and metabolism.

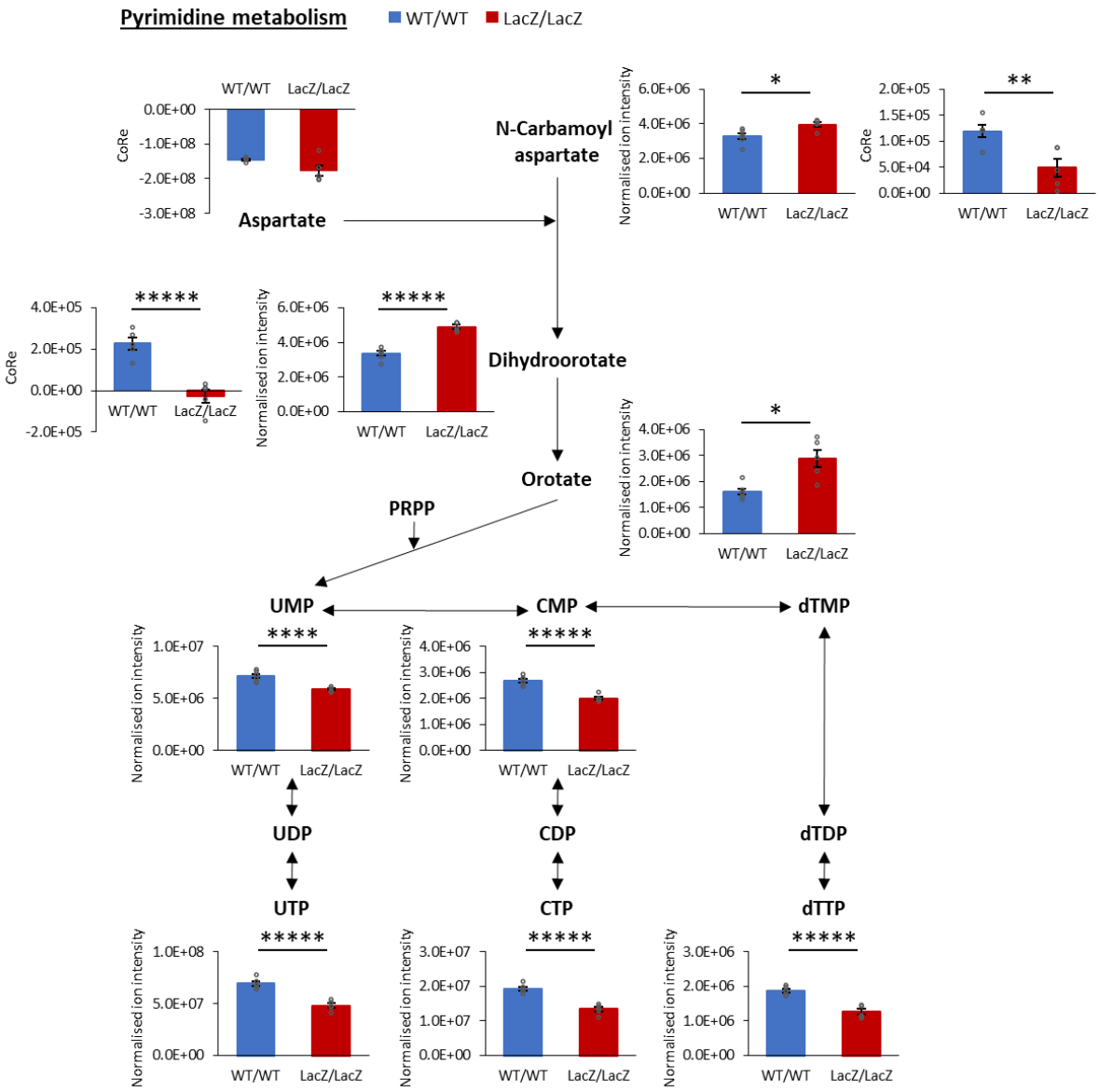

Figure 3.27: Metabolomic analysis of Fbxo7-deficient T cells shows changes to pyrimidine metabolism.

Untargeted metabolomics profiling on $CD4^+$ T cells from WT or $Fbxo7^{LacZLacZ}$ mice shows changes to pyrimidine intracellular ion intensities and consumption-release (CoRe) of associated metabolites from cell culture media.

(n=6) * p<0.05, ** p<0.01, *** p<0.005, **** p<0.001, ***** p<0.0005

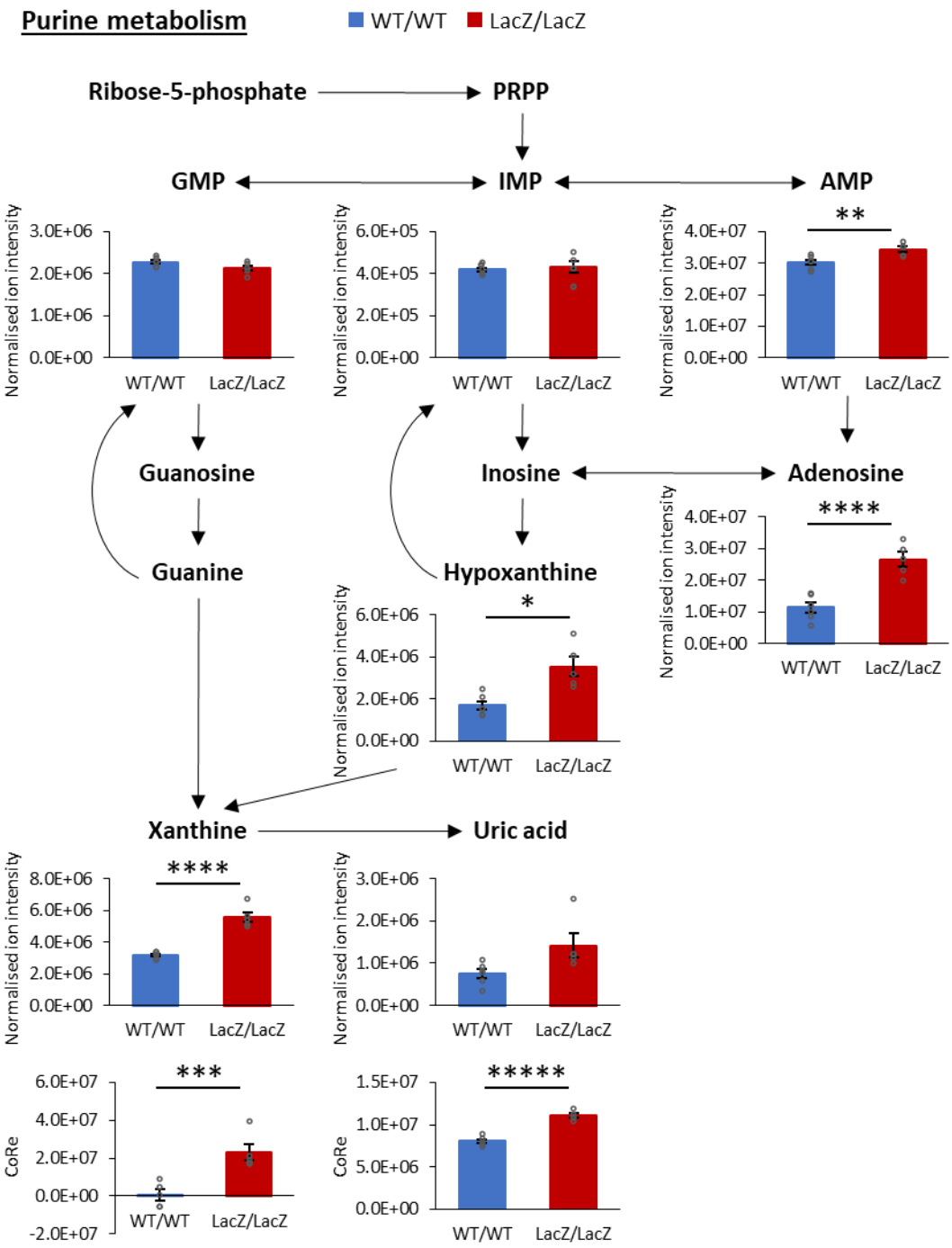

Figure 3.28: Metabolomic analysis of Fbxo7-deficient T cells shows changes to purine metabolism.

Untargeted metabolomics profiling on $CD4^+$ T cells from WT or $Fbxo7^{LacZLacZ}$ mice shows changes to purine intracellular ion intensities and consumption-release (CoRe) of associated metabolites from cell culture media.

(n=6) * p<0.05, ** p<0.01, *** p<0.005, **** p<0.001, ***** p<0.0005

Another metabolic pathway markedly altered in Fbxo7$^{LacZ/LacZ}$ T cells is the urea cycle (Fig. 3.29). In mutant cells, I observed 2.5-fold higher levels of intracellular citrulline, and it was released into the cell culture media, in contrast to WT cells where it was consumed. This trend was not observed to the same extent for other urea cycle metabolites, with arginine and ornithine only showing a 1.1-fold increase in mutant cells, and a marginal 0.9-fold reduction in arginosuccinate. Interestingly, arginine metabolite guanidinoacetate is elevated in Fbxo7-deficient T cells, suggesting heightened arginine metabolism. Together these data suggest that Fbxo7-deficient T cells have elevated citrulline synthesis and a disrupted urea cycle, compared to WT cells.

A final pathway of note from the metabolomics dataset is the alteration of tryptophan metabolism in CD4^{+} T cells lacking Fbxo7 (Fig. 3.30). Tryptophan uptake was lower in mutant T cells compared to WT, yet intracellular levels were 1.6-fold higher. Similarly, intracellular kynurenine, quinolic acid and nicotinic acid were all elevated 1.4 to 1.8-fold in mutant cells, and more kynurenine was excreted, ultimately suggesting disruption to tryptophan metabolism in the absence of Fbxo7.

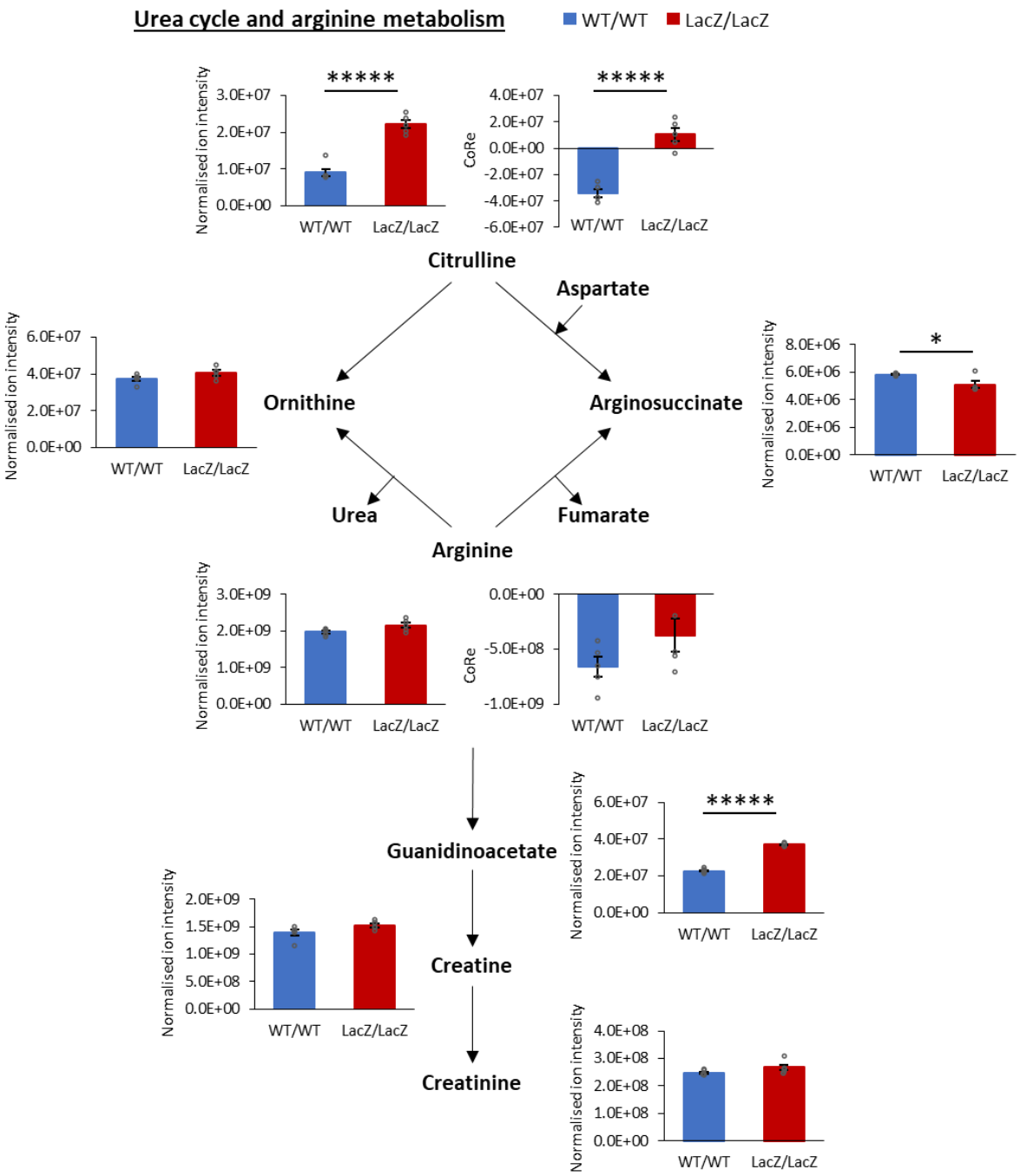

Figure 3.29: Metabolomic analysis of Fbxo7-deficient T cells shows changes to the urea cycle and arginine metabolism.

Untargeted metabolomics profiling on $CD4^+$ T cells from WT or $Fbxo7^{LacZLacZ}$ mice shows changes to urea cycle / arginine metabolism intracellular ion intensities and consumption-release (CoRe) of associated metabolites from cell culture media. (n=6) * p<0.05, ** p<0.01, *** p<0.005, **** p<0.001, ***** p<0.0005

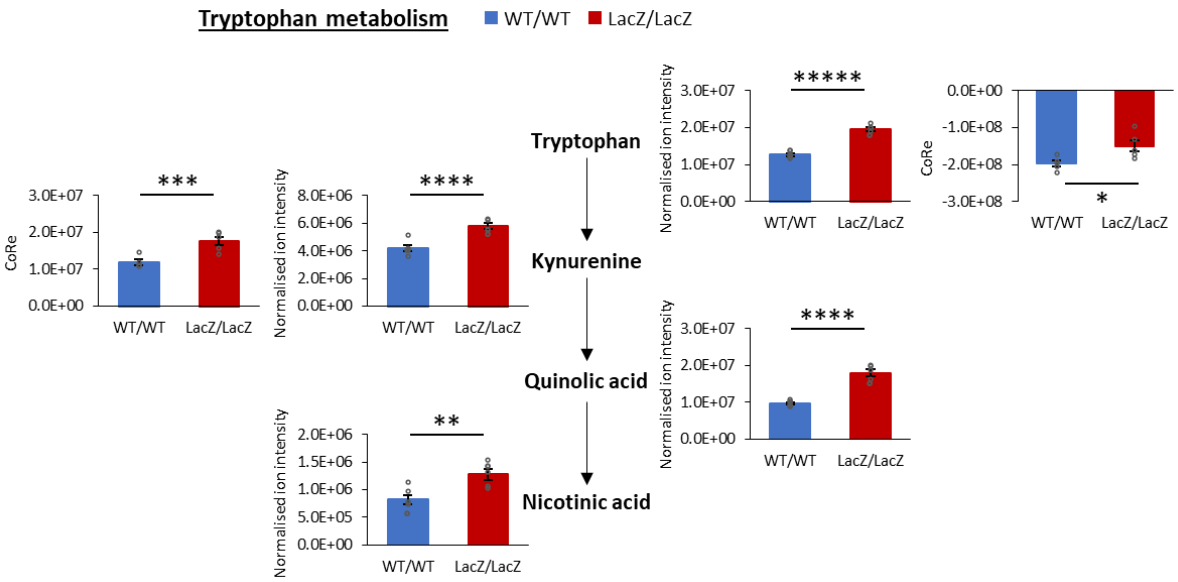

Figure 3.30: Metabolomic analysis of Fbxo7-deficient T cells shows changes to tryptophan metabolism.

Untargeted metabolomics profiling on $CD4^+$ T cells from WT or $Fbxo7^{LacZLacZ}$ mice shows changes to tryptophan intracellular ion intensities and consumption-release (CoRe) of associated metabolites from cell culture media.

(n=6) * p<0.05, ** p<0.01, *** p<0.005, **** p<0.001, ***** p<0.0005

Given the broad alterations discovered by metabolomic fingerprinting analysis, I sought to compile other putative Fbxo7 substrates identified in our historic screens that have metabolic functions. These comprise the Y2H screen that identified PFKP; an unbiased mass spectrometry (MS)-based screen on purified SCF^{Fbxo7} and $SCF^{Fbxo7\text{-}\Delta Fbox}$ ligases[81]; and a protein microarray to measure ubiquitination of over 9000 unique proteins by SCF^{Fbxo7} or $SCF^{Fbxo7\text{-}\Delta Fbox}$ control[81]. In total, 48 proteins were identified with roles in metabolism (Appendix A) and these were spread across the entire metabolic network. To determine whether any of the metabolic changes identified in Fbxo7-deficient $CD4^+$ T cells may be attributed to these putative targets, I assessed this list and metabolomics dataset in parallel. Pathvisio software[461] was used to create a metabolic map that represents the fold-change in intracellular metabolites in Fbxo7-deficient $CD4^+$ T cells compared to WT, for the key metabolic pathways measured. This map was then annotated with the putative Fbxo7 target proteins (Fig. 3.31). Alongside PFKP, glycolytic enzymes GAPDH and PKM were identified in the protein array and MS screens respectively and, if validated, may also contribute to the regulation of glycolysis by Fbxo7. Interestingly, several proteins involved in glycolytic biosynthetic pathways were also identified as putative substrates. For example, D-3-phosphoglycerate dehydrogenase (PHGDH) catalyses the first step in serine synthesis from glycolysis and both 3-phosphoserine and serine were elevated in mutant mice. Moreover, SHMT1/2 regulate the interconversion of serine and glycine as part of the folate cycle, a pathway critical for biosynthesis and survival in proliferating T cells[243]. In addition, the synthesis of conjugates for glycosylation may be disrupted as the biosynthetic enzyme N-Acetylneuraminate Synthase (NANS) was ubiquitinated by SCF^{Fbxo7} on the protein array and N-acetylneuraminic acid was elevated in mutant mice (Fig. 3.31).

I next turned my attention to the other pathways altered in the metabolomic fingerprinting analysis. CAD is a trifunctional enzyme involved in the first three steps of pyrimidine biosynthesis and was identified as an Fbxo7-interacting protein in the MS screen (Fig 3.31, Appendix A). Misregulation of CAD in Fbxo7-deficient mice may contribute to the defect in pyrimidine synthesis observed in the metabolomic fingerprinting data (Fig. 3.27). No urea cycle enzymes were identified by our screens (Appendix A), though changes to CAD may also impact this metabolic pathway since carbamoyl phosphate is a common precursor in both pyrimidine synthesis and the urea cycle. In addition, two polyamine biosynthetic enzymes were identified as putative Fbxo7 binding proteins: ornithine decarboxylase 1 (ODC1) and spermidine synthase (SRM) (Fig 3.31, Appendix A). These proteins catalyse the rate-limiting and subsequent step in spermidine synthesis from ornithine, a key urea cycle metabolite. Hence disruption of these enzymes may directly impact flux around the urea cycle. Another hit, kynurenine 3-monooxygenase (KMO), catalyses the hydroxylation of L-kynurenine in tryptophan metabolism and was ubiquitinated by SCF^{Fbxo7} in the protein array (Fig. 3.31, Appendix A).

Therefore, validating KMO as a substrate for SCF^{Fbxo7} may be interesting to further understand the altered tryptophan metabolism in $CD4^+$ T cells from our Fbxo7-deficient mice (Fig. 3.30). Finally, several enzymes involved in both fatty acid metabolism and β-oxidation, and fatty acid synthesis and elongation, were identified in our Fbxo7 screens (Fig. 3.31, Appendix A), including two acyl-CoA synthetase enzymes involved in activating medium and long fatty acids (ACSM3 & ACSL5), two enzymes in the subsequent β-oxidation cycle (ACADM & HADH), and fatty acid synthase (FASN) responsible for *de novo* biosynthesis of long-chain saturated fatty acids. Moreover, some fatty acid metabolites were downregulated in mutant T cells, suggesting that Fbxo7 may be implicated in these pathways.

Although metabolic networks are complex and this map does not identify any single Fbxo7 interacting protein responsible for the metabolic phenotypes observed, it does identify areas of notable metabolic alteration and selects putative Fbxo7 substrates that may be appropriate for further investigation.

Next page

Figure 3.31: A map of key metabolic pathways disrupted in Fbxo7-deficient T cells, annotated with putative Fbxo7 binding partners.

The Log2(fold-change) in intracellular metabolite concentration from untargeted metabolomics profiling on $CD4^+$ T cells from WT or $Fbxo7^{LacZLacZ}$ mice is represented by colour gradient as per the key (Log2(fold-change) -1 is green to +1 is red). Not every metabolite measured is displayed in this map. Proteins identified as putative Fbxo7 substrates in the yeast two-hybrid, mass spectrometry and protein microarray screens are annotated in pink ellipse.

Figure 3.31

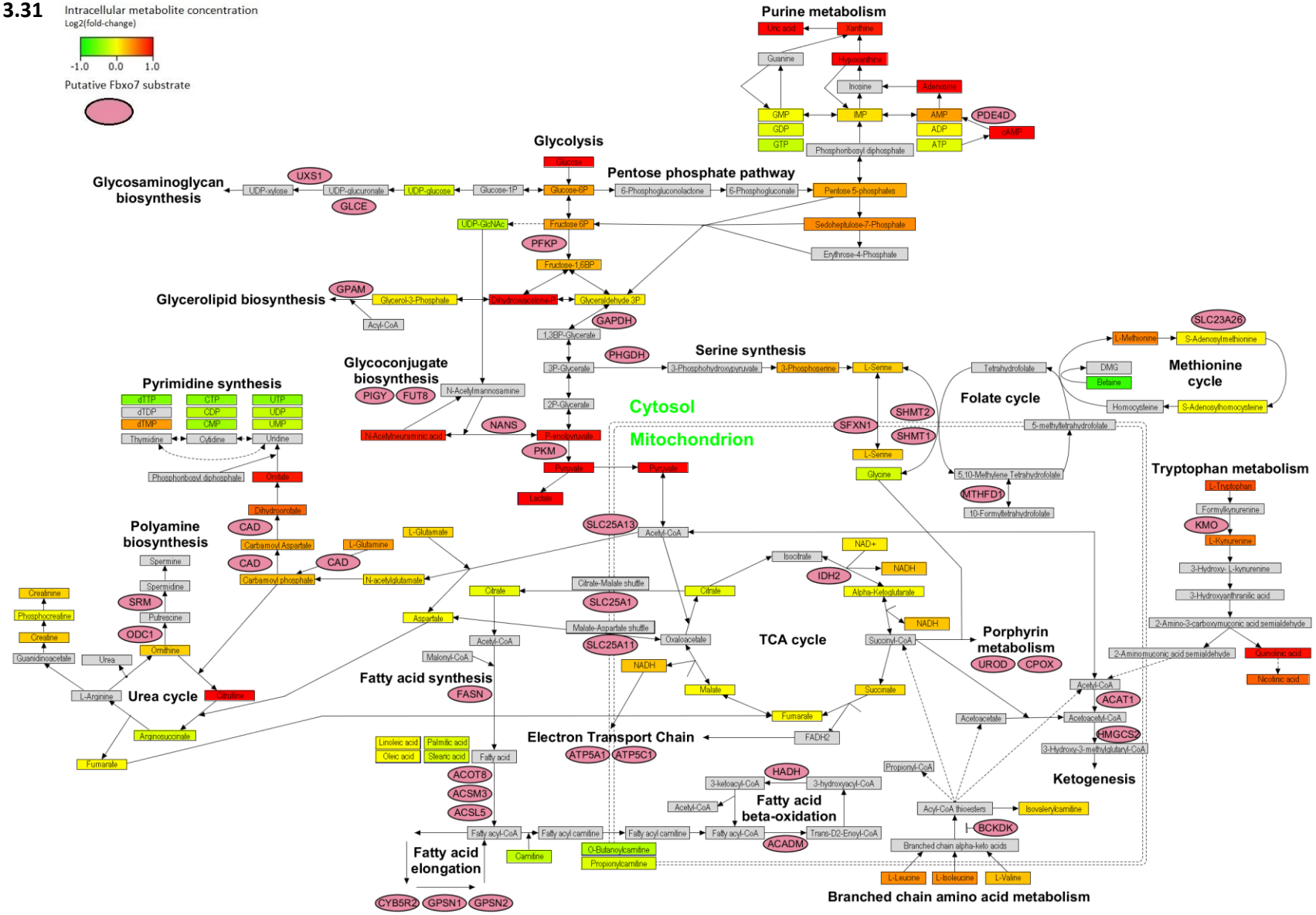
Intracellular metabolite concentration
Log2(fold-change)
-1.0
0.0
1.0
Putative Fbxo7 substrate
Purine metabolism
Uric acid
Xanthine
Guanine
Hypoxanthine
Inosine
Adenosine
GMP
GDP
GTP
IMP
AMP
ADP
ATP
PDE4D
cAMP
Phosphoribosyl diphosphate
Glycolysis
Glucose
Pentose phosphate pathway
Glycosaminoglycan biosynthesis
UXS1
UDP-xylose
UDP-glucuronate
GLCE
UDP-glucose
Glucose-1P
Glucose-6P
6-Phosphogluconolactone
6-Phosphogluconate
Pentose 5-phosphates
UDP-GlcNAc
Fructose 6P
Sedoheptulose-7-Phosphate
Erythrose-4-Phosphate
PFKP
Fructose-1,6BP
Glycerolipid biosynthesis
GPAM
Glycerol-3-Phosphate
Acyl-CoA
Dihydroxyacetone-P
Glyceraldehyde 3P
GAPDH
1,3BP-Glycerate
Glycoconjugate biosynthesis
PIGY
FUT8
N-Acetylmannosamine
N-Acetylneuraminic acid
NANS
PHGDH
Serine synthesis
3P-Glycerate
3-Phosphohydroxypyruvate
3-Phosphoserine
L-Serine
2P-Glycerate
P-enolpyruvate
PKM
Pyruvate
Lactate
Cytosol
Mitochondrion
Pyrimidine synthesis
dTTP
dTDP
dTMP
CTP
CDP
CMP
UTP
UDP
UMP
Thymidine
Cytidine
Uridine
Phosphoribosyl diphosphate
Orotate
Dihydroorotate
CAD
Carbamoyl Aspartate
Carbamoyl phosphate
L-Glutamine
L-Glutamate
N-acetylglutamate
Polyamine biosynthesis
Spermine
Spermidine
Putrescine
SRM
ODC1
Ornithine
Creatinine
Phosphocreatine
Creatine
Guanidinoacetate
Urea
L-Arginine
Urea cycle
Citrulline
Arginosuccinate
Fumarate
SLC25A13
Acetyl-CoA
Citrate
Citrate-Malate shuttle
SLC25A1
Aspartate
Malate-Aspartate shuttle
SLC25A11
Oxaloacetate
Malonyl-CoA
Fatty acid synthesis
FASN
NADH
Malate
Isocitrate
NAD+
IDH2
Alpha-Ketoglutarate
TCA cycle
Succinyl-CoA
Succinate
Fumarate
FADH2
Electron Transport Chain
ATP5A1
ATP5C1
Linoleic acid
Oleic acid
Palmitic acid
Stearic acid
Fatty acid
ACOT8
ACSM3
ACSL5
Fatty acyl-CoA
Fatty acyl carnitine
Carnitine
O-Butanoylcarnitine
Propionylcarnitine
Fatty acid elongation
CYB5R2
GPSN1
GPSN2
HADH
3-ketoacyl-CoA
3-hydroxyacyl-CoA
Acetyl-CoA
Fatty acid beta-oxidation
Trans-D2-Enoyl-CoA
ACADM
Propionyl-CoA
Acyl-CoA thioesters
Isovalerylcarnitine
BCKDK
Branched chain alpha-keto acids
L-Leucine
L-Isoleucine
L-Valine
Branched chain amino acid metabolism
Folate cycle
Tetrahydrofolate
SHMT2
SHMT1
SFXN1
5-methyltetrahydrofolate
5,10-Methylene Tetrahydrofolate
MTHFD1
10-Formyltetrahydrofolate
Glycine
L-Serine
Methionine cycle
L-Methionine
S-Adenosylmethionine
SLC23A26
DMG
Betaine
Homocysteine
S-Adenosylhomocysteine
Tryptophan metabolism
L-Tryptophan
Formylkynurenine
KMO
L-Kynurenine
3-Hydroxy- L-kynurenine
3-Hydroxyanthranilic acid
2-Amino-3-carboxymuconic acid semialdehyde
2-Aminomuconic acid semialdehyde
Quinolinic acid
Nicotinic acid
Porphyrin metabolism
UROD
CPOX
Acetoacetyl-CoA
ACAT1
Acetoacetate
HMGCS2
3-Hydroxy-3-methylglutaryl-CoA
Ketogenesis

3..7 Hematopoietic and lymphoid cells show dependency on Fbxo7

A hurdle in the execution of these studies has been the sensitivity of T cells to manipulation of Fbxo7 levels. Whilst T-ALL cells expressing an *FBXO7*-targetting shRNA were viable and showed normal levels of proliferation (data generated by Dr Shachi Patel, not shown), they did quickly adapt to lose their Fbxo7 knockdown within 1-3 weeks (Fig. 3.32) and hence their use was limited to a few passages. I also sought to overexpress Fbxo7 in T-ALL cells using the Neon electroporation system, to study the complementation of Fbxo7. Following optimisation, I co-transfected plasmids expressing untagged or FLAG-tagged Fbxo7 and mCherry at a 3:1 ratio, then measured protein expression by flow cytometry and immunoblotting (Fig. 3.33). Despite efficient electroporation yielding 44.7% mCherry$^+$ CCRF-CEM cells and 83.1% mCherry$^+$ MOLT-4 cells, neither cell line showed an increase in Fbxo7 protein levels when transfected with FLAG-tagged or untagged shRNA-resistant Fbxo7 constructs, compared to the empty vector control (Fig. 3.33). This suggests that, despite efficient electroporation, T-ALL cells downregulate exogenous Fbxo7 expression to maintain physiological Fbxo7 protein levels.

Several lines of evidence indicated a dependency of hematopoietic cells on Fbxo7. As described, T-ALL cells were somewhat resistant to manipulation of Fbxo7 levels *in vitro* (Fig. 3.32 and Fig. 3.33), and murine CD4$^+$ T cells lacking Fbxo7 showed reduced viability compared to WT (Fig. 3.22). In fact, several hematopoietic deficiencies have been previously described in this mouse model, including defective thymocyte development and significantly reduced numbers of peripheral T cells[106]. Moreover, studies have shown that T-ALL cells rely on Cdk6 inhibition of glycolysis to promote cell survival[304], and I have subsequently shown that Fbxo7 is required for Cdk6 activity towards PFKP (Fig. 3.10) and inhibits glycolysis (Fig. 3.20, Fig. 3.25, Fig. 3.26). I therefore reasoned that Fbxo7 may also be essential for viability in haematological malignancies, since Cdk6 is the major kinase expressed in these cell lineages. I assessed the requirement for Fbxo7 in over 1000 cell lines by exploring the Cancer Dependency Map[459]. Approximately 8% of cell lines were strongly selected as dependent on Fbxo7 and, consistent with my model, I found that haematopoietic and lymphoid lineages are among the significantly enriched cell lines showing a preferential dependency on Fbxo7 (Fig. 3.34). These findings indicate an essential role for Fbxo7 in these malignancies.

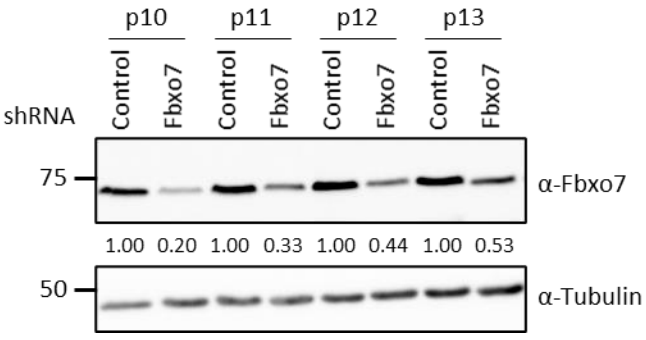

Figure 3.32: Loss of Fbxo7 knockdown with serial passage of CCRF-CEM cells.

Cell lysates were made from CCRF-CEM cells expressing a control or Fbxo7 shRNA following successive passages. Fbxo7 protein levels were analysed by immunoblot analysis. (n=1)

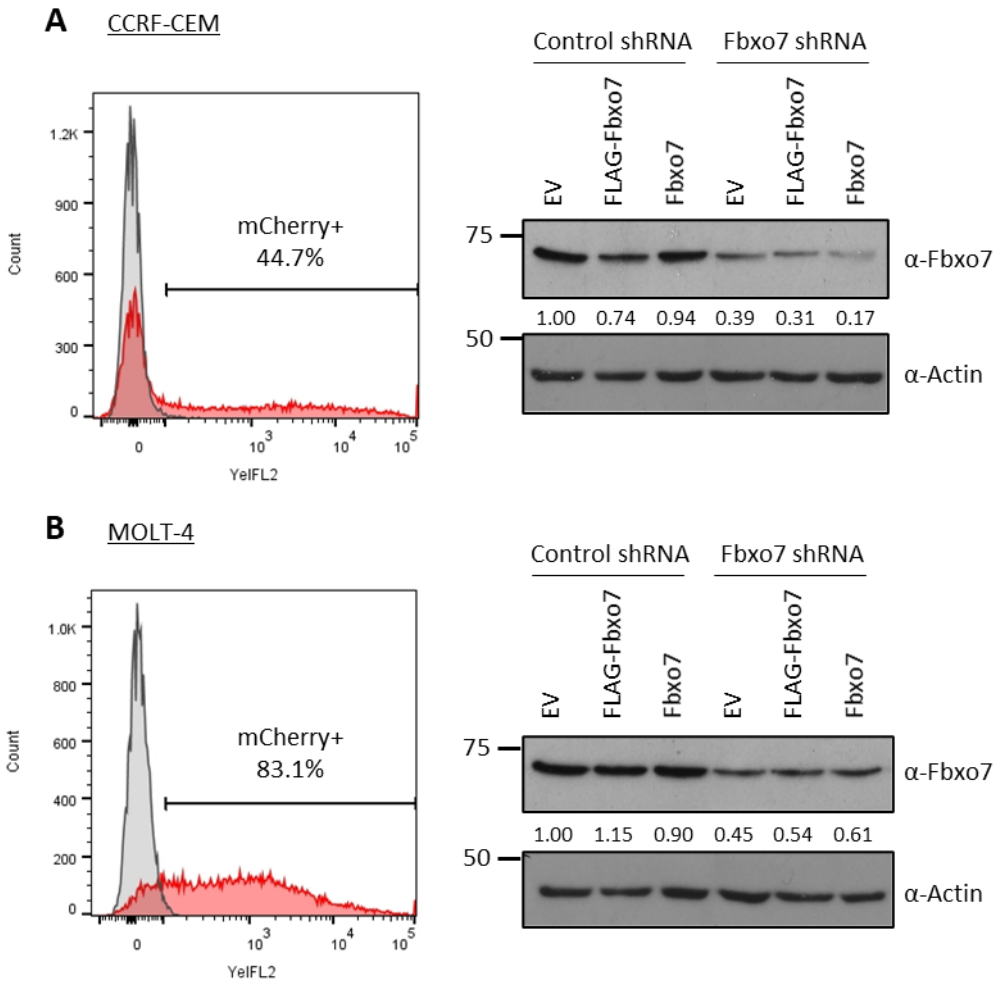

Figure 3.33: Despite efficient electroporation, T-ALL cells do not overexpress exogenous Fbxo7.

CCRF-CEM and MOLT-4 cells expressing a control or Fbxo7 shRNA were co-transfected with untagged or FLAG-tagged Fbxo7 constructs and mCherry at a 3:1 ratio. 48 hours after electroporation, the proportion of transfected mCherry$^+$ cells was measured by flow cytometry and the Fbxo7 protein detected by immunoblot from cell lysates. (n=2)

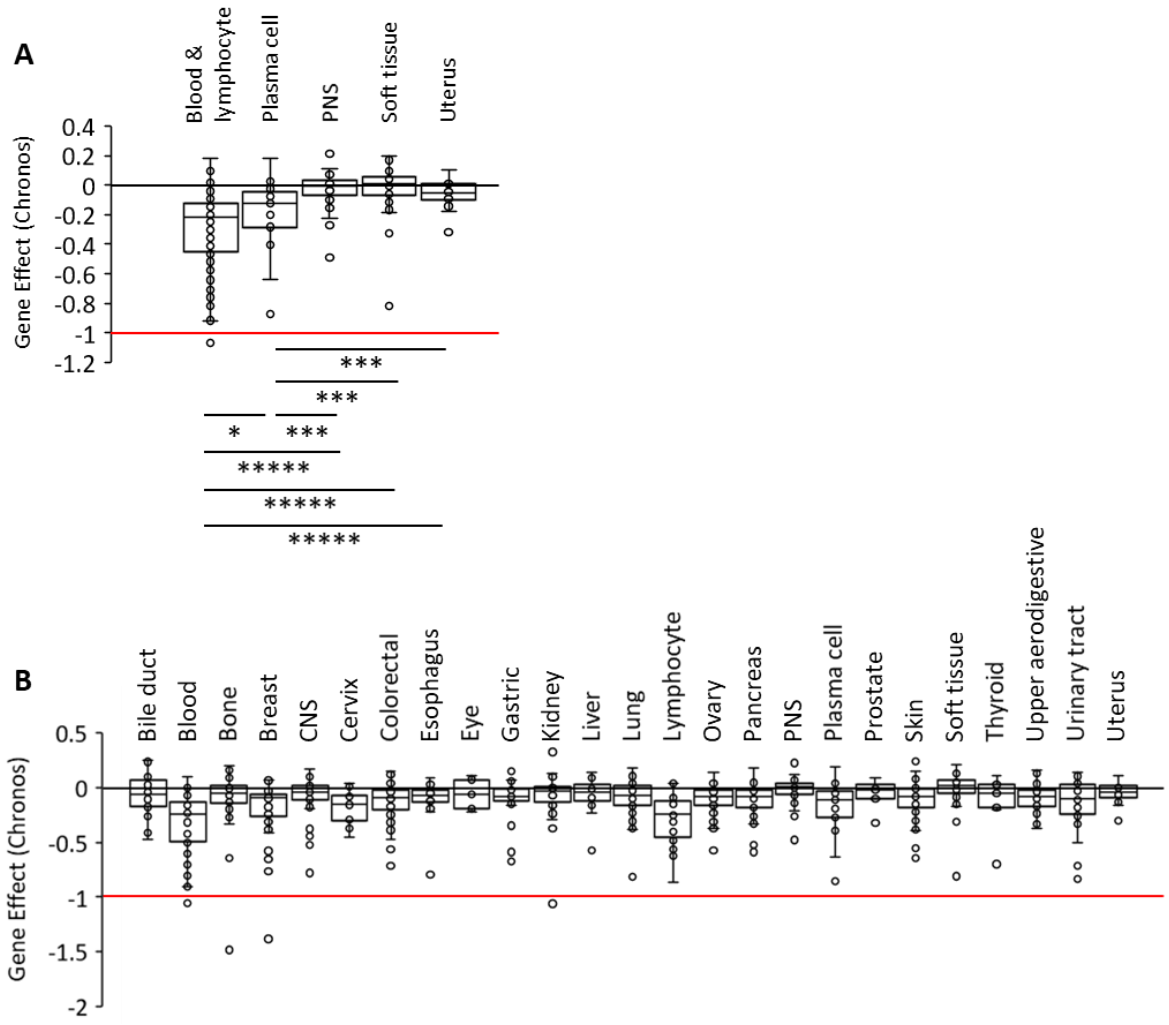

Figure 3.34: Blood, lymphocyte and plasma cell cancer lines are significantly enriched for dependency on *FBXO7*.

Chronos gene dependency scores for *FBXO7* in cancer cell lines of various lineages, plotted using data publicly available on the DepMap portal (DepMap.org). A Chronos score of 0 indicates that a gene is non-essential, whilst -1 is comparable to the median of all pan-essential genes.

(A) Blood, lymphocyte and plasma cell lines were compared, and statistics performed against selected lineages with a mean Chronos score around 0 (i.e., non-essential).

(B) Individual analysis of all cell lineages.

(Total n=1020, blood & lymphocyte n=111, plasma cell n=21, peripheral nervous system (PNS) n=32, soft tissue n=44, uterus n=34). * p<0.05, ** p<0.01, *** p<0.005, **** p<0.001, ***** p<0.0005

Discussion

In this chapter I aimed to validate a hit from our Y2H screen and determine whether PFKP interacts with, and is regulated by, Fbxo7. I verified that Fbxo7 binds and ubiquitinates PFKP and showed that this requires both the N-terminal Ubl domain and C-terminal PRR of Fbxo7. Both termini are reported to mediate substrate interactions, with HURP and cIAP binding the PRR[70,75] and others such as GSK3β, UXT-V2 and PSMA2 requiring the Ubl domain[76,81,88]. However, PFKP is the first substrate reported to require both termini of Fbxo7. Although PFKP was clearly ubiquitinated by SCF^{Fbxo7}, reducing Fbxo7 did not alter the steady state levels or half-life of PFKP, indicating non-degradative effects. This is not uncommon for SCF^{Fbxo7}, which is reported to promote the degradation of only one-third of its known substrates[70,76,86,99], whilst the other substrates are stabilised, re-localised or have their activity altered by SCF^{Fbxo7} [74,77,80,81,89,460]. However, other ligases, TRIM21, HRD1 and A20, have been reported to catalyse the ubiquitination-mediated degradation of PFKP in glioblastoma and breast cancer, and PFKL in hepatocellular carcinoma[388,399,462].

I identified the presence of two dominant species of PFKP, one of which had a 10-15 kDa increase in MW, indicative of a PTM. Whilst the intensity of this upper form correlated with the presence of Fbxo7, through the overexpression of Fbxo7 WT or inactive ΔFbox, I confirmed that it was not dependent on Fbxo7 ligase activity. Therefore, the modified subpopulation is not a multi-mono or di-ubiquitinated PFKP moiety appended by SCF^{Fbxo7}. One possibility is that, alongside its own ligase activity towards PFKP, Fbxo7 binding may additionally promote ubiquitination by another E3 ligase. This may also explain the intermediate ubiquitination of PFKP following overexpression of FLAG-Fbxo7 ΔFbox *in cellulo* ubiquitination assays, since this ligase-dead Fbxo7 mutant may still bind to PFKP. Nonetheless, this subpopulation is unaffected by proteasome inhibition and its levels do not decrease over the course of an 8-hour cycloheximide chase, indicating that it does not promote PFKP degradation. It is therefore unlikely to be ubiquitination by any of the reported PFKP-directed E3 ligases (TRIM21, HRD1 and A20)[388,399,462]. A second, possibility is that this band represents phosphorylated PFKP. Since I have shown that Fbxo7 promotes Cdk6 activity towards PFKP it is reasonable that, in the presence of Fbxo7, an increase in phosphorylated PFKP would be observed. This is consistent with my data showing a reduction in PFKP monomer/dimer forms with Fbxo7 knockdown, since a decrease in PFKP phosphorylation by Cdk6 would promote tetramer assembly. Genetic knockdown of PFKP may be used to evaluate the specificity of both antibodies and confirm that all bands discussed represent PFKP, whilst mass spectrometry analysis of the protein bands could identify if PTMs are present.

PFKP is frequently regulated by PTMs including phosphorylation, O-GlcNAcylation and acetylation, to enable a rapid physiological response to cellular signalling[304,388,395,398]. One common mechanism of

PFKP regulation by both PTMs and allosteric regulators is the disruption or stabilisation of the PFKP active tetrameric state. This is true for the phosphorylation of PFKP by Cdk6 which dissociates PFKP tetramers and inhibits glycolysis[304]. I have shown that Fbxo7 can regulate PFKP via two alternative PTMs: ubiquitination and phosphorylation. Mechanistically, I have shown that Fbxo7 ubiquitination activity towards PFKP is independent of Cdk6, whilst the previously reported interaction and phosphorylation of PFKP by Cdk6 requires Fbxo7. These two mechanisms may act in concert or opposition since the non-degradative effects of the ubiquitination remain to be elucidated. Yet ultimately a loss of Fbxo7 reduces the proportion of inactive monomer/dimer PFKP, suggesting a stabilisation of the active tetrameric state and positioning Fbxo7 as a negative regulator of glycolysis.

I found that several phenotypes observed when Fbxo7 is reduced in primary and malignant T cells, including a decrease in the inactive monomer/dimer forms of PFKP, increase in glycolysis and ROS, and reduced T cell viability, phenocopy the loss or inhibition of Cdk6[118,119,122,304]. This proposes the idea that a major role for Fbxo7 is as an activator of Cdk6, and my findings using the biosensor based on a Cdk6-phosphoacceptor in PFKP support this theory. I further hypothesise that this Cdk6-activating function conveys an essential role for Fbxo7 in hematopoietic cells. Fbxo7-deficient mice show hematopoietic defects reminiscent of $Cdk6^{-/-}$ mice, including thymic hypoplasia, reduced cellularity in the spleen, and anaemia[103,104,106,119,122]. By surveying the Depmap dataset, I also found that haematological and lymphocytic malignancies, where Cdk6 is highly expressed, are specifically dependent on Fbxo7. Moreover, I have experimentally observed that T-ALL cells resist modulation of Fbxo7 expression by shRNA, siRNA and transient overexpression. Together these provide evidence of a critical role for Fbxo7 in blood lineages, likely via Cdk6 activation.

Alongside the Cdk6-dependent changes to PFKP oligomerisation, glycolysis, oxidative stress and viability, a recent paper reported that, in T-ALL cells, PFKP dimers phosphorylated by Cdk6 can be translocated to the nucleus where, in concert with c-Myc, they induce expression of the chemotaxis CXCR4 receptor[396]. Based on my data showing that Cdk6 phosphorylation of PFKP requires Fbxo7, we hypothesise that loss of Fbxo7 may reduce nuclear PFKP, CXCR4 transcription, and cancer invasion, analogous to Cdk6 inhibition. This interesting proposal could warrant further investigation. Furthermore, Cdk6 is also reported to regulate the glycolytic enzyme PKM2 in a manner analogous to PFKP[304]. Since PKM was identified as an Fbxo7-interacting protein in our MS screen, it would be interesting to determine whether Fbxo7 also promotes this phosphorylation to elicit a compounding effect on glycolysis.

Although several effects of Fbxo7 loss replicate those of Cdk6 inhibition as described above, my data show a discrepancy in the source of the elevated oxidative stress. Wang et al. reported that PFKP

phosphorylation by Cdk6 increases glycolysis, reduces glucose-derived carbon in the PPP and hence NADPH generation, and thus increases cellular ROS[304]. Although I observed an increase in ROS in $CD4^+$ T cells from our $Fbxo7^{LacZ/LacZ}$ mice, my data cannot attribute this to a reduction in the PPP since 24-hour ^{13}C-isotype tracing showed elevated flux through both glycolysis and the oxidative PPP. It would be preferable to repeat this experiment with a time-course of ^{13}C-isotype tracing to observe the kinetics of lactate labelling, since more meaningful differences may be observed at earlier time points. The generation of ROS, antioxidant molecules and redox cofactors is dynamically modulated by a multitude of metabolic processes[463]. Given the broad metabolic alterations seen in Fbxo7-deficient T cells, it is also possible that the oxidative stress observed arises from one, or several alternative pathways. For example, intracellular glycine is reduced by 20% in mutant T cells compared to WT, and its extracellular release is 70% lower. Since glycine is critically required for glutathione synthesis[464], this deficit may impair cellular oxidative capacity. Several other studies have also reported that deficiencies in Fbxo7 are associated with an increase in ROS, with proposed mechanisms including a reduction in the NAD^+ pool and impaired mitochondrial function[465–467].

Previous work has characterised several T cell phenotypes in mice lacking Fbxo7, and these are interesting to consider in the context of my work describing Fbxo7 as a glycolytic regulator[104,106]. Whilst Fbxo7-deficient mice have fewer $CD4^+$ T cells in the periphery, these T cells expand more rapidly upon activation, and this has been attributed to reduced levels of p27 [106]. T cell activation is characterised by a predominantly glycolytic programme that is upregulated within 6 hours of TCR engagement to facilitate clonal expansion[214]. I have shown that activated $Fbxo7^{LacZ/LacZ}$ T cells have elevated glycolysis compared to WT, so they may be in a metabolic state more conducive to rapid proliferation. Therefore, there may be a metabolic contribution to the increased proliferation of activated T cells previously described. These activated Fbxo7-deficient T cells secrete increased IL-2, IFNγ (Th1 cytokines) and IL-10 (Th2/Treg cytokine), despite lower cell numbers[106]. The production of certain cytokines, including IL-2 and IFNγ, relies on specific metabolic regulation, since GAPDH and LDH both have RNA-binding functions that mediate cytokine mRNA stability and expression[214,241,249]. The upregulated glycolysis in T cells lacking Fbxo7 may reduce the availability of GAPDH and LDH to sequester IFNγ and IL-2 mRNA and hence facilitate the elevated cytokine secretion described. Increased IL-10 secretion and a proportional increase in $CD44^{High}$ $CD62L^{Low}$ markers suggest polarisation towards regulatory and central memory T cell subsets in Fbxo7-deficient mice[104]. Differentiated T cell subsets display discrete metabolic profiles, with effector $CD4^+$ T helper cells notably more glycolytic than regulatory and memory subsets. It is therefore interesting that I show Fbxo7-deficient $CD4^+$ T cells have higher levels of glycolysis despite significantly lower levels of viability

and activation, and an increase in the proportion of less glycolytic regulatory and central memory T cell subsets in mutant mice.

My analysis of the metabolome of activated $CD4^+$ T cells lacking Fbxo7 indicates that, in addition to increased glycolysis, these primary cells have numerous metabolic alterations, including in arginine metabolism and in purine and pyrimidine biosynthesis. My data show reduced pyrimidine concentrations and elevated purine metabolic intermediates in Fbxo7-deficient T cells, implying disrupted pyrimidine synthesis or usage, and altered purine metabolism. The expansion of nucleotide pools is associated with T cell activation, and nucleotides may regulate proliferation, the cell cycle and survival following activation[251,468]. Moreover, the inhibition of both purine and pyrimidine synthesis is shown to favour $Foxp3^{High}$ Treg cells[251]. Although highly speculative, it is therefore possible that the altered nucleotide metabolism highlighted in my data may contribute to the reduced viability or increased IL-10 secretion of Fbxo7-deficient T cells. That said, the limitations of this experiment should also be mentioned, since culture media composition is increasingly recognised to have profound effects on cellular metabolism[469]. This analysis was performed in traditional RPMI culture medium which Cantor, et al, have shown can particularly alter de novo pyrimidine synthesis compared to a physiological medium[469]. My metabolic fingerprinting analysis also highlights a change in arginine metabolism in Fbxo7-deficient T cells. Geiger, et al, show that within the first 24-48 hours following T cell activation, arginine uptake increases but its intracellular concentration drops due to rapid metabolism to spermidine and proline[232]. This arginine metabolism is critical to prevailing T cell function since increased arginine promotes OXPHOS over glycolysis and induces a Tm phenotype with improved persistence and anti-tumour efficacy[232]. This central role of arginine in T cell metabolism therefore makes the disrupted urea cycle and arginine metabolism in our $Fbxo7^{LacZ/LacZ}$ mouse, and putative Fbxo7 substrates ODC1 and SRM, an interesting area of future investigation. Finally, tryptophan and its metabolites are implicated in T cell fitness and their effects are two-fold. Depletion of exogenous tryptophan, such as in the tumour microenvironment, can induce cell cycle arrest and anergy, whilst metabolites such as kynurenine suppress effector T cell function, stimulate apoptosis, and polarise to Treg cells[349,470–472]. I observed an increase in intracellular tryptophan and its catabolic products in $Fbxo7^{LacZ/LacZ}$ T cells, which also secreted more kynurenine. Another interesting proposition is therefore that altered tryptophan metabolism may contribute to reduced cell viability, proliferative capacity or Treg polarisation. Interestingly, tryptophan metabolites have been shown to reduce protein aggregation in Alzheimer's disease (AD) and are proposed as endogenous anti-AD metabolites[473], highlighting that Fbxo7-induced metabolic alterations may have implications in other cell types and pathological settings.

In summary, I have identified broad metabolic alterations in primary $CD4^+$ T cells lacking Fbxo7, several of which may contribute to the T cell phenotypes observed in this $Fbxo7^{LacZ/LacZ}$ mouse. Specifically, my data validate Fbxo7 as a negative regulator of glycolysis in T cells. I propose a mechanism through which Fbxo7 can promote two PTMs on PFKP: ubiquitination and phosphorylation, to ultimately inhibit the assembly of active PFKP tetramers. Since several effects of Fbxo7 loss phenocopy that of Cdk6 inhibition, my data indicate that a key role for Fbxo7 is as a Cdk6 activator, and this conveys a particular dependency in hematopoietic cells. Given the significance of Cdk6 in diseases such as cancer, and the availability of Cdk6 kinase inhibitors, it will be interesting to ascertain whether the regulation of Cdk6 represents a common, therapeutically tractable, pathway mediating Fbxo7's effects in physiological and pathological settings.

CHAPTER 4

Fbxo7 regulation under cellular stress

Introduction

Nutrient sensing, feedback loops and metabolite-induced signalling cascades are commonplace in cellular systems to maintain dynamic homeostasis. Given the central importance of glucose as a metabolic substrate, it is perhaps unsurprising that it can also induce signalling pathways that control cell physiology. In mammals, this is largely through the action of AMPK which detects changes in glucose metabolism by sensing the ATP:AMP ratio in a cell, and is widely regarded as a central regulator of energy homeostasis[474,475]. AMPK activation by elevated AMP is responsible for the transcriptional adaptation of mammalian cells to several stresses that deplete ATP, of which nutrient starvation is one. Through AMPK-induced transcriptional reprogramming, energy balance is restored by switching off anabolic pathways that consume ATP and promoting catabolic ATP-generating pathways[475]. Moreover, AMPK is a central node that integrates several stress responses with the induction of macroautophagy (herein, called autophagy), a catabolic process in which cytoplasmic content is degraded in lysosomes to recycle the components of macromolecules[476].

Examples of starvation-induced responses in metabolic proteins include the upregulation of glutamine transporters and glutaminase to promote compensatory glutaminolysis[477], and the inhibition of acetyl-CoA carboxylase enzymes to facilitate fatty acid oxidation[478,479]. Since I discovered a role for Fbxo7 in the regulation of glycolysis (Chapter 3), I hypothesised that Fbxo7 may too be subject to regulation by nutrient starvation.

Similarly, oxidative stress induces a heterogeneous cellular stress response involving the activation of MAPK, PI3K/AKT, NFκB and p53 signalling cascades, amongst others, to mediate a delicate balance between cell survival and death depending on the nature of the insult[480]. My work (Chapter 3) and previous findings have shown that deficiencies in Fbxo7 are associated with an increase in ROS[465–467], suggesting that Fbxo7 has a ROS-neutralising role. As such, I reasoned that Fbxo7 may also be regulated by oxidative stress to promote this function when required.

In this chapter I aimed to determine whether Fbxo7 is regulated by metabolic or oxidative stress, and to outline the mechanisms through which this may occur. Moreover, I sought to investigate whether the loss of Fbxo7 would increase the sensitivity of cells to such stresses.

Results

4..1 Fbxo7 protein levels are sensitive to glucose availability

To first determine whether Fbxo7 protein levels were influenced by glucose availability, I cultured HEK293T cells and T-ALL cell lines CCRF-CEM, MOLT-4 and Jurkat E6 in 4.5 g/L or 0 g/L glucose for 48 hours prior to lysis and immunoblotting. Fbxo7 protein was consistently reduced following glucose starvation, by up to 65% (Fig. 4.1). I next tested whether this was a dose-dependent effect. The blood sugar level of a healthy person ranges from 0.6 – 1.4 g/L glucose[481]. The concentration in a diabetic patient experiencing hyperglycaemia will rise above this, and they are at risk of entering a coma above 6 g/L glucose[482], or in hypoglycaemic conditions below 0.5 g/L glucose[483]. Astonishingly, records show that some patients have survived above 20 g/L glucose in their blood[484]. To mimic a range of glycaemic conditions, I cultured CCRF-CEM and Jurkat cells in a titration of 0 – 10 g/L glucose for 48 hours prior to lysis and immunoblotting. Fbxo7 protein levels positively correlated with glucose concentration in both cell lines, in a dose-dependent manner, even at hyperglycaemic levels (Fig. 4.2). To test this relationship in a physiological setting, I isolated $CD4^+$ T cells from the spleen of WT mice and activated them for 48 hours in 4.5 g/L or 0 g/L glucose. These primary mouse $CD4^+$ T cells showed a 67% decrease in Fbxo7 when activated in the absence of glucose (Fig. 4.3). Interestingly, when these cells were maintained for a further 5 days in the presence of IL-2, the sensitivity of Fbxo7 to glucose availability was lost, suggesting that IL-2 signalling can overcome this glucose effect in activated T cells.

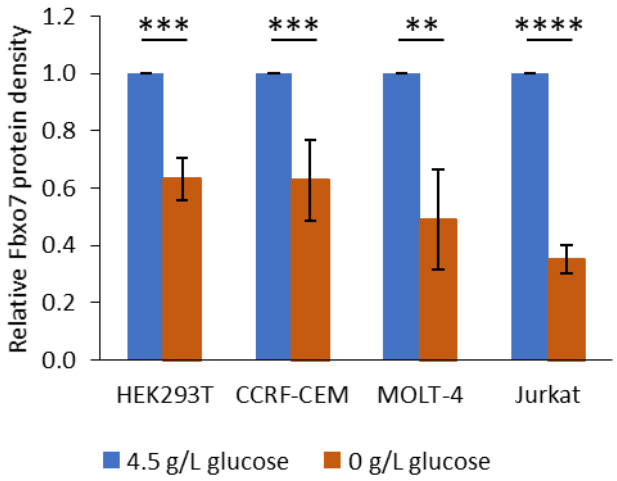

Figure 4.1: Glucose starvation reduces Fbxo7 protein levels.

HEK293T and T-ALL cells were cultured for 48 hours in media containing 0 or 4.5 g/L glucose, and cell lysates were analysed by immunoblot and quantified. (n≥3) ** p<0.01, ***p<0.001, **** p<0.0001

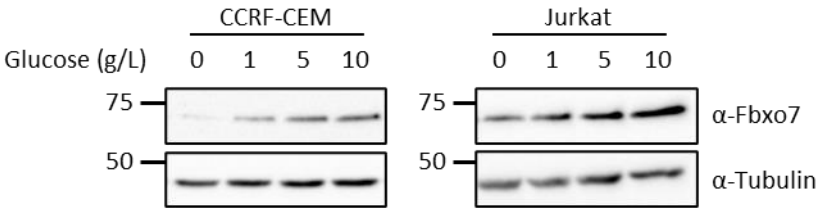

Figure 4.2: Fbxo7 protein levels positively correlate with glucose concentration in a dose-dependent manner.

CCRF-CEM and Jurkat cells were cultured for 48 hours with a titration of glucose, then lysed and analysed by immunoblot. (n=3)

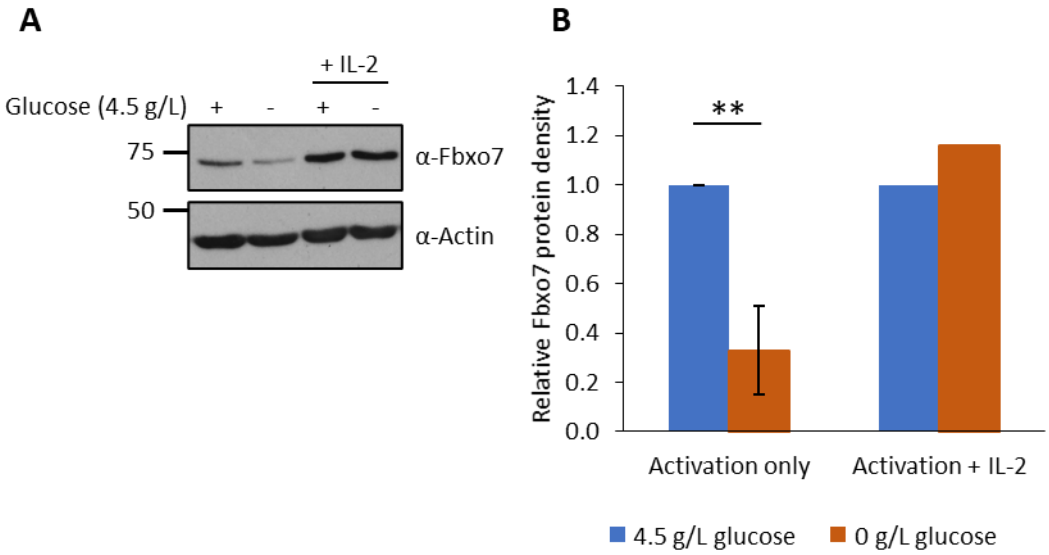

Figure 4.3: Glucose starvation reduces Fbxo7 protein levels in primary T cells, but this is overcome by IL-2.

Splenic $CD4^+$ T cells were isolated and activated *in vitro* for 48 hours in media containing 0 or 4.5 g/L glucose, and samples were taken and lysed. 40 ng/mL IL-2 was added to the remaining cells which were maintained for a further 5 days in 0 or 4.5 g/L glucose before a second set of samples were lysed. Cell lysates were analysed by immunoblot and quantified. (A) Representative immunoblot image. (B) Quantification of relative levels of Fbxo7. (Samples without IL-2 n=3, samples with IL-2 n=2) ** $p<0.01$

To understand the kinetics with which this change occurs, I performed a time course experiment of glucose addition and removal from cell culture medium. CCRF-CEM cells routinely cultured in 4.5 g/L glucose were washed and resuspended in glucose-free media, and samples were lysed at various time points following glucose removal for analysis by immunoblot (Fig. 4.4, grey bars). A 42% decrease in Fbxo7 protein was observed within 6 hours of glucose removal, and this expression level was maintained for 72 hours, suggesting a rapid signalling response. Similarly, CCRF-CEM cells that had been routinely cultured in the absence of glucose were switched to fresh media containing 4.5 g/L glucose (Fig. 4.4, yellow bars). The 34% increase in Fbxo7 protein upon the addition of glucose occurred more gradually over the 72 hours, indicating a slower adaptation. Together, these data show that there is a significant dose-dependent effect of glucose on Fbxo7 expression, and these changes can be observed within 6 hours of altering the glucose concentration.

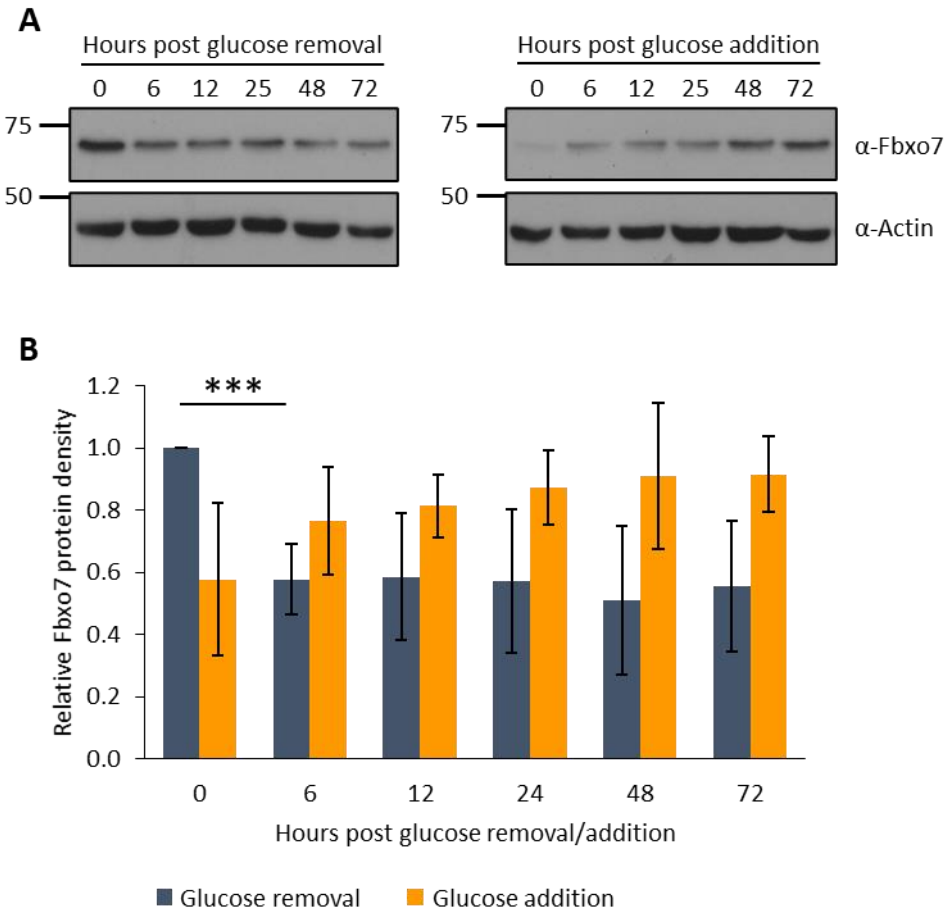

Figure 4.4: Changes to Fbxo7 protein levels occur within 6 hours of glucose modulation. CCRF-CEM cells maintained in 4.5 g/L or 0 g/L glucose had glucose acutely removed or added, and samples were taken at the indicated time intervals for 72 hours. Cells were lysed, analysed by immunoblot and quantified. (A) Representative immunoblot images. (B) Quantification of relative levels of Fbxo7. (n=4) *** $p<0.0005$

4..2 Glucose starvation induces Fbxo7 degradation by autophagy

Since Fbxo7 protein correlated with glucose availability, I sought to determine whether Fbxo7 stability was affected, and if the reduction in Fbxo7 was due to increased protein turnover during glucose starvation. CCRF-CEM cells that had been routinely cultured in 4.5 g/L glucose were washed and resuspended in media containing 4.5 g/L (maintenance) or 0 g/L (starvation) glucose, and cells were simultaneously treated with cycloheximide. A shorter Fbxo7 half-life was seen when glucose was acutely removed from cells (t½ = 4 hr in 4.5g/L glucose vs. t½ = 1.75 hr in no glucose) suggesting that glucose starvation promotes Fbxo7 protein degradation within 2 hours of glucose removal (Fig. 4.5).

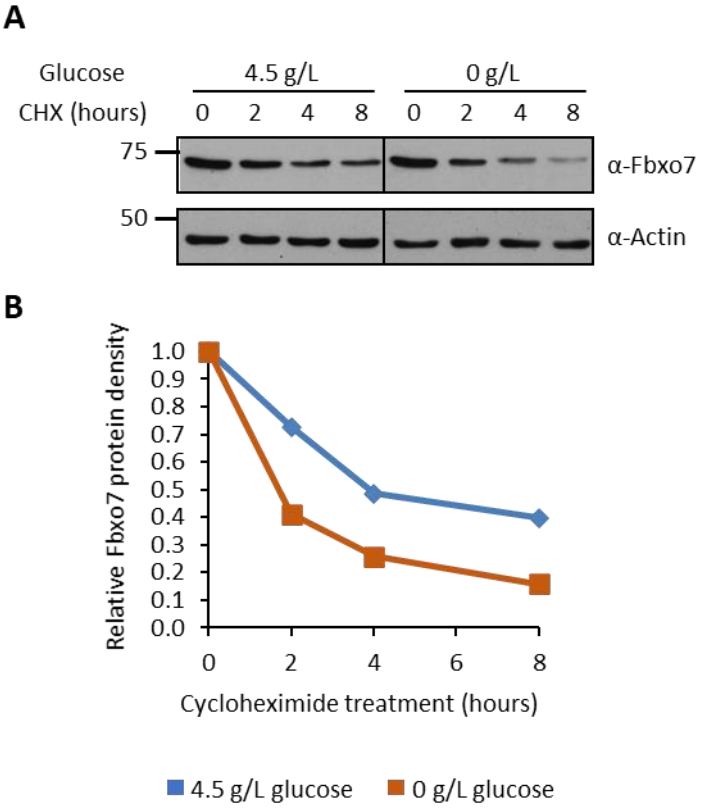

Figure 4.5: Glucose starvation reduces Fbxo7 protein half-life.

Immediately following glucose removal (0 g/L) or maintenance (4.5 g/), CCRF-CEM cells were treated with cycloheximide for up to 8 hours. Cells were lysed at time intervals, analysed by immunoblot (A) and quantified (B). (Representative of n=3)

To determine the pathway promoting Fbxo7 degradation, CCRF-CEM cells were treated with MG132 or bafilomycin A1 (BafA) to inhibit the proteasome or autophagy, respectively (Fig. 4.6). Surprisingly, proteasome inhibition with MG132 reduced Fbxo7 protein signal, but this was not dependent on glucose concentration. This phenomenon may arise from the accumulation of ubiquitinated targets upon MG132 treatment and subsequent negative feedback on Fbxo7, or may be an experimental artefact due to PTMs masking the antibody epitope. Importantly, BafA treatment rescued Fbxo7 levels after glucose withdrawal, suggesting that Fbxo7 was cleared by autophagy (Fig. 4.6).

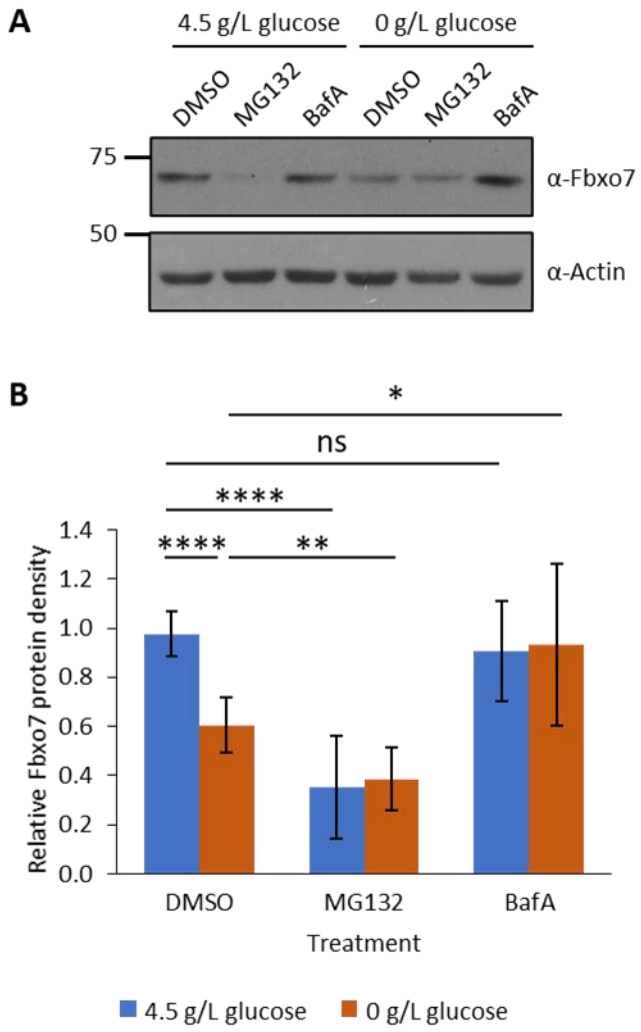

Figure 4.6: Inhibition of autophagy rescues the decrease in Fbxo7 protein induced by glucose starvation.

Immediately following glucose removal (0 g/L) or maintenance (4.5 g/), CCRF-CEM cells were treated with DMSO, 10 µM MG132 or 200 nM BafA for 5 hours. Cells were lysed, analysed by immunoblot and quantified. (A) Representative immunoblot image. (B) Quantification of relative levels of Fbxo7. (n=7). * p<0.05, ** p<0.01, ***p<0.001, **** p<0.0001

4..3 *FBXO7* is transcriptionally regulated in response to cellular stress

Glucose signalling is evidenced to have widespread impacts on gene expression, hence I investigated whether there is also a transcriptional element to the Fbxo7 response. Following 48 hours of glucose starvation, 4.5 g/L glucose was added to CCRF-CEM cells for 4 hours prior to RNA extraction and qRT-PCR analysis. As I had observed an increase in Fbxo7 protein within 6 hours of glucose addition (Fig. 4.4) I expected that, if *FBXO7* was upregulated by glucose, transcriptional changes would be measurable within this early window. Fbxo7 mRNA from glucose-starved CCRF-CEM cells was 31% lower than cells in 4.5 g/L glucose (Fig. 4.7A). Similarly, when naïve murine $CD4^+$ T cells were isolated and cultured for 4 hours in the presence (4.5 g/L) or absence of glucose, glucose starvation correlated with a 25% reduction in Fbxo7 mRNA levels (Fig. 4.7B). Together, these data indicate that *FBXO7* is a glucose-responsive gene that is transcriptionally upregulated by glucose availability in both malignant and primary cells.

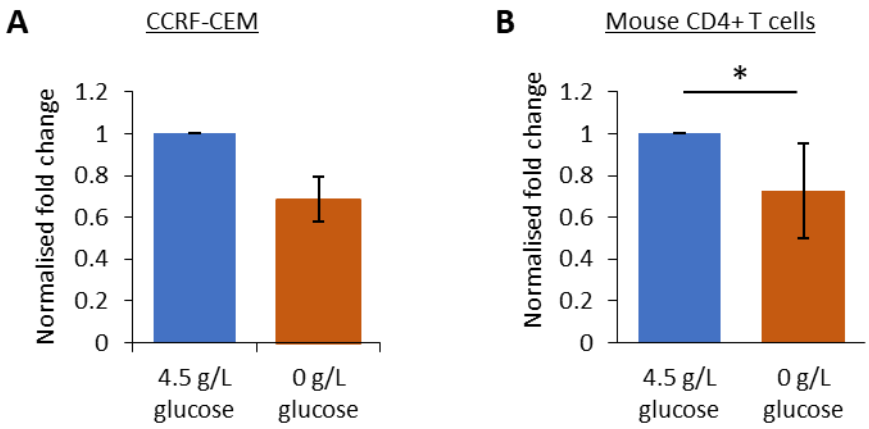

Figure 4.7: Fbxo7 mRNA is reduced by glucose starvation.

(A) CCRF-CEM cells were cultured for 48 hours in the absence of glucose. Cells were maintained in this media (0 g/L) or glucose was added (4.5 g/L) for 4 hours prior to RNA extraction and qRT-PCR analysis. Relative Fbxo7 mRNA is shown, normalised to actin. (n=2)

(B) Naïve murine $CD4^+$ T cells were isolated and incubated for 4 hours in 0 g/L or 4.5 g/L glucose. Relative Fbxo7 mRNA is shown, normalised to actin, cyclophilin and hprt. (n=6). * $p<0.05$

Since Fbxo7 is regulated by changes in glucose concentration, I sought to determine whether it is also sensitive to oxidative stress. I had previously observed elevated ROS in activated murine $CD4^+$ T cells lacking Fbxo7, thus Fbxo7 may be considered to have an anti-oxidative function (Chapter 3, Fig 3.21). I therefore reasoned that Fbxo7 may be regulated by oxidative stress in these cells as a means to promote this neutralising pathway when required. ROS accumulate during T cell activation due to the upregulation of OXPHOS[239–241], so I tested the effect of 100 µM exogenous H_2O_2 on both naïve and

activating CD4⁺ T cells following 45 minutes of exposure (Fig. 4.8). The effect of H_2O_2 in naïve cells was variable, and no significant difference was observed. However, when I exposed activating cells to H_2O_2 I observed a modest yet significant 8% upregulation in Fbxo7 mRNA (Fig. 4.8), suggesting that *FBXO7* expression is increased by oxidative stress in certain contexts.

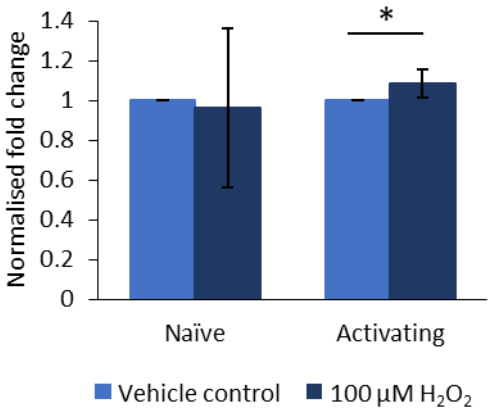

Figure 4.8: Fbxo7 mRNA is upregulated by oxidative stress in activating CD4⁺ T cells.
Murine CD4⁺ T cells were isolated and incubated for 4 hours as naïve cells or activated with α-CD3/α-CD28. These cells were exposed to 100 µM H_2O_2 or vehicle control for the last 45 minutes of the incubation/immediately following isolation, prior to RNA extraction and qRT-PCR analysis. Relative Fbxo7 mRNA is shown, normalised to actin, cyclophilin and hprt. (n=6) * $p<0.05$

Surprisingly, RNA extraction and qRT-PCR analysis from naïve and activated CD4⁺ T cells revealed a striking 80% reduction in Fbxo7 mRNA post-activation (Fig. 4.9). This occurred within 4 hours of T cell activation and was sustained up to 24 hours later. This is interesting when considered alongside protein expression data that showed an increase in Fbxo7 following prolonged culture in the presence of IL-2 (Fig. 4.3). Extensive transcriptional and metabolic reprogramming occurs following engagement of the TCR and continues throughout T cell activation as directed by cytokines. Together these data suggest that Fbxo7 is quickly transcriptionally downregulated upon TCR engagement but is later upregulated in response to IL-2.

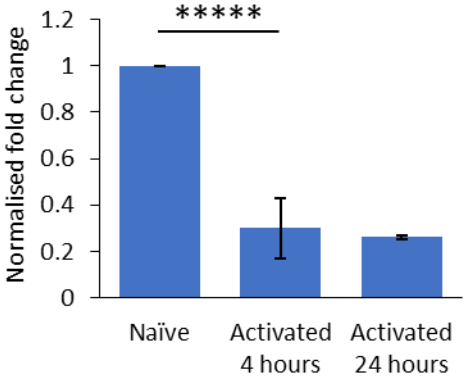

Figure 4.9: Fbxo7 mRNA is downregulated upon T cell activation.
Murine CD4⁺ T cells were isolated and activated *in vitro* for the indicated duration prior to RNA extraction and qRT-PCR analysis. Relative Fbxo7 mRNA is shown, normalised to actin, cyclophilin and hprt. (Naïve and 4 hour activated samples n=6, 24 hour activated sample n=2) ***** $p<0.00001$

4..4 Fbxo7 protein correlates with glucose availability and oxidative stress in various primary tissues

T cells, especially during activation, have a defined metabolic programme that is tightly linked to their functional output. I was therefore interested to ascertain whether Fbxo7 was also regulated by glucose availability and oxidative stress in other tissues. The thymus, pancreas, liver and lung were isolated from WT mice and processed to a single cell suspension. These cells were incubated for 3 hours in varying concentrations of glucose and Fbxo7 protein levels were analysed by immunoblot (Fig. 4.10A and C). In all tissues tested, Fbxo7 protein positively correlated with increasing glucose concentration, though the extent to which this occurred varied between tissues. The pancreas and lung showed an 8.7 and 6.5-fold increase in Fbxo7 protein at 10 g/L compared to glucose starved cells, whilst cells from the thymus and liver had a more modest 2.8 and 2.6-fold increase respectively. Nonetheless, these data confirm that Fbxo7 is regulated by glucose availability across different tissues.

The single cell suspensions from various tissues were also incubated with 100 μM H_2O_2 for 1 or 3 hours to induce oxidative stress prior to cell lysis and immunoblot analysis (Fig. 4.10B and C). Consistent with the increase in Fbxo7 mRNA in H_2O_2 treated $CD4^+$ T cells (Fig. 4.8), cells from the liver and lung displayed a dose-dependent increase in Fbxo7 protein with ongoing exposure to H_2O_2, which showed up to a 3.7-fold rise (Fig. 4.10B). Interestingly, cells from the thymus and pancreas had a 56% and 29% decrease in Fbxo7 protein respectively, following 3 hours exposure to H_2O_2, suggesting that the response to oxidative stress varies between cell and tissue types. Together, these data confirm that the regulation of Fbxo7 by glucose availability and oxidative stress is not limited to T cells, though the nature of the response may be context dependent.

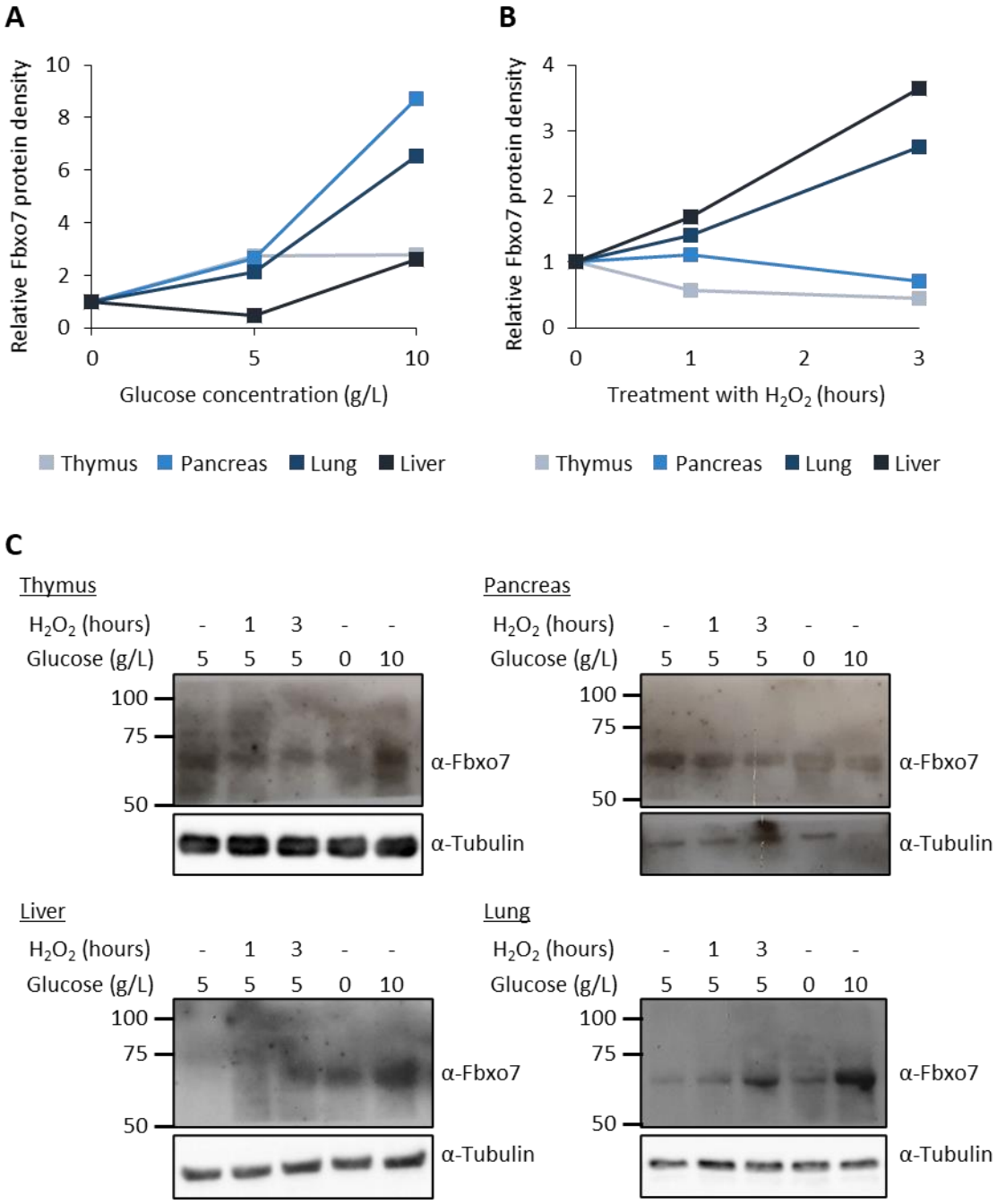

Figure 4.10: Fbxo7 protein levels are responsive to glucose availability and oxidative stress in various primary mouse tissues.

Tissues were isolated from WT mice and processed to a single cell suspension. Cells were incubated for 3 hours in a titration of glucose concentrations or treated with 100 µM H_2O_2 for 1 or 3 hours. Cells were lysed and analysed by immunoblot. (n=1)

(A) Quantification of Fbxo7 protein levels following culture in a titration of glucose for 3 hours.

(B) Quantification of Fbxo7 protein levels following exposure to 100 µM H_2O_2.

(C) Immunoblot images.

4..5 Fbxo7-deficient T cells are more sensitive to oxidative stress-induced cell death

Since Fbxo7 is regulated by glucose availability and oxidative stress, and CD4$^+$ T cells lacking Fbxo7 have elevated levels of ROS (Chapter 3, Fig 3.21), I reasoned that Fbxo7 may be involved cellular stress responses. I therefore investigated whether T cells lacking Fbxo7 had altered sensitivity to metabolic or oxidative stress. I used our mouse model in which the *FBXO7* locus is disrupted by a *LacZ* insertion and measured the viability of WT or Fbxo7-deficient CD4$^+$ T cells following *ex vivo* culture in the presence of stress. Naïve T cells cultured for 24 hours in a titration of glucose (0 to 10 g/L) all showed less than 4% variation in cell viability across the glucose concentrations, and there was no difference between WT and Fbxo7$^{LacZ/LacZ}$ cell viability (Fig. 4.11A). This suggests that glucose availability does not impact the viability of naïve T cells.

To induce oxidative stress, naïve CD4$^+$ T cells in media containing 5 g/L glucose were treated with 100 µM H_2O_2 for 1 hour. T cells lacking Fbxo7 displayed a 47.8% decrease in viability upon oxidative stress, which was up to 13% more cell death than WT cells (Fig. 4.11B & C). This suggests that T cells lacking Fbxo7 are more sensitive to cell death caused by oxidative stress.

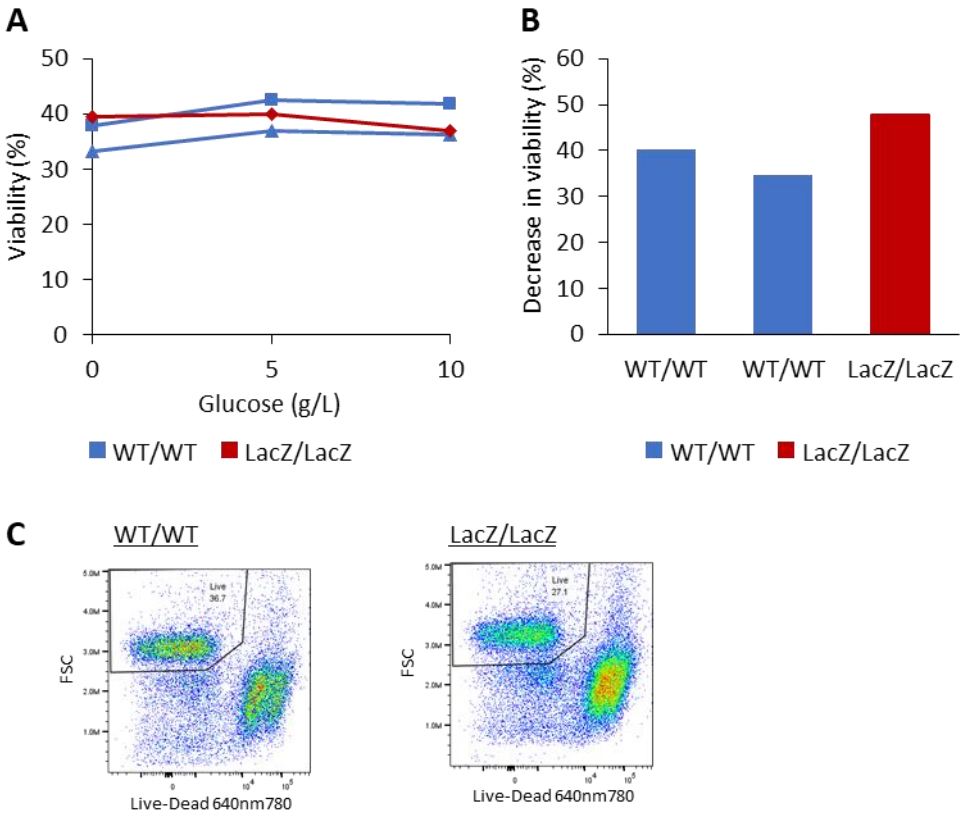

Figure 4.11: Loss of Fbxo7 reduces CD4$^+$ T cell viability in response to exogenous H_2O_2, but not glucose starvation.

Naïve CD4$^+$ T cells were incubated with (A) a titration of glucose for 24 hours or (B-C) 100 µM H_2O_2 for 1 hour, prior to flow cytometry analysis to measure the cell viability. (WT/WT n=2, LacZ/LacZ n=1)

Discussion

In this chapter I sought to determine whether Fbxo7 is regulated by changes in glucose concentration, and to outline the mechanisms through which this may occur. The cellular response to nutrient starvation typically involves an altered transcriptional programme that switches from anabolic to catabolic pathways to restore the energy balance, alongside the activation of the autophagy salvage pathway[475,476,485,486]. I have demonstrated that Fbxo7 expression is responsive to glucose concentration at both the mRNA and protein levels, utilising both these adaptive mechanisms to downregulate *FBXO7* and promote its degradation by autophagy in response to glucose starvation. It is understood that the pool of available FBPs is likely controlled by a combination of transcriptional regulation and targeted degradation/stabilisation, in part mediated by auto-ubiquitination, depending on intrinsic and extrinsic signals, and FBP substrate availability[56,57]. Whilst other FBPs are described to respond to nutrient availability, such as the muscle catabolism regulator Atrogin-1 (Fbxo32) which is transcriptionally upregulated in response to starvation[487] and the yeast FBP Grr1 which associates with Skp1 in a glucose-dependent manner to signal changes in gene expression[488], I present the first data describing the regulation of Fbxo7 by nutrient depletion and autophagy.

My data demonstrating the regulation of Fbxo7 by glucose availability may be considered alongside its role as a negative regulator of glycolysis (Chapter 3), since this suggests that Fbxo7 levels may act to adjust the glycolytic rate under different physiological and pathological conditions. I propose that, when glucose is replete, higher Fbxo7 levels may inhibit glycolysis, promoting other biosynthetic pathways (Fig 4.12). Conversely, with falling glucose concentrations, Fbxo7 may be downregulated to prioritise glycolysis over macromolecule biosynthesis. Further study could test the physiological significance of this pathway by measuring metabolic flux in response to glucose starvation, in the presence and absence of Fbxo7.

I found that Fbxo7 downregulation in response to glucose starvation was preserved at several stages throughout T cell development and function, specifically in thymus tissue, naïve and activated $CD4^+$ T cells and T-ALL cell lines. This signifies a common regulatory pathway that may have relevance in both a physiological and malignant setting. T cells undergo significant metabolic and genetic remodelling throughout their life cycle and are deeply influenced by their microenvironment. At sites of infection and in the tumour microenvironment (TME), T cells may be exposed to various cellular stresses including nutrient deprivation, oxidative stress, and hypoxia[485,489]. In fact, glucose concentrations in tumours are estimated to be 3 to 10-fold lower than in non-transformed tissues[490]. Whilst the metabolic plasticity of T cells enables them to adapt to glucose starvation by upregulating other catabolic pathways such as glutaminolysis and fatty acid oxidation[485,491], glucose availability may still alter their function as evidenced by impaired cytokine production, T cell hypo-responsiveness and

enhanced expression of inhibitory markers when cells are activated in glucose-deprived environments[340–343]. As such, a role for Fbxo7 in finetuning the glycolytic rate to reflect glucose availability, may impact on T cell survival and function in glucose depleted pathological environments such as the TME. Nonetheless, my data show that loss of Fbxo7 had no impact on the viability of naïve $CD4^+$ T cells maintained in a glucose-starved culture. This is perhaps unsurprising since naïve T cells are metabolically quiescent and do not display high levels of glycolysis[225]. The availability of additional mice would enable this investigation in the more relevant context of activated glycolytic $CD4^+$ T cells. Interestingly, the later addition of IL-2 to activated T cells abolished the glucose-dependent effect on Fbxo7, and upregulated Fbxo7 protein irrespective of glucose availability. IL-2 is a pleiotropic cytokine that sustains *MYC* expression and mTORC1 and HIF1 activation to promote the upregulation of nutrient transporters in T cells, potentiating glucose and glutamine uptake to support proliferation[492]. Interestingly, it has been shown that IL-2 production is not sensitive to glucose starvation or hypoxia[493], hence IL-2 signal transduction may overcome some effects of glucose starvation. Therefore, any functional effect of Fbxo7 regulation by glucose likely only occurs during the early stages of T cell activation.

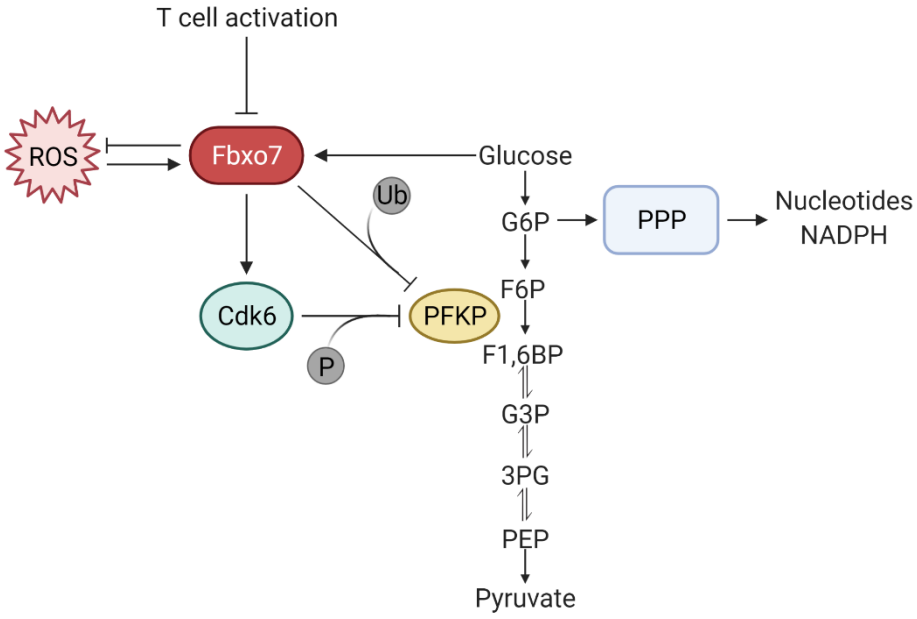

Figure 4.12: Model depicting how exposure to cellular stress may alter glycolytic regulation by Fbxo7. I propose that the adaptation of Fbxo7 levels to metabolic and oxidative stress, and T cell activation, may affect the downstream regulation of PFKP and hence alter metabolic flux through glycolysis in response to stress. Elevated ROS may upregulate Fbxo7 to promote its ROS-neutralising effect, whilst glucose starvation and T cell activation may reduce Fbxo7 levels to promote glycolysis.

My findings also suggest that Fbxo7 is regulated by oxidative stress in T cells, as *FBXO7* was upregulated by exogenous H_2O_2 treatment in activating $CD4^+$ T cells. Previous studies report that ROS are elevated in cells lacking Fbxo7, suggesting a role in neutralising ROS[465–467]. In support of this, I found that Fbxo7-deficient T cells were more sensitive to H_2O_2-induced cell death than WT cells, collectively indicating that Fbxo7 may be transcriptionally activated by oxidative stress and has a role in promoting the stress response (Fig. 4.12). In contrast, cells derived from thymus tissue displayed a reduction in Fbxo7 protein following incubation with H_2O_2. However, it is important to note that this will represent a mixed population of thymocytes and stromal cells, and that the significant genetic and metabolic differences between thymocytes and active T cells may foster altered stress responses. As such, whilst I have shown that Fbxo7 levels are altered in response to oxidative stress in T cells, the mechanisms through which this occurs and differences throughout T cell development remain to be determined.

T cell activation is a complex cellular process that requires gross transcriptional and metabolic reprogramming[225]. Interestingly, I discovered that *FBXO7* is one gene strongly downregulated in response to T cell activation, and this occurs within 4 hours of stimulation. Given the widespread transcriptional changes upon activation, we cannot eliminate the possibility that this decrease is simply due to the downregulation of genes not essential for the activation programme. However, an enticing proposition is that Fbxo7 is specifically downregulated in activating T cells as one of several mechanisms to promote glycolysis (Fig. 4.12). In this manner, reduced Fbxo7 would promote PFKP activity and glycolytic flux, which is an integral part of the required metabolic reprogramming and may facilitate efficient T cell activation. Autophagy also plays a critical role in T cell survival and can be activated by TCR engagement and cytokine stimulation[494]. Since my data demonstrate the simultaneous transcriptional downregulation and autophagic degradation of Fbxo7 in response to glucose starvation, it may be interesting to ascertain whether Fbxo7 is similarly cleared by autophagy in early T cell activation. Interestingly, Fbxo7 protein was subsequently elevated by the addition of IL-2 to activated T cells as previously discussed, perhaps to redirect glycolytic metabolites into biosynthetic pathways, or to counteract activation-induced oxidative stress, indicating differential Fbxo7 regulation through early and late-stage T cell activation.

Whilst all cells must maintain homeostasis, the environmental stresses and functional requirements of tissues differ. Glucose sensing is particularly vital in the pancreas since endocrine cells in the pancreatic islets of Langerhans are responsible for regulating blood glucose levels. Specifically, islet β cells secrete insulin when blood sugar rises, whereas α cells release the glucagon stress hormone when blood sugar falls too low[495]. Therefore, it is perhaps unsurprising that cells derived from mouse pancreas tissue showed the greatest glucose-induced increase in Fbxo7 protein of the tissues tested.

Other tissues such as the liver, skeletal muscle and adipose tissue, are important for the storage or release of glucose as required[486,495], yet I found that cells from the liver only showed a subtle increase in Fbxo7 protein in response to elevating glucose. Interestingly, a less studied phenotype reported in mice lacking Fbxo7 is a decrease in circulating fructosamine levels[496,497]. Fructosamine is a glycoprotein formed by the spontaneous glycation that is accelerated in diabetes and indicative of sustained hyperglycemia[498]. As such, fructosamine concentrations are commonly used as a measure of average blood glucose levels in diabetes patients in the previous two to four weeks[498]. This phenotype in Fbxo7-deficient mice therefore suggests blood glucose concentration may be reduced and glucose sensing, or metabolism altered. Ultimately these data only offer a crude look to the stress response of Fbxo7 in different tissues, but they do highlight responsiveness in a range of cell types. Understanding the differing mechanisms involved in tissue-specific responses, and any implications in glucose sensing in metabolic diseases such as diabetes, will require a more refined approach.

Since I have shown that a major role for Fbxo7 is activating Cdk6, I propose that Cdk6 activity will respond to stress conditions, such as fluctuating glucose levels, through the finetuning of Fbxo7 levels[499]. In addition to regulating metabolism, another critical role for Cdk6 under stress conditions has been attributed to its regulation of transcription[115,117]. Bellutti, et al, proposed that Cdk6 promotes oncogenic transformation of bone marrow cells with BCR-ABL by suppressing p53-mediated stress responses, and in the absence of Cdk6, p53's pro-apoptotic functions prevail[115]. In a Parkinson's disease mouse model with conditional loss of Fbxo7 in dopaminergic neurons, a p53 pro-apoptotic signature was detected[86]. One possibility is the progressive neuronal death observed in this mouse arises from a lack of Fbxo7 and consequently Cdk6, to offset the p53 pro-apoptotic transcriptional response. Although Fbxo7 impacts on several other cellular pathways, as a factor that selectively scaffolds Cdk6, Fbxo7 levels may help to set a threshold for Cdk6-directed stress responses, transcriptional and metabolic, in many different cell types.

In summary, the findings presented in this chapter identify Fbxo7 as a protein regulated by various sources of cellular stress at a transcriptional and post-translational level. I have established that Fbxo7 is a dose-dependent, glucose responsive protein in numerous cell types, which is both transcriptionally downregulated and targeted for autophagy in response to glucose starvation. Moreover, I have correlated Fbxo7 transcripts with T cell activation and oxidative stress and shown that Fbxo7 loss increases T cell sensitivity to oxidative stress. Aberrant cellular stress responses are associated with many human diseases, including Parkinson's disease and cancer[500,501], in which Fbxo7 mis-regulation and mutation are proposed to play a role. As such, the recognition of *FBXO7* as a stress responsive gene may have implications in both physiological cell survival and Fbxo7-associated disease pathologies.

CHAPTER 5

A role for Fbxo7 in regulating the immunomodulatory drug target, CRBN

Introduction

F-box proteins, such as Fbxo7, are the substrate recruiting components for CRL1 E3 ubiquitin ligases (also called SCF ligases). Another family, CRL4, instead use DDB1-CUL4 associated factors (DCAFs) to recruit their substrates for ubiquitination. Cereblon (CRBN) is a DCAF protein most known for its role as the primary target for IMiDs[158,159], a class of drugs that are central to the treatment of multiple myeloma (MM) and increasingly show efficacy in other haematological malignancies[156,157]. IMiDs bind to the CULT domain of CRBN[130,131] and ultimately modify substrate recognition, generating neo-substrates for $CRL4^{CRBN}$. Through this mechanism IMiDs promote the ubiquitination and degradation of several neo-substrates including the transcription factors IKZF1 and IKZF3 which play a vital role in B cell maturation and MM cell survival[160–163]. Importantly, high CRBN expression is associated with improved clinical outcomes to IMiDs, whilst mutations in *CRBN* or its depletion can contribute to IMiD resistance[159,178].

Beyond its role in IMiD sensitivity, CRBN also has several physiological substrates, many of which are involved in neuronal and brain function[130,134–136]. One such example is the BK channel which, upon polyubiquitination by CRBN, is retained in the endoplasmic reticulum to prevent epileptogenesis[136]. Interestingly, a subsequent study revealed that CRBN mutations associated with intellectual disability (ID) disrupt the CRBN-BK interaction and instead both mutant CRBN and BK are directed to SCF^{Fbxo7} for polyubiquitination and proteasomal degradation[137].

Since sustained CRBN expression is required for IMiD sensitivity[159,178], and Fbxo7 may promote the turnover of CRBN[137], I hypothesised that Fbxo7 may modulate CRBN to affect IMiD sensitivity. In this chapter, I therefore aimed to establish whether WT CRBN is a substrate for ubiquitination by Fbxo7, and if this promotes CRBN degradation. I sought to test the effect of the IMiD, lenalidomide, on Fbxo7 and CRBN proteins, and to ascertain whether the loss of Fbxo7 altered MM cell sensitivity to lenalidomide.

Results

5..1 CRBN is a substrate for ubiquitination by Fbxo7

To investigate whether CRBN is a substrate for Fbxo7, I performed a ubiquitination assay in HEK293T cells expressing a control or Fbxo7-targetting shRNA. I overexpressed FLAG-CRBN in these cells, alongside the re-expression of Fbxo7 constructs into the Fbxo7-knockdown cells. Immunoblot analysis displays characteristic smears of CRBN polyubiquitination in all samples, including those with Fbxo7 knockdown (Fig. 5.1), illustrating that CRBN is ubiquitinated by other E3 ligases besides Fbxo7. Given that CRBN is also an E3 ubiquitin ligase, and that E3 ligases are shown to auto-ubiquitinate in the absence of their substrates[56,57], some of this likely represents auto-ubiquitination by CRBN itself. Interestingly, there was no change to this baseline CRBN ubiquitination upon Fbxo7 knockdown (Fig. 5.1, lane 1 vs. lane 2), but overexpression of WT Fbxo7 did promote an increase in CRBN ubiquitination (Fig. 5.1, lane 2 vs. lane 3) that was dependent on the Fbxo7 F-box domain (Fig. 5.1, lane 4). This increase in CRBN polyubiquitination that is specifically dependent on SCF^{Fbxo7} ligase activity is consistent with the hypothesis that CRBN is a substrate for ubiquitination by Fbxo7. The lack of a reciprocal result upon Fbxo7 knockdown is perhaps an indication of adaptive mechanisms whereby other E3 ligases, or CRBN auto-ubiquitination, compensate for the lack of Fbxo7 activity towards CRBN.

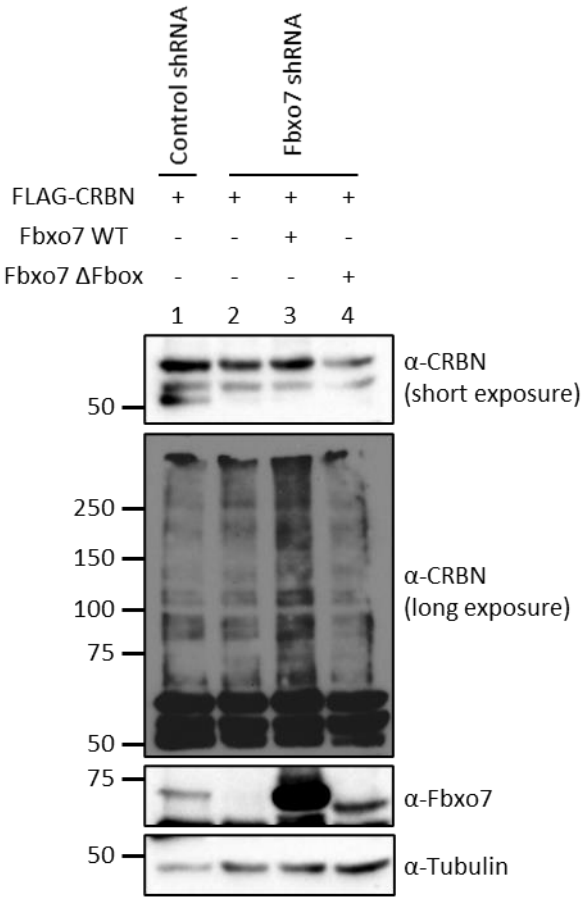

Figure 5.1: Fbxo7 ubiquitinates CRBN in HEK293T cells.

HEK293T cells expressing a control or Fbxo7 shRNA were transfected with FLAG-CRBN and Fbxo7 constructs as indicated. Cells were treated with 10 μM MG132 prior to cell lysis and analysis by immunoblot. Immunoblot for CRBN shows the degree of ubiquitination. Endogenous CRBN is a 51 kDa protein. Higher bands represent FLAG-CRBN and ubiquitinated populations. (n=3)

5..2 Fbxo7 ubiquitination promotes CRBN degradation

Since Fbxo7 is reported to promote the degradation of mutant CRBN in ID[137], I hypothesised that Fbxo7 ubiquitination may also target WT CRBN for degradation. I first examined whether Fbxo7 and CRBN protein levels correlated in HEK293T cells expressing a control or Fbxo7-targeting shRNA by immunoblot analysis (Fig. 5.2A & B). This showed a subtle, but not significant, decrease in endogenous CRBN with Fbxo7 knockdown, in opposition with a role for Fbxo7 in CRBN degradation. Since I had seen no difference in CRBN ubiquitination in these cells due to the possible action of other compensating E3 ligases but had observed an increase with Fbxo7 overexpression (Fig. 5.1), I also investigated the effect of Fbxo7 WT and ΔFbox overexpression on CRBN levels (Fig. 5.2C & D). These data show a significant 20% decrease in CRBN protein levels upon Fbxo7 overexpression, which is not phenocopied by the ΔFbox mutant, indicating that it is specifically reliant on SCF^{Fbxo7} ligase activity.

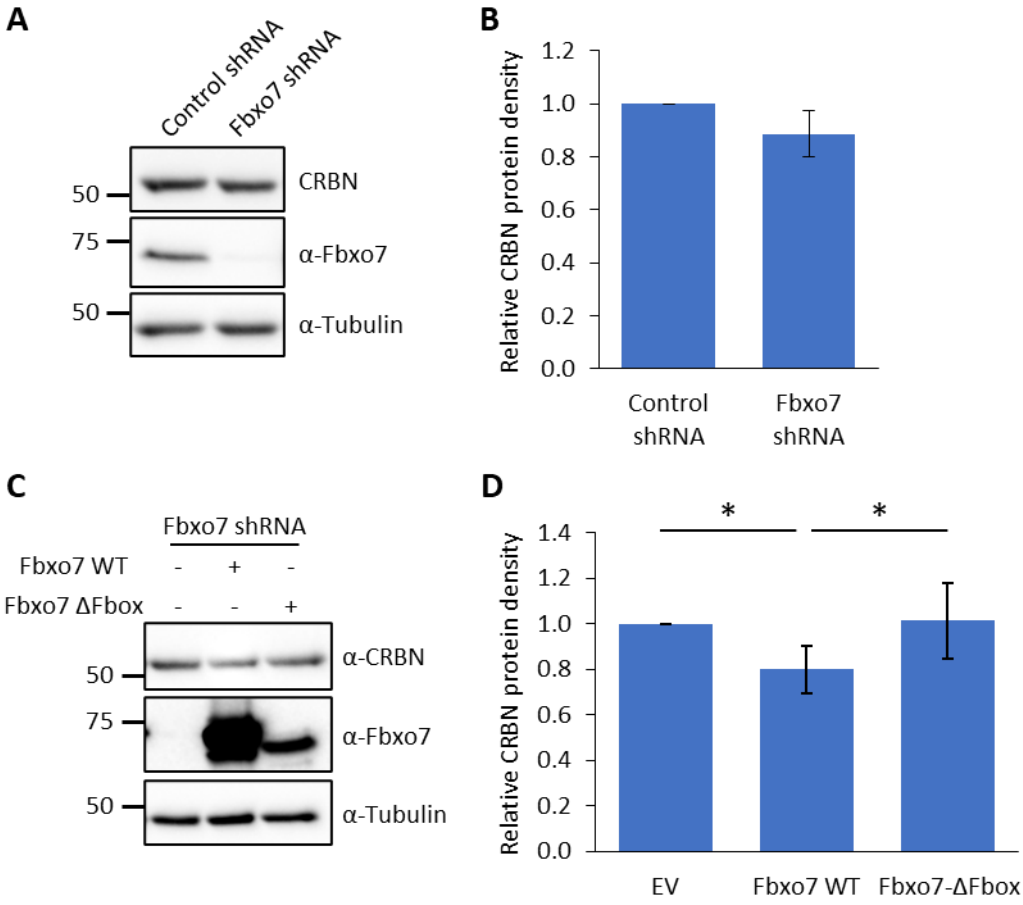

Figure 5.2: CRBN protein levels inversely correlate with Fbxo7 expression.

(A) & (B) Lysates from HEK293T cells expressing a control or Fbxo7 shRNA were analysed by immunoblot. (A) Shows a representative image. (B) Quantification of relative levels of CRBN. (n=4) (C) & (D) HEK293T cells expressing an Fbxo7 shRNA were transfected with Fbxo7 WT and ΔFbox constructs prior to lysis and analysis by immunoblot. (C) Shows a representative image. (D) Quantification of relative levels of CRBN. (n=5) * $p<0.05$

To support this, I transfected Fbxo7-knockdown HEK293T cells with Fbxo7 WT or ΔFbox constructs and subsequently treated them with DMSO or the proteasome inhibitor MG132, to test whether it rescued the decrease in CRBN protein levels with Fbxo7 overexpression (Fig. 5.3). As expected, immunoblot analysis shows a reduction in CRBN protein levels with the overexpression of WT Fbxo7, that is not seen with Fbxo7-ΔFbox (Fig. 5.3, lanes 1-3). CRBN accumulated with MG132 treatment in all three samples, indicating that it is degraded by the proteasome even in the absence of Fbxo7 (Fig. 5.3, lanes 4-6). This is consistent with CRBN ubiquitination by other E3 ubiquitin ligases in the absence of Fbxo7 ligase activity (Fig. 5.1). Nonetheless, MG132 treatment did rescue the reduction in CRBN protein levels induced by Fbxo7 overexpression (Fig. 5.3, lane 1 vs. lane 2 compared to lane 4 vs. lane 5), which may support the theory that Fbxo7 ubiquitination targets CRBN for proteasomal degradation.

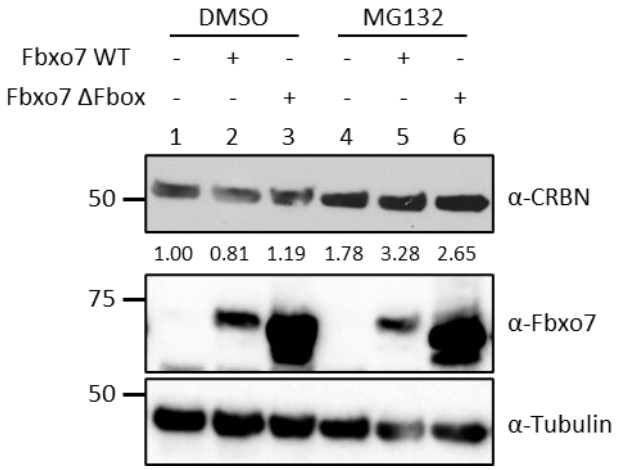

Figure 5.3: CRBN protein levels increase with MG132 treatment.
HEK293T cells expressing an Fbxo7 shRNA were transfected with Fbxo7 WT or ΔFbox constructs. Cells were treated with DMSO or 10 μM MG132 for 4 hours prior to lysis and immunoblot analysis. (n=2)

Lastly, I performed a cycloheximide chase experiment to examine CRBN stability in the presence and absence of Fbxo7. However, I found that CRBN has a long half-life, and no change was seen in cells with reduced Fbxo7 (Fig. 5.4). This protein stability was surprising since CRBN accumulated following a 4-hour treatment with MG132 (Fig. 5.3), suggesting proteasomal degradation in this timeframe. Nonetheless, I did observe an interesting higher MW CRBN species that may represent a PTM. This CRBN species was stabilised upon Fbxo7 knockdown, indicating a role for Fbxo7 in regulating PTMs on CRBN.

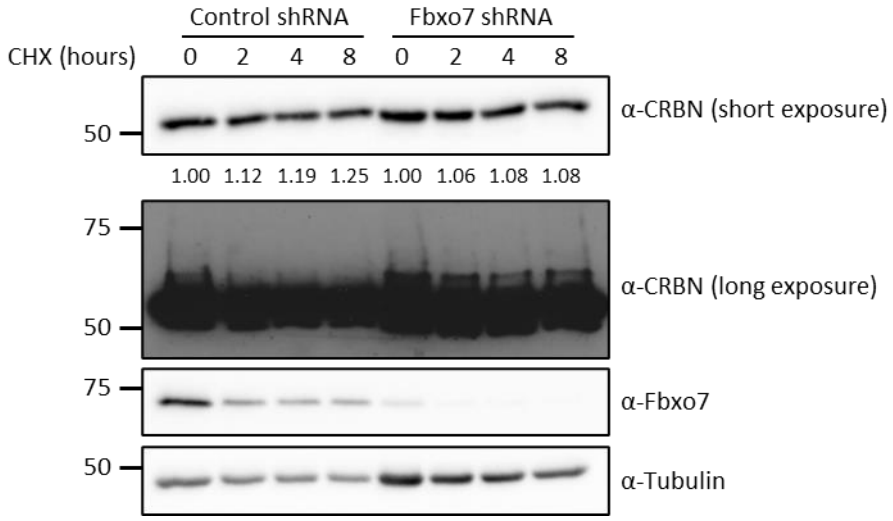

Figure 5.4: CRBN half-life is unchanged in the absence of Fbxo7.

Representative immunoblot of CRBN half-life in HEK293T cells expressing a control or Fbxo7 shRNA and treated with cycloheximide for up to 8 hours. (n=4)

5..3 Fbxo7 and CRBN protein interaction predictions

As CRBN is a substrate for ubiquitination by Fbxo7, I was interested to explore the interaction between these two proteins. I used the AlphaFold Protein Structure Database (https://alphafold.ebi.ac.uk)[502,503] to model the 3D structural interaction between full-length Fbxo7 and CRBN proteins (Fig. 5.5). Five models were generated and ranked according to their predicted confidence scores. AlphaFold produces a per-residue estimate of its confidence on a scale of 0 – 100 (termed pLDDT). The confidence scores for Fbxo7 and CRBN protein folding show that, whilst CRBN was folded with reasonable confidence apart from its unstructured N-terminal region, Fbxo7 structural predictions had lower confidence (Fig. 5.5A). In particular, the regions corresponding to the linker and Cdk6 binding domain, and C-terminal PRR, had pLDDT values <50, which is an indication of intrinsic disorder.

All five models showed notable similarity and positioned the α-helices of the CRBN DDB1-binding domain between the Ubl domain and FP/F-box domains of Fbxo7 (Fig. 5.5B). In models 1-4 the Fbxo7 Ubl domain is positioned close to the CRBN N-terminal linker (labelled A) and first α-helix of the CRBN DDB1-binding domain (labelled B). These four models also predict that the most C-terminal α-helix of Fbxo7 (in the linker before the disordered PRR, labelled C) wraps around the other face of the CRBN DDB1-binding domain. Whilst model 5 predicts the same positioning of CRBN relative to the Fbxo7 Ubl domain, it shows a more compact structure in which CRBN sits deeper into the cleft between the Fbxo7 Ubl domain and FP/F-box domains. Together, these predictions suggest that the DDB1-binding domain of CRBN, and the Fbxo7 Ubl domain, may be important for the protein interaction.

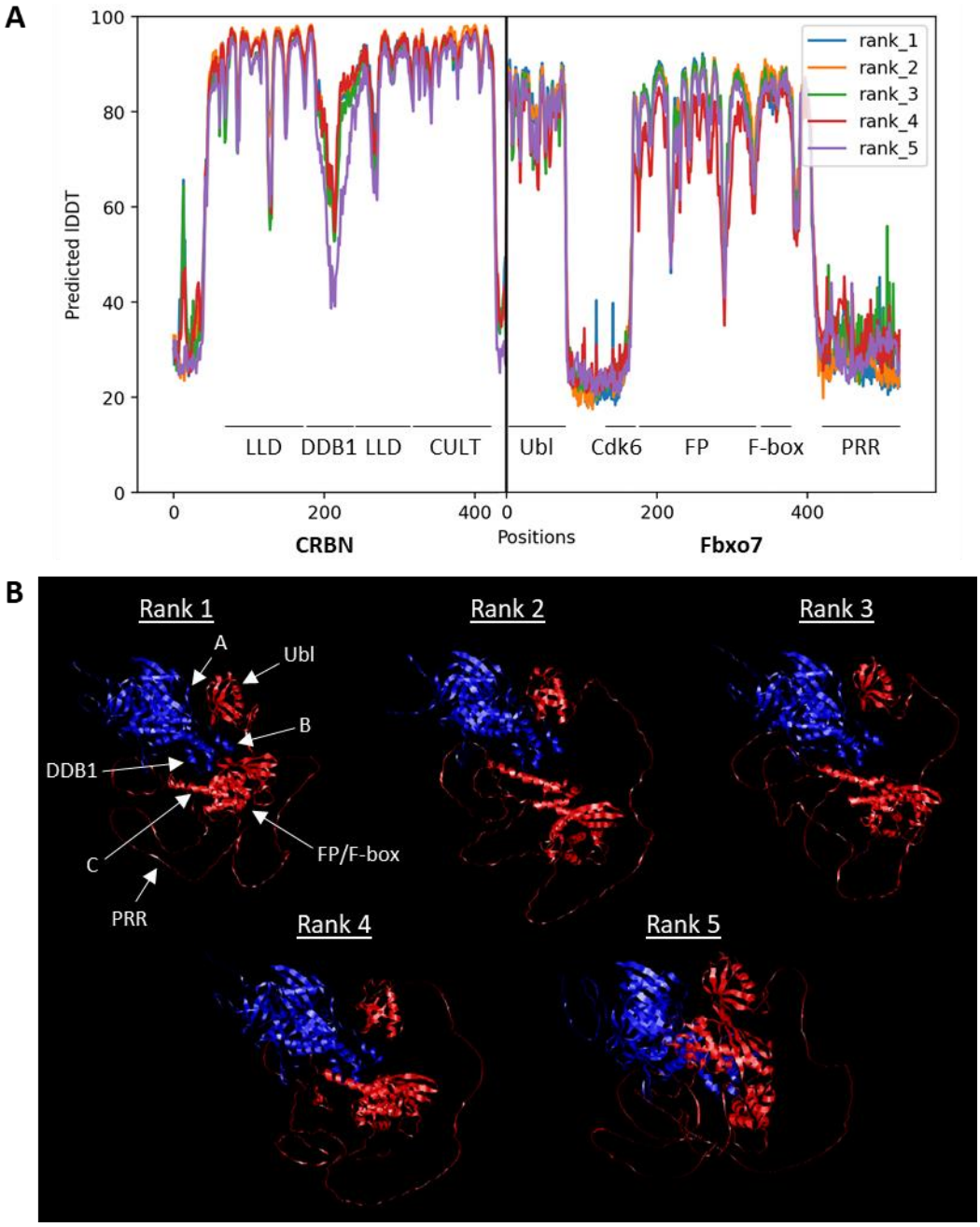

Figure 5.5: 3D structure predictions for the interaction between Fbxo7 (red) and CRBN (blue) using AlphaFold Protein Structure Database.

(A) Modelling error represented by AlphaFold's per-residue confidence estimate, predicted LDDT (pLDDT). Regions with pLDDT > 90 are expected to be modelled to a high accuracy, 70-90 are modelled well, 50-70 represent low confidence, and <50 indicates structural disorder. Annotations underneath represent approximate locations of Fbxo7 and CRBN protein domains.

(B) 3D structure models generated by the AlphaFold deep learning system. Fbxo7: red. CRBN: blue. Key features are labelled by white arrows. Ubl: Fbxo7 Ubl domain. FP/F-box: Fbxo7 FP and F-box domains. PRR: Fbxo7 PRR. DDB1: CRBN DDB1-binding domain. A: CRBN N-terminal linker. B: First α-helix of the CRBN DDB1-binding domain. C: Most C-terminal α-helix of Fbxo7.

5..4 Lenalidomide induces cell line-specific changes to Fbxo7 and CRBN proteins

In the screen that first identified the CRBN-dependent decrease in Ikaros proteins induced by lenalidomide, Fbxo7 was also found to be downregulated by 2 µM lenalidomide treatment[161]. This screen was performed in 293FT cells in a 384w format, but the finding was not reproduced in the follow-up 96w assay. As such, we sought to validate whether lenalidomide affects Fbxo7 protein levels. HEK293T cells were treated with a titration of lenalidomide for 24 hours prior to lysis and analysis by immunoblot (Fig. 5.6). We observed a dose-dependent decrease in Fbxo7 protein levels in response to lenalidomide, culminating in a 48% reduction following treatment with 10 µM IMiD, thus supporting the original screen by Lu, et al[161].

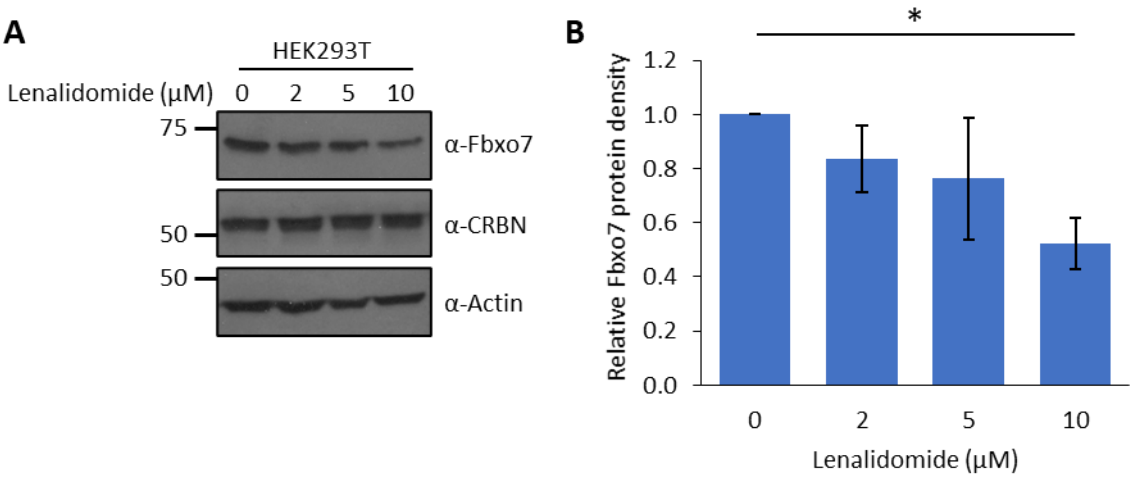

Figure 5.6: Fbxo7 protein levels are reduced by lenalidomide treatment in HEK293T cells. HEK293T cells were treated with a titration of lenalidomide for 24 hours prior to cell lysis and analysis by immunoblot. (A) Shows a representative immunoblot. (B) Quantification of relative levels of CRBN. (n=3) * $p<0.05$

Experiment performed by Omar Helmy, reproduced here with permission.

Next, I tested this response in a selection of more clinically relevant MM cell lines (OPM2, MM1S and U266) which are all categorised as IMiD sensitive. As before, cells were treated with a titration of lenalidomide for 24 hours prior to lysis and immunoblot analysis. Unlike in HEK293T cells, Fbxo7 was not downregulated by lenalidomide in any of the MM cell lines tested (Fig. 5.7 and 5.8), suggesting that different drug responses are induced in MM cells. Whilst it is widely understood that IMiDs alter CRBN substrate specificity, there are contradicting reports of their effect on CRBN protein levels[161,504,505]. In all three cell lines, my data consistently show no change to steady-state CRBN protein levels with lenalidomide treatment (Fig. 5.7 and 5.8). However, interestingly, there was a dose-dependent increase in CRBN laddering when U266 cells were treated with a titration of lenalidomide (Fig. 5.8), suggesting that lenalidomide promotes CRBN ubiquitination in these cells.

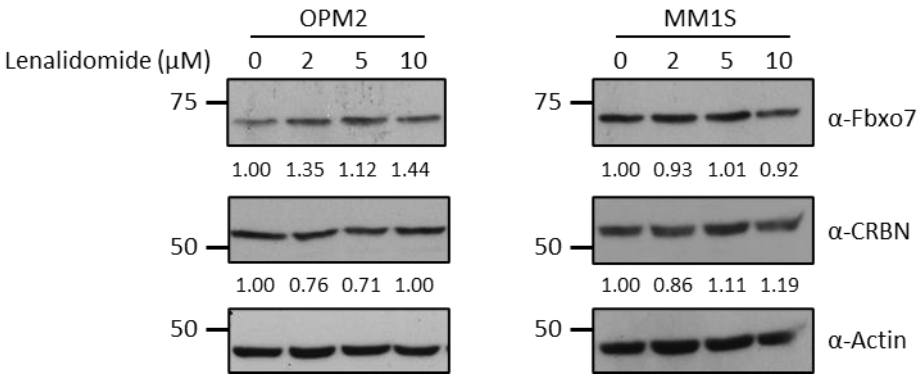

Figure 5.7: Fbxo7 and CRBN protein levels are unchanged by lenalidomide treatment in OPM2 and MM1S cells.

OPM2 and MM1S cells were treated with a titration of lenalidomide for 24 hours prior to cell lysis and analysis by immunoblot. (n=2)

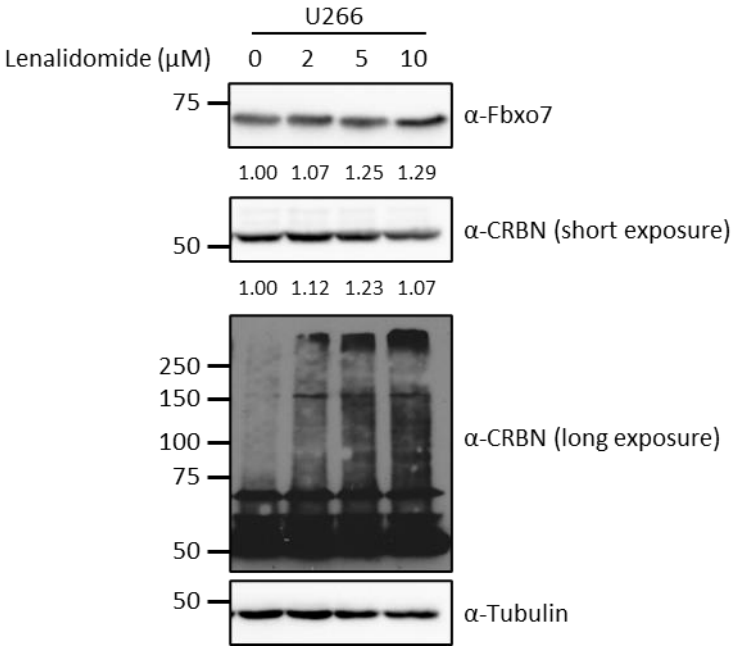

Figure 5.8: Lenalidomide treatment promotes CRBN ubiquitination in U266 cells.

U266 cells were treated with a titration of lenalidomide for 24 hours prior to cell lysis and analysis by immunoblot. (n=3)

5..5 Attempts to generate Fbxo7-knockdown MM cells

Since I have shown that CRBN is a substrate for ubiquitination by Fbxo7, I was interested to ascertain whether the lenalidomide-induced ubiquitination of CRBN in U266 cells was the action of SCF^{Fbxo7}. I therefore aimed to generate U266 cells with an Fbxo7 knockdown to investigate the dependence of this response on Fbxo7. Several approaches were taken to produce these cells. Firstly, I used Lipofectamine RNAiMAX, a lipid-mediated transfection reagent, to treat U266 cells with a control or Fbxo7-targeting siRNA for 48 hours prior to cell lysis, but this only yielded a 9% reduction in Fbxo7 protein levels (Fig. 5.9A). Since the Neon electroporation system reports high transfection efficiency in immune cells, I next tested this method for Fbxo7 siRNA delivery to U266 cells. Four electroporation protocols identified from published work[506–508] were tested in parallel to deliver the Fbxo7 siRNA or scrambled control, yet none produced an Fbxo7 knockdown (Fig. 5.9B).

Alongside my efforts to transfect MM cells with an Fbxo7-targeting siRNA, I also transduced both U266 and MM1S cells with a control or Fbxo7-targeting shRNA using a retroviral system. Whilst neither U266 cell lines survived the infection and puromycin selection, infection of MM1S cells did generate populations of transduced cells, as visualised by the expression of the GFP marker (Fig. 5.9C). Interestingly, the MM1S cells expressing a plasmid containing the Fbxo7 shRNA were slower to recover and expand following transduction than control cells (Fig. 5.9C). Upon recovery of sufficient cells, lysates from these MM1S shRNA-expressing cell lines were analysed by immunoblot (Fig. 5.9D). This showed only a modest 29% reduction in Fbxo7 protein levels in cells expressing the Fbxo7 shRNA compared to control, despite high expression of the GFP marker and ongoing selection in puromycin.

Together, these data illustrate the challenge of genetically manipulating MM cell lines and suggest that akin to my findings in T cells (Chapter 3), expression of the Fbxo7-targeting shRNA was suppressed by MM cells in culture.

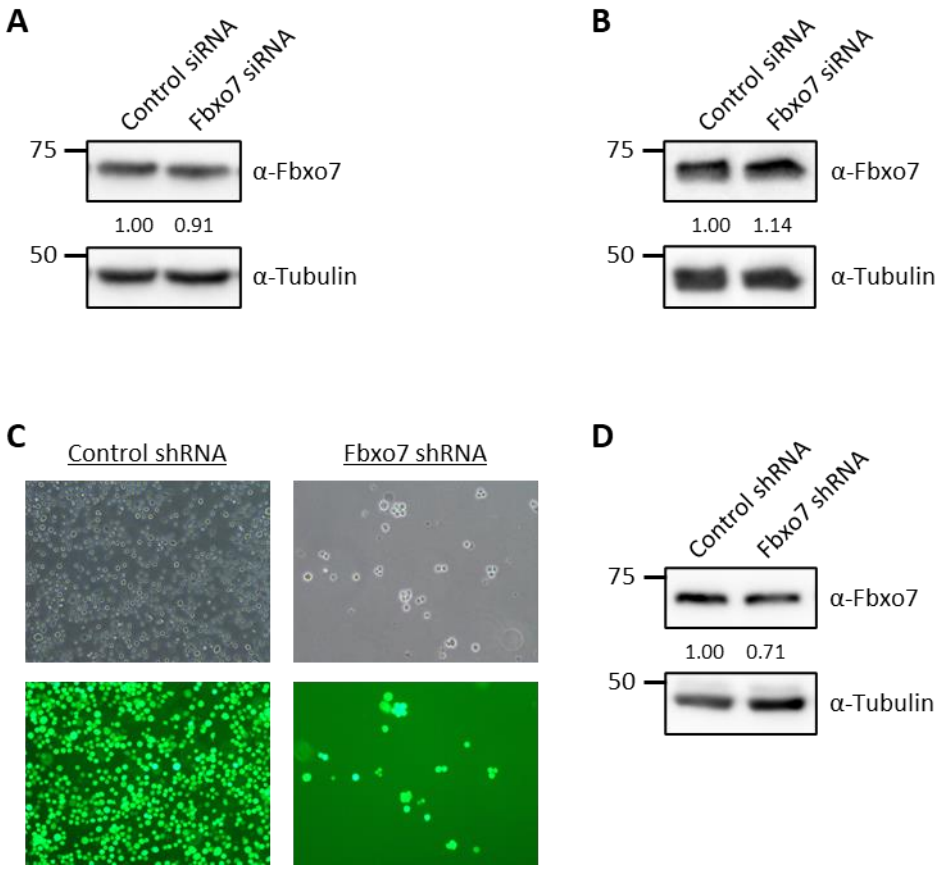

Figure 5.9: Attempts to generate MM cells with an Fbxo7 knockdown.

(A)-(B) U266 cells were treated with a control or Fbxo7-targeting siRNA for 48 hours using (A) Lipofectamine RNAiMAX (n=3) or (B) Neon electroporation (n=4) delivery systems.

(C)-(D) MM1S cells were transduced with retroviral plasmids containing control or Fbxo7-targeting shRNA alongside a GFP marker and puromycin resistance gene. (C) Microscopy images of GFP expression in transduced cells. (D) Immunoblot of Fbxo7 protein levels in transduced cells.

5..6 Fbxo7 knockdown does not sensitise Nalm6 cells to lenalidomide-induced cytotoxicity

Since I was unable to generate an Fbxo7 knockdown in MM cells, I investigated whether the loss of Fbxo7 altered the sensitivity of a B cell line, Nalm6, to lenalidomide. Nalm6 is a B cell precursor leukaemia cell line, thus of the same cell lineage but different malignancy to MM. Nalm6 cells expressing a control or Fbxo7-targeting shRNA (Fig. 5.10A) were seeded in a 96w plate and treated with titrating concentrations of lenalidomide for 72 hours. The IMiD-sensitive cell line MM1S was tested in parallel as a positive control. Drug-induced cytotoxicity was measured by a colorimetric assay in which a tetrazolium salt is reduced to an orange formazan product by living cells, and thus absorbance at 450 nm is directly proportional to the number of viable cells. Nalm6 cells were resistant to lenalidomide-induced cytotoxicity and no cell death was observed, regardless of Fbxo7 expression (Fig. 5.10B). Nonetheless, a dose-dependent reduction in cell viability was measured in MM1S cells treated with increasing concentrations of lenalidomide (Fig. 5.10B), and 50 µM camptothecin reduced the viability of all three cell lines by over 75% (data not shown), validating the functionality of the assay. Unfortunately, these data only identify Nalm6 as a lenalidomide-resistant cell line and do not address whether the loss of Fbxo7 affects IMiD sensitivity.

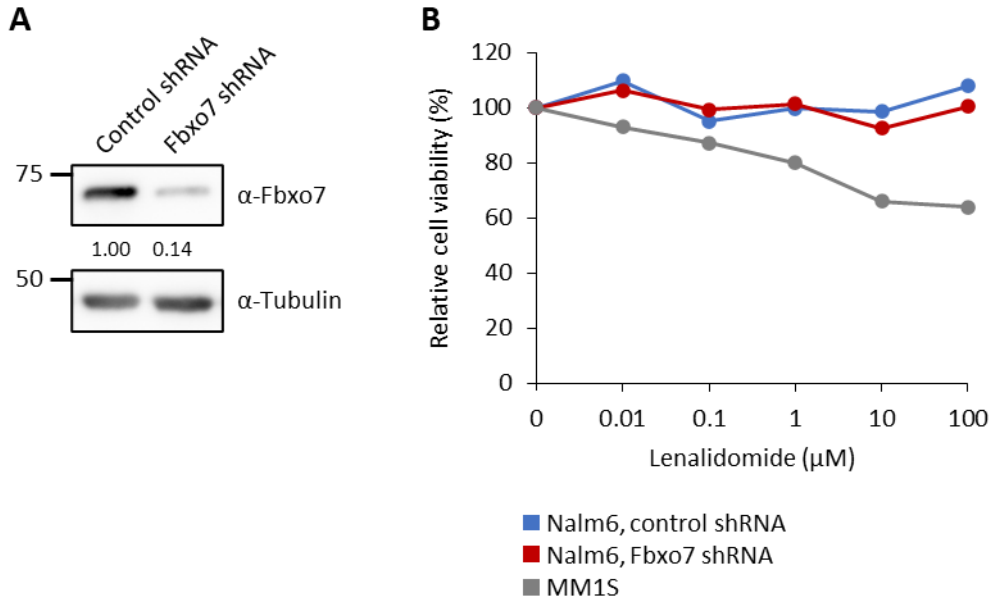

Figure 5.10: Nalm6 cell viability following lenalidomide treatment is not affected by the loss of Fbxo7.

Nalm6 cells expressing a control or Fbxo7 shRNA, and WT MM1S cells, were seeded in a 96w plate and treated with a titration of lenalidomide for 72 hours. CCK8 reagent (Abcam) was used to measure cell viability. (A) Immunoblot showing Fbxo7 protein levels in Nalm6 cell lines. (B) Quantification of relative cell viability by CCK8 reagent. (n=1)

Discussion

In this chapter I aimed to determine whether CRBN is ubiquitinated and regulated by Fbxo7. I have presented evidence that supports that CRBN is a substrate for ubiquitination by Fbxo7 and my data suggest that this promotes the proteasomal degradation of CRBN. During the execution of this work, Liu, et al.[505] also published that CRBN is targeted for degradation by SCF^{Fbxo7}. Using a CRISPR-Cas9 screen, this study established that the CSN9 signalosome complex, which inhibits CRL activity via cullin deneddylation, is required for MM sensitivity to IMiDs. They describe that CSN9 knock-out reduces CRBN protein levels and demonstrated that this was specifically reliant on Cul1 and Fbxo7 protein expression, indicating that CSN9 inhibits SCF^{Fbxo7}-mediated CRBN degradation to promote IMiD sensitivity. Through this mechanism, Liu, et al. elegantly demonstrated that, whilst loss of CSN9 promotes IMiD resistance, the simultaneous loss of Fbxo7 restores IMiD sensitivity by maintaining CRBN protein levels[505]. My work complements this to specifically show the polyubiquitination of CRBN by SCF^{Fbxo7} and verify that this is dependent on Fbxo7 ligase activity. Moreover, my data indicate that the degradation of CRBN occurs via the UPS since the change in CRBN protein levels may be rescued by proteasome inhibition. Based on the data presented both here and by Liu, et al[505], I propose a model where the SCF^{Fbxo7}-mediated degradation of CRBN reduces IMiD sensitivity in MM cells (Fig. 5.11).

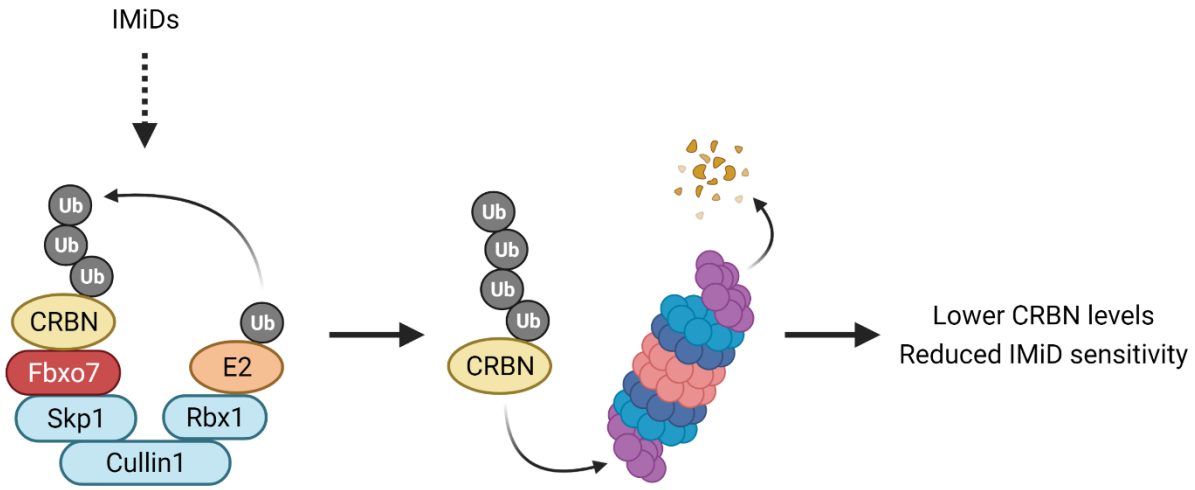

Figure 5.11: Proposed model through which Fbxo7 may reduce IMiD sensitivity.

SCF^{Fbxo7} ubiquitination targets CRBN for proteasomal degradation and this lowers CRBN levels to impair IMiD sensitivity. In some instances, IMiDs can promote CRBN ubiquitination and Fbxo7 may be the E3 ubiquitin ligase responsible (represented by dashed arrow).

In addition to the polyubiquitination of CRBN, I have also shown that Fbxo7 destabilises a higher MW species of CRBN, that may represent a post-translationally modified form. One possibility is that this PTM acts as a degron for SCF^{Fbxo7} recognition thus, in the presence of Fbxo7, it is rapidly polyubiquitinated and degraded. The PhosphoSitePlus database reports that CRBN contains five experimentally determined phosphorylation sites: one in the N-terminal disordered region, two flanking either side of the DDB1-binding domain and two in the CULT domain[509]. Since my Alphafold structural predictions suggest that the DDB1-binding domain sits close to the Fbxo7 Ubl domain, we may postulate that one of these DDB1-flanking phosphorylation sites could promote binding. Alternatively, this higher MW species may represent mono-ubiquitinated CRBN that is added by another E3 ubiquitin ligase. The action of other E3 ligases towards CRBN is supported by the background laddering in my ubiquitination assay. In this scenario, Fbxo7 may function as an E4 ubiquitin ligase to extend the ubiquitin chain. This would be the first example of Fbxo7 acting in this manner, though studies have shown that several other E3 ligases may also act as E4 chain elongating factors including the U-box E3s UBE4A and UBE4B[30–33], and the HECT-domain ligase Hul5[510]. Further investigation of this population could test its stability in response to β-glycerophosphate and CIP alkaline phosphatase which should increase and decrease phosphorylation respectively, or mass spectrometry analysis of the protein band to determine if PTMs are present.

In screens to identify proteins differentially degraded in the presence of lenalidomide, Lu, et al. reported a 40% decrease in Fbxo7 levels but this was not replicated in their follow-up assay[161]. I therefore sought to validate the effect of lenalidomide treatment on Fbxo7 protein levels. Whilst I confirmed that Fbxo7 protein is significantly lower in lenalidomide treated HEK293T cells, this was not observed in three lenalidomide-sensitive MM cell lines, suggesting that the mechanism of Fbxo7 downregulation may not contribute to the clinical activity of IMiDs. Although it is widely understood that IMiDs alter CRBN substrate specificity, there are contradicting reports of their effect on CRBN protein levels[161,504,505]. Whilst the screens by Lu, et al, reported no change to CRBN protein levels[161], subsequent studies reported an increase in CRBN protein with short term (16 hour) treatment of MM cells with lenalidomide or pomalidomide[505], and a paradoxical decrease following prolonged exposure (5 days)[504]. However, both these effects were subtle. My data show no change in CRBN protein levels following 24-hour treatment with a titration of lenalidomide. However, most interestingly, my data illustrate that lenalidomide promotes the dose-dependent ubiquitination of CRBN in U266 cells. Previous work has shown that CRBN auto-ubiquitination is inhibited by the IMiD thalidomide[158], thus the lenalidomide-induced ubiquitination that I observe is likely the action of another E3 ubiquitin ligase. One candidate is SCF^{Fbxo7}. Whilst further work is required to identify the E3 ligase responsible, it is enticing to consider that IMiD treatment may promote the SCF^{Fbxo7}-dependent ubiquitination and

degradation of CRBN to downregulate CRBN and promote the emergence of IMiD resistance (Fig. 5.11, dashed line).

IMiD resistance is also proposed to emerge through an increase in the cell's oxidative capacity. IMiDs inhibit thioredoxin reductase, an enzyme involved in hydrogen peroxide decomposition, in a CRBN-dependent manner, and this increases intracellular ROS[181]. Therefore, cells with a lower oxidative capacity are more vulnerable to the oxidative stress-induced cytotoxic effect of IMiDs, whilst those with increased capacity may emerge as IMiD resistant[180,181]. My work, alongside others, has shown that Fbxo7 deficiencies are associated with an increase in ROS[465–467]. As such, it is possible that Fbxo7 may contribute to reduced IMiD sensitivity in two ways: promoting CRBN degradation and increasing cellular oxidative capacity (Fig. 5.12).

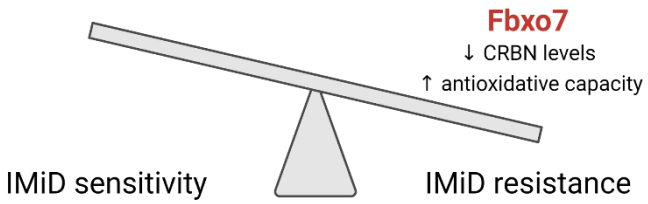

Figure 5.12: Fbxo7 may contribute to IMiD resistance by reducing CRBN protein levels and increasing cellular oxidative capacity.

Unfortunately, I was unable to generate MM cells with an Fbxo7 knockdown in order to test the hypothesis that reduced Fbxo7 expression would increase IMiD sensitivity. Immune cells are generally regarded as difficult to transfect which made the delivery of siRNA challenging. The observations that MM1S cells transduced with a plasmid containing an Fbxo7-targeting shRNA recovered and expanded more slowly than control cells, and subsequently supressed the effects of the shRNA, is particularly interesting. In Chapter 3 I presented data from the Cancer Dependency Map which also illustrates that plasma cell cancer lines are significantly dependent on Fbxo7 (Fig. 3.34). Together these data cumulatively suggest an essential role for Fbxo7 in hematopoietic lineages.

To summarise, I have presented data to support that SCF^{Fbxo7} ubiquitinates CRBN and promotes its proteasomal degradation. Alongside increasing CRBN protein levels, I have also revealed that loss of Fbxo7 stabilises a higher MW species of CRBN that may represent a PTM such as a phospho-degron or mono-ubiquitination that Fbxo7 elongates through E4 ligase activity. Finally, I also discovered that lenalidomide can promote the ubiquitination of CRBN in a dose-dependent manner, something that could be attributed to SCF^{Fbxo7} activity. Alongside published work[159,178,505], my data support the hypothesis that Fbxo7 may reduce the IMiD sensitivity of MM cells through a mechanism that downregulates CRBN. Fbxo7 overexpression has been observed in several cancers including T cell lymphoma and ALCL[67] which both have ongoing clinical trials with IMiD-based treatment regimens[511]. Therefore, my findings may have clinical significance in the emergence of IMiD resistant clones in these settings. Interestingly, the combination of IMiD treatment with proteasome and neddylation inhibitors has demonstrated increased cytotoxicity in a preclinical setting, as well as improved clinical response[505], further suggesting that inhibiting Fbxo7-mediated CRBN degradation may enhance IMiD sensitivity.

CHAPTER 6

General discussion

Ubiquitination regulates an array of cellular processes including the cell cycle, DNA repair, differentiation, and metabolism. Fbxo7 is a protein with a growing number of identified substates which it ubiquitinates as part of the SCF complex[70,74,76,77,80,81,86,89,99,460], in addition to having several SCF-independent roles[55]. Together these confer functions for Fbxo7 in a host of cellular processes including mitophagy, the cell cycle, proteasome regulation and cell differentiation. The findings presented in this thesis characterise novel functions for Fbxo7 in regulating metabolism and the stress response. The synergy between these two networks is widely acknowledged and typified by the function of proteins such as AMPK, the master regulator of energy homeostasis, which critically couples cellular stress and ATP depletion to the metabolic programme to restore an energy balance[474,475]. Previous studies have described roles for several FBPs in both homeostatic metabolic regulation and its reprogramming in disease. Much of this research has focused on the Warburg effect, and Skp2, Fbxw7 and Fbxl10 are among those implicated in glycolytic regulation in cancer[409,417,437,438]. In particular, Fbxl10 is associated with a plethora of metabolic pathways including glycolysis, pyrimidine synthesis and OXPHOS, via a non-canonical role as a histone demethylase[435]. The widespread metabolic defects I have highlighted in T cells from Fbxo7-deficient mice, suggest that Fbxo7 may similarly influence several pathways, and contribute yet another example of the critical involvement of FBPs in metabolic regulation.

Specifically, I present Fbxo7 as a negative regulator of glycolysis which promotes two distinct PTMs on the rate-limiting enzyme, PFKP: ubiquitination and phosphorylation. Mechanistically, I have shown that Fbxo7 ubiquitination activity towards PFKP is independent of Cdk6, whilst the previously reported[304] interaction and phosphorylation of PFKP by Cdk6 requires Fbxo7. I propose that Fbxo7 ultimately destabilises active PFKP tetramers to inhibit glycolysis in T cells. PFKP is regulated by several PTMs and allosteric regulators which frequently alter its oligomeric state[512], hence this Fbxo7-dependent mechanism appears typical for modes of PFKP regulation. Since I have demonstrated that Fbxo7 is regulated by glucose availability and is transcriptionally downregulated and degraded by autophagy upon glucose starvation, Fbxo7 may serve to adapt the cells metabolic output to nutrient availability. In this manner, Fbxo7 downregulation could increase PFKP activity during glucose deprivation, acting synergistically with allosteric activation by ADP and AMP to promote catabolic glycolysis[364,372–374]. Interestingly, the FBP Skp2 is activated by AMPK in response to metabolic stress, and this similarly increases glucose uptake and glycolytic flux through mechanisms such as the upregulation of PFKFB3[409–411]. This elevated PFKFB3 produces the PFKP allosteric activator F2,6BP, serving as a third mean to increase PFKP activity during metabolic stress. Ultimately, Fbxo7 may be positioned amongst several regulating networks to fine-tune the metabolic response to cellular stress.

Beyond glycolysis, I have identified that a range of metabolic pathways are disrupted in Fbxo7-deficient T cells. Of note and potential physiological significance is the disruption of nucleotide biosynthesis, and arginine and tryptophan metabolism, which can influence T cell proliferation, survival and differentiation[232,251,349,468,470–472]. Through the comparative analysis of metabolomic fingerprinting data and hits from multiple Fbxo7 substrate screens, I have compiled an infographic that can be used to identify other putative metabolic substrates of Fbxo7 that may contribute to the metabolic defects observed. The regulation of PFKP, and thus glycolysis, by Fbxo7 is perhaps just one of several metabolic functions, and this initial analysis may guide further study.

As alluded to above, a role for Fbxo7 in metabolism and cellular stress responses may impact the physiology and function of T cells. I observed that T cells lacking Fbxo7 had elevated ROS, reduced viability and were slower to activate *in vitro*, and previous characterisation of these cells include reports of impaired T cell development, faster proliferation of activated T cells, and altered cytokine profiles[104,106]. Metabolic reprogramming is central for T cell development and function and so some of these defects may be explained, in part, by the newly described metabolic role for Fbxo7. For instance, the elevated glycolysis I observed may place Fbxo7-deficient T cells in a metabolic state that supports their increased proliferation following activation and may also reduce the RNA-binding capabilities of GAPDH and LDH to account for the increased IL-2 and IFNγ production[104,106]. Metabolic regulation by Fbxo7 may be particularly important for T cells in stressful pathological settings. At sites of infection and in the TME, T cells may be exposed to various cellular stresses including nutrient deprivation, oxidative stress, and hypoxia[485,489]. In these environments, metabolic plasticity is essential to promote T cell survival and efficient effector functions[340–343]. As such, *FBXO7*, particularly as a glucose and oxidative-stress responsive gene, may impact T cell survival and function in pathology. As the use of T cell transfer therapies grow, their constant development has led to the manipulation of T cell metabolism *ex vivo* to improve their longevity and cytotoxicity upon reinfusion. This includes modulating pathways such as those affected by Fbxo7 loss in our mouse model. Therefore, understanding the regulation of the metabolic network and the impact of this in T cells, can provide insight for future therapeutic advances.

Since several phenotypes observed in Fbxo7-deficient hematopoietic cells phenocopy the loss or inhibition of Cdk6[118,119,122,304], and I demonstrated that Fbxo7 knockdown reduces Cdk6 activity, I propose that a major role for Fbxo7 in these cells is as an activator of Cdk6. This is further supported by the observation that haematological and lymphocytic malignancies, where Cdk6 is highly expressed, are specifically dependent on *FBXO7* in the Depmap dataset, and experimental evidence that shows T-ALL and MM cells resist manipulation of *FBXO7* expression. Since I have shown that Fbxo7 may respond to glucose starvation and oxidative stress, I propose that Fbxo7 may fine-tune the

Cdk6 response to such perturbations. Under stress conditions, Cdk6 is reported to play a critical role in regulating transcription. Bellutti, et al. propose that Cdk6 promotes oncogenic transformation of bone marrow cells by suppressing p53-mediated stress responses, and in the absence of Cdk6, p53's pro-apoptotic functions prevail[115]. Another study reports that a Parkinson's disease mouse model with Fbxo7-loss also displays a p53 pro-apoptotic signature[86], thus we may speculate that one explanation is the loss of Cdk6 activity in this setting. Much of the work in this thesis has been discussed in the context of cancer, but Fbxo7 mis-regulation and mutation are also associated with a variety of other pathological conditions including anaemia, male sterility and Parkinson's disease. Whilst it is important to note that there are significant differences in some phenotypes of $Cdk6^{-/-}$ and $Fbxo7^{-/-}$ mice, it is possible that Fbxo7 levels may help to set a threshold for Cdk6-directed stress responses in many different cell types, and this may represent a common pathway that mediates Fbxo7's effects in a physiological and pathological setting.

Alongside a role in metabolism and the stress response, I have identified another disease-relevant function for Fbxo7 in cancer where it can ubiquitinate the primary IMiD target, CRBN. I propose that this ubiquitination by SCF^{Fbxo7} promotes the degradation of CRBN and that, since sustained CRBN expression is required for IMiD efficacy[159,178], CRBN turnover by Fbxo7 may consequently affect IMiD sensitivity. In support of this, Liu, et al. describe a mechanism whereby the SCF^{Fbxo7}-mediated degradation of CRBN is inhibited by CSN9 cullin deneddylation, and in the absence of CSN9, Fbxo7 reduces IMiD sensitivity[505]. Since I have also shown that IMiDs can promote the ubiquitination of CRBN, it is possible that this mechanism presents a means for prolonged IMiD exposure to promote CRBN turnover and the emergence of resistant clones. To combat CRBN downregulation and IMiD resistance, IMiDs have been tested in combination with proteasome and NAE inhibitors and this approach shows promise in both newly diagnosed and relapsed MM patients[505,513,514]. Fbxo7 overexpression is reported in cancers including T cell lymphoma and ALCL in which IMiD-based treatment regimens are being tested[67,511]. It may therefore be advantageous to consider Fbxo7 expression status in these cancers since it may correlate with patient response to IMiDs and indicate situations where combination therapy may be beneficial. Therefore, whilst only preliminary, my data suggest that the regulation of CRBN by Fbxo7 may affect IMiD sensitivity, and such knowledge may help to design effective therapeutic strategies.

In conclusion, I have identified two novel substrates for Fbxo7 ubiquitination that may have significance in disease. I first discovered a role for Fbxo7 in metabolism, highlighting a range of metabolic pathways disrupted by Fbxo7 loss in T cells, and specifically validating Fbxo7 as a negative regulator of glycolysis that inhibits the gatekeeper enzyme, PFKP. I subsequently found that Fbxo7 is a stress-responsive gene that is regulated by both glucose availability and oxidative stress at

transcriptional and post-translational levels and propose that Fbxo7 levels may fine-tune metabolism under different homeostatic and stress conditions. Finally, I identified CRBN as a substrate for ubiquitination by SCF^{Fbxo7} and propose that this targets CRBN for proteasomal degradation, which may have relevance for IMiD sensitivity. Together, these newly described functions position Fbxo7 as a nexus to link various cellular stress responses to metabolism and show the importance of Fbxo7 in the physiology and pathology of lymphocytes.

References

1. Schulman, B. A. & Wade Harper, J. Ubiquitin-like protein activation by E1 enzymes: the apex for downstream signalling pathways. *Nat. Rev. Mol. Cell Biol.* **10**, 319–331 (2009).

2. Pickart, C. M. Mechanisms underlying ubiquitination. *Annu. Rev. Biochem* **70**, 503–33 (2001).

3. Stewart, M. D., Ritterhoff, T., Klevit, R. E. & Brzovic, P. S. E2 enzymes: more than just middle men. *Cell Res.* **26**, 423–440 (2016).

4. Ye, Y. & Rape, M. Building ubiquitin chains: E2 enzymes at work. *Nat. Rev. Mol. Cell Biol.* **10**, 755–764 (2009).

5. Zheng, N. & Shabek, N. Ubiquitin Ligases: Structure, Function, and Regulation. *Annu. Rev. Biochem.* **86**, 129–157 (2017).

6. Morreale, F. E. & Walden, H. Types of Ubiquitin Ligases. *Cell* **165**, 248-248.e1 (2016).

7. Park, C.-W. & Ryu, K.-Y. Cellular ubiquitin pool dynamics and homeostasis. *BMB Rep.* **47**, 475–482 (2014).

8. Reyes-Turcu, F. E., Ventii, K. H. & Wilkinson, K. D. Regulation and Cellular Roles of Ubiquitin-Specific Deubiquitinating Enzymes. *Annu. Rev. Biochem.* **78**, 363–397 (2009).

9. Yau, R. & Rape, M. The increasing complexity of the ubiquitin code. *Nat. Cell Biol.* **18**, 579–586 (2016).

10. Herhaus, L. & Dikic, I. Expanding the ubiquitin code through post-translational modification. *EMBO Rep.* **16**, 1071–1083 (2015).

11. Ordureau, A. *et al.* Quantitative proteomics reveal a feedforward mechanism for mitochondrial PARKIN translocation and ubiquitin chain synthesis. *Mol. Cell* **56**, 360–375 (2014).

12. Swaney, D. L., Rodríguez-Mias, R. A. & Villén, J. Phosphorylation of ubiquitin at Ser65 affects its polymerization, targets, and proteome-wide turnover. *EMBO Rep.* **16**, 1131–1144 (2015).

13. Akutsu, M., Dikic, I. & Bremm, A. Ubiquitin chain diversity at a glance. *J. Cell Sci.* **129**, 875–880 (2016).

14. Li, W. & Ye, Y. Polyubiquitin chains: functions, structures, and mechanisms. *Cell. Mol. Life Sci.* **65**, 2397–2406 (2008).

15. Flick, K., Raasi, S., Zhang, H., Yen, J. L. & Kaiser, P. A ubiquitin-interacting motif protects polyubiquitinated Met4 from degradation by the 26S proteasome. *Nat. Cell Biol.* **8**, 509–515 (2006).

16. Wang, G. *et al.* K63-linked ubiquitination in kinase activation and cancer. *Front. Oncol.* **2**, 1–13 (2012).

17. Yuan, W.-C. *et al.* K33-Linked Polyubiquitination of Coronin 7 by Cul3-KLHL20 Ubiquitin E3 Ligase Regulates Protein Trafficking. *Mol. Cell* **54**, 586–600 (2014).

18. Liu, J. *et al.* Rhbdd3 controls autoimmunity by suppressing the production of IL-6 by dendritic cells via K27-linked ubiquitination of the regulator NEMO. *Nat. Immunol.* **15**, 612–622 (2014).

19. Gatti, M. *et al.* RNF168 Promotes Noncanonical K27 Ubiquitination to Signal DNA Damage. *Cell Rep.* **10**, 226–238 (2015).

20. Meyer, H. & Rape, M. Enhanced Protein Degradation by Branched Ubiquitin Chains. *Cell* **157**, 910–921 (2014).

21. Swatek, K. N. & Komander, D. Ubiquitin modifications. *Cell Res.* **26**, 399–422 (2016).

22. Hoppe, T. Multiubiquitylation by E4 enzymes: 'One size' doesn't fit all. *Trends Biochem. Sci.* **30**, 183–187 (2005).

23. Antoniou, N. *et al.* The role of E3, E4 ubiquitin ligase (UBE4B) in human pathologies. *Cancers (Basel).* **12**, 1–15 (2020).

24. Grossman, S. R. *et al.* Polyubiquitination of p53 by a ubiquitin ligase activity of p300. *Science (80-.).* **300**, 342–344 (2003).

25. Shi, D. *et al.* CBP and p300 are cytoplasmic E4 polyubiquitin ligases for p53. *Proc. Natl. Acad. Sci.* **106**, 16275–16280 (2009).

26. Imai, Y. *et al.* CHIP is associated with Parkin, a gene responsible for familial Parkinson's Disease, and enhances its ubiquitin ligase activity. *Mol. Cell* **10**, 55–67 (2002).

27. Hatakeyama, S., Yada, M., Matsumoto, M., Ishida, N. & Nakayama, K. I. U Box Proteins as a New Family of Ubiquitin-Protein Ligases. *J. Biol. Chem.* **276**, 33111–33120 (2001).

28. Johnson, E. S., Ma, P. C. M., Ota, I. M. & Varshavsky, A. A proteolytic pathway that recognizes ubiquitin as a degradation signal. *J. Biol. Chem.* **270**, 17442–17456 (1995).

29. Koegl, M. *et al.* A novel ubiquitination factor, E4, is involved in multiubiquitin chain assembly. *Cell* **96**, 635–644 (1999).

30. Baranes-Bachar, K. *et al.* The Ubiquitin E3/E4 Ligase UBE4A Adjusts Protein Ubiquitylation and Accumulation at Sites of DNA Damage, Facilitating Double-Strand Break Repair. *Mol. Cell* **69**, 866-878.e7 (2018).

31. Matsumoto, M. *et al.* Molecular clearance of ataxin-3 is regulated by a mammalian E4. *EMBO J.* **23**, 659–669 (2004).

32. Wu, H. *et al.* UBE4B promotes Hdm2-mediated degradation of the tumor suppressor p53. *Nat. Med.* **17**, 347–355 (2011).

33. Zhang, Y., Lv, Y., Zhang, Y. & Gao, H. Regulation of p53 level by UBE4B in breast cancer. *PLoS One* **9**, 5–10 (2014).

34. Berndsen, C. E. & Wolberger, C. New insights into ubiquitin E3 ligase mechanism. *Nat. Struct. Mol. Biol.* **21**, 301–307 (2014).

35. Metzger, M. B., Pruneda, J. N., Klevit, R. E. & Weissman, A. M. RING-type E3 ligases: Master manipulators of E2 ubiquitin-conjugating enzymes and ubiquitination. *Biochim. Biophys. Acta - Mol. Cell Res.* **1843**, 47–60 (2014).

36. Petroski, M. D. & Deshaies, R. J. Function and regulation of cullin–RING ubiquitin ligases. *Nat. Rev. Mol. Cell Biol.* **6**, 9–20 (2005).

37. Skaar, J. R., Pagan, J. K. & Pagano, M. Mechanisms and function of substrate recruitment by F-box proteins. *Nat. Rev. Mol. Cell Biol.* **14**, 369–381 (2013).

38. He, Y. J., McCall, C. M., Hu, J., Zeng, Y. & Xiong, Y. DDB1 functions as a linker to recruit receptor WD40 proteins to CUL4-ROC1 ubiquitin ligases. *Genes Dev.* **20**, 2949–2954 (2006).

39. Lee, J. & Zhou, P. DCAFs, the Missing Link of the CUL4-DDB1 Ubiquitin Ligase. *Mol. Cell* **26**,

775–780 (2007).

40. Rossi, M. *et al.* Regulation of the CRL4Cdt2 Ubiquitin Ligase and Cell-Cycle Exit by the SCFFbxo11 Ubiquitin Ligase. *Mol. Cell* **49**, 1159–1166 (2013).

41. Kuchay, S. *et al.* FBXL2- and PTPL1-mediated degradation of p110-free p85β regulatory subunit controls the PI(3)K signalling cascade. *Nat. Cell Biol.* **15**, 472–480 (2013).

42. Fukutomi, T., Takagi, K., Mizushima, T., Ohuchi, N. & Yamamoto, M. Kinetic, Thermodynamic, and Structural Characterizations of the Association between Nrf2-DLGex Degron and Keap1. *Mol. Cell. Biol.* **34**, 832–846 (2014).

43. Harper, J. W. & Schulman, B. A. Cullin-RING Ubiquitin Ligase Regulatory Circuits: A Quarter Century beyond the F-Box Hypothesis. *Annu. Rev. Biochem.* **90**, 403–429 (2021).

44. Yoshida, Y. *et al.* E3 ubiquitin ligase that recognizes sugar chains. *Nature* **418**, 438–442 (2002).

45. Glenn, K. A., Nelson, R. F., Wen, H. M., Mallinger, A. J. & Paulson, H. L. Diversity in Tissue Expression, Substrate Binding, and SCF Complex Formation for a Lectin Family of Ubiquitin Ligases. *J. Biol. Chem.* **283**, 12717–12729 (2008).

46. Lai, Y., Li, J., Li, X. & Zou, C. Lipopolysaccharide modulates p300 and Sirt1 to promote PRMT1 stability via an SCF Fbxl17 -recognized acetyldegron. *J. Cell Sci.* **130**, 3578–3587 (2017).

47. Havens, C. G. & Walter, J. C. Article Docking of a Specialized PIP Box onto Chromatin-Bound PCNA Creates a Degron for the Ubiquitin Ligase CRL4 Cdt2. *Mol. Cell* **35**, 93–104 (2009).

48. Havens, C. G. & Walter, J. C. Mechanism of CRL4 Cdt2 , a PCNA-dependent E3 ubiquitin ligase. **7**, 1568–1582 (2011).

49. Michishita, M. *et al.* Positively charged residues located downstream of PIP box, together with TD amino acids within PIP box, are important for CRL4Cdt2-mediated proteolysis. *Genes to Cells* **16**, 12–22 (2011).

50. Tedesco, D., Lukas, J. & Reed, S. I. The pRb-related protein p130 is regulated by phosphorylation-dependent proteolysis via the protein-ubiquitin ligase SCFSkp2. *Genes Dev.* **16**, 2946–2957 (2002).

51. Spruck, C. *et al.* A CDK-Independent Function of Mammalian Cks1. *Mol. Cell* **7**, 639–650 (2001).

52. Ganoth, D. *et al.* The cell-cycle regulatory protein Cks1 is required for SCF Skp2 -mediated ubiquitinylation of p27. *Nat. Cell Biol.* **3**, 321–324 (2001).

53. Wang, H. *et al.* FBXL5 Regulates IRP2 Stability in Iron Homeostasis via an Oxygen-Responsive [2Fe2S] Cluster. *Mol. Cell* **78**, 31-41.e5 (2020).

54. Zeng, Z. *et al.* Structural Basis of Selective Ubiquitination of TRF1 by SCFFbx4. *Dev. Cell* **18**, 214–225 (2010).

55. Nelson, D. E., Randle, S. J. & Laman, H. Beyond ubiquitination: the atypical functions of Fbxo7 and other F-box proteins. *Open Biol.* **3**, 130131 (2013).

56. Zhou, P. & Howley, P. M. Ubiquitination and Degradation of the Substrate Recognition Subunits of SCF Ubiquitin–Protein Ligases. *Mol. Cell* **2**, 571–580 (1998).

57. Galan, J.-M. & Peter, M. Ubiquitin-dependent degradation of multiple F-box proteins by an autocatalytic mechanism. *Proc. Natl. Acad. Sci.* **96**, 9124–9129 (1999).

58. Liu, J., Furukawa, M., Matsumoto, T. & Xiong, Y. NEDD8 modification of CUL1 dissociates p120CAND1, an inhibitor of CUL1-SKP1 binding and SCF ligases. *Mol. Cell* **10**, 1511–1518 (2002).

59. Zheng, J. *et al.* CAND1 binds to unneddylated CUL1 and regulates the formation of SCF ubiquitin E3 ligase complex. *Mol. Cell* **10**, 1519–1526 (2002).

60. Pierce, N. W. *et al.* Cand1 Promotes Assembly of New SCF Complexes through Dynamic Exchange of F Box Proteins. *Cell* **153**, 206–215 (2013).

61. Wu, S. *et al.* CAND1 controls in vivo dynamics of the cullin 1-RING ubiquitin ligase repertoire. *Nat. Commun.* **4**, 1642 (2013).

62. Reitsma, J. M. *et al.* Composition and Regulation of the Cellular Repertoire of SCF Ubiquitin Ligases. *Cell* **171**, 1326-1339.e14 (2017).

63. Liu, X. *et al.* Cand1-Mediated Adaptive Exchange Mechanism Enables Variation in F-Box Protein Expression. *Mol. Cell* **69**, 773-786.e6 (2018).

64. Reichermeier, K. M. *et al.* PIKES Analysis Reveals Response to Degraders and Key Regulatory Mechanisms of the CRL4 Network. *Mol. Cell* **77**, 1092-1106.e9 (2020).

65. Skaar, J. R., D'Angiolella, V., Pagan, J. K. & Pagano, M. SnapShot: F Box Proteins II. *Cell* **137**, 1358.e1-1358.e2 (2009).

66. Cenciarelli, C. *et al.* Identification of a family of human F-box proteins. *Curr. Biol.* **9**, 1177–1179 (1999).

67. Laman, H. *et al.* Transforming activity of Fbxo7 is mediated specifically through regulation of cyclin D/cdk6. *EMBO J.* **24**, 3104–3116 (2005).

68. Randle, S. J. & Laman, H. Structure and Function of Fbxo7/PARK15 in Parkinson's Disease. *Curr. Protein Pept. Sci.* **18**, 715–724 (2017).

69. Lee, J. E. *et al.* The Steady-State Repertoire of Human SCF Ubiquitin Ligase Complexes Does Not Require Ongoing Nedd8 Conjugation. *Mol. Cell. Proteomics* **10**, M110.006460 (2011).

70. Hsu, J.-M., Lee, Y.-C. G., Yu, C.-T. R. & Huang, C.-Y. F. Fbx7 Functions in the SCF Complex Regulating Cdk1-Cyclin B-phosphorylated Hepatoma Up-regulated Protein (HURP) Proteolysis by a Proline-rich Region. *J. Biol. Chem.* **279**, 32592–32602 (2004).

71. Kuo, T., Chang, P., Huang, S., Chou, C. & Chao, C. C.-K. Knockdown of HURP inhibits the proliferation of hepacellular carcinoma cells via downregulation of gankyrin and accumulation of p53. *Biochem. Pharmacol.* **83**, 758–768 (2012).

72. Bertrand, M. J. M. *et al.* cIAP1 and cIAP2 Facilitate Cancer Cell Survival by Functioning as E3 Ligases that Promote RIP1 Ubiquitination. *Mol. Cell* **30**, 689–700 (2008).

73. Mahoney, D. J. *et al.* Both cIAP1 and cIAP2 regulate TNF -mediated NF- B activation. *Proc. Natl. Acad. Sci.* **105**, 11778–11783 (2008).

74. Kuiken, H. J. *et al.* Identification of F-box only protein 7 as a negative regulator of NF-kappaB signalling. *J. Cell. Mol. Med.* **16**, 2140–2149 (2012).

75. Chang, Y.-F., Cheng, C., Chang, L., Jong, Y. & Yuo, C. The F-box protein Fbxo7 interacts with human inhibitor of apoptosis protein cIAP1 and promotes cIAP1 ubiquitination. *Biochem. Biophys. Res. Commun.* **342**, 1022–1026 (2006).

76. Spagnol, V. *et al.* The E3 ubiquitin ligase SCF(Fbxo7) mediates proteasomal degradation of

UXT isoform 2 (UXT-V2) to inhibit the NF-κB signaling pathway. *Biochim. Biophys. Acta - Gen. Subj.* **1865**, 129754 (2021).

77. Kang, J. & Chung, K. C. The F-box protein FBXO7 positively regulates bone morphogenetic protein-mediated signaling through Lys-63-specific ubiquitination of neurotrophin receptor-interacting MAGE (NRAGE). *Cell. Mol. Life Sci.* **72**, 181–195 (2015).

78. Shimizu, D. *et al.* NRAGE promotes the malignant phenotype of hepatocellular carcinoma. *Oncol. Lett.* **11**, 1847–1854 (2016).

79. Du, Q., Zhang, Y., Tian, X.-X., Li, Y. & Fang, W.-G. MAGE-D1 inhibits proliferation, migration and invasion of human breast cancer cells. *Oncol. Rep.* **22**, 659–665 (2009).

80. Udasin, R. G. *et al.* The p105 NF-κB precursor is a pseudo substrate of the ubiquitin ligase FBXO7, and its binding to the ligase stabilizes it and results in stimulated cell proliferation. *Biochem. Biophys. Res. Commun.* **558**, 224–230 (2021).

81. Teixeira, F. R. *et al.* Gsk3β and Tomm20 are substrates of the SCFFbxo7/PARK15 ubiquitin ligase associated with Parkinson's disease. *Biochem. J.* **473**, 3563–3580 (2016).

82. Di Maio, R. *et al.* α-synuclein binds to TOM20 and inhibits mitochondrial protein import in Parkinson's disease. *Sci. Transl. Med.* **8**, 1–15 (2016).

83. Franco-Iborra, S. *et al.* Defective mitochondrial protein import contributes to complex I-induced mitochondrial dysfunction and neurodegeneration in Parkinson's disease. *Cell Death Dis.* **9**, (2018).

84. De Miranda, B. R., Rocha, E. M., Castro, S. L. & Greenamyre, J. T. Protection from α-Synuclein induced dopaminergic neurodegeneration by overexpression of the mitochondrial import receptor TOM20. *npj Park. Dis.* **6**, (2020).

85. Cohen, P. & Frame, S. The renaissance of GSK3. *Nat. Rev. Mol. Cell Biol.* **2**, 769–776 (2001).

86. Stott, S. R. W. *et al.* Loss of FBXO7 results in a Parkinson's-like dopaminergic degeneration via an RPL23–MDM2–TP53 pathway. *J. Pathol.* **249**, 241–254 (2019).

87. Rousseau, A. & Bertolotti, A. Regulation of proteasome assembly and activity in health and disease. *Nat. Rev. Mol. Cell Biol.* **19**, 697–712 (2018).

88. Vingill, S. *et al.* Loss of FBXO7 (PARK15) results in reduced proteasome activity and models a parkinsonism-like phenotype in mice. *EMBO J.* **35**, 2008–2025 (2016).

89. Wang, Q., Crnković, V., Preisinger, C. & Stegmüller, J. The parkinsonism-associated protein FBXO7 cooperates with the BAG6 complex in proteasome function and controls the subcellular localization of the complex. *Biochem. J.* **478**, 2179–2199 (2021).

90. Correa-Vela, M. *et al.* Impaired proteasome activity and neurodegeneration with brain iron accumulation in FBXO7 defect. *Ann. Clin. Transl. Neurol.* **7**, 1436–1442 (2020).

91. McCutchen-Maloney, S. L. *et al.* cDNA Cloning, Expression, and Functional Characterization of PI31, a Proline-rich Inhibitor of the Proteasome. *J. Biol. Chem.* **275**, 18557–18565 (2000).

92. Zaiss, D. M. W., Standera, S., Holzhütter, H., Kloetzel, P. & Sijts, A. J. A. M. The proteasome inhibitor PI31 competes with PA28 for binding to 20S proteasomes. *FEBS Lett.* **457**, 333–338 (1999).

93. Rathje, C. C. *et al.* A Conserved Requirement for Fbxo7 During Male Germ Cell Cytoplasmic Remodeling. *Front. Physiol.* **10**, 1–16 (2019).

94. Bader, M. *et al.* A Conserved F Box Regulatory Complex Controls Proteasome Activity in Drosophila. *Cell* **145**, 371–382 (2011).

95. Bader, M., Arama, E. & Steller, H. A novel F-box protein is required for caspase activation during cellular remodeling in Drosophila. *Development* **137**, 1679–1688 (2010).

96. Zaiss, D. M. W., Standera, S., Kloetzel, P.-M. & Sijts, A. J. A. M. PI31 is a modulator of proteasome formation and antigen processing. *Proc. Natl. Acad. Sci.* **99**, 14344–14349 (2002).

97. Kirk, R. *et al.* Structure of a Conserved Dimerization Domain within the F-box Protein Fbxo7 and the PI31 Proteasome Inhibitor. *J. Biol. Chem.* **283**, 22325–22335 (2008).

98. Burchell, V. S. *et al.* The Parkinson's disease–linked proteins Fbxo7 and Parkin interact to mediate mitophagy. *Nat. Neurosci.* **16**, 1257–1265 (2013).

99. Liu, Y. *et al.* Chemical inhibition of FBXO7 reduces inflammation and confers neuroprotection by stabilizing the mitochondrial kinase PINK1. *JCI insight* **5**, (2020).

100. Lomonosov, M. *et al.* Expression of Fbxo7 in Haematopoietic Progenitor Cells Cooperates with p53 Loss to Promote Lymphomagenesis. *PLoS One* **6**, e21165 (2011).

101. Laman, H. Fbxo7 Gets Proactive with Cyclin D/cdk6. *Cell Cycle* **5**, 279–282 (2006).

102. Meziane, E. K., Randle, S. J., Nelson, D. E., Lomonosov, M. & Laman, H. Knockdown of Fbxo7 reveals its regulatory role in proliferation and differentiation of haematopoietic precursor cells. *J. Cell Sci.* **124**, 2175–2186 (2011).

103. Randle, S. J., Nelson, D. E., Patel, S. P. & Laman, H. Defective erythropoiesis in a mouse model of reduced Fbxo7 expression due to decreased p27 expression. *J. Pathol.* **237**, 263–272 (2015).

104. Ballesteros Reviriego, C. *et al.* FBXO7 sensitivity of phenotypic traits elucidated by a hypomorphic allele. *PLoS One* **14**, e0212481 (2019).

105. Harris, R., Randle, S. & Laman, H. Analysis of the FBXO7 promoter reveals overlapping Pax5 and c-Myb binding sites functioning in B cells. *Biochem. Biophys. Res. Commun.* **554**, 41–48 (2021).

106. Patel, S. P., Randle, S. J., Gibbs, S., Cooke, A. & Laman, H. Opposing effects on the cell cycle of T lymphocytes by Fbxo7 via Cdk6 and p27. *Cell. Mol. Life Sci.* **74**, 1553–1566 (2017).

107. Goel, S., DeCristo, M. J., McAllister, S. S. & Zhao, J. J. CDK4/6 Inhibition in Cancer: Beyond Cell Cycle Arrest. *Trends Cell Biol.* **28**, 911–925 (2018).

108. Lukas, J., Bartkova, J. & Bartek, J. Convergence of mitogenic signalling cascades from diverse classes of receptors at the cyclin D-cyclin-dependent kinase-pRb-controlled G1 checkpoint. *Mol. Cell. Biol.* **16**, 6917–6925 (1996).

109. Sherr, C. J. & Roberts, J. M. CDK inhibitors: positive and negative regulators of G1-phase progression. *Genes Dev.* **13**, 1501–1512 (1999).

110. Tigan, A., Bellutti, F., Kollmann, K., Tebb, G. & Sexl, V. CDK6—a review of the past and a glimpse into the future: from cell-cycle control to transcriptional regulation. *Oncogene* **35**, 3083–3091 (2016).

111. Kollmann, K. *et al.* A Kinase-Independent Function of CDK6 Links the Cell Cycle to Tumor Angiogenesis. *Cancer Cell* **24**, 167–181 (2013).

112. Kollmann, K. & Sexl, V. CDK6 and p16INK4A in lymphoid malignancies. *Oncotarget* **4**, 1858–

1859 (2013).

113. Scheicher, R. *et al.* CDK6 as a key regulator of hematopoietic and leukemic stem cell activation. *Blood* **125**, 90–101 (2015).

114. Laurenti, E. *et al.* CDK6 levels regulate quiescence exit in human hematopoietic stem cells. *Cell Stem Cell* **16**, 302–313 (2015).

115. Bellutti, F. *et al.* CDK6 Antagonizes p53-Induced Responses during Tumorigenesis. *Cancer Discov.* **8**, 884–897 (2018).

116. Buss, H. *et al.* Cyclin-Dependent Kinase 6 Phosphorylates NF-κB P65 at Serine 536 and Contributes to the Regulation of Inflammatory Gene Expression. *PLoS One* **7**, 1–13 (2012).

117. Handschick, K. *et al.* Cyclin-Dependent Kinase 6 Is a Chromatin-Bound Cofactor for NF-κB-Dependent Gene Expression. *Mol. Cell* **53**, 193–208 (2014).

118. Hu, M. G. *et al.* CDK6 kinase activity is required for thymocyte development. *Blood* **117**, 6120–6131 (2011).

119. Hu, M. G. *et al.* A Requirement for Cyclin-Dependent Kinase 6 in Thymocyte Development and Tumorigenesis. *Cancer Res.* **69**, 810–818 (2009).

120. Jena, N. *et al.* CDK6-mediated repression of CD25 is required for induction and maintenance of Notch1-induced T-cell acute lymphoblastic leukemia. *Leukemia* **30**, 1033–1043 (2016).

121. Meyerson, M. & Harlow, E. Identification of G1 kinase activity for cdk6, a novel cyclin D partner. *Mol. Cell. Biol.* **14**, 2077–2086 (1994).

122. Malumbres, M. *et al.* Mammalian cells cycle without the D-type cyclin-dependent kinases Cdk4 and Cdk6. *Cell* **118**, 493–504 (2004).

123. Asghar, U., Witkiewicz, A. K., Turner, N. C. & Knudsen, E. S. The history and future of targeting cyclin-dependent kinases in cancer therapy. *Nat. Rev. Drug Discov.* **14**, 130–146 (2015).

124. Liu, M., Liu, H. & Chen, J. Mechanisms of the CDK4/6 inhibitor palbociclib (PD 0332991) and its future application in cancer treatment (Review). *Oncol. Rep.* 901–911 (2018) doi:10.3892/or.2018.6221.

125. Deng, J. *et al.* CDK4/6 Inhibition Augments Antitumor Immunity by Enhancing T-cell Activation. *Cancer Discov.* **8**, 216–233 (2018).

126. Goel, S. *et al.* CDK4/6 inhibition triggers anti-tumour immunity. *Nature* **548**, 471–475 (2017).

127. Mistry, B. V. *et al.* Expression profiling of WD40 family genes including DDB1- A nd CUL4- A ssociated factor (DCAF) genes in mice and human suggests important regulatory roles in testicular development and spermatogenesis. *BMC Genomics* **21**, 1–21 (2020).

128. Jackson, S. & Xiong, Y. CRL4s: the CUL4-RING E3 ubiquitin ligases. *Trends Biochem. Sci.* **34**, 562–570 (2009).

129. Higgins, J. J., Pucilowska, J., Lombardi, R. Q. & Rooney, J. P. A mutation in a novel ATP-dependent Lon protease gene in a kindred with mild mental retardation. *Neurology* **63**, 1927–1931 (2004).

130. Fischer, E. S. *et al.* Structure of the DDB1-CRBN E3 ubiquitin ligase in complex with thalidomide. *Nature* **512**, 49–53 (2014).

131. Chamberlain, P. P. *et al.* Structure of the human Cereblon-DDB1-lenalidomide complex

reveals basis for responsiveness to thalidomide analogs. *Nat. Struct. Mol. Biol.* **21**, 803–809 (2014).

132. Jo, S., Lee, K., Song, S., Jung, Y. & Park, C. Identification and functional characterization of cereblon as a binding protein for large-conductance calcium-activated potassium channel in rat brain. *J. Neurochem.* **94**, 1212–1224 (2005).

133. Hohberger, B. & Enz, R. Cereblon is expressed in the retina and binds to voltage-gated chloride channels. *FEBS Lett.* **583**, 633–637 (2009).

134. Chen, Y. A. *et al.* The cullin 4A/B-DDB1-cereblon E3 ubiquitin ligase complex mediates the degradation of CLC-1 chloride channels. *Sci. Rep.* **5**, 1–13 (2015).

135. Fu, S. *et al.* CUL4-DDB1-CRBN E3 Ubiquitin Ligase Regulates Proteostasis of ClC-2 Chloride Channels: Implication for Aldosteronism and Leukodystrophy. *Cells* **9**, 1332 (2020).

136. Liu, J. *et al.* CRL4ACRBN E3 ubiquitin ligase restricts BK channel activity and prevents epileptogenesis. *Nat. Commun.* **5**, 3924 (2014).

137. Song, T. *et al.* CRL4 antagonizes SCFFbxo7-mediated turnover of cereblon and BK channel to regulate learning and memory. *PLoS Genet.* **14**, 1–26 (2018).

138. Capdevila, J. *et al.* Control of Vertebrate Limb Outgrowth by the Proximal Factor Meis2 and Distal Antagonism of BMPs by Gremlin. *Mol. Cell* **4**, 839–849 (1999).

139. Crowley, M. A. *et al.* Further evidence for the possible role of MEIS2 in the development of cleft palate and cardiac septum. *Am. J. Med. Genet. Part A* **152A**, 1326–1327 (2010).

140. Aizawa, M., Abe, Y., Ito, T., Handa, H. & Nawa, H. mRNA distribution of the thalidomide binding protein cereblon in adult mouse brain. *Neurosci. Res.* **69**, 343–347 (2011).

141. Choi, T.-Y. *et al.* Cereblon Maintains Synaptic and Cognitive Function by Regulating BK Channel. *J. Neurosci.* **38**, 3571–3583 (2018).

142. Ando, H. *et al.* Cereblon Control of Zebrafish Brain Size by Regulation of Neural Stem Cell Proliferation Cereblon Control of Zebrafish Brain Size by Regulation of Neural Stem Cell Proliferation. *ISCIENCE* **15**, 95–108 (2019).

143. Rajadhyaksha, A. M. *et al.* Behavioral characterization of cereblon forebrain-specific conditional null mice : A model for human non-syndromic intellectual disability. *Behav. Brain Res.* **226**, 428–434 (2012).

144. Sheereen, A. *et al.* A missense mutation in the CRBN gene that segregates with intellectual disability and self-mutilating behaviour in a consanguineous Saudi family. *J. Med. Genet.* **54**, 236–240 (2017).

145. Nguyen, T. Van *et al.* Glutamine Triggers Acetylation-Dependent Degradation of Glutamine Synthetase via the Thalidomide Receptor Cereblon. *Mol. Cell* **61**, 809–820 (2016).

146. Lee, K. M., Jo, S., Kim, H., Lee, J. & Park, C. S. Functional modulation of AMP-activated protein kinase by cereblon. *Biochim. Biophys. Acta - Mol. Cell Res.* **1813**, 448–455 (2011).

147. Kwon, E., Li, X., Deng, Y., Chang, H. W. & Kim, D. Y. AMPK is down-regulated by the CRL4A-CRBN axis through the polyubiquitination of AMPKα isoforms. *FASEB J.* **33**, 6539–6550 (2019).

148. Yang, S. J. *et al.* Ubiquitin-dependent proteasomal degradation of AMPK gamma subunit by Cereblon inhibits AMPK activity. *Biochim. Biophys. Acta - Mol. Cell Res.* **1867**, 118729 (2020).

149. Lee, K. M. *et al.* Disruption of the cereblon gene enhances hepatic AMPK activity and

prevents high-fat diet-induced obesity and insulin resistance in mice. *Diabetes* **62**, 1855–1864 (2013).

150. Eichner, R. *et al.* Immunomodulatory drugs disrupt the cereblon-CD147-MCT1 axis to exert antitumor activity and teratogenicity. *Nat. Med.* **22**, 735–743 (2016).

151. Min, Y. *et al.* Cereblon negatively regulates TLR4 signaling through the attenuation of ubiquitination of TRAF6. *Cell Death Dis.* **7**, 1–12 (2016).

152. Singhal, S. *et al.* Antitumor Activity of Thalidomide in Refractory Multiple Myeloma. *N. Engl. J. Med.* **341**, 1565–1571 (1999).

153. Wang, B., Duan, J. & Zhou, L. The paradoxical pharmacological mechanisms of lenalidomide and bortezomib in the treatment of multiple myeloma. *Anticancer. Drugs* **32**, 227–232 (2021).

154. International Agency for Research on Cancer. World Health Organisation. *Global Multiple Myeloma Statistics*. https://gco.iarc.fr/today/data/factsheets/cancers/35-Multiple-myeloma-fact-sheet.pdf (2020).

155. Office for National Statistics. *Cancer survival by stage at diagnosis for England*. (2019).

156. Holstein, S. A. & McCarthy, P. L. Immunomodulatory Drugs in Multiple Myeloma: Mechanisms of Action and Clinical Experience. *Drugs* **77**, 505–520 (2017).

157. Ito, T., Yamaguchi, Y. & Handa, H. Exploiting ubiquitin ligase cereblon as a target for small-molecule compounds in medicine and chemical biology. *Cell Chem. Biol.* **28**, 987–999 (2021).

158. Ito, T. *et al.* Identification of a Primary Target of Thalidomide Teratogenicity. *Science (80-.).* **327**, 1345–1350 (2010).

159. Zhu, Y. X. *et al.* Cereblon expression is required for the antimyeloma activity of lenalidomide and pomalidomide. *Blood* **118**, 4771–4779 (2011).

160. Krönke, J. *et al.* Lenalidomide Causes Selective Degradation of IKZF1 and IKZF3 in Multiple Myeloma Cells. *Science (80-.).* **343**, 301–305 (2014).

161. Lu, G. *et al.* The Myeloma Drug Lenalidomide Promotes the Cereblon-Dependent Destruction of Ikaros Proteins. *Science (80-.).* **343**, 305–309 (2014).

162. Bjorklund, C. C. *et al.* Rate of CRL4CRBN substrate Ikaros and Aiolos degradation underlies differential activity of lenalidomide and pomalidomide in multiple myeloma cells by regulation of c-Myc and IRF4. *Blood Cancer J.* **5**, e354–e354 (2015).

163. Lopez-Girona, A. *et al.* Lenalidomide downregulates the cell survival factor, interferon regulatory factor-4, providing a potential mechanistic link for predicting response. *Br. J. Haematol.* **154**, 325–336 (2011).

164. Manni, S. *et al.* Inactivation of CK1α in multiple myeloma empowers drug cytotoxicity by affecting AKT and β-catenin survival signaling pathways. *Oncotarget* **8**, 14604–14619 (2017).

165. Krönke, J. *et al.* Lenalidomide induces ubiquitination and degradation of CK1α in del(5q) MDS. *Nature* **523**, 183–188 (2015).

166. List, A. *et al.* Lenalidomide in the Myelodysplastic Syndrome with Chromosome 5q Deletion. *N. Engl. J. Med.* **355**, 1456–1465 (2006).

167. Yamamoto, J. *et al.* ARID2 is a pomalidomide-dependent CRL4CRBN substrate in multiple myeloma cells. *Nat. Chem. Biol.* **16**, 1208–1217 (2020).

168. Matyskiela, M. E. *et al.* SALL4 mediates teratogenicity as a thalidomide-dependent cereblon substrate. *Nat. Chem. Biol.* **14**, 981–987 (2018).

169. Quach, H. *et al.* Mechanism of action of immunomodulatory drugs (IMiDS) in multiple myeloma. *Leukemia* **24**, 22–32 (2010).

170. D'Souza, C., Prince, H. M. & Neeson, P. J. Understanding the Role of T-Cells in the Antimyeloma Effect of Immunomodulatory Drugs. *Front. Immunol.* **12**, 1–8 (2021).

171. Henry, J. Y. *et al.* Enhanced cross-priming of naive CD8 + T cells by dendritic cells treated by the IMiDs ® immunomodulatory compounds lenalidomide and pomalidomide. *Immunology* **139**, 377–385 (2013).

172. LeBlanc, R. *et al.* Immunomodulatory drug costimulates T cells via the B7-CD28 pathway. *Blood* **103**, 1787–1790 (2004).

173. Schafer, P. H. *et al.* Enhancement of Cytokine Production and AP-1 Transcriptional Activity in T Cells by Thalidomide-Related Immunomodulatory Drugs. *J. Pharmacol. Exp. Ther.* **305**, 1222–1232 (2003).

174. Davies, F. E. *et al.* Thalidomide and immunomodulatory derivatives augment natural killer cell cytotoxicity in multiple myeloma. *Blood* **98**, 210–216 (2001).

175. Ogawara, H. *et al.* High Th1/Th2 ratio in patients with multiple myeloma. *Leuk. Res.* **29**, 135–140 (2005).

176. Wu, L. *et al.* Lenalidomide Enhances Natural Killer Cell and Monocyte-Mediated Antibody-Dependent Cellular Cytotoxicity of Rituximab-Treated CD20 + Tumor Cells. *Clin. Cancer Res.* **14**, 4650–4657 (2008).

177. Hsu, A. K. *et al.* The immunostimulatory effect of lenalidomide on NK-cell function is profoundly inhibited by concurrent dexamethasone therapy. *Blood* **117**, 1605–1613 (2011).

178. Kort, K. M. *et al.* Targeted sequencing of refractory myeloma reveals a high incidence of mutations in CRBN and Ras pathway genes. **128**, 1226–1233 (2016).

179. Zhou, N. *et al.* RUNX proteins desensitize multiple myeloma to lenalidomide via protecting IKZFs from degradation. *Leukemia* **33**, 2006–2021 (2019).

180. Mountjoy, L. *et al.* Prediction of immunomodulatory drugs (IMiDs) sensitivity in myeloma via determination of baseline anti-oxidative stress capacity. *Leukemia* **34**, 3060–3063 (2020).

181. Sebastian, S. *et al.* Multiple myeloma cells' capacity to decompose H2O2 determines lenalidomide sensitivity. *Blood* **129**, 991–1007 (2017).

182. Heiden, M. G. V., Cantley, L. C. & Thompson, C. B. Understanding the warburg effect: The metabolic requirements of cell proliferation. *Science (80-.).* **324**, 1029–1033 (2009).

183. Navale, A. M. & Paranjape, A. N. Glucose transporters: physiological and pathological roles. *Biophys. Rev.* **8**, 5–9 (2016).

184. Judge, A. & Dodd, M. S. Metabolism. *Essays Biochem.* **64**, 607–647 (2020).

185. Khan, T. *et al.* Revisiting Glycogen in Cancer: A Conspicuous and Targetable Enabler of Malignant Transformation. *Front. Oncol.* **10**, 1–10 (2020).

186. Bolaños, J. P., Almeida, A. & Moncada, S. Glycolysis: a bioenergetic or a survival pathway? *Trends Biochem. Sci.* **35**, 145–149 (2010).

187. Icard, P. & Lincet, H. A global view of the biochemical pathways involved in the regulation of the metabolism of cancer cells. *Biochim. Biophys. Acta - Rev. Cancer* **1826**, 423–433 (2012).

188. Cho, E. S., Cha, Y. H., Kim, H. S., Kim, N. H. & Yook, J. I. The Pentose Phosphate Pathway as a Potential Target for Cancer Therapy. *Biomol. Ther. (Seoul).* **26**, 29–38 (2018).

189. Chang, C. & Pearce, E. L. Emerging concepts of T cell metabolism as a target of immunotherapy. *Nat. Immunol.* **17**, 364–368 (2016).

190. Patra, K. C. & Hay, N. The pentose phosphate pathway and cancer. *Trends Biochem. Sci.* **39**, 347–354 (2014).

191. Au, S. W. N., Gover, S., Lam, V. M. S. & Adams, M. J. Human glucose-6-phosphate dehydrogenase: The crystal structure reveals a structural NADP+ molecule and provides insights into enzyme deficiency. *Structure* **8**, 293–303 (2000).

192. Shuvalov, O. *et al.* One-carbon metabolism and nucleotide biosynthesis as attractive targets for anticancer therapy. *Oncotarget* **8**, 23955–23977 (2017).

193. Ducker, G. S. & Rabinowitz, J. D. One-Carbon Metabolism in Health and Disease. *Cell Metab.* **25**, 27–42 (2017).

194. DeBerardinis, R. J. *et al.* Beyond aerobic glycolysis: Transformed cells can engage in glutamine metabolism that exceeds the requirement for protein and nucleotide synthesis. *Proc. Natl. Acad. Sci.* **104**, 19345–19350 (2007).

195. Chen, C., Hsu, S., Ann, D. K., Yen, Y. & Kung, H. Arginine Signaling and Cancer Metabolism. *Cancers (Basel).* **13**, 3541 (2021).

196. Takahama, Y. Journey through the thymus: Stromal guides for T-cell development and selection. *Nat. Rev. Immunol.* **6**, 127–135 (2006).

197. Godfrey, D. I., Kennedy, J., Suda, T. & Zlotnik, A. A developmental pathway involving four phenotypically and functionally distinct subsets of CD3-CD4-CD8- triple-negative adult mouse thymocytes defined by CD44 and CD25 expression. *J. Immunol.* **150**, 4244–52 (1993).

198. Livák, F., Tourigny, M., Schatz, D. G. & Petrie, H. T. Characterization of TCR gene rearrangements during adult murine T cell development. *J. Immunol.* **162**, 2575–80 (1999).

199. Rothenberg, E. V., Moore, J. E. & Yui, M. A. Launching the T-cell-lineage developmental programme. *Nat. Rev. Immunol.* **8**, 9–21 (2008).

200. Von Boehmer, H. Unique features of the pre-T-cell receptor aα-chain: Not just a surrogate. *Nat. Rev. Immunol.* **5**, 571–577 (2005).

201. Maillard, I. *et al.* The requirement for Notch signaling at the β-selection checkpoint in vivo is absolute and independent of the pre-T cell receptor. *J. Exp. Med.* **203**, 2239–2245 (2006).

202. Dose, M. *et al.* c-Myc mediates pre-TCR-induced proliferation but not developmental progression. *Blood* **108**, 2669–2677 (2006).

203. Ciofani, M. & Zúñiga-Pflücker, J. C. Notch promotes survival of pre-T cells at the β-selection checkpoint by regulating cellular metabolism. *Nat. Immunol.* **6**, 881–888 (2005).

204. Juntilla, M. M., Wofford, J. A., Birnbaum, M. J., Rathmell, J. C. & Koretzky, G. A. Akt1 and Akt2 are required for αβ thymocyte survival and differentiation. *Proc. Natl. Acad. Sci. U. S. A.* **104**, 12105–12110 (2007).

205. Henao-Mejia, J. *et al.* The MicroRNA miR-181 Is a Critical Cellular Metabolic Rheostat

Essential for NKT Cell Ontogenesis and Lymphocyte Development and Homeostasis. *Immunity* **38**, 984–997 (2013).

206. Takaba, H. & Takayanagi, H. The Mechanisms of T Cell Selection in the Thymus. *Trends Immunol.* **38**, 805–816 (2017).

207. Zhao, Y., Niu, C. & Cui, J. Gamma-delta (γδ) T Cells: Friend or Foe in Cancer Development. *J. Transl. Med.* **16**, 1–13 (2018).

208. Mossmann, D., Park, S. & Hall, M. N. mTOR signalling and cellular metabolism are mutual determinants in cancer. *Nat. Rev. Cancer* **18**, 744–757 (2018).

209. Yang, K. *et al.* Metabolic signaling directs the reciprocal lineage decisions of and T cells. *Sci. Immunol.* **3**, 1–13 (2018).

210. Rathmell, J. C., Farkash, E. A., Gao, W. & Thompson, C. B. IL-7 Enhances the Survival and Maintains the Size of Naive T Cells. *J. Immunol.* **167**, 6869–6876 (2001).

211. Herbel, C. *et al.* Clinical significance of T cell metabolic reprogramming in cancer. *Clin. Transl. Med.* **5**, 29 (2016).

212. Cekic, C., Sag, D., Day, Y. & Linden, J. Extracellular adenosine regulates naive T cell development and peripheral maintenance. *J. Exp. Med.* **210**, 2693–2706 (2013).

213. Klein Geltink, R. I., Kyle, R. L. & Pearce, E. L. Unraveling the Complex Interplay Between T Cell Metabolism and Function. *Annu. Rev. Immunol.* **36**, 461–488 (2018).

214. Menk, A. V. *et al.* Early TCR Signaling Induces Rapid Aerobic Glycolysis Enabling Distinct Acute T Cell Effector Functions. *Cell Rep.* **22**, 1509–1521 (2018).

215. Cunningham, C. A., Bergsbaken, T. & Fink, P. J. Cutting Edge: Defective Aerobic Glycolysis Defines the Distinct Effector Function in Antigen-Activated CD8 + Recent Thymic Emigrants. *J. Immunol.* **198**, 4575–4580 (2017).

216. Wang, R. *et al.* The Transcription Factor Myc Controls Metabolic Reprogramming upon T Lymphocyte Activation. *Immunity* **35**, 871–882 (2011).

217. Pollizzi, K. N. *et al.* mTORC1 and mTORC2 selectively regulate CD8+ T cell differentiation. *J. Clin. Invest.* **125**, 2090–2108 (2015).

218. Purtic, B., Pitcher, L. A., van Oers, N. S. C. & Wulfing, C. T cell receptor (TCR) clustering in the immunological synapse integrates TCR and costimulatory signaling in selected T cells. *Proc. Natl. Acad. Sci.* **102**, 2904–2909 (2005).

219. Liechtenstein, T., Dufait, I., Lanna, A., Breckpot, K. & Escors, D. Modulating Co-Stimulation During Antigen Presentation to Enhance Cancer Immunotherapy. *Immunol. Endocr. Metab. Agents - Med. Chem.* **12**, 224–235 (2012).

220. Kim, J. W., Tchernyshyov, I., Semenza, G. L. & Dang, C. V. HIF-1-mediated expression of pyruvate dehydrogenase kinase: A metabolic switch required for cellular adaptation to hypoxia. *Cell Metab.* **3**, 177–185 (2006).

221. Jacobs, S. R. *et al.* Glucose Uptake Is Limiting in T Cell Activation and Requires CD28-Mediated Akt-Dependent and Independent Pathways. *J. Immunol.* **180**, 4476–4486 (2008).

222. Wieman, H. L., Wofford, J. A. & Rathmell, J. C. Cytokine Stimulation Promotes Glucose Uptake via Phosphatidylinositol-3 Kinase/Akt Regulation of Glut1 Activity and Trafficking. *Mol. Biol. Cell* **18**, 1437–1446 (2007).

223. Frauwirth, K. A. *et al.* The CD28 Signaling Pathway Regulates Glucose Metabolism. *Immunity* **16**, 769–777 (2002).

224. Finlay, D. K. *et al.* PDK1 regulation of mTOR and hypoxia-inducible factor 1 integrate metabolism and migration of CD8+ T cells. *J. Exp. Med.* **209**, 2441–2453 (2012).

225. Balyan, R., Gautam, N. & Gascoigne, N. R. J. The Ups and Downs of Metabolism during the Lifespan of a T Cell. *Int. J. Mol. Sci.* **21**, 7972 (2020).

226. Dumont, F. J. & Su, Q. Mechanism of action of the immunosuppressant rapamycin. *Life Sci.* **58**, 373–395 (1995).

227. Osthus, R. C. *et al.* Deregulation of Glucose Transporter 1 and Glycolytic Gene Expression by c-Myc. *J. Biol. Chem.* **275**, 21797–21800 (2000).

228. Kim, J., Gao, P., Liu, Y., Semenza, G. L. & Dang, C. V. Hypoxia-Inducible Factor 1 and Dysregulated c-Myc Cooperatively Induce Vascular Endothelial Growth Factor and Metabolic Switches Hexokinase 2 and Pyruvate Dehydrogenase Kinase 1. *Mol. Cell. Biol.* **27**, 7381–7393 (2007).

229. Dang, C. V, Le, A. & Gao, P. MYC-Induced Cancer Cell Energy Metabolism and Therapeutic Opportunities. *Clin. Cancer Res.* **15**, 6479–6483 (2009).

230. Ma, E. H. *et al.* Serine Is an Essential Metabolite for Effector T Cell Expansion. *Cell Metab.* **25**, 345–357 (2017).

231. Sinclair, L. V. *et al.* Control of amino-acid transport by antigen receptors coordinates the metabolic reprogramming essential for T cell differentiation. *Nat. Immunol.* **14**, 500–508 (2013).

232. Geiger, R. *et al.* L-Arginine Modulates T Cell Metabolism and Enhances Survival and Anti-tumor Activity. *Cell* **167**, 829-842.e13 (2016).

233. Srivastava, M. K., Sinha, P., Clements, V. K., Rodriguez, P. & Ostrand-Rosenberg, S. Myeloid-derived suppressor cells inhibit T-cell activation by depleting cystine and cysteine. *Cancer Res.* **70**, 68–77 (2010).

234. Owen, O. E., Kalhan, S. C. & Hanson, R. W. The key role of anaplerosis and cataplerosis for citric acid cycle function. *J. Biol. Chem.* **277**, 30409–30412 (2002).

235. Yang, C. *et al.* Glutamine oxidation maintains the TCA cycle and cell survival during impaired mitochondrial pyruvate transport. *Mol. Cell* **56**, 414–424 (2014).

236. Yaqoob, P. & Calder, P. C. Glutamine requirement of proliferating T lymphocytes. *Nutrition* **13**, 646–651 (1997).

237. Carr, E. L. *et al.* Glutamine Uptake and Metabolism Are Coordinately Regulated by ERK/MAPK during T Lymphocyte Activation. *J. Immunol.* **185**, 1037–1044 (2010).

238. Gao, P. *et al.* c-Myc suppression of miR-23a/b enhances mitochondrial glutaminase expression and glutamine metabolism. *Nature* **458**, 762–765 (2009).

239. Sena, L. A. *et al.* Mitochondria Are Required for Antigen-Specific T Cell Activation through Reactive Oxygen Species Signaling. *Immunity* **38**, 225–236 (2013).

240. Tan, H. *et al.* Profiling Reveals Dynamic Signaling Networks and Bioenergetics Pathways Underlying T Cell Activation Resource Integrative Proteomics and Phosphoproteomics Profiling Reveals Dynamic Signaling Networks and Bioenergetics Pathways Underlying T Cell

Activation. *Immunity* **46**, 488–503 (2017).

241. Chang, C. *et al.* Posttranscriptional Control of T Cell Effector Function by Aerobic Glycolysis. *Cell* **153**, 1239–1251 (2013).

242. Laniewski, N. G. & Grayson, J. M. Antioxidant Treatment Reduces Expansion and Contraction of Antigen-Specific CD8 + T Cells during Primary but Not Secondary Viral Infection. *J. Virol.* **78**, 11246–11257 (2004).

243. Ron-Harel, N. *et al.* Mitochondrial Biogenesis and Proteome Remodeling Promote One-Carbon Metabolism for T Cell Activation. *Cell Metab.* **24**, 104–117 (2016).

244. Yang, K. *et al.* T Cell Exit from Quiescence and Differentiation into Th2 Cells Depend on Raptor-mTORC1-Mediated Metabolic Reprogramming. *Immunity* **39**, 1043–1056 (2013).

245. Shi, L. Z. *et al.* HIF1α-dependent glycolytic pathway orchestrates a metabolic checkpoint for the differentiation of TH17 and Treg cells. *J. Exp. Med.* **208**, 1367–1376 (2011).

246. Gerriets, V. A. *et al.* Foxp3 and Toll-like receptor signaling balance Treg cell anabolic metabolism for suppression. *Nat. Immunol.* **17**, 1459–1466 (2016).

247. Szabo, S. J. *et al.* A novel transcription factor, T-bet, directs Th1 lineage commitment. *Cell* **100**, 655–669 (2000).

248. Chornoguz, O. *et al.* mTORC1 Promotes T-bet Phosphorylation To Regulate Th1 Differentiation. *J. Immunol.* **198**, 3939–3948 (2017).

249. Peng, M. *et al.* Aerobic glycolysis promotes T helper 1 cell differentiation through an epigenetic mechanism. *Science (80-.).* **354**, 481–484 (2016).

250. Klysz, D. *et al.* Glutamine-dependent α-ketoglutarate production regulates the balance between T helper 1 cell and regulatory T cell generation. *Sci. Signal.* **8**, 1–13 (2015).

251. Metzler, B., Gfeller, P. & Guinet, E. Restricting Glutamine or Glutamine-Dependent Purine and Pyrimidine Syntheses Promotes Human T Cells with High FOXP3 Expression and Regulatory Properties. *J. Immunol.* **196**, 3618–3630 (2016).

252. Michalek, R. D. *et al.* Cutting Edge: Distinct Glycolytic and Lipid Oxidative Metabolic Programs Are Essential for Effector and Regulatory CD4 + T Cell Subsets . *J. Immunol.* **186**, 3299–3303 (2011).

253. Zheng, W. & Flavell, R. A. The Transcription Factor GATA-3 Is Necessary and Sufficient for Th2 Cytokine Gene Expression in CD4 T Cells. *Cell* **89**, 587–596 (1997).

254. Zhu, J., Guo, L., Watson, C. J., Hu-Li, J. & Paul, W. E. Stat6 Is Necessary and Sufficient for IL-4's Role in Th2 Differentiation and Cell Expansion. *J. Immunol.* **166**, 7276–7281 (2001).

255. Delgoffe, G. M. *et al.* The kinase mTOR regulates the differentiation of helper T cells through the selective activation of signaling by mTORC1 and mTORC2. *Nat. Immunol.* **12**, 295–304 (2011).

256. Tibbitt, C. A. *et al.* Single-Cell RNA Sequencing of the T Helper Cell Response to House Dust Mites Defines a Distinct Gene Expression Signature in Airway Th2 Cells. *Immunity* **51**, 169-184.e5 (2019).

257. Yasuda, K., Takeuchi, Y. & Hirota, K. The pathogenicity of Th17 cells in autoimmune diseases. *Semin. Immunopathol.* **41**, 283–297 (2019).

258. Ivanov, I. I. *et al.* The Orphan Nuclear Receptor RORγt Directs the Differentiation Program of

Proinflammatory IL-17+ T Helper Cells. *Cell* **126**, 1121–1133 (2006).

259. Berod, L. *et al.* De novo fatty acid synthesis controls the fate between regulatory T and T helper 17 cells. *Nat. Med.* **20**, (2014).

260. Karmaus, P. W. F. *et al.* Metabolic heterogeneity underlies reciprocal fates of TH17 cell stemness and plasticity. *Nature* **565**, 101–105 (2019).

261. Zheng, S. G., Wang, J., Wang, P., Gray, J. D. & Horwitz, D. A. IL-2 Is Essential for TGF-β to Convert Naive CD4 + CD25 − Cells to CD25 + Foxp3 + Regulatory T Cells and for Expansion of These Cells. *J. Immunol.* **178**, 2018–2027 (2007).

262. Bluestone, J. A. & Abbas, A. K. Natural versus adaptive regulatory T cells. *Nat. Rev. Immunol.* **3**, 253–257 (2003).

263. Angelin, A. *et al.* Foxp3 Reprograms T Cell Metabolism to Function in Low-Glucose, High-Lactate Environments. *Cell Metab.* **25**, 1282-1293.e7 (2017).

264. Gualdoni, G. A. *et al.* The AMP analog AICAR modulates the T reg /T h 17 axis through enhancement of fatty acid oxidation. *FASEB J.* **30**, 3800–3809 (2016).

265. Lee, J. *et al.* Regulator of Fatty Acid Metabolism, Acetyl Coenzyme A Carboxylase 1, Controls T Cell Immunity. *J. Immunol.* **192**, 3190–3199 (2014).

266. Pollizzi, K. N. *et al.* Asymmetric inheritance of mTORC1 kinase activity during division dictates CD8+ T cell differentiation. *Nat. Immunol.* **17**, 704–711 (2016).

267. Verbist, K. C. *et al.* Metabolic maintenance of cell asymmetry following division in activated T lymphocytes. *Nature* **532**, 389–393 (2016).

268. Buck, M. D. *et al.* Mitochondrial Dynamics Controls T Cell Fate through Article Mitochondrial Dynamics Controls T Cell Fate through Metabolic Programming. *Cell* **166**, 63–76 (2016).

269. Sukumar, M. *et al.* Inhibiting glycolytic metabolism enhances CD8+ T cell memory and antitumor function. *J. Clin. Invest.* **123**, 4479–4488 (2013).

270. Pearce, E. L. *et al.* Enhancing CD8 T-cell memory by modulating fatty acid metabolism. *Nature* **460**, 103–107 (2009).

271. van der Windt, G. J. W. *et al.* Mitochondrial Respiratory Capacity Is a Critical Regulator of CD8 + T Cell Memory Development. *Immunity* **36**, 68–78 (2012).

272. O'Sullivan, D. *et al.* Memory CD8+ T Cells Use Cell-Intrinsic Lipolysis to Support the Metabolic Programming Necessary for Development. *Immunity* **41**, 75–88 (2014).

273. Cui, G. *et al.* IL-7-induced glycerol transport and TAG synthesis promotes memory CD8+ T cell longevity. *Cell* **161**, 750–761 (2015).

274. Hanahan, D. & Weinberg, R. A. The hallmarks of cancer. *Cell* **100**, 57–70 (2000).

275. Hanahan, D. & Weinberg, R. A. Hallmarks of cancer: The next generation. *Cell* **144**, 646–674 (2011).

276. Warburg, O. On the origin of cancer cells. *Science* **123**, 309–14 (1956).

277. Hu, J. *et al.* Heterogeneity of tumor-induced gene expression changes in the human metabolic network. *Nat. Biotechnol.* **31**, 522–529 (2013).

278. Rosario, S. R. *et al.* Pan-cancer analysis of transcriptional metabolic dysregulation using The Cancer Genome Atlas. *Nat. Commun.* **9**, (2018).

279. Gaude, E. & Frezza, C. Tissue-specific and convergent metabolic transformation of cancer correlates with metastatic potential and patient survival. *Nat. Commun.* **7**, 1–9 (2016).

280. Seth Nanda, C., Venkateswaran, S. V., Patani, N. & Yuneva, M. Defining a metabolic landscape of tumours: genome meets metabolism. *Br. J. Cancer* **122**, 136–149 (2020).

281. Wang, J. *et al.* Glucose transporter GLUT1 expression and clinical outcome in solid tumors: a systematic review and meta-analysis. *Oncotarget* **8**, (2017).

282. Zhu, A., Lee, D. & Shim, H. Metabolic Positron Emission Tomography Imaging in Cancer Detection and Therapy Response. *Semin. Oncol.* **38**, 55–69 (2011).

283. Wang, C. *et al.* Identification of transaldolase as a novel serum biomarker for hepatocellular carcinoma metastasis using xenografted mouse model and clinic samples. *Cancer Lett.* **313**, 154–166 (2011).

284. Xu, X., zur Hausen, A., Coy, J. F. & Löchelt, M. Transketolase-like protein 1 (TKTL1) is required for rapid cell growth and full viability of human tumor cells. *Int. J. Cancer* **124**, 1330–1337 (2009).

285. Jiang, P. *et al.* p53 regulates biosynthesis through direct inactivation of glucose-6-phosphate dehydrogenase. *Nat. Cell Biol.* **13**, 310–316 (2011).

286. Locasale, J. W. *et al.* Phosphoglycerate dehydrogenase diverts glycolytic flux and contributes to oncogenesis. *Nat. Genet.* **43**, 869–874 (2011).

287. Nilsson, R. *et al.* Metabolic enzyme expression highlights a key role for MTHFD2 and the mitochondrial folate pathway in cancer. *Nat. Commun.* **5**, 3128 (2014).

288. Yang, L., Venneti, S. & Nagrath, D. Glutaminolysis: A Hallmark of Cancer Metabolism. *Annu. Rev. Biomed. Eng.* **19**, 163–194 (2017).

289. van Geldermalsen, M. *et al.* ASCT2/SLC1A5 controls glutamine uptake and tumour growth in triple-negative basal-like breast cancer. *Oncogene* **35**, 3201–3208 (2016).

290. Yang, L. *et al.* Metabolic shifts toward glutamine regulate tumor growth, invasion and bioenergetics in ovarian cancer. *Mol. Syst. Biol.* **10**, 728 (2014).

291. Reynolds, M. R. *et al.* Control of glutamine metabolism by the tumor suppressor Rb. *Oncogene* **33**, 556–566 (2014).

292. Seyfried, T. N., Flores, R. E., Poff, A. M. & D'Agostino, D. P. Cancer as a metabolic disease: implications for novel therapeutics. *Carcinogenesis* **35**, 515–527 (2014).

293. Sancho, P., Barneda, D. & Heeschen, C. Hallmarks of cancer stem cell metabolism. *Br. J. Cancer* **114**, 1305–1312 (2016).

294. Lee, K. *et al.* MYC and MCL1 Cooperatively Promote Chemotherapy-Resistant Breast Cancer Stem Cells via Regulation of Mitochondrial Oxidative Phosphorylation. *Cell Metab.* **26**, 633-647.e7 (2017).

295. Kuntz, E. M. *et al.* Targeting mitochondrial oxidative phosphorylation eradicates therapy-resistant chronic myeloid leukemia stem cells. *Nat. Med.* **23**, 1234–1240 (2017).

296. Hayes, J. D., Dinkova-kostova, A. T. & Tew, K. D. Review Oxidative Stress in Cancer. *Cancer Cell* **38**, 167–197 (2020).

297. Kamata, H. *et al.* Reactive Oxygen Species Promote TNFα-Induced Death and Sustained JNK Activation by Inhibiting MAP Kinase Phosphatases. *Cell* **120**, 649–661 (2005).

298. Zhang, Y. *et al.* Redox Biology Redox regulation of tumor suppressor PTEN in cell signaling. *Redox Biol.* **34**, 101553 (2020).

299. Kong, H. *et al.* Metabolic determinants of cellular fitness dependent on mitochondrial reactive oxygen species. *Sci. Adv.* **6**, 1–15 (2020).

300. Woo, D. K. *et al.* Mitochondrial Genome Instability and ROS Enhance Intestinal Tumorigenesis in APCMin/+ Mice. *Am. J. Pathol.* **180**, 24–31 (2012).

301. Bensaad, K. *et al.* TIGAR, a p53-Inducible Regulator of Glycolysis and Apoptosis. *Cell* **126**, 107–120 (2006).

302. Tang, Z. & He, Z. TIGAR promotes growth, survival and metastasis through oxidation resistance and AKT activation in glioblastoma. *Oncol. Lett.* 2509–2517 (2019) doi:10.3892/ol.2019.10574.

303. Liu, Z. *et al.* TIGAR Promotes Tumorigenesis and Protects Tumor Cells From Oxidative and Metabolic Stresses in Gastric Cancer. *Front. Oncol.* **9**, 1–13 (2019).

304. Wang, H. *et al.* The metabolic function of cyclin D3-CDK6 kinase in cancer cell survival. *Nature* **546**, 426–430 (2017).

305. Kalluri, R. & Weinberg, R. A. The basics of epithelial-mesenchymal transition. *J. Clin. Invest.* **119**, 1420–1428 (2009).

306. Rios Garcia, M. *et al.* Acetyl-CoA Carboxylase 1-Dependent Protein Acetylation Controls Breast Cancer Metastasis and Recurrence. *Cell Metab.* **26**, 842-855.e5 (2017).

307. Jiang, F., Ma, S., Xue, Y., Hou, J. & Zhang, Y. LDH-A promotes malignant progression via activation of epithelial-to-mesenchymal transition and conferring stemness in muscle-invasive bladder cancer. *Biochem. Biophys. Res. Commun.* **469**, 985–992 (2016).

308. Sciacovelli, M. & Frezza, C. Europe PMC Funders Group Metabolic reprogramming and epithelial-to-mesenchymal transition in cancer. **284**, 3132–3144 (2018).

309. Jiang, J. *et al.* Redox regulation in tumor cell epithelial – mesenchymal transition : molecular basis and therapeutic strategy. *Nat. Publ. Gr.* **2**, 1–12 (2017).

310. Piskounova, E. *et al.* Oxidative stress inhibits distant metastasis by human melanoma cells. *Nature* **527**, 186–191 (2015).

311. Martínez-Reyes, I. & Chandel, N. S. Cancer metabolism: looking forward. *Nat. Rev. Cancer* **21**, 669–680 (2021).

312. Ngo, B. *et al.* Limited Environmental Serine and Glycine Confer Brain Metastasis Sensitivity to PHGDH Inhibition. *Cancer Discov.* **10**, 1352–1373 (2020).

313. Burrell, R. A., McGranahan, N., Bartek, J. & Swanton, C. The causes and consequences of genetic heterogeneity in cancer evolution. *Nature* **501**, 338–345 (2013).

314. Plas, D. R., Talapatra, S., Edinger, A. L., Rathmell, J. C. & Thompson, C. B. Akt and Bcl-x L Promote Growth Factor-independent Survival through Distinct Effects on Mitochondrial Physiology. *J. Biol. Chem.* **276**, 12041–12048 (2001).

315. Rathmell, J. C. *et al.* Akt-Directed Glucose Metabolism Can Prevent Bax Conformation Change and Promote Growth Factor-Independent Survival. *Mol. Cell. Biol.* **23**, 7315–7328 (2003).

316. Christofk, H. R. *et al.* The M2 splice isoform of pyruvate kinase is important for cancer metabolism and tumour growth. *Nature* **452**, 230–233 (2008).

317. David, C. J., Chen, M., Assanah, M., Canoll, P. & Manley, J. L. HnRNP proteins controlled by c-Myc deregulate pyruvate kinase mRNA splicing in cancer. *Nature* **463**, 364–368 (2010).

318. Liu, Y. & Yang, C. Oncometabolites in cancer: Current understanding and challenges. *Cancer Res.* **81**, 2820–2823 (2021).

319. Dang, L. *et al.* Cancer-associated IDH1 mutations produce 2-hydroxyglutarate. *Nature* **462**, 739–744 (2009).

320. Xu, W. *et al.* Oncometabolite 2-hydroxyglutarate is a competitive inhibitor of α-ketoglutarate-dependent dioxygenases. *Cancer Cell* **19**, 17–30 (2011).

321. Figueroa, M. E. *et al.* Leukemic IDH1 and IDH2 Mutations Result in a Hypermethylation Phenotype, Disrupt TET2 Function, and Impair Hematopoietic Differentiation. *Cancer Cell* **18**, 553–567 (2010).

322. Wang, P. *et al.* Oncometabolite D-2-Hydroxyglutarate Inhibits ALKBH DNA Repair Enzymes and Sensitizes IDH Mutant Cells to Alkylating Agents. *Cell Rep.* **13**, 2353–2361 (2015).

323. Duncan, C. G. *et al.* A heterozygous IDH1R132H/WT mutation induces genome-wide alterations in DNA methylation. *Genome Res.* **22**, 2339–2355 (2012).

324. San-Millán, I., Julian, C. G., Matarazzo, C., Martinez, J. & Brooks, G. A. Is Lactate an Oncometabolite? Evidence Supporting a Role for Lactate in the Regulation of Transcriptional Activity of Cancer-Related Genes in MCF7 Breast Cancer Cells. *Front. Oncol.* **9**, 1–10 (2020).

325. Losman, J. & Kaelin, W. G. What a difference a hydroxyl makes: mutant IDH, (R)-2-hydroxyglutarate, and cancer. *Genes Dev.* **27**, 836–852 (2013).

326. Tateishi, K. *et al.* Extreme Vulnerability of IDH1 Mutant Cancers to NAD+ Depletion. *Cancer Cell* **28**, 773–784 (2015).

327. Satoh, K. *et al.* Global metabolic reprogramming of colorectal cancer occurs at adenoma stage and is induced by MYC. *Proc. Natl. Acad. Sci. U. S. A.* **114**, E7697–E7706 (2017).

328. Priolo, C. *et al.* AKT1 and MYC induce distinctive metabolic fingerprints in human prostate cancer. *Cancer Res.* **74**, 7198–7204 (2014).

329. Morotti, M. *et al.* Hypoxia-induced switch in SNAT2/SLC38A2 regulation generates endocrine resistance in breast cancer. *Proc. Natl. Acad. Sci. U. S. A.* **116**, 12452–12461 (2019).

330. Wang, Y. *et al.* Coordinative metabolism of glutamine carbon and nitrogen in proliferating cancer cells under hypoxia. *Nat. Commun.* **10**, 201 (2019).

331. Pavlova, N. N. & Thompson, C. B. The Emerging Hallmarks of Cancer Metabolism. *Cell Metab.* **23**, 27–47 (2016).

332. Eichner, L. J. *et al.* Genetic Analysis Reveals AMPK Is Required to Support Tumor Growth in Murine Kras-Dependent Lung Cancer Models. *Cell Metab.* **29**, 285-302.e7 (2019).

333. Guo, J. Y. *et al.* Autophagy suppresses progression of K-ras-induced lung tumors to oncocytomas and maintains lipid homeostasis. *Genes Dev.* **27**, 1447–1461 (2013).

334. Yang, A. *et al.* Autophagy sustains pancreatic cancer growth through both cell-autonomous and nonautonomous mechanisms. *Cancer Discov.* **8**, 276–287 (2018).

335. Jayashankar, V. & Edinger, A. L. Macropinocytosis confers resistance to therapies targeting cancer anabolism. *Nat. Commun.* **11**, 1–15 (2020).

336. Commisso, C. *et al.* Macropinocytosis of protein is an amino acid supply route in Ras-transformed cells. *Nature* **497**, 633–637 (2013).

337. Yang, L. *et al.* Targeting Stromal Glutamine Synthetase in Tumors Disrupts Tumor Microenvironment-Regulated Cancer Cell Growth. *Cell Metab.* **24**, 685–700 (2016).

338. Whitaker-Menezes, D. *et al.* Evidence for a stromal-epithelial 'lactate shuttle' in human tumors: MCT4 is a marker of oxidative stress in cancer-associated fibroblasts. *Cell Cycle* **10**, 1772–1783 (2011).

339. Zhang, W. *et al.* Stromal control of cystine metabolism promotes cancer cell survival in chronic lymphocytic leukaemia. *Nat. Publ. Gr.* **14**, 276–286 (2012).

340. Ottensmeier, C. H. *et al.* Upregulated Glucose Metabolism Correlates Inversely with CD8 + T-cell Infiltration and Survival in Squamous Cell Carcinoma. *Cancer Res.* **76**, 4136–4148 (2016).

341. Chang, C.-H. *et al.* Metabolic Competition in the Tumor Microenvironment Is a Driver of Cancer Progression. *Cell* **162**, 1229–1241 (2015).

342. Ho, P. *et al.* Phosphoenolpyruvate Is a Metabolic Checkpoint of Anti-tumor T Cell Responses. *Cell* **162**, 1217–1228 (2015).

343. Ecker, C. *et al.* Differential Reliance on Lipid Metabolism as a Salvage Pathway Underlies Functional Differences of T Cell Subsets in Poor Nutrient Environments. *Cell Rep.* **23**, 741–755 (2018).

344. Brand, A. *et al.* LDHA-Associated Lactic Acid Production Blunts Tumor Immunosurveillance by T and NK Cells. *Cell Metab.* **24**, 657–671 (2016).

345. Quinn, W. J. *et al.* Lactate Limits T Cell Proliferation via the NAD(H) Redox State. *Cell Rep.* **33**, 108500 (2020).

346. Mendler, A. N. *et al.* Tumor lactic acidosis suppresses CTL function by inhibition of p38 and JNK/c-Jun activation. *Int. J. Cancer* **131**, 633–640 (2012).

347. Colegio, O. R. *et al.* Functional polarization of tumour-associated macrophages by tumour-derived lactic acid. *Nature* **513**, 559–563 (2014).

348. Godin-Ethier, J., Hanafi, L.-A., Piccirillo, C. A. & Lapointe, R. Indoleamine 2,3-Dioxygenase Expression in Human Cancers: Clinical and Immunologic Perspectives. *Clin. Cancer Res.* **17**, 6985–6991 (2011).

349. Munn, D. H. & Mellor, A. L. Indoleamine 2,3-dioxygenase and tumor-induced tolerance. *J. Clin. Invest.* **117**, 1147–1154 (2007).

350. Zhang, Z. *et al.* T Cell Dysfunction and Exhaustion in Cancer. *Front. Cell Dev. Biol.* **8**, (2020).

351. Patsoukis, N. *et al.* PD-1 alters T-cell metabolic reprogramming by inhibiting glycolysis and promoting lipolysis and fatty acid oxidation. *Nat. Commun.* **6**, 1–13 (2015).

352. Siska, P. J. *et al.* Suppression of Glut1 and Glucose Metabolism by Decreased Akt/mTORC1 Signaling Drives T Cell Impairment in B Cell Leukemia. *J. Immunol.* **197**, 2532–2540 (2016).

353. Dugnani, E. *et al.* Integrating T cell metabolism in cancer immunotherapy. *Cancer Lett.* **411**, 12–18 (2017).

354. Pellegrino, M. *et al.* Manipulating the Metabolism to Improve the Efficacy of CAR T-Cell Immunotherapy. *Cells* **10**, 14 (2020).

355. Nabe, S. *et al.* Reinforce the antitumor activity of CD8+ T cells via glutamine restriction. *Cancer Sci.* **109**, 3737–3750 (2018).

356. Leone, R. D. *et al.* Glutamine blockade induces divergent metabolic programs to overcome tumor immune evasion. *Science (80-.).* **366**, 1013–1021 (2019).

357. Sukumar, M. *et al.* Mitochondrial Membrane Potential Identifies Cells with Enhanced Stemness for Cellular Therapy. *Cell Metab.* **23**, 63–76 (2016).

358. Menk, A. V. *et al.* 4-1BB costimulation induces T cell mitochondrial function and biogenesis enabling cancer immunotherapeutic responses. *J. Exp. Med.* **215**, 1091–1100 (2018).

359. Long, A. H. *et al.* 4-1BB costimulation ameliorates T cell exhaustion induced by tonic signaling of chimeric antigen receptors. *Nat. Med.* **21**, 581–590 (2015).

360. Tsurutani, N. *et al.* Costimulation Endows Immunotherapeutic CD8 T Cells with IL-36 Responsiveness during Aerobic Glycolysis. *J. Immunol.* **196**, 124–134 (2016).

361. Ligtenberg, M. A. *et al.* Coexpressed Catalase Protects Chimeric Antigen Receptor–Redirected T Cells as well as Bystander Cells from Oxidative Stress–Induced Loss of Antitumor Activity. *J. Immunol.* **196**, 759–766 (2016).

362. Calcinotto, A. *et al.* Modulation of microenvironment acidity reverses anergy in human and murine tumor-infiltrating T lymphocytes. *Cancer Res.* **72**, 2746–2756 (2012).

363. Ninomiya, S. *et al.* Tumor indoleamine 2,3-dioxygenase (IDO) inhibits CD19-CAR T cells and is downregulated by lymphodepleting drugs. *Blood* **125**, 3905–3916 (2015).

364. Hasawi, N. Al, Alkandari, M. F. & Luqmani, Y. A. Phosphofructokinase: A mediator of glycolytic flux in cancer progression. *Crit. Rev. Oncol. Hematol.* **92**, 312–321 (2014).

365. Dunaway, G. A., Kasten, T. P., Sebo, T. & Trapp, R. Analysis of the phosphofructokinase subunits and isoenzymes in human tissues. *Biochem. J.* **251**, 677–683 (1988).

366. Mulukutla, B. C., Yongky, A., Daoutidis, P. & Hu, W. Bistability in Glycolysis Pathway as a Physiological Switch in Energy Metabolism. *PLoS One* **9**, e98756 (2014).

367. Kim, N. H. *et al.* Snail reprograms glucose metabolism by repressing phosphofructokinase PFKP allowing cancer cell survival under metabolic stress. *Nat. Commun.* **8**, 1–12 (2017).

368. Moon, J. S. *et al.* Krüppel-like Factor 4 (KLF4) activates the transcription of the gene for the platelet isoform of phosphofructokinase (PFKP) in breast cancer. *J. Biol. Chem.* **286**, 23808–23816 (2011).

369. Wang, G. *et al.* Differential phosphofructokinase-1 isoenzyme patterns associated with glycolytic efficiency in human breast cancer and paracancer tissues. *Oncol. Lett.* **6**, 1701–1706 (2013).

370. Marinho-Carvalho, M. M., Zancan, P. & Sola-Penna, M. Modulation of 6-phosphofructo-1-kinase oligomeric equilibrium by calmodulin: Formation of active dimmers. *Mol. Genet. Metab.* **87**, 253–261 (2006).

371. Webb, B. A. *et al.* Structures of human phosphofructokinase-1 and atomic basis of cancer-associated mutations. *Nature* **523**, 111–114 (2015).

372. Costa Leite, T., Da Silva, D., Guimarães Coelho, R., Zancan, P. & Sola-Penna, M. Lactate favours the dissociation of skeletal muscle 6-phosphofructo-1-kinase tetramers down-regulating the enzyme and muscle glycolysis. *Biochem. J.* **408**, 123–130 (2007).

373. Zancan, P., Almeida, F. V. R., Faber-Barata, J., Dellias, J. M. & Sola-Penna, M. Fructose-2,6-bisphosphate counteracts guanidinium chloride-, thermal-, and ATP-induced dissociation of skeletal muscle key glycolytic enzyme 6-phosphofructo-1-kinase: A structural mechanism for PFK allosteric regulation. *Arch. Biochem. Biophys.* **467**, 275–282 (2007).

374. Zancan, P., Marinho-Carvalho, M. M., Faber-Barata, J., Dellias, J. M. M. & Sola-Penna, M. ATP and fructose-2,6-bisphosphate regulate skeletal muscle 6-phosphofructo-1-kinase by altering its quaternary structure. *IUBMB Life* **60**, 526–533 (2008).

375. Hers, H. G. & Van Schaftingen, E. Fructose 2,6-bisphosphate 2 years after its discovery. *Biochem. J.* **206**, 1–12 (1982).

376. Wu, C., Khan, S. A., Peng, L. & Lange, A. J. Roles for fructose-2,6-bisphosphate in the control of fuel metabolism: Beyond its allosteric effects on glycolytic and gluconeogenic enzymes. *Adv. Enzyme Regul.* **46**, 72–88 (2006).

377. Coelho, W. S., Costa, K. C. & Sola-Penna, M. Serotonin stimulates mouse skeletal muscle 6-phosphofructo-1-kinase through tyrosine-phosphorylation of the enzyme altering its intracellular localization. *Mol. Genet. Metab.* **92**, 364–370 (2007).

378. Gomes Alves, G. & Sola-Penna, M. Epinephrine modulates cellular distribution of muscle phosphofructokinase. *Mol. Genet. Metab.* **78**, 302–306 (2003).

379. Silva, A. P. P., Alves, G. G., Araújo, A. H. B. & Sola-Penna, M. Effects of insulin and actin on phosphofructokinase activity and cellular distribution in skeletal muscle. *An. Acad. Bras. Cienc.* **76**, 541–548 (2004).

380. Marinho-Carvalho, M. M., Costa-Mattos, P. V., Spitz, G. A., Zancan, P. & Sola-Penna, M. Calmodulin upregulates skeletal muscle 6-phosphofructo-1-kinase reversing the inhibitory effects of allosteric modulators. *Biochim. Biophys. Acta - Proteins Proteomics* **1794**, 1175–1180 (2009).

381. Tarui, S. *et al.* Phosphofructokinase deficiency in skeletal muscle. A new type of glycogenosis. *Biochem. Biophys. Res. Commun.* **19**, 517–523 (1965).

382. Shen, J. *et al.* PFKP is highly expressed in lung cancer and regulates glucose metabolism. *Cell. Oncol.* **43**, 617–629 (2020).

383. Wang, F., Li, L. & Zhang, Z. Platelet isoform of phosphofructokinase promotes aerobic glycolysis and the progression of non-small cell lung cancer. *Mol. Med. Rep.* **23**, 74 (2020).

384. Peng, M. *et al.* Intracellular citrate accumulation by oxidized ATM-mediated metabolism reprogramming via PFKP and CS enhances hypoxic breast cancer cell invasion and metastasis. *Cell Death Dis.* **10**, 228 (2019).

385. Prasad, C. P., Södergren, K. & Andersson, T. Reduced production and uptake of lactate are essential for the ability of WNT5A signaling to inhibit breast cancer cell migration and invasion. *Oncotarget* **8**, 71471–71488 (2017).

386. Umar, S. M. *et al.* Prognostic and therapeutic relevance of phosphofructokinase platelet-type (PFKP) in breast cancer. *Exp. Cell Res.* **396**, 112282 (2020).

387. Wang, Z. *et al.* Comprehensive identification of a two-genesignature as a novel potential prognostic model for patients with medulloblastoma. *Am. J. Transl. Res.* **12**, 1600–1613 (2020).

388. Lee, J. H. *et al.* Stabilization of phosphofructokinase 1 platelet isoform by AKT promotes tumorigenesis. *Nat. Commun.* **8**, 1–14 (2017).

389. Wang, J. *et al.* The platelet isoform of phosphofructokinase contributes to metabolic reprogramming and maintains cell proliferation in clear cell renal cell carcinoma. *Oncotarget* **7**, 27142–27157 (2016).

390. Chen, G., Liu, H., Zhang, Y., Liang, J. & Zhu, Y. Silencing PFKP inhibits starvation-induced autophagy , glycolysis , and epithelial mesenchymal transition in oral squamous cell carcinoma. *Exp. Cell Res.* **370**, 46–57 (2018).

391. Liu, B. *et al.* Prognostic Roles of Phosphofructokinase Platelet in Clear Cell Renal Cell Carcinoma and Correlation with Immune Infiltration. *Int. J. Gen. Med.* **Volume 14**, 3645–3658 (2021).

392. Xu, C. *et al.* Cistrome analysis of YY1 uncovers a regulatory axis of YY1:BRD2/4-PFKP during tumorigenesis of advanced prostate cancer. *Nucleic Acids Res.* **49**, 4971–4988 (2021).

393. Yeerken, D. *et al.* PFKP is transcriptionally repressed by BRCA1/ZBRK1 and predicts prognosis in breast cancer. *PLoS One* **15**, e0233750 (2020).

394. Chiaradonna, F., Ricciardiello, F. & Palorini, R. The Nutrient-Sensing Hexosamine Biosynthetic Pathway as the Hub of Cancer Metabolic Rewiring. *Cells* **7**, 53 (2018).

395. Yi, W. *et al.* Phosphofructokinase 1 Glycosylation Regulates Cell Growth and Metabolism. *Science (80-.).* **337**, 975–980 (2012).

396. Gao, X. *et al.* Nuclear PFKP promotes CXCR4-dependent infiltration by T cell acute lymphoblastic leukemia. *J. Clin. Invest.* **131**, (2021).

397. Broxmeyer, H. E. All in for nuclear PFKP–induced CXCR4 metastasis: a T cell acute lymphoblastic leukemia prognostic marker. *J. Clin. Invest.* **131**, (2021).

398. Lee, J. *et al.* EGFR-Phosphorylated Platelet Isoform of Phosphofructokinase 1 Promotes PI3K Activation. *Mol. Cell* **70**, 197-210.e7 (2018).

399. Fan, Y. *et al.* Anti-Warburg effect by targeting HRD1-PFKP pathway may inhibit breast cancer progression. *Cell Commun. Signal.* **19**, 18 (2021).

400. Spitz, G. A., Furtado, C. M., Sola-Penna, M. & Zancan, P. Acetylsalicylic acid and salicylic acid decrease tumor cell viability and glucose metabolism modulating 6-phosphofructo-1-kinase structure and activity. *Biochem. Pharmacol.* **77**, 46–53 (2009).

401. Penso, J. & Beitner, R. Detachment of glycolytic enzymes from cytoskeleton of Lewis lung carcinoma and colon adenocarcinoma cells induced by clotrimazole and its correlation to cell viability and morphology. *Mol. Genet. Metab.* **76**, 181–188 (2002).

402. Xiao, Y. *et al.* Inhibition of PFKFB3 induces cell death and synergistically enhances chemosensitivity in endometrial cancer. *Oncogene* **40**, 1409–1424 (2021).

403. Zhang, W. *et al.* Skp2 is over-expressed in breast cancer and promotes breast cancer cell proliferation. *Cell Cycle* **15**, 1344–1351 (2016).

404. Gstaiger, M. *et al.* Skp2 is oncogenic and overexpressed in human cancers. *Proc. Natl. Acad. Sci. U. S. A.* **98**, 5043–5048 (2001).

405. Frescas, D. & Pagano, M. Deregulated proteolysis by the F-box proteins SKP2 and β-TrCP: tipping the scales of cancer. *Nat. Rev. Cancer* **8**, 438–449 (2008).

406. Randle, S. J. & Laman, H. F-box protein interactions with the hallmark pathways in cancer. *Semin. Cancer Biol.* **36**, 3–17 (2016).

407. Kim, S. Y., Herbst, A., Tworkowski, K. A., Salghetti, S. E. & Tansey, W. P. Skp2 Regulates Myc Protein Stability and Activity. *Mol. Cell* **11**, 1177–1188 (2003).

408. Han, F. *et al.* The critical role of AMPK in driving Akt activation under stress, tumorigenesis and drug resistance. *Nat. Commun.* **9**, 4728 (2018).

409. Chan, C.-H. *et al.* The Skp2-SCF E3 Ligase Regulates Akt Ubiquitination, Glycolysis, Herceptin Sensitivity, and Tumorigenesis. *Cell* **149**, 1098–1111 (2012).

410. Robey, R. B. & Hay, N. Is Akt the 'Warburg kinase'?-Akt-energy metabolism interactions and oncogenesis. *Semin. Cancer Biol.* **19**, 25–31 (2009).

411. Yu, X. *et al.* Skp2-mediated ubiquitination and mitochondrial localization of Akt drive tumor growth and chemoresistance to cisplatin. *Oncogene* **38**, 7457–7472 (2019).

412. Elstrom, R. L. *et al.* Akt Stimulates Aerobic Glycolysis in Cancer Cells. *Cancer Res.* **64**, 3892–3899 (2004).

413. Akhoondi, S. *et al.* FBXW7/hCDC4 Is a General Tumor Suppressor in Human Cancer. *Cancer Res.* **67**, 9006–9012 (2007).

414. Sundqvist, A. *et al.* Control of lipid metabolism by phosphorylation-dependent degradation of the SREBP family of transcription factors by SCFFbw7. *Cell Metab.* **1**, 379–391 (2005).

415. Olson, B. L. *et al.* SCFCdc4 acts antagonistically to the PGC-1α transcriptional coactivator by targeting it for ubiquitin-mediated proteolysis. *Genes Dev.* **22**, 252–264 (2008).

416. Fu, L. *et al.* Perifosine Inhibits Mammalian Target of Rapamycin Signaling through Facilitating Degradation of Major Components in the mTOR Axis and Induces Autophagy. *Cancer Res.* **69**, 8967–8976 (2009).

417. Ji, S. *et al.* FBW7 (F-box and WD Repeat Domain-Containing 7) Negatively Regulates Glucose Metabolism by Targeting the c-Myc/TXNIP (Thioredoxin-Binding Protein) Axis in Pancreatic Cancer. *Clin. Cancer Res.* **22**, 3950–3960 (2016).

418. Zhan, P. *et al.* FBXW7 negatively regulates ENO1 expression and function in colorectal cancer. *Lab. Investig.* **95**, 995–1004 (2015).

419. Shimizu, K., Nihira, N. T., Inuzuka, H. & Wei, W. Physiological functions of FBW7 in cancer and metabolism. *Cell. Signal.* **46**, 15–22 (2018).

420. Qin, Y. *et al.* PRMT5 enhances tumorigenicity and glycolysis in pancreatic cancer via the FBW7/cMyc axis. *Cell Commun. Signal.* **17**, 30 (2019).

421. Guo, X. *et al.* miR-181d and c-myc-mediated inhibition of CRY2 and FBXL3 reprograms metabolism in colorectal cancer. *Cell Death Dis.* **8**, e2958–e2958 (2017).

422. Li, M. & Zhang, P. The function of APC/CCdh1 in cell cycle and beyond. *Cell Div.* **4**, 2 (2009).

423. Almeida, A., Bolanos, J. P. & Moncada, S. E3 ubiquitin ligase APC/C-Cdh1 accounts for the Warburg effect by linking glycolysis to cell proliferation. *Proc. Natl. Acad. Sci.* **107**, 738–741 (2010).

424. Colombo, S. L. *et al.* Molecular basis for the differential use of glucose and glutamine in cell proliferation as revealed by synchronized HeLa cells. *Proc. Natl. Acad. Sci.* **108**, 21069–21074 (2011).

425. Wu, Q. *et al.* APC/C-CDH1–Regulated IDH3β Coordinates with the Cell Cycle to Promote Cell Proliferation. *Cancer Res.* **79**, 3281–3293 (2019).

426. Estévez-García, I. O. *et al.* Glucose and glutamine metabolism control by APC and SCF during the G1-to-S phase transition of the cell cycle. *J. Physiol. Biochem.* **70**, 569–581 (2014).

427. Duan, S. & Pagano, M. Linking metabolism and cell cycle progression via the APC/CCdh1 and SCF TrCP ubiquitin ligases. *Proc. Natl. Acad. Sci.* **108**, 20857–20858 (2011).

428. Tudzarova, S. *et al.* Two ubiquitin ligases, APC/C-Cdh1 and SKP1-CUL1-F (SCF)- -TrCP, sequentially regulate glycolysis during the cell cycle. *Proc. Natl. Acad. Sci.* **108**, 5278–5283 (2011).

429. Bassermann, F. *et al.* The Cdc14B-Cdh1-Plk1 Axis Controls the G2 DNA-Damage-Response Checkpoint. *Cell* **134**, 256–267 (2008).

430. Wang, Q. *et al.* Alterations of anaphase-promoting complex genes in human colon cancer cells. *Oncogene* **22**, 1486–1490 (2003).

431. Rada, P. *et al.* SCF/B-TrCP Promotes Glycogen Synthase Kinase 3-Dependent Degradation of the Nrf2 Transcription Factor in a Keap1-Independent Manner. *Mol. Cell. Biol.* **31**, 1121–1133 (2011).

432. Tsuchiya, Y. *et al.* Dual Regulation of the Transcriptional Activity of Nrf1 by B-TrCP- and Hrd1-Dependent Degradation Mechanisms. *Mol. Cell. Biol.* **31**, 4500–4512 (2011).

433. Biswas, M., Phan, D., Watanabe, M. & Chan, J. Y. The Fbw7 Tumor Suppressor Regulates Nuclear Factor E2-related Factor 1 Transcription Factor Turnover through Proteasome-mediated Proteolysis. *J. Biol. Chem.* **286**, 39282–39289 (2011).

434. Tan, M.-K. M., Lim, H.-J., Bennett, E. J., Shi, Y. & Harper, J. W. Parallel SCF Adaptor Capture Proteomics Reveals a Role for SCFFBXL17 in NRF2 Activation via BACH1 Repressor Turnover. *Mol. Cell* **52**, 9–24 (2013).

435. Janzer, A. *et al.* The H3K4me3 Histone Demethylase Fbxl10 Is a Regulator of Chemokine Expression, Cellular Morphology, and the Metabolome of Fibroblasts. *J. Biol. Chem.* **287**, 30984–30992 (2012).

436. Polytarchou, C., Pfau, R., Hatziapostolou, M. & Tsichlis, P. N. The JmjC Domain Histone Demethylase Ndy1 Regulates Redox Homeostasis and Protects Cells from Oxidative Stress. *Mol. Cell. Biol.* **28**, 7451–7464 (2008).

437. Yu, X., Wang, J., Wu, J. & Shi, Y. A systematic study of the cellular metabolic regulation of Jhdm1b in tumor cells. *Mol. Biosyst.* **11**, 1867–1875 (2015).

438. Hong, X. *et al.* MiR-448 promotes glycolytic metabolism of gastric cancer by downregulating KDM2B. *Oncotarget* **7**, 22092–22102 (2016).

439. Tzatsos, A. *et al.* KDM2B promotes pancreatic cancer via Polycomb-dependent and -independent transcriptional programs. *J. Clin. Invest.* **123**, 727–739 (2013).

440. Ueda, T. *et al.* Fbxl10 overexpression in murine hematopoietic stem cells induces leukemia involving metabolic activation and upregulation of Nsg2. *Blood* **125**, 3437–3446 (2015).

441. Chen, B. B. *et al.* E3 Ligase Subunit Fbxo15 and PINK1 Kinase Regulate Cardiolipin Synthase 1 Stability and Mitochondrial Function in Pneumonia. *Cell Rep.* **7**, 476–487 (2014).

442. Liu, Y. *et al.* The Proapoptotic F-box Protein Fbxl7 Regulates Mitochondrial Function by Mediating the Ubiquitylation and Proteasomal Degradation of Survivin. *J. Biol. Chem.* **290**, 11843–11852 (2015).

443. Rodel, F. *et al.* Survivin as a Prognostic/Predictive Marker and Molecular Target in Cancer Therapy. *Curr. Med. Chem.* **19**, 3679–3688 (2012).

444. Jonkers, W. & Rep, M. Lessons from Fungal F-Box Proteins. *Eukaryot. Cell* **8**, 677–695 (2009).

445. Benanti, J. A., Cheung, S. K., Brady, M. C. & Toczyski, D. P. A proteomic screen reveals SCFGrr1 targets that regulate the glycolytic–gluconeogenic switch. *Nat. Cell Biol.* **9**, 1184–1191 (2007).

446. Liu, Y. & Mallampalli, R. K. Small molecule therapeutics targeting F-box proteins in cancer. *Semin. Cancer Biol.* **36**, 105–119 (2016).

447. Zhou, L. *et al.* Cdh1-mediated Skp2 degradation by dioscin reprogrammes aerobic glycolysis and inhibits colorectal cancer cells growth. *EBioMedicine* **51**, 102570 (2020).

448. Rana, S. *et al.* Selective degradation of CDK6 by a palbociclib based PROTAC. *Bioorg. Med. Chem. Lett.* **29**, 1375–1379 (2019).

449. Su, S. *et al.* Potent and Preferential Degradation of CDK6 via Proteolysis Targeting Chimera Degraders. *J. Med. Chem.* **62**, 7575–7582 (2019).

450. Brees, C. & Fransen, M. A cost-effective approach to microporate mammalian cells with the Neon Transfection System. *Anal. Biochem.* **466**, 49–50 (2014).

451. Su, X., Lu, W. & Rabinowitz, J. D. Metabolite Spectral Accuracy on Orbitraps. *Anal. Chem.* **89**, 5940–5948 (2017).

452. Gaude, E. *et al.* muma, An R Package for Metabolomics Univariate and Multivariate Statistical Analysis. *Curr. Metabolomics* **1**, 180–189 (2013).

453. Hadley, W. *ggplot2: Elegant graphics for data analysis*. (Springer-Verlag, 2016).

454. Horikoshi, M. & Tang, Y. ggfortify: Data Visualization Tools for Statistical Analysis Results. (2018).

455. Tang, Y., Horikoshi, M. & Li, W. ggfortify: Unified Interface to Visualize Statistical Results of Popular R Packages. *R J.* **8**, 474 (2016).

456. Blighe, K., Rana, S. & Lewis, M. EnhancedVolcano: Publication-ready volcano plots with enhanced colouring and labeling. (2021).

457. Soamalala, J. *et al.* Fluorescent Peptide Biosensor for Probing CDK6 Kinase Activity in Lung Cancer Cell Extracts. *ChemBioChem* **22**, 1065–1071 (2021).

458. Pfaffl, M. W. A new mathematical model for relative quantification in real-time RT-PCR. *Nucleic Acids Res.* **29**, 45e – 45 (2001).

459. Tsherniak, A. *et al.* Defining a Cancer Dependency Map. *Cell* **170**, 564-576.e16 (2017).

460. Vingill, S. *et al.* Loss of FBXO 7 (PARK 15) results in reduced proteasome activity and models a parkinsonism-like phenotype in mice. **35**, 2008–2025 (2016).

461. Kutmon, M. *et al.* PathVisio 3: An Extendable Pathway Analysis Toolbox. *PLoS Comput. Biol.* **11**, 1–13 (2015).

462. Feng, Y. *et al.* A20 targets PFKL and glycolysis to inhibit the progression of hepatocellular carcinoma. *Cell Death Dis.* **11**, 89 (2020).

463. Panieri, E. & Santoro, M. M. ROS homeostasis and metabolism: a dangerous liason in cancer cells. *Cell Death Dis.* **7**, e2253–e2253 (2016).

464. Franco, R., Schoneveld, O. J., Pappa, A. & Panayiotidis, M. I. The central role of glutathione in the pathophysiology of human diseases. *Arch. Physiol. Biochem.* **113**, 234–258 (2007).

465. Delgado-Camprubi, M., Esteras, N., Soutar, M. P., Plun-Favreau, H. & Abramov, A. Y. Deficiency of Parkinson's disease-related gene Fbxo7 is associated with impaired mitochondrial metabolism by PARP activation. *Cell Death Differ.* **24**, 120–131 (2017).

466. Zhou, Z. D. *et al.* F-box protein 7 mutations promote protein aggregation in mitochondria and inhibit mitophagy. **24**, 6314–6330 (2015).

467. Tian, R. *et al.* Genome-wide CRISPRi/a screens in human neurons link lysosomal failure to ferroptosis. *Nat. Neurosci.* **24**, 1020–1034 (2021).

468. Quéméneur, L. *et al.* Differential Control of Cell Cycle, Proliferation, and Survival of Primary T Lymphocytes by Purine and Pyrimidine Nucleotides. *J. Immunol.* **170**, 4986–4995 (2003).

469. Cantor, J. R. *et al.* Physiologic Medium Rewires Cellular Metabolism and Reveals Uric Acid as an Endogenous Inhibitor of UMP Synthase. *Cell* **169**, 258-272.e17 (2017).

470. Mezrich, J. D. *et al.* An Interaction between Kynurenine and the Aryl Hydrocarbon Receptor Can Generate Regulatory T Cells. *J. Immunol.* **185**, 3190–3198 (2010).

471. Gandhi, R. *et al.* Activation of the aryl hydrocarbon receptor induces human type 1 regulatory T cell–like and Foxp3+ regulatory T cells. *Nat. Immunol.* **11**, 846–853 (2010).

472. Sorgdrager, F. J. H., Naudé, P. J. W., Kema, I. P., Nollen, E. A. & Deyn, P. P. De. Tryptophan Metabolism in Inflammaging: From Biomarker to Therapeutic Target. *Front. Immunol.* **10**, 1–8 (2019).

473. Weaver, D., Gupta, M., Meek, A., Wang, Y. & Wu, F. Alzheimer's Disease as a Disorder of Tryptophan Metabolism (2745). *Neurology* **94**, 2745 (2020).

474. Hardie, D. G., Carling, D. & Carlson, M. THE AMP-ACTIVATED/SNF1 PROTEIN KINASE SUBFAMILY: Metabolic Sensors of the Eukaryotic Cell? *Annu. Rev. Biochem.* **67**, 821–855 (1998).

475. Garcia, D. & Shaw, R. J. AMPK: Mechanisms of Cellular Energy Sensing and Restoration of Metabolic Balance. *Mol. Cell* **66**, 789–800 (2017).

476. Kroemer, G., Mariño, G. & Levine, B. Autophagy and the Integrated Stress Response. *Mol. Cell* **40**, 280–293 (2010).

477. Blagih, J. *et al.* The Energy Sensor AMPK Regulates T Cell Metabolic Adaptation and Effector Responses In Vivo. *Immunity* **42**, 41–54 (2015).

478. Jeon, S., Chandel, N. S. & Hay, N. AMPK regulates NADPH homeostasis to promote tumour cell survival during energy stress. *Nature* **485**, 661–665 (2012).

479. Ren, Y. & Shen, H. Critical role of AMPK in redox regulation under glucose starvation. *Redox Biol.* **25**, 101154 (2019).

480. Martindale, J. L. & Holbrook, N. J. Cellular response to oxidative stress: Signaling for suicide and survival. *J. Cell. Physiol.* **192**, 1–15 (2002).

481. Institute for Quality and Efficiency in Health Care (IQWiG). Hyperglycemia and hypoglycemia in type 1 diabetes. https://www.ncbi.nlm.nih.gov/books/NBK279340/ (2006).

482. Kitabchi, A. E. *et al.* Management of Hyperglycemic Crises in Patients With Diabetes. *Diabetes Care* **24**, 131–153 (2001).

483. Ben-Ami, H., Nagachandran, P., Mendelson, A. & Edoute, Y. Drug-Induced Hypoglycemic Coma in 102 Diabetic Patients. *Arch. Intern. Med.* **159**, 281 (1999).

484. Gopalakrishnan, M., Manappallil, R. G., Ramdas, D. & Jayaraj, J. The survival story of a diabetic ketoacidosis patient with blood sugar levels of 1985 mg/dL. *Asian J. Med. Sci.* **8**, 60–61 (2017).

485. Nicoli, F. Angry, Hungry T-Cells: How Are T-Cell Responses Induced in Low Nutrient Conditions? *Immunometabolism* 10–14 (2020) doi:10.20900/immunometab20200004.

486. Towle, H. C. Glucose as a regulator of eukaryotic gene transcription. *Trends Endocrinol. Metab.* **16**, 489–494 (2005).

487. Sandri, M. *et al.* Foxo Transcription Factors Induce the Atrophy-Related Ubiquitin Ligase Atrogin-1 and Cause Skeletal Muscle Atrophy. *Cell* **117**, 399–412 (2004).

488. Li, F. N. & Johnston, M. Grr1 of Saccharomyces cerevisiae is connected to the ubiquitin proteolysis machinery through Skp1: Coupling glucose sensing to gene expression and the cell cycle. *EMBO J.* **16**, 5629–5638 (1997).

489. Leone, R. D. & Powell, J. D. Metabolism of immune cells in cancer. *Nat. Rev. Cancer* **20**, 516–531 (2020).

490. Hirayama, A. *et al.* Quantitative Metabolome Profiling of Colon and Stomach Cancer Microenvironment by Capillary Electrophoresis Time-of-Flight Mass Spectrometry. *Cancer Res.* **69**, 4918–4925 (2009).

491. Zhang, Y. *et al.* Enhancing CD8+ T Cell Fatty Acid Catabolism within a Metabolically Challenging Tumor Microenvironment Increases the Efficacy of Melanoma Immunotherapy. *Cancer Cell* **32**, 377-391.e9 (2017).

492. Ross, S. H. & Cantrell, D. A. Signaling and Function of Interleukin-2 in T Lymphocytes. *Annu. Rev. Immunol.* **36**, 411–433 (2018).

493. Cham, C. M., Driessens, G., O'Keefe, J. P. & Gajewski, T. F. Glucose deprivation inhibits multiple key gene expression events and effector functions in CD8+ T cells. *Eur. J. Immunol.* **38**, 2438–2450 (2008).

494. Merkley, S. D., Chock, C. J., Yang, X. O., Harris, J. & Castillo, E. F. Modulating T Cell Responses via Autophagy: The Intrinsic Influence Controlling the Function of Both Antigen-Presenting Cells and T Cells. *Front. Immunol.* **9**, 2914 (2018).

495. Röder, P. V., Wu, B., Liu, Y. & Han, W. Pancreatic regulation of glucose homeostasis. *Exp. Mol. Med.* **48**, e219 (2016).

496. International Mouse Phenotyping Consortium. www.mousephenotype.org.

497. Dickinson, M. E. *et al.* High-throughput discovery of novel developmental phenotypes. *Nature* **537**, 508–514 (2016).

498. Bergman, M. *et al.* Review of methods for detecting glycemic disorders. *Diabetes Res. Clin. Pract.* **165**, 108233 (2020).

499. Zhou, Z. D., Sathiyamoorthy, S., Angeles, D. C. & Tan, E. K. Linking F-box protein 7 and parkin to neuronal degeneration in Parkinson's disease (PD). *Mol. Brain* **9**, 1–11 (2016).

500. Chen, M. & Xie, S. Therapeutic targeting of cellular stress responses in cancer. *Thorac. Cancer* **9**, 1575–1582 (2018).

501. Puspita, L., Chung, S. Y. & Shim, J. Oxidative stress and cellular pathologies in Parkinson's disease. *Mol. Brain* **10**, 53 (2017).

502. Varadi, M. *et al.* AlphaFold Protein Structure Database: massively expanding the structural coverage of protein-sequence space with high-accuracy models. *Nucleic Acids Res.* 1–6 (2021) doi:10.1093/nar/gkab1061.

503. Jumper, J. *et al.* Highly accurate protein structure prediction with AlphaFold. *Nature* **596**, 583–589 (2021).

504. Díaz-Rodríguez, E. & Pandiella, A. Modulation of cereblon levels by anti-myeloma agents. *Leuk. Lymphoma* **57**, 167–176 (2016).

505. Liu, J. *et al.* A genome-scale CRISPR-Cas9 screening in myeloma cells identifies regulators of immunomodulatory drug sensitivity. *Leukemia* **33**, 171–180 (2019).

506. Raimondi, L. *et al.* Targeting of multiple myeloma-related angiogenesis by miR-199a-5p mimics: in vitro and in vivo anti-tumor activity. *Oncotarget* **5**, 3039–3054 (2014).

507. Robinson, S. R. Investigating the role of the ribonuclease DIS3 in haematological cancers (A thesis submitted for the degree of Doctor of Philosophy at the University of Brighton and the University of Sussex). (2016).

508. Keats Lab. Multiple Myeloma: Neon transfection conditions. https://www.keatslab.org/myeloma-cell-lines/neon-transfection-conditions.

509. Hornbeck, P. V *et al.* PhosphoSitePlus, 2014: mutations, PTMs and recalibrations. *Nucleic Acids Res.* **43**, D512–D520 (2015).

510. Crosas, B. *et al.* Ubiquitin Chains Are Remodeled at the Proteasome by Opposing Ubiquitin Ligase and Deubiquitinating Activities. *Cell* **127**, 1401–1413 (2006).

511. National Library of Medicine & (US). ClinicalTrials.gov. https://clinicaltrials.gov.

512. Lang, L., Chemmalakuzhy, R., Shay, C. & Teng, Y. PFKP Signaling at a Glance: An Emerging Mediator of Cancer Cell Metabolism. in *Advances in Experimental Medicine and Biology* 243–258 (2019). doi:10.1007/978-3-030-12668-1_13.

513. Ntanasis-Stathopoulos, I., Terpos, E. & Dimopoulos, M. A. Optimizing Immunomodulatory Drug With Proteasome Inhibitor Combinations in Newly Diagnosed Multiple Myeloma. *Cancer J.* **25**, 2–10 (2019).

514. Das, D. S. *et al.* Synergistic anti-myeloma activity of the proteasome inhibitor marizomib and the IMiD ® immunomodulatory drug pomalidomide. *Br. J. Haematol.* **171**, 798–812 (2015).

Appendix A

Hits from Fbxo7 yeast two-hybrid, mass spectrometry and protein array screens that have metabolic functions.

Screen	Gene	Gene name	Metabolic pathway	Metabolic role
Protein array	GAPDH	Glyceraldehyde-3-Phosphate Dehydrogenase	Glycolysis	Catalyses the conversion of glyceraldehyde-3-phosphate to 1,3-bisphosphoglycerate
Y2H	PFKP	Phosphofructokinase, Platelet	Glycolysis	Catalyses the conversion of F6P to F1,6BP, the rate limiting step in glycolysis
Mass spec.	PKM	Pyruvate Kinase M1/2	Glycolysis	Catalyses the conversion of PEP to pyruvate
Protein array	IDH2	Isocitrate Dehydrogenase 2	TCA cycle	Catalyses the oxidative decarboxylation of isocitrate to α-ketoglutarate
Protein array Mass spec.	ATP5C1	ATP Synthase F1 Subunit Gamma	OXPHOS	A subunit of mitochondrial ATP synthase
Mass spec.	ATP5A1	ATP Synthase F1 Subunit Alpha	OXPHOS	Subunit of mitochondrial membrane ATP synthase
Protein array	SHMT1	Cytoplasmic serine hydroxymethyltransferase	1C metabolism	Catalyses the cleavage of serine to glycine accompanied with the production of 5,10-methylenetetrahydrofolate
Protein array	SHMT2	Mitochondrial serine hydroxymethyltransferase	1C metabolism	Catalyses the cleavage of serine to glycine accompanied with the production of 5,10-methylenetetrahydrofolate
Protein array	SLC25A26	Solute Carrier Family 25 Member 26	1C metabolism	Mediates the transport of S-adenosylmethionine (SAM) into the mitochondria
Mass spec.	MTHFD1	Methylenetetrahydrofolate Dehydrogenase 1	1C metabolism	Trifunctional enzyme that catalyses three sequential reactions in the interconversion of 1-carbon derivatives of tetrahydrofolate.
Mass spec.	SFXN1	Sideroflexin 1	1C metabolism	Mitochondrial serine transporter that mediates transport of serine into mitochondria
Mass spec.	PHGDH	Phosphoglycerate Dehydrogenase	Serine synthesis	Catalyses the first step of the phosphorylated L-serine biosynthesis pathway
Protein array	KMO	Kynurenine 3-Monooxygenase	Tryptophan metabolism	Catalyses the hydroxylation of L-kynurenine
Protein array	BCKDK	Branched Chain Keto Acid Dehydrogenase Kinase	Amino acid metabolism	Catalyses the phosphorylation and inactivation of the branched-chain alpha-ketoacid dehydrogenase (BCKD) complex, the key regulatory enzyme of the valine, leucine and isoleucine catabolic pathways
Y2H	ACAT1	Acetyl-CoA Acetyltransferase 1	Amino acid metabolism Ketogenesis	Catalyses the reversible formation of acetoacetyl-CoA from two molecules of acetyl-CoA

Y2H	ODC1	Ornithine Decarboxylase 1	Polyamine biosynthesis	Catalyses the conversion of ornithine to putrescine, the rate-limiting step of the polyamine biosynthesis pathway
Mass spec.	SRM	Spermidine Synthase	Polyamine biosynthesis	Catalyses the conversion of putrescine and decarboxylated S-adenosylmethionine to spermidine
Protein array	PDE4D	Phosphodiesterase 4D	Nucleotide metabolism	Hydrolyses the second messenger cAMP to control its availability
Mass spec.	CAD	Carbamoyl-Phosphate Synthetase 2, Aspartate Transcarbamylase, and Dihydroorotase	Nucleotide biosynthesis	Trifunctional multi-domain enzyme involved in the first three steps of pyrimidine biosynthesis
Mass spec.	EPRS	Glutamyl-Prolyl-TRNA Synthetase 1	Fatty acid uptake	A multifunctional aminoacyl-tRNA synthetase that also recruits the GAIT complex to bind 3'-UTR of mRNA and suppress the IFNy response, and functions downstream of mTORC1 to promote the uptake of long-chain fatty acids
Protein array	ACOT8	Acyl-CoA Thioesterase 8	Fatty acid metabolism	Catalyses the hydrolysis of acyl-CoAs to the free fatty acid and coenzyme A
Protein array	ACSL5	Acyl-CoA Synthetase Long Chain Family Member 5	Fatty acid metabolism	Catalyses the activation of fatty acids by CoA to produce an acyl-CoA, the first step in fatty acid metabolism (long chains)
Protein array	ACSM3	Acyl-CoA Synthetase Medium Chain Family Member 3	Fatty acid metabolism	Catalyses the activation of fatty acids by CoA to produce an acyl-CoA, the first step in fatty acid metabolism (medium chains)
Y2H	ACADM	Acyl-CoA Dehydrogenase Medium Chain	Fatty acid metabolism	Catalyses the initial step of the beta-oxidation cycle for medium-chain fatty acyl-CoAs
Protein array	HADH	Hydroxyacyl-CoA Dehydrogenase	Fatty acid metabolism	Catalyses the third step of the beta-oxidation cycle for medium and short-chain fatty acyl-CoAs
Mass spec.	FASN	Fatty Acid Synthase	Fatty acid synthesis	A multifunctional enzyme that catalyses the *de novo* biosynthesis of long-chain saturated fatty acids from acetyl-CoA and malonyl-CoA
Y2H	CYB5R2	Cytochrome B5 Reductase 2	Fatty acid synthesis	Involved in desaturation and elongation of fatty acids as part of the fatty acid desaturation complex, and cholesterol biosynthesis
Protein array	GPSN1 (TECRL)	Trans-2,3-Enoyl-CoA Reductase Like	Fatty acid synthesis	Proposed to be involved in very long-chain fatty acid elongation
Protein array	GPSN2 (TECR)	Trans-2,3-Enoyl-CoA Reductase	Fatty acid synthesis	Catalyses reduction of trans-2,3-enoyl-CoA to saturated acyl-CoA, the last step in very long-chain fatty acid elongation
Protein array	GPAM	Glycerol-3-Phosphate Acyltransferase, Mitochondrial	Glycerolipid biosynthesis	Esterifies the acyl-group from acyl-ACP to glycerol-3-phosphate, an essential step in glycerolipids biosynthesis
Protein array	FUT8	Fucosyltransferase 8	Glycosylation	Catalyses the transfer of fucose from GDP-fucose to N-linked type complex glycopeptides

Protein array	NANS	N-Acetylneuraminate Synthase	Glycosylation	Catalyses N-acetylmannosamine 6-phosphate to N-acetylneuraminic acid (sialic acid) for N-glycan biosynthesis
Protein array	PIGY	Phosphatidylinositol Glycan Anchor Biosynthesis Class Y	Glycosylation	Component of the GPI-GlcNAc transferase which catalyses the first step in the production of GPI-anchors
Protein array	UXS1	UDP-Glucuronate Decarboxylase 1	Glycosylation	Catalyses the NAD-dependent decarboxylation of UDP-glucuronate to UDP-xylose which is used in glycosaminoglycan biosynthesis
Protein array	GLCE	Glucuronic Acid Epimerase	Glycosylation	Catalyses the epimerisation of D-glucuronic acid to L-iduronic acid, with a role in glycosaminoglycan metabolism
Mass spec.	SLC25A13	Solute Carrier Family 25 Member 13	Metabolite transport	Catalyses the Ca^{2+}-dependent exchange of mitochondrial aspartate with cytoplasmic glutamate across the mitochondrial inner membrane
Mass spec.	SLC25A1	Solute Carrier Family 25 Member 1	Metabolite transport	Catalyses the exchange of mitochondrial citrate with cytosolic malate across the inner mitochondrial membrane
Mass spec.	SLC25A11	Solute Carrier Family 25 Member 11	Metabolite transport	Catalyses the exchange of mitochondrial α-ketoglutarate with cytosolic malate or other dicarboxylic acids across the inner mitochondrial membrane
Mass spec.	HSPA5	Heat Shock Protein Family A (Hsp70) Member 5 / 78 KDa Glucose-Regulated Protein	Cellular homeostasis	Chaperone for protein folding in the endoplasmic reticulum. Is upregulated in response to glucose. Has roles in the unfolded protein response, apoptosis, and senescence in response to stress
Mass spec.	IRS4	Insulin Receptor Substrate 4	Cellular homeostasis	A tyrosine kinase activated by insulin with a role in glucose homeostasis
Protein array	GLRX2	Glutaredoxin 2	Cellular homeostasis	Glutathione-dependent oxidoreductase that regulates mitochondrial redox homeostasis and protects against oxidative stress
Protein array	UROD	Uroporphyrinogen Decarboxylase	Porphyrin metabolism	Catalyses the decarboxylation of four acetate groups of uroporphyrinogen-III to yield coproporphyrinogen-III, a key process in heme biosynthesis
Y2H	CPOX	Coproporphyrinogen Oxidase	Porphyrin metabolism	Catalyses the stepwise oxidative decarboxylation of coproporphyrinogen III to protoporphyrinogen IX, the sixth step in the heme biosynthetic pathway
Protein array	HMGCS2	3-Hydroxy-3-Methylglutaryl-CoA Synthase 2	Ketogenesis	Condenses acetyl-CoA with acetoacetyl-CoA to form HMG-CoA, the first irreversible step in ketogenesis
Y2H	PPA2	Inorganic Pyrophosphatase 2	Phosphate metabolism	Catalyses the hydrolysis of pyrophosphate to inorganic phosphate in phosphate metabolism, which has implications in DNA and RNA synthesis, fatty acid and amino acid activation, and cyclic nucleotide synthesis
Protein array	DHRS2	Dehydrogenase/Reductase 2		Displays NADPH-dependent dicarbonyl reductase activity towards α-diketones
Protein array	ASPHD1	Aspartate Beta-Hydroxylase Domain Containing 1		Predicted to enable dioxygenase activity and to be involved in peptidyl-amino acid modification
Mass spec.	ATAD3A	ATPase Family AAA Domain Containing 3A		Mitochondrial membrane protein with proposed roles in mitochondrial DNA replication and protein synthesis, mitochondrial network organisation, and mitochondrial and cholesterol metabolism